CRANFIELD INSTITUTE OF TECHNOLOGY

DEPARTMENT OF AERODYNEMICS

PhD THESIS

ACADEMIC YEAR 1988-89

S. KARNI

FAR - FIELD BOUNDARIES AND THEIR NUMERICAL TREATMENT

SUPERVISOR: PROFESSOR P.L. ROE

JULY 1989

"...Actually, the sea is bluer than this and the waves are playful but gentle....Long cool evenings full of moussaka, local fish, wine and ouzo. Is a Ph.D worth it? Two Ph.D's even?..."

Phil and Sue Roe, on the back of a postcard sent from the Greek Island of Lesbos (1988).

SUMMARY

Many computational problems of theoretical and practical interest are not naturally bounded by physical boundaries. Aerodynamic examples include flow calculations past aerofoils or past wing-body configurations, semi-bounded channel flows etc. Other examples include simulations of Turbomachinery flows, problems in Underwater Acoustics etc. To obtain a numerical solution, the problem has first to be converted to a finite region, by introducing an artificial boundary at some finite distance. Boundary conditions must be specified at the artificial boundary for well-posedness of the truncated problem. They should simulate an open boundary across which the fluid flows and should ideally allow outgoing waves to pass through without generating reflections. Indeed, reflections at the boundary not only degrade the accuracy of transient solutions but also inhibit convergence to steady-state. In many problems of practical interest, perfect absorption cannot be achieved. Instead one aims at minimizing the amount of reflected energy using asymptotic expansions based on various asymptotic arguments. The more accurate the boundary statements, the closer the artificial boundaries can be located to the regions of aerodynamic interest, thereby reducing the computational domain and costs.

We present a thorough numerical study of the efficiency of several widely used boundary conditions in absorbing outgoing waves. We identify the key parameters upon which the level of absorption at the boundaries depends and expose the limitations of some of the existing recipes. We show that substantial reflections may occur even under conditions which are considerably milder than those encountered in practical calculations. We then introduce an unconventional approach to the treatment of artificial boundaries. It is proposed that in the far field the governing equations are modified in a boundary-layer like manner. Two closely related far field modifications are derived and analysed: (a) Slowing down the outgoing waves and (b) Attenuating the outgoing waves. Under the first modification the outgoing waves are prevented from reaching the boundary hence from reflecting. Under the second, the outgoing waves are attenuated to practically zero strength before reaching the boundary. Both modifications do not alter the propagation of the incoming waves to allow the launching of correct information from the boundary into the interior. Analytic conditions are derived to ensure that no reflections are generated due to the change of coefficients in the governing equations. Reflection analysis is also performed on the discrete level. Well-posedness of the modified systems is established as well as stability of the resulting interface problem. The modifications are extended to two space dimensions and are applied to a variety of one and multidimensional test problems. Results indicate that the proposed far field modifications are attractive in genuinely time-dependent calculations. Preliminary steady state calculations with the unsteady 2D Euler equations show significantly improved convergence properties.

CONTENTS

CHAPTER IV

LIST OF ILLUSTRATIONS

LIST OF FIGURES

with boundary conditions (ii)-(v).

(II.4) - 1D Euler Equations on a mildly expanding grid - A reflection study with boundary conditions (ii), (iii) and (v).

(II.5) - 1D Euler equations - Internal reflection of simple waves: (a) (u) wave and (b) (u-c) wave.

(II.6) - Strong focussing of an error generated at the boundary (a) 2D and (b) 3D linearised Euler equations.

(II.7) - 2D linearised Euler equations - High frequency initial data: (a) p, (b) q, (c) p-q and (d) p+q profiles.

(II.8) - 2D linearised Euler equations - High frequency boundary conditions.

(II.9) - 2D linearised Euler equations - Reflection of a smooth wave from a high frequency boundary.

(II.10) - 2D linearised Euler equations - Combined Low-High frequency boundary conditions.

(III.1) - 1D wave equation - Slowing down outgoing waves with (a)-(c) constant and (d) smoothly varying slowing down coefficients.

(III.2) - 1D Euler equations with various constant slowing down coefficients.

(III.3) - 1D Euler equations - (a) Piecewise constant and (b) Smoothly varying slowing down coefficients.

(III.4) - 2D linearised Euler equations - Exact solution for initial data (3.8.5).

(III.5) - 2D linearised Euler equations - Numerical solution for initial data (3.8.5) with (a)-(c) constant and (d) smoothly varying slowing down coefficients.

(III.6) - 2D linearised Euler equations with smoothly varying slowing down coeeficients - Numerical solution by (a) System I and (b) System II.

(III.7) - 2D linearised Euler equations - Exact solution for initial data (3.8.7).

(III.8) - 2D linearised Euler equations - Numerical solution for initial data (3.8.7).

(IV.1) - Linear advection equation - Gradually attenuated solution.

(IV.2) - 1D wave equation - Gradual attenuation of outgoing waves.

(IV.3) - 1D isothermal Euler equations - (a) Gradual attenuation of an outgoing compression wave (b) Incoming wave unaffected.

(IV.4) - 2D linearised Euler equations - Gradual attenuation of an outgoing pressure wave.

(IV.5) - 2D linearised Euler equations with gradual attenuation - Profiles along main diagonal.

(IV.6) - 2D linearised Euler equations with initial data (3.8.5)- Combined far field treatment.

(IV.7) - 2D Euler equations - Subsonic flow past a circular arc: Steady state (a) Mach number and (b) Pressure contours.

(IV.8) - 2D Euler equations - Transonic flow past a circular arc: Steady state (a) Mach number and (b) Pressure contours.

NOTATION

It has proved necessary to define the notation within the text on a sectional basis. The following however make frequent and largely consistent appearances throughout. The list is not comprehensive.

a	Slowing down coefficient
A, B	Jacobian matrices
A^*, B^*	Modified Jacobian matrices
α_k, β_k	Wave strengths
c_1, c_2	Attenuation coefficients
c	Speed of sound
C	Damping matrix
C_g	Group velocity
C_p	Phase velocity
$\Delta x, \Delta y, \Delta t$	Spatial and temporal grid spacings
E	Specific total energy
γ	Specific heat ratio
h	Specific enthalpy
I	Identity matrix
κ, μ	Space amplification factors
$\mathbb{K}$	Space shift operator
$\underline{\ell}_j, \underline{r}_j$	Left and right eigenvectors of the Jacobian matrix
L, R	Matrices of left and right eigenvectors respectively
λ	Characteristic speed
λ_j	Eigenvalues of the Jacobian matrix
Λ	Diagonal matrix of eigenvalues
Λ^*	Diagonal matrix of modified eigenvalues
M	Mach number
$M(\vartheta)$	$= A\cos(\vartheta)+B\sin(\vartheta)$ Jacobian matrix in the (ϑ) direction
ν	Courant or CFL number
p	Pressure
q	Radial velocity
r	Radial distance
ρ	Density
S	Entropy function
t	Time coordinate
T, R	Transmission and Reflection coefficients
ϑ	Angle of incidence
u, v	Velocity components in the x and y directions
φ	Solution function of the wave equation
w	Scalar variable
$\underline{w}$	Vector of variables
ω	Wave frequency
x, y	Cartesien space coordinates
ξ, η	Wave numbers in the x and y directions
Z	Time amplification factor
$\mathbb{Z}$	Time shift operator

Superscripts and Subscripts:

w_j^n, v_j^n	Numerical solutions at node j and time level n
$(\ )_0$	Linearised conditions about a mean state
$(\ )_\infty$	Free stream conditions

INTRODUCTION

In a large class of CFD applications it is required to solve problems which are not naturally bounded by physical boundaries. Aerodynamic examples include flow calculations past aerofoils or past wing-body configurations (infinite in 2 and 3 space dimensions), calculations of semi-bounded channel flows (infinite in 1 space dimension) etc. Other examples include the simulation of Turbomachinery flows, problems in Underwater Acoustics, Elasticity, Numerical Weather Prediction etc. In order to obtain a numerical solution, the problem first has to be converted to a finite region. For a certain class of problems, this can be achieved by coordinate mapping techniques, provided the solution is simple at infinity and that it is smooth in the transformed coordinate [24]. The transformed problem requires boundary conditions at infinity which are available and can be specified without introducing errors. However, if the solution in the far field is oscillatory, mapping techniques fail. The outgoing waves cannot be resolved accurately in the transformed coordinate and reflections occur at critical grid points. For this large class of problems, the only means of limiting the unbounded physical region is by introducing an artificial boundary at some finite region. This, however, is at the price of having to specify boundary conditions (BCS) at the artificial boundary to ensure well-posedness of the truncated problem. To appreciate the difficulty in specifying BCS, consider the steady state calculation of transonic flow past an aerofoil. In the far field the flow is subsonic, implying that the solution at every point depends on the solution at every other point in its neighbourhood. If a boundary is introduced, part of this neighbourhood is discarded and the only means of conveying the *infinite* amount of lost information is through a *finite* number of BCS, often just a single one. " Boundary Conditions are a mathematical model for the rest of the Universe" (G. Moretti) and the task of their specification is often far from trivial.

Clearly, even if physical conditions at infinity are known, they are unlikely to be correct at the artificial boundary itself, unless

the boundary is located at a very large distance. Imposing infinity conditions at the artificial boundary usually results in reflections of the outgoing waves which should ideally pass through the boundary and leave the domain of computation. This obviously degrades the accuracy of the solution during the time-dependent phase. In problems where steady state solutions are sought by means of integrating the time-dependent equations, the reflected waves carry energies which are damped very slowly and inhibit convergence to steady state [66]. Moreover, the solution is knowingly inaccurate although it is hoped that the inaccuracies are confined to the neighbourhood of the remote boundary.

The number of required BCS is dictated by the theory of characteristics, which is strictly valid in one space dimension. In one dimensional problems, the theory also establishes the actual analytic BCS that perfectly absorb outgoing waves. When discretized and incorporated into a numerical model, truncation errors are introduced. In multidimensional problems the situation is more complex and one usually resorts to 1 Dimensional arguments normal to the boundary, to asymptotic expansions or to procedures guided by practical experience. The errors in this case are due to neglecting terms in the asymptotic expansions as well as due to the discretisation procedure.

The philosophy of constructing absorbing BCS is to match them to a known (asymptotic) behaviour of the outgoing waves. This behaviour can either be deduced from the governing equations or directly from its discrete approximation. Clearly, if the BC is exactly satisfied by an outgoing wave, no other waves are generated at the boundary which may propagate back into the domain of computation. It should also be apparent that artificial boundaries do not constitute a difficulty in problems where all characteristic speeds are pointing out of the computational domain (ie supersonic boundaries). In such cases, even if errors are generated at the boundary, there is no mechanism by which the errors can propagate back into the interior of the domain. The difficulty thus lies in the subsonic case, where

there is at least one characteristic speed pointing into the interior.

The present work is devided into two main parts, each of which is preceded by an introduction which is more specific to the content that follows. In broad terms, the first part surveys existing open boundary treatments, emphasising the different strategies and the degree of approximation involved in each of the recipes. This is followed by a thorough numerical study of the absorbing features of several of the proposed recipes. The aim of the study is to expose the limits of the conventional far field treatments and to identify the parameters upon which the level of absorption depends. It is found that even under mild conditions, substantial reflections may occur, which although classified as high-order effect, can become quite troublesome. Acquaintance with two closely related theories is vital for the understanding of artificial boundary treatment: The theory of *Well-posedness* of mixed Initial Boundary Value Problems (IBVPS) and the theory of *Stability* of discrete numerical models in the presence of boundaries. The first part of this work begins by glancing at some illuminating aspects of both theories, which are viewed in the light of the *Theory of Wave Propagation.* This by no means is intended to be a comprehensive account of the theories. Its aim is to familiarise the reader with the predominant concepts and to assist in introducing notations and terminology which are later referred to. The second part of this work contains its main original contribution. It presents a less conventional strategy to handle remote boundaries, based on modifying the governing equations in an outer absorbing 'sponge' layer and forcing the solution to a desirable far field behaviour. Two new far field modifications are proposed: (i) To slow down the outgoing waves and (ii) To attenuate the outgoing waves. Both modifications are analysed on the continuous and discrete levels, well-posedness of the modified systems is established and stability of the numerical model is proved. The proposed modifications are implemented in a variety of one and multidimensional test cases. Results show improved time accuracy of solutions and indicate significant acceleration in rate of convergence to steady state.

Acknowledgements

First, I am deeply indebted to my supervisor Professor P.L. Roe for introducing me to the topic of this work; for having original and inspiring ideas as to how to go about solving it; for always having the time and patience to listen and to advise; for not showing his impatience when progress was nearly brought to a halt and for never being too busy for a laugh or a joke. I owe much of my CFD knowledge to him and wish a little bit of his originality and clarity of thought would have clung to me and not only the way I organize my desk. I want to thank my husband, Doron, but I do not know how. " My heart is full..." said the screenwriter and the truth is often so banal. No words can express my deep gratitude to Theresa and Fred Haines for giving little Yali a warm home and endless love and providing me with the peace of mind I needed to concentrate on this work. The completion of this thesis is largely a result of their joint efforts. As to Yali, he is a living proof that despite all, there is no such thing as conservation and someone ought to be thanked for that. I would like to thank my parents for the faith they always had in me and for their continuous encouragement and support. I just hope they will not feel obliged to read this thesis only because I went through the trouble of writing it. I would like to thank B'nai B'rith, Leo Baeck Lodge, for their generous financial support over the years. I am happy to acknowledge Mr. A.D. French for providing the basic code for the 2D unsteady Euler calculations and for getting me out of the programming muddle in which I had been. Last but not least, I would like to thank Mrs. Pauline Forshaw for her dedication in typing this thesis and for being so helpful and kind duringg the last stages of its preparation.

PART ONE

Introduction

The study of numerical solutions to hyperbolic mixed IBVPS involves analysis on various levels. Hyperbolic systems of equations are characterised by the existence of a set of channels, ie characteristic curves, along which information may propagate. In one space dimension only a finite number of such curves exists, while in multidimensional problems information may be carried in an infinite number of directions. The solution inside a given domain Ω is determined partly by the initial conditions and partly by the data on the boundary $\partial\Omega$. Similarly, the solution on the boundary itself usually depends both on the boundary data and on information arriving from the domain Ω. It is therefore clear that the manner in which boundary data are specified at the boundary must be consistent with that arriving at the boundary, if it is to yield a mathematically well-posed problem. The physical significance of the boundary data is a completely separate issue.

Apart from very simple cases, sclutions to IBVPS are obtained numerically, by applying a discrete model to approximate the analytic problem. Numerical solutions, by nature, cannot be obtained on infinite domains and therefore always involve boundaries. Some problems are naturally limited by physical boundaries. In other cases, artificial boundaries have to be introduced in order to truncate the unlimited physical domain so that a numerical solution can be obtained. Numerical schemes of sufficient order of accuracy always break down in the neighbourhood of a boundary and in either situation, special measures are required.

In order to update the numerical solution at the boundary, one needs to make a sufficient number of independent statements. This to some extent is analogous to the analytic situation. However, 'sufficient' very often results in more conditions that would have been allowed analytically, and self-consistency becomes more

complicated. Instead of well-posedness one talks about the stability of the mixed IBVP. Clearly well-posedness and stability are closely related to one another. Yet stability is inherently more complicated because numerical approximations are always dispersive even when the analytic problem is not.

Over the last 15 years a substantial effort has been devoted to the modelling of open boundaries. An adequate account of the related published studies would occupy many pages and is beyond the scope of the present work. The admirable versatility of approaches reflects not merely differences of tastes. It also portrays the lack of sufficient generality in each of the individual approaches and accordingly the lack of consensus over the issue. In order to be numerically applicable, the BCS must yield a well-posed problem and their discrete numerical approximation must be stable. We therefore begin Chapter I by discussing well-posedness of hyperbolic problems with boundaries. We highlight the particular difficulty of numerical boundary treatment and move on to discuss the concept of stability in the presence of boundaries. Both well-posedness and stability theories are related to the theory of wave propagation and are viewed in this light. Chapter I continues by surveying existing recipes for the modelling of open boundaries and emphasises the degree of approximation involved in each of the individual recipes. In Chapter II we select a particular dissipative scheme, namely the Lax-Wendroff scheme, and analyse its dispersive and dissipative properties in more detail. The analysis predicts a pathological behaviour which is confirmed by experiments. Chapter II concludes with a thorough numerical study of the (in)efficiency of various recipes in absorbing outgoing waves. Reflections from artificial boundaries are studied, exposing the key parameters upon which the level of absorption depends. Internal reflections due to grid expansion are presented. Strong focussing of an error generated at the boundary is demonstrated in a multidimensional setup. The need for nonreflecting upwind boundaries naturally emerges, upwind BCS following [35] and [86] are adapted to systems but fail to perform as satisfactorily as they do in the scalar case.

(1.1) Well-Posedness of Hyperbolic Initial Boundary Value Problems, Characteristic Curves and Boundary Conditions

Consider the 1st order hyperbolic linear system of equations in one space dimension

$$\begin{aligned} \underline{w}_t + A\underline{w}_x &= 0 \\ \underline{w}(x,0) &= \underline{f}(x) \end{aligned} \tag{1.1.1}$$

where $\underline{w} = \underline{w}(x,t)$ is the vector of N dependent variables and A is a constant coefficient NxN matrix. Hyperbolicity implies that A possesses real eigenvalues $\{\lambda_j\}$, and a complete set of right eigenvectors $\{\underline{r}_j\}$. Let $\{\underline{\ell}_j\}$ denote the (complete) set of left eigenvectors, then the following relations hold

$$\begin{aligned} A\underline{r}_j &= \lambda_j \underline{r}_j \qquad j = 1,\ldots,N \\ \underline{\ell}_j A &= \lambda_j \underline{\ell}_j \qquad j = 1,\ldots,N \\ \underline{\ell}_j \cdot \underline{r}_k &= \delta_{jk} \end{aligned} \tag{1.1.2}$$

Let R be the matrix with columns $\underline{r}_j$, let L be the matrix with rows $\underline{\ell}_j$ and let Λ be the diagonal matrix with λ_j along its diagonal.

$$R = (\underline{r}_1,\ldots,\underline{r}_N) \qquad L = \begin{pmatrix} \underline{\ell}_1 \\ \vdots \\ \underline{\ell}_N \end{pmatrix} \qquad \Lambda = \operatorname{diag}(\lambda_1\ldots,\lambda_N) \tag{1.1.3}$$

Then it follows from (1.1.2) that

$$LR = RL = I \qquad LAR = \Lambda \tag{1.1.4}$$

If (1.1.1) is to be solved on the limited domain $[0,\infty)$, then in addition to the initial distribution $\underline{w}(x,0)$ one often needs to specify BCS at x=0. These BCS may or may not arise from physical considerations (eg solid walls, open boundaries etc.). In either situation they cannot be specified arbitrarily. A theory has been developed (eg Kreiss [48]) to determine whether a given set of equations and boundary conditions are to yield a well-posed problem:

Definition

An IBVP is said to be *well-posed* if it possesses a unique solution continuously dependent on the initial and boundary data

According to the theory in [48], testing for well-posedness amounts to ensuring that the combination of governing equations and set of BCS do not admit exponentially growing solutions,

$$\underline{w} = \underline{w}_0 e^{st+i\xi x} \qquad \text{with} \quad \text{Real}(s) \geq 0 \tag{1.1.5}$$

This theory has recently been reviewed by Higdon [34], and interpreted in terms of wave propagation.

Not every set of BCS yields a well-posed problem. This can be appreciated from the following example. Let (1.1.1) be premultiplied by the matrix L, which in the linear case is constant

$$\begin{aligned} L\underline{w}_t + LA\underline{w}_x &= 0 \\ (L\underline{w})_t + LAR\,(L\underline{w})_x &= 0 \\ \bar{\underline{w}}_t + \Lambda\bar{\underline{w}}_x &= 0 \end{aligned} \tag{1.1.6}$$

with $\bar{\underline{w}} = L\underline{w}$. Equation (1.1.6) is in fact a set of N scalar equations

$$(\bar{\underline{w}}_j)_t + \lambda_j(\bar{\underline{w}}_j)_x = 0 \qquad j = 1,\ldots,N \tag{1.1.7}$$

implying that

$$(\bar{\underline{w}}_j) = \underline{\ell}_j \cdot \underline{w} = \text{constant} \quad \text{on} \quad dx/dt = \lambda_j \tag{1.1.8}$$

$\bar{\underline{w}}_j$ are called the characteristic variables or the *Riemann Invariants*, and the curves along which they remain constant are the characteristic curves. In the linear case λ_j = const and characteristic curves are straight lines. Initial values of $\bar{\underline{w}}_j$ are supplied by the data, which then propagate along the characteristics. If $\lambda_j > 0$, the propagation is from left to right (in our case incoming). Similarly, if $\lambda_j < 0$, propagation is from right to left (outgoing).

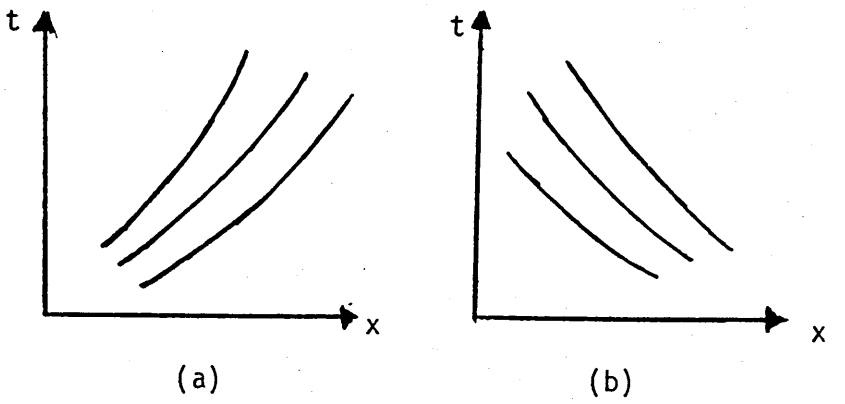

Ill. (I.1) - (a) Incoming and (b) outgoing characteristic curves for the left hand IBVP.

For the left hand IBVP, it is clearly not allowed to prescribe the values of $\bar{\underline{w}}_j$ for $\lambda_j < 0$, as those are pre-determined by initial data. An attempt to do so may result in a contradiction in which case a solution cannot exist. On the other hand, the solution requires information about the incoming $\bar{\underline{w}}_j$, to ensure uniqueness. It is obvious then, that one is only free to impose as many BCS as there are incoming characteristics at the boundary. A general set of BCS defines the incoming $\bar{\underline{w}}_j$ in terms of the outgoing $\bar{\underline{w}}_j$ and possibly some forcing terms.

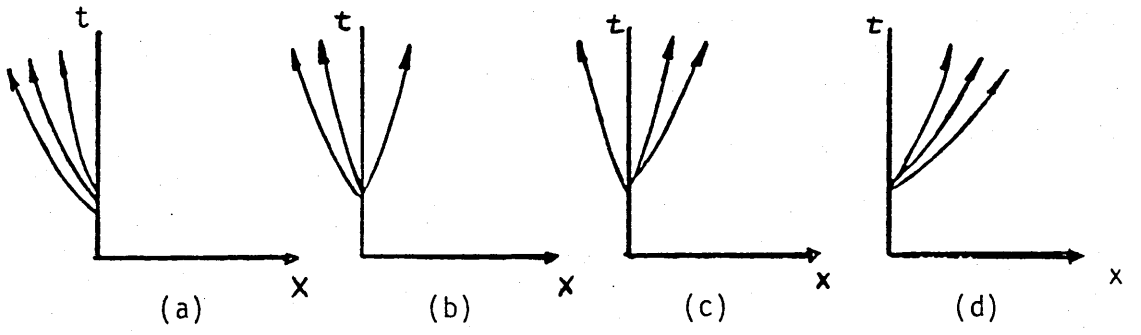

Ill. (1.2) - Required number of boundary conditions - Impose 0,1,2 and 3 bc's respectively.

In the non linear case we have

$$\underline{W}_t + A(\underline{W})\underline{W}_x = 0$$

$$L(\underline{W})\underline{W}_t + L(\underline{W})\underline{W}_x = 0$$

$$L(\underline{W})\ (\underline{W}_t + \Lambda(\underline{W})\underline{W}_x) = 0 \qquad (1.1.9)$$

implying

$$\underline{\ell}_j \cdot d\underline{W} = 0 \quad \text{along} \quad dx/dt = \lambda_j(\underline{W}) \qquad (1.1.10)$$

which is an Ordinary Differential Equation (ODE) obeyed along the characteristic curve. Equation (1.1.8) is a particular case of (1.1.10) where the ODE can be integrated along the characteristic curve to yield the Riemann Invariant. Charecteristic equations like (1.1.8) and (1.1.10) are often used as BCS at open boundaries. Examples shall be given in the following sections. A common practice in many applications is to locally linearise the system with respect tc a mean state $\underline{W}_0$, and to use (1.1.8) instead of (1.1.10).

(1.2) Numerical Solutions and Boundary Conditions

The simplest hyperbolic equation (Eqn. (1.1.6)) is the linear advection equation

$$w_t + \lambda w_x = 0 \qquad (1.2.1)$$

$$w(x,0) = f(x) \qquad -\infty < x < \infty$$

with solution

$$w(x,t) = f(x-\lambda t) \qquad (1.2.2)$$

Let the infinite domain be truncated by introducing boundaries at $x = 0$ and at $x = x_0$. Let us also assume, without loss of generality, that $\lambda > 0$. Characteristic analysis suggests that a BC is required at $x = 0$ but not at $x = x_0$.

One may attempt to solve (1.2.1) numerically, using a two level explicit scheme

$$w_j^{n+1} = \sum_{k=-L}^{R} c_k w_{j+1}^{N} \qquad (1.2.3)$$

The stencil of (1.2.3) is of width L+R+1. If $L > 0$ ($R > 0$) the scheme cannot be used to update the leftmost (rightmost) point and a special boundary treatment is needed. While at $x = 0$, this is consistent with the analytic requirement, at $x = x_0$ it is not, yet one is forced to supplement (1.2.3) by a boundary procedure (BP) where analysis forbids to impose a BC. In view of (1.2.2) the BP should simulate right travelling waves propagating at a speed $\lambda > 0$. Ideally, the boundary should allow the oncoming waves to pass through without reflections. In practice, particularly in multidimensional problems, this is very difficult to achieve.

Note that while an analytic boundary consists of a single point, a numerical boundary may stretch over several grid points depending on the stencil of the numerical scheme. If $R = 1$, the numerical Right Hand Boundary (RHB) consists of one point, but if $R > 1$, a BP has to be applied to more than one point. $R = 0$ implies a one sided stencil, and no BP is required at all at the RHB. At first sight, this appears to have solved the problem. However, unless $L = 1$, reducing the

scheme to first order accuracy, a BP will be required at the LHB.

(1.3) Finite Representation of the Solution on the Grid

Investigating the features of a linear numerical scheme is best done by means of Fourier or Normal Mode Analysis in the frequency domain. The initial data can be expressed in terms of its Fourier Transform.

$$w(x,0) = f(x) = \int_{-\infty}^{\infty} \hat{f}(\xi) e^{i\xi x} \, d\xi \tag{1.3.1}$$

where ξ is the wave number of dimension length^{-1}, and $\hat{f}(\xi)$ its amplitude. Small ξ implies long waves while large ξ implies short waves. Let a grid be defined by $x_j = j\Delta x$, with Δx the grid spacing and consider a single Fourier mode $f(x) = e^{i\xi x}$. When sampled at a finite number of grid points it has the representation

$$f(j\Delta x) = e^{i\xi j\Delta x} = (e^{i\xi\Delta x})^j \tag{1.3.2}$$

This seemingly harmless sampling procedure introduces an error which is best appreciated by noticing that the highest possible frequency representable on the grid is $|\xi\Delta x| = \pi$, and in general, only frequencies in the range

$$\xi\Delta x \in (-\pi, \pi] \tag{1.3.3}$$

can be represented. Frequencies outside the band (1.3.3) are folded into it, and get misinterpreted. This is illustrated in Ill. (I.3). Note that in the discrete context, the terms low and high frequencies refer to the grid spacing Δx and not to the space coordinate x. It is often said that low frequencies are the physics while high frequencies are the numerics. Indeed, it is due to the finite size of the grid that waves appear as high frequencies, with an increasing number of poorly resolved frequencies as the grid gets coarser. If one could afford infinitely fine grids, all frequencies would be well resolved hence physically meaningful (excluding of course discontinuities).

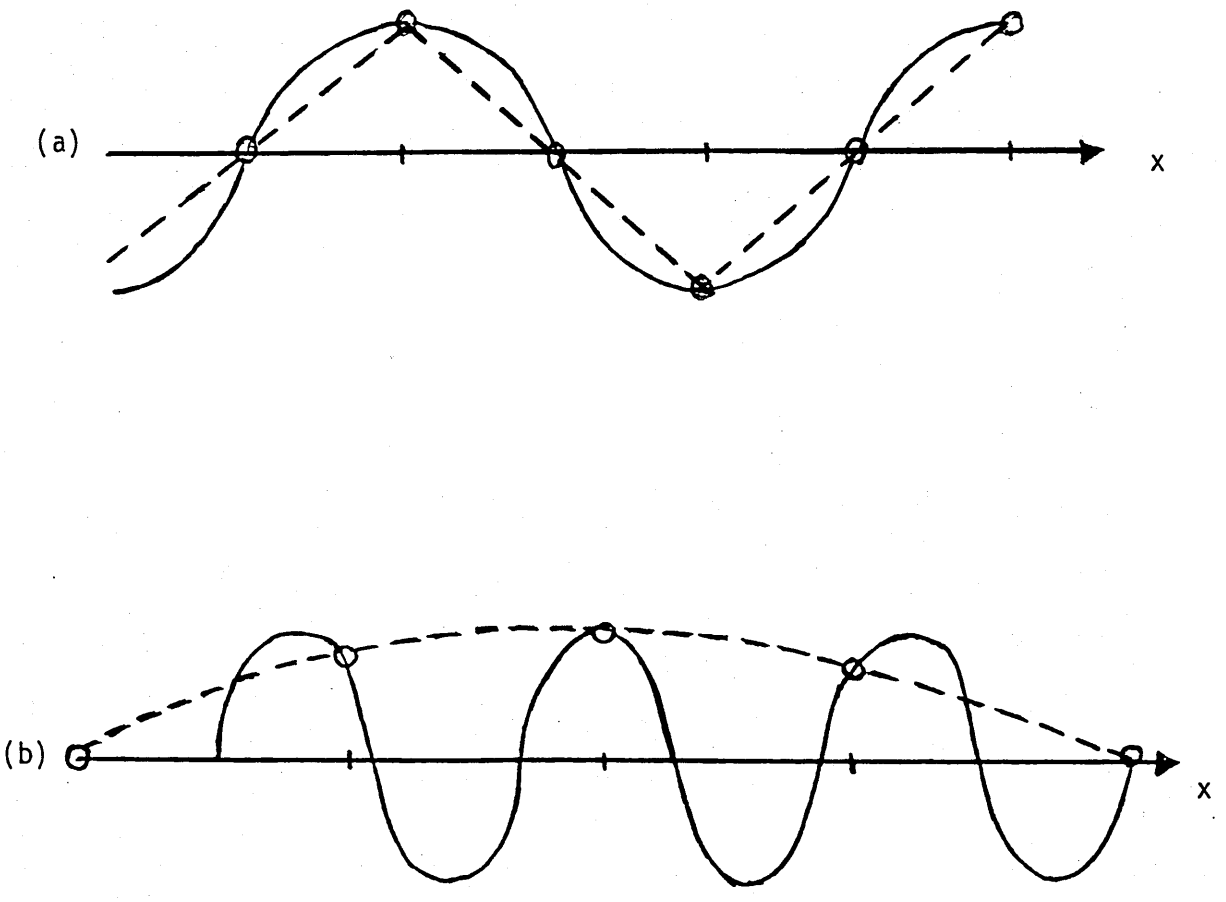

Ill. (I.3) - Misinterpretation of waves on a coarse grid -
(a) Low frequency interpreted as high frequency.
(b) High frequency interpreted as low frequency.

(1.4) Stability of Finite Differences Models and Boundary Conditions

Stability of a finite difference model depends on the combination of the interior numerical scheme and the numerical boundary procedures. Even when the analytic problem is well-posed, it sometimes takes more than good will to make it numerically stable. We therefore glance very briefly at several stability conditions, presented in a gradual degree of severity, starting from the well-known Von Neumann stability criterion for pure Initial Value Problems (IVPS) through the Godunov-Ryabenkii necessary stability condition in the presence of a boundary, and to the Gustafsson Kreiss and Sundström (GKS) stability condition which is both necessary and sufficient. As mentioned in the introduction, this by no means is intended to be a comprehensive account of stability theory. Its aim is to gently lead the reader through the tangle of stability theory to the physical concepts of travelling waves and energy distributions which have proved very revealing in the analysis to follow. It also provides an opportunity to appreciate the degree of complexity involved in rigorous stability analysis. For the sake of simplicity we concentrate on schemes of the form (1.2.3).

Advancing the solution from one time step to the next can be viewed as the act of the solution operator S on the vector of data $\underline{w}^n$

$$\underline{w}^{n+1} = S\underline{w}^n = S^2\underline{w}^{n-1} = \ldots = S^{n+1}\underline{w}^0 \qquad (1.4.1)$$

$\underline{w}^0$ being the vector of initial data. In the course of the numerical calculation, errors may be introduced (eg computer rounding errors), which in view of linearity also satisfy (1.4.1), and should clearly not be allowed to grow unboundedly. Suppose that we want to obtain the solution at a fixed time T, and are trying to get there by a sequence of calculations letting the time step Δt become increasingly smaller. As $T = N \cdot \Delta t$ is fixed, the required number of steps, N, is becoming increasingly larger, and by (1.4.1) we need to consider operators of the form S^n, as $n \to \infty$

Definition

The scheme is said to be stable in some norm $\| \ \|$ if

$$\| S^n \underline{w} \| \leq C \| \underline{w} \| \tag{1.4.2}$$

$\forall$ admissible $\underline{w}$, for some constant $C > 0$ as $n \to \infty$.

By the Lax Equivalence Theorem [60], stability of a consistent numerical approximation guarantees convergence to the analytic solution in the same norm $\| \ \|$, as the mesh is refined ($\Delta x, \Delta t \to 0$). The ℓ_2 norm

$$\| \underline{w} \|_2^2 = \sum_j w_j^2 \tag{1.4.3}$$

is sometimes regarded as a natural norm in that it can be related to amplification factors through Parseval's Equality [78]. In practical calculations, however, it is often not clear which norm is best for stability measurements and other norms may be found preferable.

Substituting a single Fourier mode

$$w_j^n = e^{i\omega t + i\xi x} \qquad t = n\Delta t \qquad \xi = j\Delta x \tag{1.4.4}$$

into (1.2.3), we obtain

$$e^{i\omega\Delta t} = \sum_{k=-L}^{R} c_k e^{i\xi k\Delta x} \tag{1.4.5}$$

Equation (1.4.5) is called the *dispersion relation* of the numerical approximation, relating the wave number ξ to the frequency ω. Note that although equation (1.2.1) is non-dispersive, its finite difference approximation always is. Misinterpreted frequencies, mentioned in the previous section, then become a major source of trouble.

The Von Neumann Stability Condition

Let a finite difference model (1.2.3) admit solutions of the form (1.4.4) with $\xi \in \mathbb{R}$. A necessary condition for stability is

$$|e^{i\omega\Delta t}| \leq 1 \qquad \forall \xi \in \mathbb{R} \tag{1.4.6}$$

For later purposes it is useful to introduce the notations

$$Z = e^{i\omega\Delta t} \qquad \varkappa = e^{i\xi\Delta x} \tag{1.4.7}$$

The travelling wave solution (1.4.4) then reads

$$w_j^n = Z^n \varkappa^j \tag{1.4.8}$$

and the dispersion relation

$$Z = \sum_{k=-L}^{R} c_k \varkappa^k \tag{1.4.9}$$

In these notations the Von Neumann condition becomes

$$|Z| \leq 1 \ (+ O(\Delta t)) \qquad \forall \ |\varkappa| = 1 \tag{1.4.10}$$

In the absence of boundaries, $|\varkappa| = 1$ are the only admissible modes. Indeed, modes with $|\varkappa|>1$ grow unboundedly as $j \to \infty$ and those with $|\varkappa|<1$ do so as $j \to -\infty$. Numerical calculations, however, are not performed on infinite domains. Let the domain be truncated so that j assumes positive values $j \geq 0$. It is immediately apparent that modes with $|\varkappa|<1$ are now perfectly admissible, having a finite ℓ_2 norm. This leads to a natural extension of (1.4.10) in the presence of a boundary.

Godunov Ryabenkii Stability Condition

A necessary condition for the left hand IBVP to be stable is that no modes of the form (1.4.8) are admitted which have

$$|x|\leq 1 \qquad |Z|>1 \tag{1.4.11)a}$$

Likewise, the right hand IBVP should admit no modes which have

$$|x|\geq 1 \qquad |Z|>1 \tag{1.4.11)b}$$

(Admissible modes here are modes of finite norm which satisfy both the interior scheme and the boundary conditions).

The Godunov-Ryabenkii stability condition rules out modes which are growing exponentially with time. Usually this criterion is not sufficient to ensure stability. The only theory which provides a condition both necessary and sufficient for stability of IBVPS is the GKS stability theory [27]. The condition is obtained at the expense of choosing a very complicated and restrictive norm $\|\ \|$ in (1.4.2) which accounts for initial, boundary and forcing data. GKS instability does not imply ℓ_2 instability and it is only conjectured that GKS stability implies ℓ_2 stability [76]. Testing for GKS stability may become extremely laborious even in relatively simple problems. It is an extension of the Godunov-Ryabenkii condition in that it considers modes of the form (1.4.8) with $|Z|>1$ in the limit $|Z| \to 1$.

Definition

Consider the left hand IBVP. An Eigensolution of (1.2.3) is a mode (1.4.8) with

$$|Z|\geq 1 \qquad |x|<1 \tag{1.4.12)a}$$

A Generalised Eigensolution is a mode (1.4.8) with

$$|Z|=1 \qquad |\varkappa|=1 \tag{1.4.13a}$$

so that when Z is perturbed $Z \rightarrow Z+\Delta Z$ and $|Z+\Delta Z|>1$, $\varkappa$ is perturbed $\varkappa \rightarrow \varkappa+\Delta\varkappa$ with $|\varkappa+\Delta\varkappa|<1$.

Similarly, consider the right hand IBVP. An Eigensolution is a mode (1.4.8) with

$$|Z|>1 \qquad |\varkappa|>1 \tag{1.4.12b}$$

A Generalised Eigensolution is a mode (1.4.8) with

$$|Z|=1 \qquad |\varkappa|=1 \tag{1.4.13b}$$

so that when Z is perturbed $Z \rightarrow Z+\Delta Z$ and $|Z+\Delta Z|>1$, $\varkappa$ is perturbed $\varkappa \rightarrow \varkappa+\Delta\varkappa$, with $|\varkappa+\Delta\varkappa|>1$.

Thus a Generalised Eigensolution is a limit of Eigensolution as $|Z|\rightarrow 1$.

The GKS Stability Condition

A necessary and sufficient condition for an IBVP to be stable is that it does not admit Eigensolutions or Generalised Eigensolutions.

This concludes our brief review of stability conditions. The reader is referred to [60,47,27] for a comprehensive discussion of stability theory. Ref. [9] is very instructive in the implementation of the various stability criteria to a test problem. We move on to introduce the concept of group velocity which is associated with the perturbation test of the GKS stability condition.

(1.5) GKS Stability and Group Velocity

Although the GKS stability theory was developed in the early 70's, its physical interpretation and in particular that associated with the search for Generalised Eigensolutions, remained obscure. It was not until quite recently [75] that a connection has been established between the perturbation test involved with finding Generalised Eigensolutions and the fundamental concept of Group Velocity in the theory of dispersive waves. This has been the work of Trefethen [74-78], which shed much light on the important role of Group Velocity in the analysis of numerical approximations to hyperbolic problems.

Associating a direction of propagation with a given normal mode is important not only for understanding the underlying mechanisms of instability, but also for energy distribution analysis [21,84] and for the assessment of rate of convergence to steady state [41,65]. Associating such a direction with the Godunov Ryabenkii unstable modes (1.4.11) can be achieved in a natural way. A mode with $|Z|>1$ and $|x|<1$ can be thought of being shifted to the right as n increases. Similarly, a mode with $|Z|>1$ $|x|>1$ as moving to the left. A stable numerical model should clearly not admit such modes since they grow exponentially in time. It is less obvious why Generalised Eigensolutions (1.4.13) are unstable. Assigning a direction of propagation with such modes can only be accomplished through the notion of Group Velocity. It can then be established [76] that they represent a much milder instability and grow only linearly in time.

It is interesting to observe how the concept of group velocity keeps emerging in the theory of dispersive waves in a surprisingly versatile manner. Consider the simple example of a superposition of two sinusoidal waves of neighbouring frequencies and wave numbers

$$w(x,t) = \cos(\omega_1 t-\xi_1 x) + \cos(\omega_2 t-\xi_2 x) \qquad (1.5.1)$$

$$\omega_1 = \omega_0 + \Delta\omega \qquad \xi_1 = \xi_0 + \Delta\xi$$
$$\omega_2 = \omega_0 - \Delta\omega \qquad \xi_2 = \xi_0 - \Delta\xi$$

By a known trigonometrical identity

$$w(x,t) = 2\cos(\Delta\omega\cdot t - \Delta\xi\cdot x)\cos(\omega_0 t - \xi_0 x) \tag{1.5.2}$$

which describes a wave of the original frequency and wave number $\cos(\omega_0 t-\xi_0 x)$ multiplied by a slowly varying sinusoidal envelope $2\cos(\Delta\omega\cdot t-\Delta\xi\cdot x)$, giving rise to 'groups' of waves (see Ill. (I.4)). An observer that fixes his attention on a particular point on the wave train, say point A, moves his eyes with the *Phase Velocity*

$$\omega_0 t-\xi_0 x = 0 \qquad C_p = x/t = \omega_0/\xi_0 \tag{1.5.3}$$

An observer that follows a particular point on the envelope, say point B, moves his eyes with the *Group Velocity*

$$\Delta\omega\cdot t-\Delta\xi\cdot x=0 \qquad C_g = x/t = \Delta\omega/\Delta\xi \rightarrow d\omega/d\xi \tag{1.5.4}$$

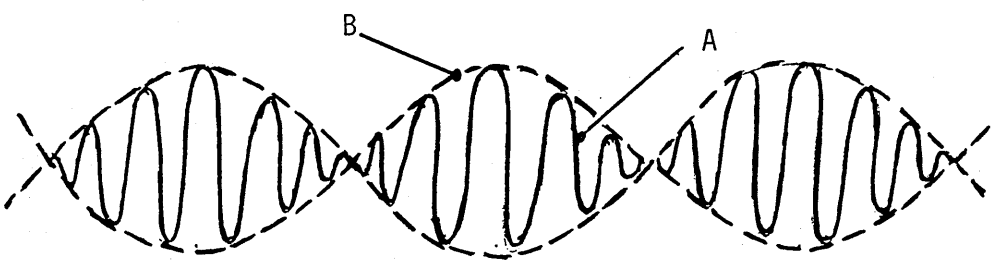

Ill. (I.4) - Groups of waves

Even from this simple example it is clear that if one is not interested in the details of the motion but rather in some average

distribution of the amplitude, then it is C_g rather than C_p that determines the speed of propagation. This argument can be made more precise, by using variational methods (see Whitham [87], p.390).

In general, any PDE that admits travelling wave solutions (1.4.4) also defines a dispersion relation $\omega=\omega(\xi)$ from which the phase and group speeds can be deduced

$$C_p = \omega(\xi)/\xi \qquad\qquad C_g = d\omega(\xi)/d\xi$$

Unless ω is a homogeneous linear function of ξ, the two speeds are not equal and we may either have $C_p > C_g$ or $C_p < C_g$. We have seen C_g emerging from a simple example (1.5.1). In the more general case

$$w(x,t) = \int_{-\infty}^{\infty} f(\xi) e^{i(\omega(\xi)t-\xi x)}\, d\xi \qquad (1.5.5)$$

and one may ask which values of ξ contribute most to the integral in (1.5.5) for a given (x,t). Denote by $\vartheta(x,t)$ the phase

$$\vartheta(x,t) = \omega t-\xi x = t\ (\omega-\xi\cdot x/t) \qquad (1.5.6)$$

and examine the behaviour of (1.5.5) at large times when the ratio x/t is held fixed, thus concentrating on waves which are moving at that particular speed. For large t, the phase ϑ oscillates very rapidly and most wave numbers make very little or no net contribution at all. The predominant contribution to the integral comes from points where the phase is varying slowly so that neighbouring Fourier modes tend to reinforce one another. These points satisfy.

$$d\vartheta/d\xi = 0 \qquad \Longrightarrow \qquad x/t = d\omega/d\xi = C_g$$

This method is known as the method of *stationary phase* [7,87]. It implies that after sufficiently long time, that is after the waves have dispersed and separated, we shall see a local wave number of ξ moving with speed $C_g = d\omega/d\xi$. (For a full discussion see Brillouin [7] and Whitham [87], pp.363-402).

In terms of $\varkappa$ and Z

$$C_g = -\frac{d\omega}{d\xi} = -\frac{\Delta x}{\Delta t}\frac{\varkappa}{Z}\frac{dZ}{d\varkappa} \tag{1.5.7}$$

Returning now to the perturbation test of the GKS stability condition (1.4.13), it can be shown (Trefethen [76]) that Generalised Eigensolutions (1.4.13) have <u>real</u> group velocity which points into the interior of the domain (ie positive for (1.4.13)$_a$ and negative for (1.4.13)$_b$). If admitted, such modes represent spontaneous radiation of energy from the boundary and clearly constitutes a source of instability.

(1.6) <u>Absorbing Boundary Conditions in One Space Dimension</u>

Consider the 1D scalar wave equation

$$\left(\frac{\partial^2}{\partial t^2} - \lambda^2 \frac{\partial^2}{\partial x^2} \right) \varphi = 0 \tag{1.6.1}$$

which admits left and right moving single frequency solutions

$$\varphi(x,t) = ae^{i\omega(x+\lambda t)} + be^{i\omega(x-\lambda t)} \tag{1.6.2}$$

and requires for well-posedness two initial conditions $\varphi(x,0)$ and $\varphi_t(x,0)$. If an artificial boundary is introduced at $x=x_0$, and the problem is solved on $x \leq x_0$, well-posedness of the truncated problem requires a BC at $x=x_0$. A single frequency right moving wave is of the form $\varphi=ae^{i\omega(x-\lambda t)}$ and exactly satisfies

$$\left(\frac{\partial}{\partial t} + \lambda \frac{\partial}{\partial x} \right) \varphi = 0 \tag{1.6.3}$$

Equation (1.6.3) is a perfectly absorbing BC for the truncated problem. To appreciate it we define the *Reflection Coefficient* R=a/b

and substitute (1.6.2) into (1.6.3). R=0 immediately follows.

Equation (1.6.3) is known as the *Sommerfeld Radiation Condition* [69] and has been implemented in a variety of ways to simulate open boundaries (eg Orlanski [56] and references therein). It repeatedly emerges as a first order approximation to absorbing BCS in several space dimensions.

A slightly different approach to the same end has been taken by Hedstrom [33] who considers first order hyperbolic systems

$$\underline{w}_t + A\underline{w}_x = 0$$

Let the eigenvalues of A be ordered $\lambda_1 < \cdots < \lambda_m < 0 < \lambda_{m+1} < \cdots < \lambda_N$, implying that the system admits (m) left moving waves and (N-m) right moving waves. A k^{th} simple wave disturbance satisfies

$$d\underline{w} = c_k \underline{r}_k$$

If a boundary is successively crossed by right moving waves, then changes on the boundary satisfy

$$d\underline{w} = \sum_{k=m+1}^{N} c_k \underline{r}_k$$

or equivalently

$$\frac{\partial \underline{w}}{\partial t}\, dt = \sum_{k=m+1}^{N} c_k \underline{r}_k \qquad (1.6.4)$$

For well-posedness, (m) BCS are required at the RHB corresponding to the (m) incoming Riemann Invariants. Using the orthogonality property (1.1.2)c it can be verified that

$$\underline{\ell}_j \cdot \frac{\partial \underline{w}}{\partial t} = 0 \qquad j = 1, \cdots, m \qquad (1.6.5)$$

are exactly satisfied by a general outgoing solution (1.6.4).

Equation (1.6.5) can be viewed as a negative statement, namely, that *no* left running waves are crossing the RHB. In the linear case $\underline{\ell}_j$ is constant and (1.6.5) can be integrated to give

$$\underline{\ell}_j \cdot \underline{w} = \text{const.} \quad j = 1, \cdots, m \tag{1.6.6}$$

implying the constancy of the incoming characteristic variables often referred to as the *Zero Incoming Riemann Invariant* condition.

As a specific example, consider the 1D Euler equations

$$\begin{pmatrix} \rho \\ u \\ p \end{pmatrix}_t + \begin{pmatrix} u & \rho & 0 \\ 0 & u & 1/\rho \\ 0 & \rho c^2 & u \end{pmatrix} \begin{pmatrix} \rho \\ u \\ p \end{pmatrix} = 0 \tag{1.6.7}$$

with left eigenvectors

$$\begin{aligned} \ell_1 &= (0 \ , \ \rho c \ , \ -1) & \lambda_1 &= u - c \\ \ell_2 &= (-c^2 \ , \ 0 \ , \ 1) & \lambda_2 &= u \\ \ell_3 &= (0 \ , \ \rho c \ , \ 1) & \lambda_3 &= u + c \end{aligned} \tag{1.6.8}$$

Let $u>0$. At the LHB (inflow boundary) the perfectly absorbing BCS are

$$\begin{aligned} \ell_2 \cdot \frac{\partial w}{\partial t} &= \frac{\partial p}{\partial t} - c^2 \frac{\partial \rho}{\partial t} = 0 \\ \ell_3 \cdot \frac{\partial w}{\partial t} &= \frac{\partial p}{\partial t} + \rho c \frac{\partial u}{\partial t} = 0 \end{aligned} \tag{1.6.9ab}$$

and at the RHB (outflow)

$$\ell_1 \cdot \frac{\partial w}{\partial t} = \frac{\partial p}{\partial t} - \rho c \frac{\partial u}{\partial t} = 0 \tag{1.6.9c}$$

As a side remark we note that if the wave equation (1.6.1) is written as a first order system in $p=\varphi_t$ and $u=\varphi_x$, the zero incoming Riemann Invariant condition at $x=x_0$ reads

$$\frac{\partial u}{\partial t} + \lambda \frac{\partial p}{\partial t} = 0$$

which is precisely the time derivative of the Sommerfeld Radiation condition (1.6.3) in the linear case λ = const.

It is BCS (1.6.9), derived from one dimensional principles, that are the most commonly used in multidimensional applications. Their implementation does not require apriori knowledge of conditions at infinity which are not always available. However, when used in connection with a marching algorithm towards a steady state limit, the gradient form (1.6.9) determines the solution only up to a constant which renders the converged solution dependent on initial data. To drive the far field pressure towards its free stream value, Rudy & Strikwerda [65,66] suggest to modify (1.6.9)c

$$\frac{\partial p}{\partial t} - \rho c \frac{\partial u}{\partial t} + \alpha(p - p_\infty) = 0 \qquad (1.6.10)$$

The parameter α is determined by linear 1D analysis to yield most rapid decay of the transient solution, and may need adjustments in multidimensional setups. Another drawback to (1.6.10) is that in the steady state limit $p=p_\infty$ at the boundary itself which is inaccurate.

Instead of matching the BC to the outgoing part of the analytic solution, it can be matched to that of the discrete solution. This is the approach taken in the early work of Lindman [51]. Let a grid be defined by $x_j = j\Delta x$, $t_n = n\Delta t$, with Δx and Δt the grid spacing. Let $\varphi_j^n \approx \varphi(x_j, t_n)$ and consider the discrete approximation to (1.6.1)

$$\frac{\varphi_j^{n+1} - 2\varphi_j^n + \varphi_j^{n-1}}{(\Delta t)^2} - \lambda^2 \frac{\varphi_{j+1}^n - 2\varphi_j^n + \varphi_{j-1}^n}{(\Delta x)^2} = 0 \qquad (1.6.11)$$

with the discrete dispersion relation

$$\left(\frac{2i}{\Delta t}\right)^2 \sin^2\left(\frac{\omega\Delta t}{2}\right) - \left(\frac{2\lambda i}{\Delta x}\right)^2 \sin^2\left(\frac{\xi\Delta x}{2}\right) = 0 \qquad (1.6.12)$$

For each frequency ω, equation (1.6.12) defines two admissible wave numbers $\pm\xi(\omega)$

$$\varphi_j^n = e^{i\omega n\Delta t}\,(ae^{i\xi j\Delta x} + be^{-i\xi j\Delta x}) \tag{1.6.13}$$

(compare (1.6.2)). As a boundary operator, Lindman considers a specific discrete approximation of the Sommerfeld Radiation condition and the results are thus restricted to this form of boundary operator

$$\left(\frac{\varphi_j^{n+1}+\varphi_{j-1}^{n+1}}{2} - \frac{\varphi_j^n+\varphi_{j-1}^n}{2}\right) + \nu G\left(\frac{\varphi_j^{n+1}+\varphi_j^n}{2} - \frac{\varphi_{j-1}^{n+1}+\varphi_{j-1}^n}{2}\right) = 0$$

$\nu=\lambda\Delta t/\Delta x$ is the CFL number and G is an operator yet to be chosen that yields optimal absorption at the RHB. To determine G substitute (1.6.13) into (1.6.14). The reflection coefficient is

$$R = e^{-i\xi\Delta x}\,\frac{\tan\frac{\omega\Delta t}{2} - \nu\hat{G}\tan\frac{\xi\Delta x}{2}}{\tan\frac{\omega\Delta t}{2} + \nu\hat{G}\tan\frac{\xi\Delta x}{2}} \tag{1.6.14}$$

If G is chosen so that its symbol in the frequency domain $\hat{G}_0$ satisfies

$$\hat{G}_0 = \frac{1}{\nu}\,(\tan\tfrac{\omega\Delta t}{2})/(\tan\tfrac{\xi\Delta x}{2}) \tag{1.6.15}$$

then the boundary operator (1.6.13) yields perfect absorption. Unfortunately $\hat{G}_0$ does not represent any finite difference operator G_0 and the problem reduces to finding useful approximations to G_0, which are given in [51]. It is interesting to note that although a perfectly absorbing analytic BC exsists, namely equation (1.6.3), the discrete strategy leads only to a sequence of approximate BCS.

A similar approach was taken by Engquist & Majda [15, section 5] who factorize the symbol of the difference operator (1.6.12) into

$$\left(\frac{2i}{\Delta t}\sin\frac{\omega\Delta t}{2} - \frac{2\lambda i}{\Delta t}\sin\frac{\xi\Delta x}{2}\right)\left(\frac{2i}{\Delta t}\sin\frac{\omega\Delta t}{2} + \frac{2\lambda i}{\Delta t}\sin\frac{\xi\Delta x}{2}\right) = 0$$

describing left and right moving waves respectively. Thus, if a boundary operator is such that its dispersion relation is

$$\left(\frac{2i}{\Delta t} \sin \frac{\omega \Delta t}{2} + \frac{2\lambda i}{\Delta t} \sin \frac{\xi \Delta x}{2} \right) = 0 \qquad (1.6.16)$$

it would yield perfect absorption. Again, equation (1.6.16) is not directly realisable on the grid and is replaced by high order approximations.

Vichnevetsky and Pariser [85] investigate the semi-discrete form of the advection equation

$$\left(\frac{dw}{dt}\right)_j + \lambda \frac{w^n_{j+1} - w^n_{j-1}}{2\Delta x} = 0 \qquad (1.6.17)$$

Based on centered differences, equation (1.6.17) admmits two spatial modes ξ_1 and ξ_2 with the same frequency,

$$w = e^{i\omega t} \left(ae^{i\xi_1 j\Delta x} + be^{i\xi_2 j\Delta x}\right) \qquad (1.6.18)$$

in contrast with the analytic equation which admits only one. Associating a direction of propagation with each mode is less straight forward and is established by applying group velocity analysis. The authors then consider a semi-discrete boundary operator

$$\left(\frac{dw}{dt}\right)_j = aw_j + bw_{j-1} + cw_{j-2} + \cdots$$

and choose the coefficients to yield optimal reflection coefficient.

Finally Higdon [35,36] considers boundary operators for the discrete wave equation (1.6.11) and attacks the problem from a slightly different angle. In terms of $\varkappa$ and Z defined in section (1.4), equation (1.6.11) reads

$$(Z - 2 + Z^{-1}) = \nu^2(\varkappa - 2 + \varkappa^{-1})$$

and admits two solutions $\varkappa_1$ and $\varkappa_2$ for any fixed Z_0. Let $\mathbb{K}$ and $\mathbb{Z}$ be the shift operators in space and time $\mathbb{K}w_j^n=w_{j+1}^n$ $\mathbb{Z}w_j^n=w_j^{n+1}$, then a general finite difference boundary operator is a polynomial in these operators $B(\mathbb{Z}^{-1},\mathbb{K}^{-1})=0$ and the reflection coefficient is given by

$$R = - \frac{B(Z_0^{-1},\varkappa_2^{-1})}{B(Z_0^{-1},\varkappa_1^{-1})}$$

For the boundary to be perfectly absorbing $(Z_0^{-1},\varkappa_2^{-1})$ must be roots of the polynomial $B(Z^{-1},\varkappa^{-1})=0$. Since B can only possess a finite number of roots, the corresponding boundary operator can only annihilate a finite number of modes, depending on the degree of B. To absorb, for example, low frequency waves $(Z,\varkappa)=(1,1)$, the problem reduces to constructing polynomials with $(Z,\varkappa)=(1,1)$ as roots. Not all such boundary operators lead to a stable model but it can be shown [35] that

$$\text{(i)} \quad \left\{ I - \frac{I + \mathbb{Z}^{-1}}{2} \frac{I + \mathbb{K}^{-1}}{2} \right\}^P \varphi_j^n = 0 \qquad (1.6.19)_a$$

$$\text{(ii)} \quad \left\{ I - \mathbb{Z}^{-1}\mathbb{K}^{-1} \right\}^P \varphi_j^n = 0 \qquad (1.6.19)_b$$

combined with the interior scheme (1.6.11) are GKS stable. Although the suggested boundary operators have one dimensional stencils, they are analysed in the context of the multidimensional wave equation. It is shown that the reflection coefficient in both cases is

$$R = - \left(\frac{\lambda - \cos\vartheta}{\lambda + \cos\vartheta} \right)^P + O(\omega\Delta t)$$

where $\lambda=\Delta t/\Delta x$ and ϑ is the angle of incidence. Best absorption is thus at some non-zero angle of incidence.

An advantage of the direct discrete approach over the analytic

approach is that it can be targetted at absorbing non-physical parasitic modes, typically modes of saw-tooth character, which cannot be handled by any analytic approach. For example, to absorb a mode $(Z,\varkappa)=(-1,-1)$ one can apply

$$\left\{ I - \frac{I - \mathbb{Z}^{-1}}{2} \frac{I - \mathbb{K}^{-1}}{2} \right\}^{P} \varphi_j^n = 0 \qquad (1.6.20)$$

This adavantage has also been realised by Vichnevetsky and Pariser [86] who design high frequency nonreflecting BCS for the semi discrete form (1.6.17). Clearly, the left running mode in this case is totally spurious, being a direct consequence of the central differences approximation of the spatial derivative. Such spurious waves are of saw-tooth nature and are easily recognisable as numerical noise. Yet, when reflected from a (upwind) boundary they become smooth waves which are indistinguishable from consistent numerical solutions. Their absorption can become quite vital in some applications (see also review paper [84]).

(1.7) Absorbing Boundary Conditions in 2 and 3 Space Dimensions

Engquist and Majda [14,15] consider the 2D wave equation

$$\left(\frac{\partial^2}{\partial t^2} - \frac{\partial^2}{\partial x^2} - \frac{\partial^2}{\partial y^2} \right) \varphi = 0 \qquad (2.7.1)$$

solved on a strip $0\le x\le x_0$ with an absorbing boundary at $x=x_0$. Plane wave solutions $\varphi=\exp(i\xi x+i\eta y+i\omega t)$ satisfy the dispersion relation $\xi^2+\eta^2=\omega^2$ or equivalently $\xi^{\pm}=\pm\sqrt{\omega^2-\eta^2}$, $\omega^2-\eta^2\ge 0$. Like in the 1D case, for fixed (ω,η) the solution is a superposition of left and right moving waves

$$\varphi = e^{i(\eta y+\omega t)} \left(a e^{i\xi^+ x} + b^{i\xi^- x} \right)$$

A BC that exactly annihilate right moving waves is thus

$$\left(\frac{\partial}{\partial x} + \sqrt{\omega^2 - \eta^2} \right) \varphi = 0 \qquad (1.7.2)$$

which formally corresponds to the *Pseudo-Differential Operator*

$$\left(\frac{\partial}{\partial x} + \sqrt{\frac{\partial^2}{\partial t^2} - \frac{\partial^2}{\partial y^2}} \right) \varphi = 0 \qquad (1.7.3)$$

Unless $\partial/\partial y \equiv 0$ (corresponding to $\eta=0$ ie normal incidence), equation (1.7.3) is not a rational function in $(\partial/\partial t, \partial/\partial y)$ and yields a BC which is non-local in both t and y. To be numerically useful, it has to be approximated in a well-posed manner. Approximations about normal incidence naturally lead to BCS which are perfectly absorbing in that direction. For waves in other directions the p^{th} order approximation yields reflections of order $O(\eta/\omega)^{2P}$. The essential requirement of well-posedness turns out to be less trivial than anticipated. Taylor expansions of $\sqrt{1 - \eta^2/\omega^2}$ for small η/ω yield an ill-posed second order approximation, admitting solutions of the form (1.1.5). Approximating the square root by a rational function based on Padé expansion can be proved well-posed [14,15]. The first members of this family are

$$\text{(i)} \quad \left(\frac{\partial}{\partial t} + \frac{\partial}{\partial x} \right) \varphi = 0$$

$$\text{(ii)} \quad \left(\frac{\partial^2}{\partial t^2} + \frac{\partial^2}{\partial x \partial t} - \frac{1}{4} \frac{\partial^2}{\partial y^2} \right) \varphi = 0 \qquad (1.7.4)$$

If equation (1.7.1) is used to eliminate the y derivatives in (1.7.4), the p^{th} order boundary operator in (1.7.4) is equivalent to the p^{th} order generalised Sommerfeld radiation condition

$$\left(\frac{\partial}{\partial t} + \frac{\partial}{\partial x} \right)^P \varphi = 0$$

with a reflection coefficient

$$R = - \left(\frac{1 - \cos\vartheta}{1 + \cos\vartheta} \right)^P$$

The same approach was applied to the Transonic Small Perturbation equation in [16] and have been thoroughly studied numerically by Kwak in [49,50]. The theory is extended to the elastic wave equation [11,14] but well-posedness is not established. Several subsequent papers by various authors report instabilities encountered in their implementation [13,53].

Also in [14], a general theory is developed for first order symmetric systems which uses the complicated theory of pseudo-differential operators. A recent extremely elegant report by Giles [20] treats the same class of equations using the language of eigenvectors, Taylor expanded about normal incidence. Consider the NxN linear hyperbolic system of equations

$$\underline{w}_t + A\underline{w}_x + B\underline{w}_y = 0 \qquad (1.7.5)$$

Plane wave solutions $\underline{w} = \underline{w}_0 e^{i(\xi x+\eta y+\omega t)}$ satisfy

$$(\omega I + \xi A + \eta B)\ \underline{w}_0 = 0$$

or equivalently

$$(\xi I + \omega A^{-1} + \eta A^{-1}B)\ \underline{w}_0 = 0 \qquad (1.7.6)$$

Non-trivial solutions exist provided

$$\det(\xi I + \omega A^{-1} + \eta A^{-1}B) = 0 \qquad (1.7.7)$$

which is the dispersion relation for the system (1.7.5). For fixed (η,ω), equation (1.7.7) defines N roots ξ_k and N corresponding right

eigenvectors $\underline{r}_k=\underline{r}_k(\eta,\omega)$

$$(\omega A^{-1} + \eta A^{-1}B)\underline{r}_k = -\xi_k \underline{r}_k \qquad k=1,\cdots,N$$

and admits a general solution

$$\underline{w} = \left(\sum_{k=1}^{N} a_k \underline{r}_k \exp(i\xi_k x) \right) e^{i(\eta y+\omega t)} \tag{1.7.8}$$

The main difficulty is to establish which of the modes in (1.7.8) are incoming and which are outgoing. Assume that $\xi_1,\cdots,\xi_m$ are incoming modes. Denote by $\underline{\ell}_k=\underline{\ell}_k(\eta,\omega)$ the k^{th} left eigenvector and recall the orthogonality property (1.6.5)c. The perfectly absorbing BCS expressing the constancy of the incoming Riemann Invariant are

$$\underline{\ell}_k(\eta,\omega)\cdot\underline{w} = 0 \qquad k=1,\cdots,m \tag{1.7.9}$$

(compare (1.6.5) & (1.6.6)). In their exact form, BCS (1.7.9) are impractical since their implementation requires a Fourier transform in both y and t. Approximations are sought for angles close to normal incidence. Denote $\eta/\omega = \vartheta$, then

$$\ell_k^L(\eta,\omega) = \underline{\ell}_k(\vartheta) = \underline{\ell}_k(0) + \vartheta \frac{\partial}{\partial\vartheta}(\underline{\ell}_k(0)) + \frac{\vartheta^2}{2}\frac{\partial^2}{\partial\vartheta^2}(\underline{\ell}_k(0)) + \cdots$$

The p^{th} order approximation is given by

$$\left(\sum_{\ell=1}^{m} \frac{\vartheta^\ell}{\ell!} \frac{\partial^\ell}{\partial\vartheta^\ell}(\underline{\ell}_k) \right)\cdot\underline{w} = 0 \qquad k=1,\cdots,m \tag{1.7.10}$$

The corresponding BC is obtained by identifying ϑ with the operator $(\partial/\partial y)/(\partial/\partial t)$ and multiplying by $(\partial/\partial t)^p$ to clear all denominators. Well-posedness is established if it is not possible for incoming waves alone to satisfy (1.7.10) implying spontaneous radiation of energy from the boundary. This general derivation is applied to the Euler equations and it is found that the second order *inflow* conditions are ill-posed, admitting one unstable mode while the *outflow* condition is

well-posed.

A hierarcy of far field BCS based on a different asymptotic argument is derived by Bayliss & Turkel [4,5] for equations which display a wave-like far field behaviour. The same approach was extended to elliptic problems in [6] (see also [19]). Instead of expanding the solution about normal incidence, they consider an expansion of the solution in inverse powers of the radial distance r.

A spherical outgoing wave solution has the form

$$\varphi = \frac{f(r-t)}{r}$$

and is exactly annihilated by the boundary operator

$$\left(\frac{\partial}{\partial t} + \frac{\partial}{\partial r} + \frac{1}{r}\right) \varphi = 0 \tag{1.7.11}$$

A more general outgoing wave has the form

$$\varphi = \sum_{j=1}^{N} \frac{f_j(r-t,\vartheta,\phi)}{r^j}$$

where f_j may be treated as arbitrary functions. One can verify that

$$\prod_{\ell=1}^{p} \left(\frac{\partial}{\partial t} + \frac{\partial}{\partial r} + \frac{2\ell+1}{r}\right) \varphi = O\left(\frac{1}{r}\right)^{2p+1} \tag{1.7.12}$$

becoming better approximations as $r \to \infty$ and yielding well-posed problems [4].

BCS (1.7.12) are employed in the 2D linearised Euler equations

$$\begin{aligned} &p_t + u_0 p_x + \rho_0 c_0^2 (u_x + v_y) = 0 \\ &u_t + u_0 u_x + \rho_0^{-1} p_x = 0 \\ &v_t + u_0 v_x + \rho_0^{-1} p_y = 0 \end{aligned} \tag{1.7.13}$$

It can be shown that under a suitable coordinate transformation, pressure deviations from the mean pressure satisfy $p_{tt} - p_{\xi\xi} - p_{\eta\eta} = 0$. Conditions (1.7.12), slightly modified for circular outgoing waves, are transformed back into physical coordinates. The first member of this family reads

$$p_t + \frac{\rho_0 c_0}{\beta} \frac{x}{d} (u_t - u_0 v_y) - \rho_0 c_0 \beta \frac{y}{d} (v_t + u_0 v_x) + c_0 \beta \frac{p-p_0}{2d} = 0 \qquad (1.7.14)$$

where $\beta^2 = 1-M_0^2$ and $d^2 = x^2/\beta^2 + y^2$. In steady state calculations, the spatial variations of y were ignored, enforcing $p=p_0$ in the steady state limit (compare (1.6.10)). An equivalent formulation involving pressure derivatives only is [64]

$$p_t + \frac{\beta^2 c_0}{\beta d - M_0 x} \left(x \frac{\partial p}{\partial x} + y \frac{\partial p}{\partial y} + - (p-p_0) \right) = 0 \qquad (1.7.15)$$

In a recent paper by Roe [64], the Euler equations are combined in ratios (i) + $\rho_0 c_0 \cos\vartheta$ (ii) + $\rho_0 c_0 \sin\vartheta$ (iii) to yield a ϑ dependent equation in which all directional derivatives act in one plane. Each of these characeristic planes is spanned by the vectors

$$(1 , u_0 + c_0 \cos\vartheta , c_0 \sin\vartheta)$$
$$(0 , \sin\vartheta , -\cos\vartheta)$$

in the (t,x,y) directions. The first operator acts along a particular bicharacteristic while the second acts in space only. Specifying ϑ implies considering disturbances in that specific characteristic plane. Roe takes lead from the BC (1.7.15) and chooses ϑ so that the direction of the bicharacteristic coincides with the direction of the derivative in (1.7.15), obtained from global far field asymptotic considerations. This is accomplished by setting

$$\sin\vartheta = \frac{\beta^2 y}{\beta d - M_0 x}$$

With this choice of ϑ, substituting (1.7.15) into the characteristic equation results in another outgoing characteristic equation involving velocity derivatives only

$$(x-\beta M_0 d)\,\frac{\partial u}{\partial t} + \beta^3 d c_0\,\frac{\partial u}{\partial x} + \beta^2 y\left(\frac{\partial v}{\partial t} + u_0\,\frac{\partial v}{\partial y}\right) + c_0(\beta d - M_0 x)\,\frac{\partial v}{\partial y} = \frac{p-p_0}{2\rho_0} \qquad (1.7.17)$$

which can be used to update the combination $(x-\beta M_0 d)\,u + \beta^2 y v$ at the boundary. Roe's BCS applied to simpler equations are presented in Appendix A.

The statement of zero reflection at the boundary is not accurate in quasi one dimensional flows. Writing the equations in terms of the incoming and outgoing characteristic variables reveals that the two are coupled through the presence of a source-like term which accounts for the non-Cartesien geometry. As a consequence, an outgoing wave generates an incoming wave as it propagates. At the boundary, this interaction should be modelled and the BC should in fact be reflecting. In [28], Hagstrom & Hariharan derive a reflecting BC for the spherically symmetric isentropic Euler equations, based on expanding the characteristic variables as a series in inverse powers of the radial distance r.

The linearised Euler equations with spherical symmetry read

$$\begin{aligned} p_t + q_r + 2q/r &= 0 \\ q_t + p_r &= 0 \end{aligned} \qquad (1.7.18)$$

In terms of the outgoing and incoming characteristic variables $R=q+p$ and $S=q-p$, the equations become

$$R_t + R_r = -\frac{R+S}{r}$$
$$S_t - S_r = \frac{R+S}{r} \qquad (1.7.19)$$

In the far field, R and S tend to constants and can therefore be expanded in a series

$$R = R_0 + {}^{R_1}/_{r} + {}^{R_2}/_{r^2} + \cdots$$
$$S = R_0 + {}^{S_1}/_{r} + {}^{S_2}/_{r^2} + \cdots \qquad (1.7.20)$$

It follows from the definition of R and S and from the fact that $q \to 0$ in the far field that $R_0 = -S_0 = p_0$. Substituting (1.7.20) into (1.7.19) and collecting like terms leads to the first order approximation

$$(R_1)_t + (R_1)_r = 0 \quad \Longrightarrow \quad R_1(r,t) = R_1(r-t,0)$$
$$(S_1)_t - (S_1)_r = 0 \quad \Longrightarrow \quad S_1(r,t) = S_1(r+t,0)$$

implying that R_1 and S_1 are genuine Riemann Invariants. Since S_1 is initially zero, $S_1 \equiv 0$ at all later times. The first non-zero correction to the incoming characteristic variable is obtained through the second order approximation

$$(S_2)_t - (S_2)_r = R_1(r-t) \qquad (1.7.21)$$

Expressed in terms of $\tau = r-t$ and r, equation (1.7.21) reads

$$-2(S_2)_\tau - (S_2)_r = R_1(\tau)$$

At the boundary r=a, $(S_2)_r = O(1/a)$ and can be neglected. Also at the boundary $\partial\tau/\partial t = -1$ yielding

$$(S_2)_t = \frac{1}{2} R_1(a-t)$$

or equivalently up to $O(1/a)^2$

$$\frac{\partial S}{\partial t} = \frac{1}{2} (R(a,t) - R_0)$$

which is the proposed reflecting BC.

An interesting, yet not numerically practical strategy was taken by Smith [67] who proposed to solve the wave equation twice, once with Dirichlet BC and once with Neumann BC. The superposition of both solutions leads to cancellation of all reflections. Open BCS for the steady 2D Euler equations based on a Fourier expansion of the solution at the boundary were obtained in [18] and [17]. Other open BCS can be found in references [3,25,30,73].

We end here the brief survey of the modelling of open boundaries. We hope to have given a flavour of the predominant concepts in the design of nonreflecting BCS as well as of the rather involved analysis required to establish well-posedness and stability. Although establishing well-posedness is sometimes regarded as unecessary formalism of mainly cosmetic value, the above examples show that often, when well-posedness cannot be established, instabilities are encountered in practice. They also show that not all sensible strategies yield well-posed problems.

(2.1) The Lax-Wendroff (LW) Scheme and Group Velocity

The main drawback of the concept of group velocity is that it is strictly valid in non-dissipative cases only (ie ω is a real function if ξ). In the presence of dissipation (1.5.5) becomes an integral in the complex plane and the argument of stationary phase needs to be extended to the method of steepest descent or saddle point [87]. As a result, group velocity analysis strictly applies to non-dissipative numerical approximations. It is also valid for dissipative models which admit isolated non-dissipative modes [74]. Indeed, modes with $|Z|<1$ do not grow with time, hence cannot generate an instability.

Dissipation, thus, reduces the number of potentially unstable modes. In some cases, dissipativity of either the interior scheme or boundary condition is sufficient to guarantee stability [22]. In an elegant article [78], the *stability* of a difference model is presented as the consequence of a competition between the destablising mechanism of *dispersion*, and the stablising mechanism of *dissipation*.

It is precisely because of its stablising nature that dissipation is regarded as a desirable feature in practical applications. Even if the basic scheme is non dissipative, some level of dissipation is always added to prevent non-linear instabilities. Examples include various variants of the LW scheme [29,52,55,61,62], Runge-Kutta (RK) type schemes [39,40] and others [32,57].

As is often the case in practical calculations, one is seeking steady state solutions by means of marching the time dependent equations for sufficiently long time until steady state is reached. For this class of problems, although modes with $|Z|<1$ are not unstable, if $|Z| \approx 1$ they are dissipated very slowly, and inhibit convergence to steady state. Group velocity analysis in these cases, though strictly not applicable, will still make good predictions, provided dissipation levels are sufficiently weak. As a typical representative of the class of dissipative schemes we select the LW scheme, variants of which are in wide practical use. The pathological behaviour predicted by the analysis that follows has wider implications and encompasses the class of symmetric two-level explicit schemes of optimal accuracy, the class of RK schemes (see Appendix F) and others [38].

The LW scheme to approximate the advection equation (1.2.1) is

$$w_j^{n+1} = w_j^n - \frac{\nu}{2}\left(w_{j+1}^n - w_{j-1}^n\right) + \frac{\nu^2}{2}\left(w_{j+1}^n - 2w_j^n + w_{j-1}^n\right) \qquad (2.1.1)$$

with

$$\nu = \lambda\, \Delta t/\Delta x \qquad (2.1.2)$$

the CFL number. The scheme is Cauchy stable (ie stable as a pure IVP) if $|\nu| \leq 1$. The *dispersion relation* for (2.1.1) is

$$e^{i\omega\Delta t} = 1 + i\nu\sin\xi\Delta x + \nu^2(\cos\xi\Delta x - 1) \qquad (2.1.3)$$

which is both non-linear and complex reflecting both its dispersive and dissipative nature. For small ω and ξ both sides of (2.1.3) can be Taylor expanded to give as expected

$$\omega = \lambda\xi + \text{higher order terms}$$

In terms of Z and $\varkappa$ (2.1.3) reads

$$Z = 1 - \frac{\nu}{2}(\varkappa^{-1}-\varkappa) + \frac{\nu^2}{2}(\varkappa - 2 + \varkappa^{-1}) \qquad (2.1.4)$$

For a given frequency $\omega = \omega_0$, $Z = Z_0$ is fixed and (2.1.4) is a quadratic equation in $\varkappa$ yielding two solutions

$$\varkappa_1 = \frac{1}{\nu(\nu+1)}\,(\nu^2 + Z_0 - 1 + \Delta)$$

$$\varkappa_2 = \frac{1}{\nu(\nu+1)}\,(\nu^2 + Z_0 - 1 - \Delta) \qquad (2.1.5)$$

$$\Delta^2 = (1-Z_0)^2 + \nu^2(2Z_0 - 1)$$

That every frequency ω_0 has two distinct roots $\varkappa_1$ and $\varkappa_2$ is a direct result of using 3 grid points (j-1,j,j+1) to approximate the $\partial/\partial x$ term in (1.2.1). In the steady state limit $\omega\Delta t \to 0$ ($Z \to 1$) we observe that

$$\varkappa_1 \to 1 \qquad \varkappa_2 \to \frac{\nu-1}{\nu+1} \qquad (2.1.6)$$

Indicating that $\varkappa_1$ solutions are consistent solutions to (1.2.1) while $\varkappa_2$ are spurious numerical by-products of sawtooth character ($|\nu|\leq 1$). Inspecting (2.1.3), two extreme cases are observed

$\xi\Delta x = 0$ $\quad\omega\Delta t = 0$ $\quad\omega$ is real

$\xi\Delta x = \pi$ $\quad\omega$ is purely imaginary

In the latter case $e^{i\omega\Delta t} = 1-2\nu^2 \approx 1$ for very small CFL numbers. In the intermediate range $\xi\in\mathbb{R}$ let ω be complex

$$\omega = \omega_R+i\omega_I \qquad \omega_R,\omega_I\in\mathbb{R}$$

The dispersion relation can be separated into its real and imaginary parts

$$\begin{aligned} e^{-\omega_I\Delta t}\cos\omega_R\Delta t &= 1 + \nu^2(\cos\xi\Delta x-1) \\ e^{-\omega_I\Delta t}\sin\omega_R\Delta t &= \nu\sin\xi\Delta x \end{aligned} \tag{2.1.7}$$

Eliminating ω_I in (2.1.7) yields

$$\tan\omega_R\Delta t = \frac{\nu\sin\xi\Delta x}{1+\nu^2(\cos\xi\Delta x-1)} \tag{2.1.8}$$

Figure (II.1) gives ω_R and ω_I as a function of $\xi\Delta x$. As expected, for $\nu << 1$, $\omega_I \approx 0$ over the whole range of $\xi\Delta x$. In fact $\omega_I\Delta t$ is maximal when $\xi\Delta x = \pi$, hence

$$\omega_I\Delta t \le \max(\omega_I\Delta t) = -\ln(1-2\nu^2) \approx 2\nu^2 \tag{2.1.9}$$

for all $\xi\Delta x$. Implicit differentiation of (2.1.8) yields the approximate group velocity

$$C_g(\xi\Delta x) \approx \frac{d\omega_R}{d\xi} = \lambda\,\frac{\cos\xi\Delta x+\nu^2(1-\cos\xi\Delta x)}{[1-\nu^2(1-\cos\xi\Delta x)]^2+\nu^2\sin^2\xi\Delta x} \tag{2.1.10}$$

with the understanding that (2.1.10) is valid only in the limit of small CFL numbers. We observe that

$$C_g(\xi\Delta x = 0) = \lambda$$

$$C_g(\xi\Delta x = \pi) = -\lambda/(1-2\nu^2) \qquad (2.1.11)$$

As expected, well resolved waves propagate at the correct speed, while poorly resolved waves not only travel with the wrong speed but may also move in the wrong direction, if

$$\nu^2 < \frac{1}{2} \qquad (2.1.12)$$

For intermediate values of $\xi\Delta x$, C_g may also assume negative values depending on whether

$$\cos\xi\Delta x <> -\frac{\nu^2}{1-\nu^2} \qquad (2.1.13)$$

The same result can be obtained by implicit differentiation of (2.1.3)

$$C(\xi\Delta x) = \frac{\cos\xi\Delta x + i\nu\sin\xi\Delta x}{1 + i\nu\sin\xi\Delta x - \nu^2(1-\cos\xi\Delta x)} \qquad (2.1.14)$$

A feature common to many practical calculations is stretching grids. The grids are fine in regions where large gradients need to be resolved (eg near a shock wave or at leading and trailing edges in a flow past an aerofoil), while in the far field they become coarser. Highly stretched grids introduce the combination of small CFL numbers which "prolong the life" of the high frequencies with an increasing number of poorly resolved frequencies as the grid gets coarser. In view of the large dispersion errors in the high frequencies, this combination is highly undesirable.

We now turn to a series of numerical experiments which were set up in order to investigate the behaviour of discrete travelling waves in the far field, and to expose the parameters upon which the efficiency of the bc's in absorbing the waves depends.

(2.|) Numerical Experiments

(2.|.1) Boundary Conditions

In the following experiments five BCS are tested:

(i) Specify the pressure $P=P_{\infty}$, use outgoing characteristic equations to update the remaining quantities.

(ii) Specify Zero incoming Riemann Invariant, extrapolate outgoing Riemann Invariants using characteristic equations.

(iii) Specify Roe's conditions for the treatment of the acoustic waves (See Appendix A).

(iv) Over specify - Impose free stream conditions at the far field boundary.

(v) Under specify - all variables are obtained through 0^{th} order extrapolation from the interior of domain.

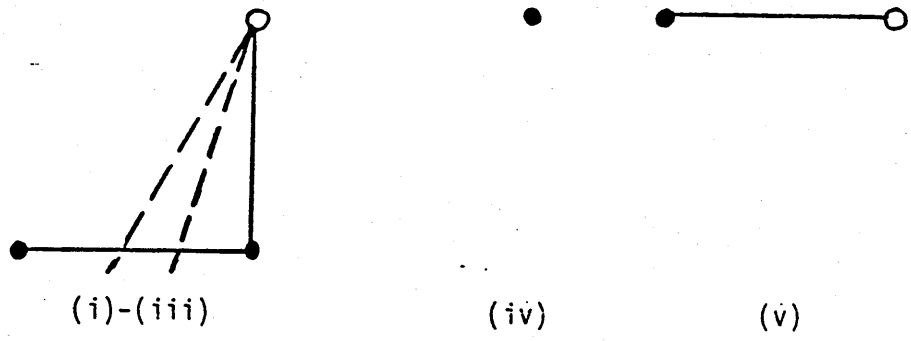

Ill. (II.1) - stencils of boundary conditions (i) - (v).

The stencils for BCS (i)-(v) are sketched in Ill. (II.1). Those are imposed at $x=x_{max}$ in the 1D case and at $r=r_{max}$ in the quasi 1D case. (see Ill. (II.2).

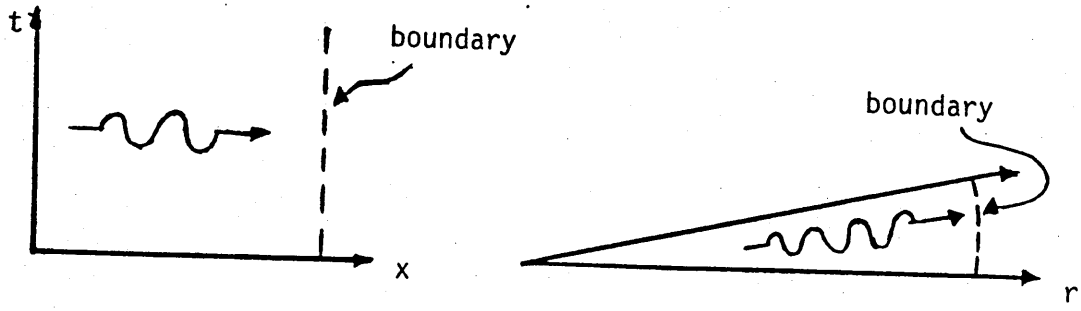

III. (II.2) - Computational domains in the (a) 1D and (b) quasi 1D setups.

Several comments should be made about the above choice of BCS:
(a) Multidimensional disturbances decay as they move away from the origin. At sufficiently large distances conditions are therefore not far off those at infinity, and it is hoped that no 'great harm' is done by imposing infinity conditions at the boundary itself. For that reason, specifying $p=p_\infty$ at a finite distance is physically wrong. Yet, various variants of bc (i) where $p=p_\infty$ is either explicitly specified or implicitly implied are widely used. Among those we find the BCS derived by Rudy & Strikwerda [65,66], Bayliss & Turkel [4,5] (see discussion in sections (1.6) & (1.7)), Hall [29] and others. Although local error estimates incurred by imposing this BC can be obtained, its overall effect on the solution remains to be investigated numerically. 1D disturbances do not decay, hence specifying $p=p_\infty$ at the boundary in 1D problems, although mathematically well-posed, is usually not physically sensible.

(b) Bc (ii) uses the theory of characteristics which is correct for 1D problems. In genuinely multidimensional flows, 1D analysis is only valid for disturbances normal to the boundary and asymptotic expansions are required for waves in other directions. The gradient form of the BCS implies that converged steady state solutions are weak limits in that they depend on initial data. See discussion in Chapter I section (1.7) and the references cited therein. See also remark in [64] p. 222.

(c) All the information required in bc (iii) is supplied by interior points. No assumption is required as to the state prevailing outside the region of computation which is not always available. The converged steady state solutions are again weak limits.

(d) Both BCS (iv) and (v) violate the Theory of Characteristics hence are mathematically ill-posed. (v) is also unstable as it is encompassed by the theorem in [72].

(2.2.2) Numerical Tests

Test A (Figure (II.2)a-e)

The governing equations are the 1D unsteady Euler equations which have the conservation form

$$\underline{W}_t + \underline{F}(\underline{W})_x = 0 \qquad (2.2.1)a$$

$$\underline{W} = (\rho, \rho u, e)^T \qquad \underline{F} = (\rho u, \rho u^2 + p, ue + up)^T$$

Using the ideal gas assumption p is found from

$$e = \frac{p}{\gamma - 1} + \frac{1}{2}\rho u^2 \qquad (2.2.1)b$$

In the above, ρ represents density, u velocity, p pressure, e energy and γ the specific heat ratio. Let c be the sound speed, h the specific enthalpy and s the entropy.

The eigenstructure of the Jacobian matrix $A(\underline{W}) = \partial\underline{F}/\partial\underline{W}$ is given by

$$R = (\underline{r}_1, \underline{r}_2, \underline{r}_3) = \begin{pmatrix} 1 & 1 & 1 \\ u-c & u & u+c \\ h-uc & \frac{1}{2}u^2 & h+uc \end{pmatrix} \qquad (2.2.3)a$$

$$A = \text{diag}\ (\lambda_1,\lambda_2,\lambda_3) = \text{diag}\ (u-c\ ,\ u,\ u+c) \qquad (2.2.3)_b$$

The characteristic equations are (see (1.1.10)

$$\begin{aligned} dp-\rho c\,du &= 0 \quad \text{on} \quad dx/dt = u-c \\ dp-c^2 d\rho &= 0 \quad \text{on} \quad dx/dt = u \\ dp+\rho c\,du &= 0 \quad \text{on} \quad dx/dt = u+c \end{aligned} \qquad (2.2.4)$$

and similarly the wave strengths

$$\begin{aligned} \alpha_1 &= (\Delta p - \rho c \Delta u)/2c^2 \\ \alpha_2 &= (c^2\Delta\rho - \Delta p)/c^2 \\ \alpha_3 &= (\Delta p + \rho c \Delta u)/2c^2 \end{aligned} \qquad (2.2.5)$$

Initial data is the uniform state $(\rho,u,p)=(1,0,1)$. High pressure is fed through the LHB $(\rho,e)=(2,4)$ giving rise to a moderate right moving shock wave followed by a contact discontinuity. The waves are expected to disappear through the RHB, and the new state is expected to occupy the whole domain. The test is conducted on a regular grid at CFL number = 0.5. The method of solution is Roe's field decomposition [62], with LW scheme applied to each characteristic field. No flux limiter is used. BC (i) is inappropriate in a 1D set-up. Indeed figure (II.2)$_a$ shows a typical reflection of a shock wave from a surface of constant pressure. BCS (ii) seem to have completely absorbed both waves. Both (iii) and (v) give similar results with a slight over estimate of u by BC (v). The performance of (v) is particularly surprising, being formally unstable. Conditions (iv) are again inadequate leading to strong reflections of a sawtooth character. These are typical numerical rather than physical reflections, and can be confirmed as (u) waves travelling in the *wrong* direction. Owing to dissipation, the reflections are confined to the neighbourhood of the boundary and the solution is rescued from complete contamination.

Test B (Figure (II.3)a-e)

The same test is repeated with $\nu = 0.0625$. Larger phase errors are expected with lower level of dissipation particularly at high frequencies. As a result, wave propagation is much more oscillatory. Bc's (ii) (iii) and (v), while coping reasonably well with the shock wave, fail to absorb the contact discontinuity. A strong reflected (u) wave travelling in the *wrong* direction can be observed. In the absence of dissipation, the contaminated region is much larger. BCS (iv) generate reflections which completely contaminate the solution.

Test C (Figure (II.4)a-c)

The same test is repeated on a mildly expanding grid. Unless expansion is very mild, the effect of grid stretching is the formal loss of accuracy [58,59,63,81]. In Appendix B we present an adaptation of the L-W scheme to non uniform grids which is conservative and preserves second order accuracy. Grid expansion rate is $\Delta x_{j+1}/\Delta x_j = 1.05$. With a total of 50 grid nodes, $\Delta x_{max}/\Delta x_{min} = 11.47$. Both rate of expansion and consequently the range of CFL numbers in the problem are not as severe as encountered in practical flow computations. Yet such conditions are sufficient to expose the inadequacy of all BCS to absorb the waves.

Test D (Figure (II.5)a,b)

The governing equations are (2.2.1). The grid is stretched at a rate of 2% in both directions and is illustrated below.

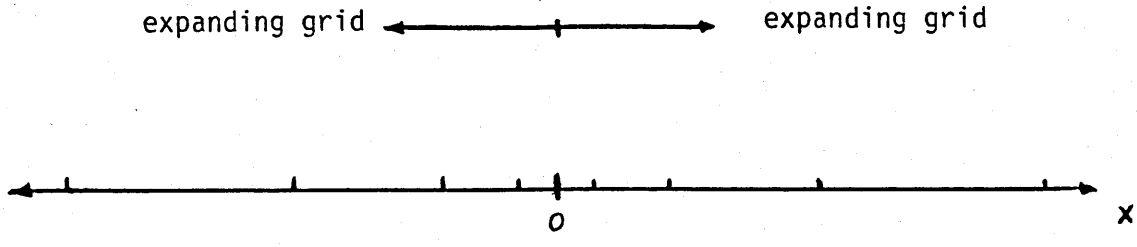

Ill. (II.3) - Grid set-up for internal reflection test.

Initial data correspond to a (u) wave and a ($u-c$) wave respectively. The initial wave, while moving in the correct direction, gradually penetrates the coarse part of the grid. At some critical point, the local wave number becomes such that the corresponding group velocity changes sign. For $|\nu| \ll 1$ this corresponds to a wave length $\approx 4\Delta x$. The wave is internally reflected and propagates as a sawtooth wave, until it reaches the coarse region where it reflects again and the low frequency is recovered. This trapped wave continues to bounce back and forth until it dissipates. In computations which march in time towards a steady state limit, internal reflections can be quite troublesome as steady state cannot be reached before these waves have dissipated. Trapped waves under non-dissipative schemes have been studied in [21,84]. Analysis suggests and experiments confirm that in far field conditions, dissipative schemes behave in much the same way.

Test E (Figure (II.6)a,b)

The governing equations are the 2D linearised Euler equations (see Appendix D)

$$\underline{w}_t + A\underline{w}_x + B\underline{w}_y = 0 \tag{2.2.7}$$

$$\underline{w} = \begin{pmatrix} p \\ u \\ v \end{pmatrix} \qquad A = \begin{pmatrix} 0 & 1 & 0 \\ 1 & 0 & 0 \\ 0 & 0 & 0 \end{pmatrix} \qquad B = \begin{pmatrix} 0 & 0 & 1 \\ 0 & 0 & 0 \\ 1 & 0 & 0 \end{pmatrix}$$

Second differentiation of (2.2.7) shows that

$$\begin{aligned} p_{tt} - p_{xx} - p_{yy} &= 0 \\ (u_y - v_x)_t &= 0 \end{aligned} \tag{2.2.8}$$

Axi-symmetric flows satisfy

$$\begin{pmatrix} p \\ q \end{pmatrix}_t + \begin{pmatrix} 0 & 1 \\ 1 & 0 \end{pmatrix} \begin{pmatrix} p \\ q \end{pmatrix}_r + \begin{pmatrix} q/r \\ 0 \end{pmatrix} = 0 \qquad (2.2.9)$$

with $q=q(r)$ the radial velocity. The emergence of a non-homogeneous source-like term is due to the non-Cartesian geometry. The simple wave structure of (2.2.9) is

$$R = \begin{pmatrix} 1 & 1 \\ -1 & 1 \end{pmatrix} \qquad \Lambda = \text{diag } (-1 \ , \ 1) \qquad (2.2.10)$$

The characteristic equations are

$$\begin{aligned} dp-dq - q/r dr &= 0 \quad \text{on} \quad dr/dt = -1 \\ dp+dq + q/r dr &= 0 \quad \text{on} \quad dr/dt = 1 \end{aligned} \qquad (2.2.11)$$

and the wave strengths due to the homogeneous and source-like terms are respectively

$$\begin{aligned} \alpha_1 &= \tfrac{1}{2}(\Delta p-\Delta q) \qquad \beta_1 = \tfrac{1}{2}\, q/r \\ \alpha_2 &= \tfrac{1}{2}(\Delta p+\Delta q) \qquad \beta_2 = \tfrac{1}{2}\, q/r \end{aligned} \qquad (2.2.12)$$

Initial data are

$$p(r,0) = 1+e^{-\sigma r^2} \qquad q(r,0) = 0$$

Due to symmetry, the problem is solved on $[0,r_{max}]$ with reflection conditions at the origin. The initial pressure hump is expected to decay as it moves away from the origin. The expected free boundary solution is

$$(p,q) = (1,0) \qquad (2.2.13)$$

The method of solution is again Roe's field decomposition, with both flux and source-like terms projected onto the eigenvectors (2.2.10).

BC (i) is now appropriate. Although specifying $p = p_\infty$ is not far off the true situation, the wave partially reflects at the boundary and then focusses very strongly as it converges towards the origin, reaching an intolerable error at the origin itself. The wave continues to bounce back and forth and requires a good number of 'round trips' before the solution converges. Moving the artificial boundary to a very large distance (200 nodes) compared with the region occupied by the initial disturbance (5 nodes) seems to have only a limited effect. This is summarised in the tables below.

No. of grid points	Signal's amplitude near the RHB	Max. reflected amplitude at origin
30	1.080	1.627
40	1.063	1.522
50	1.051	1.500
60	1.043	1.459
80	1.033	1.400
100	1.023	1.357
200	1.013/4	1.247

Table I: Focussing of pressure wave against boundary distance

No. of Points	1st focussing	2nd	3rd	4th
30	1.627	1.511	1.416	1.381
40	1.552	1.443	1.360	1.312
50	1.500	1.396	1.320	1.276
60	1.459	1.360	1.291	1.251
80	1.400	1.309	1.248	1.213
100	1.357	1.274	1.220	1.189
200	1.247	1.185	1.142	-

Table II - Maximal Reflected amplitude at the origin for successive reflections.

This example constitutes a worst case. Due to symmetry all disturbances reflect from the far field boundary to meet at the origin and focussing is particularly strong, becoming even more pronounced in a 3D set-up (figure (II.6)b). A similar behaviour, albeit in a less pronounced manner, is expected whenever $p = p_\infty$ is specified. BCS (ii)-(v) completely absorbed the wave including BC (iv) which in a way is a more strict version of (i).

Test F (Figure (II.7)a-d)

The governing equations are (2.2.9) and the method of solution is the same as in Test E. The initial state

$$p(r,0) = e^{-\sigma(r-r_0)^2}\cos\pi r \qquad q(r,0) = 0 \tag{2.2.14}$$

is expected to break into two wave packets of half the original strength moving in opposite directions. This can be observed to happen in the figures. Yet, both wave packets are moving 'backwards', resulting in the situation where the designated left running $(p-q)$ wave reaches the RHB. The BCS, being unable to absorb waves of the wrong family, reflect the oncoming waves disguised as friendly smooth solutions, which can no longer be distinguished from consistent physical solutions. BCS (iii) and (v) displayed similar behaviour. BCS targetted at absorbing waves which 'lost their way' can be designed. Since such waves are a numerical phenomenon which is entirely scheme dependent, the BCS are derived directly from the numerical dispersion relation.

(2.2.3) Upwind or High Frequency Boundary Conditions

We choose to follow the procedure suggested by Higdon [35], aimed at absorbing high frequencies (see discussion in section (1.6)). The saw-tooth wave has $\varkappa_0 = -1$ and by the discrete dispersion relation (2.1.4) $Z_0 = 1 - 2\nu^2 \simeq 1$ for $|\nu| \ll 1$. The proposed BC therefore takes the form

$$\left\{ I - \frac{I + \mathbb{Z}^{-1}}{2} \frac{I - \mathbb{K}^{-1}}{2} \right\} w_j^{n+1} = 0 \qquad (2.2.15)$$

Test G (Figure (II.8)a,b)

We have adapted (2.7.15) to systems in two ways:

(a) To the Riemann Invariants in BC (ii), neglecting the non-homogeneous term near the far field boundary.

$$\left\{ I - \frac{I + \mathbb{Z}^{-1}}{2} \frac{I - \mathbb{K}^{-1}}{2} \right\} (p-q)_{Imax}^{n+1} = 0$$
$$\left\{ I - \frac{I + \mathbb{Z}^{-1}}{2} \frac{I - \mathbb{K}}{2} \right\} (p+q)_{Imax}^{n+1} = 0 \qquad (2.2.16)$$

(b) To Roe's condition (iii), neglecting again the non-homogeneous term near the far field boundary (see Appendix A)

$$\left\{ I - \frac{I + \mathbb{Z}^{-1}}{2} \frac{I - \mathbb{K}^{-1}}{2} \right\} p_{Imax}^{n+1} = 0$$
$$\left\{ I - \frac{I + \mathbb{Z}^{-1}}{2} \frac{I - \mathbb{K}^{-1}}{2} \right\} q_{Imax}^{n+1} = 0 \qquad (2.2.17)$$

Absorption in both cases is greatly improved.

Test H (Figure (II.9)a,b)

It is easy to see that $(\varkappa_0, Z_0) = (1,1)$ are bounded away from zero in (2.7.15) hence low frequencies cannot be absorbed by this procedure. This is confirmed in the figures.

Test I (Figure (II.10)$_{a,b}$)

A natural way to absorb both low and high frequencies is

$$\left\{ I - \frac{I + \mathbb{Z}^{-1}}{2} \frac{I - \mathbb{K}^{-1}}{2} \right\} (p-q)^{n+1}_{Imax} = 0$$

$$\left\{ I - \frac{I + \mathbb{Z}^{-1}}{2} \frac{I + \mathbb{K}^{-1}}{2} \right\} (p+q)^{n+1}_{Imax} = 0 \qquad (2.2.18)$$

The first of these equations is constructed to absorb high frequency $(p-q)$ waves travelling 'backwards', ie to the right. The second is constructed to absorb $(p+q)$ waves moving in the physically correct direction, ie also to the right. These combined low-high frequency boundary procedures thus cover the extreme cases of right moving waves - the lowest and the highest possible frequencies. However, by the same construction, they are also expected to be sensitive to wave number. Indeed, the Figures show wave packets centred about $\xi h=0$ and $\xi h=\pi$ being absorbed by the BCS (2.2.18). Wave packets are not pure Fourier modes. They also contain neighboring frequencies to the ones they have been centred about. This explains the weak reflections which can be noticed in the Figures.

PART TWO

Introduction

Having presented a variety of examples where absorbing BCS give rise to strong reflections, we now present a new and less conventional approach to the treatment of far field boundaries. It is proposed to introduce an outer absorbing layer in which the governing equations are modified in a boundary-like manner, so that by the time waves have reached the boundary itself they are easy to handle. For example, one may gradually decrease the value of the specific heat ratio γ, speed so that the outer boundaries become supersonic [S. Abarbanel, private communication], or one may force the equation to a desirable solution in the far field ([46], discussed in more detail in Chapter IV).

Any attempt to modify the governing equations in the far field creates an interface to one side of which the original equations are solved, and to the other, the modified equations. The interface, just like the far field boundary itself, should behave as it it were not there, allowing waves to cross it without reflections. It is therefore vital to ensure full transmission of waves across the interface, certainly of outgoing waves but also of incoming ones.

Common to the above mentioned far field modifications is that they do not distinguish between incoming and outgoing disturbances and treat both in the same manner. In problems of genuine time dependence, however, correct physical information should be allowed to propagate from the boundaries into the interior. To be applicable to this class of problem, the far field modification needs to be of a one-way character and act on the outgoing waves without affecting the incoming ones. In one dimensional problems, the task of distinguishing between incoming and outgoing disturbances is straightforward. In multidimensional problems, it is a lot more complicated as waves may propagate in an infinite number of directions. In either case, characteristic field decomposition and simple wave analysis is required for the construction of one-way far

field modifications.

The notion of replacing an isotropic equation by a modified equation which have the same properties in some directions but different properties in others has been used before. One Way Wave Equations (OWWEs), sometimes referred to as Parabolic or Paraxial Wave Equations have long been applied to describe wave propagation with a preferred direction. Applications are widely ranging in Seismology, Geophysics, Underwater Acoustics (eg [1,2] and references therein). OWWEs have also been applied as absorbing BCS at artificial boundaries [14]. The above One Way approximations have all been derived from the second order scalar wave equation. The modifications presented in this section are based on formulating the wave equation as a first order system. This is shown to offer a wider choice of far field modifications some of which are no longer equivalent to a modified second order scalar equation hence 'beyond its reach'.

Although the proposed modifications have one-way absorbing mechanisms and are therefore suitable for far field boundary treatment in their own right, they may also be used in conjunction with absorbing BCS to enhance the performance of either of them.

Two closely related far field modifications are presented in Part Two of this work. In Chapter III, one-way absorbing boundaries by slowing down outgoing waves are studied. In section (3.1) the concept of slowing down the outgoing waves is presented in one and two space dimensions. The 1D modification is analysed in sections (3.2) and (3.3) on both the continuous and discrete levels, transmission conditions are derived and stability is established. In sections (3.4) - (3.7), several 2D extensions are presented and analysed, their well-posedness is established and their physical grounds are validated. Numerical experiments are given in section (3.8) for one and two space dimension problems. Conservation aspects are studied in section (3.9) and in section (3.10) the relation between the proposed modifications and preconditioning techniques is commented upon. In Chapter IV, we discuss one-way absorbing boundaries by gradual wave

attenuation. In sections (4.1) and (4.2), the modification is analysed on the continuous level and full transmission of waves is established. In section (4.3), the modification is analysed on the discrete level and stability is prooved. The modification is extended to 2D is presented in section (4.4). The two proposed far field treatments, namely slowing down and attenuating the outgoing waves are combined into a single far field modification is section (4.5). Numerical experiments in both one and two space dimensions are presented in section (4.6).

(3.1) The Concept of Slowing Down Outgoing Waves

Consistent boundary conditions do not generate waves unless being hit by outgoing waves, trying to leave the computational domain. Starting from a uniform initial state, and since propagation speeds are finite, there is a period of time during which those BCS are inactive and have no influence on the solution throughout the flow field. They do not play a role until the first disturbances generated at the aerofoil or at any other obstacle, have reached the outer boundary, and if the solution is required only in the immediate vicinity of the aerofoil, until they have propagated back. Meanwhile, the flow field around the aerofoil may have already started to converge to steady state, which will be destroyed by the reflected waves as soon as they reach the aerofoil.

This period of time can be prolonged by setting the outer boundaries very far away from the aerofoil. This implies a larger computational domain, and if the grid is to remain of a manageable size, it is usually highly stretched on which second order accuracy is likely to be lost [58,59,63,81]. Alternatively one can modify the set of governing PDEs so that the outgoing waves are slowed down. Upon a suitable choice of slowing down rate, one can ensure that within a given time T (possibly $T \to \infty$) the outgoing waves will not have reached the outer boundary hence not reflect back.

Slowing down the waves is a mathematical device to prevent waves from reflecting at the far field boundary. The modified set of equations has partially lost its physical significance, in that some disturbances no longer propagate at the correct physical speed. Mathematically, this is achieved by modifying the coefficients of the governing equations and by doing so creating an interface. Reflections from the interface clearly defeat the object of the whole exercise. Conditions ensuring full transmission of all waves across the interface for general hyperbolic systems are derived in section (3.2). Perhaps not surprisingly, the same conditions also turn out to retain, though in a limited sense, the physical structure of the

unmodified system - The Riemann Invariant and simple wave structure, the jump conditions etc. In that respect, the physical significance of the modified system is only partially lost.

Consider the 1D wave equation

$$\varphi_{tt} - \lambda^2 \varphi_{xx} = 0 \qquad (3.1.1)$$

to be solved on $\alpha \in [0,\infty)$. Denote by $\lambda^{\pm}$ the two families of characteristics, with respective slopes $dx/dt = \pm\lambda$. For well-posedness, equation (3.1.1) requires initial data and one BC at x=0. Let an artificial boundary be introduced at $x=X_0$ and assume that we are only interested in the solution near x=0. In the absence of a numerical boundary at $x=X_0$, the solution at x=0 is completely determined by the BC at x=0 and by the information propagated along the λ^- characteristics. In the presence of a numerical boundary at $x=X_0$, disturbances originally travelling in the positive x direction may reflect from $x=X_0$ and reach x=0 at a later time. (See Ill. (III.1)).

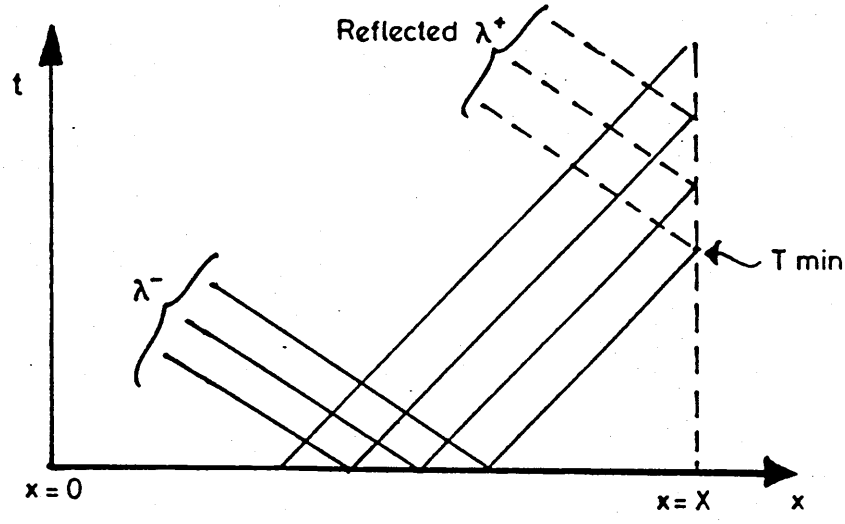

Ill. (III.1) - λ^+ and λ^- characteristics of equation (3.1.1)

Let T_{min} indicate the time the first non-zero λ^+ wave reaches the RHB. By slowing down the right going waves, T_{min} can be increased, possibly

even $T_{min} \longrightarrow \infty$ (see Ill. (III.2)).

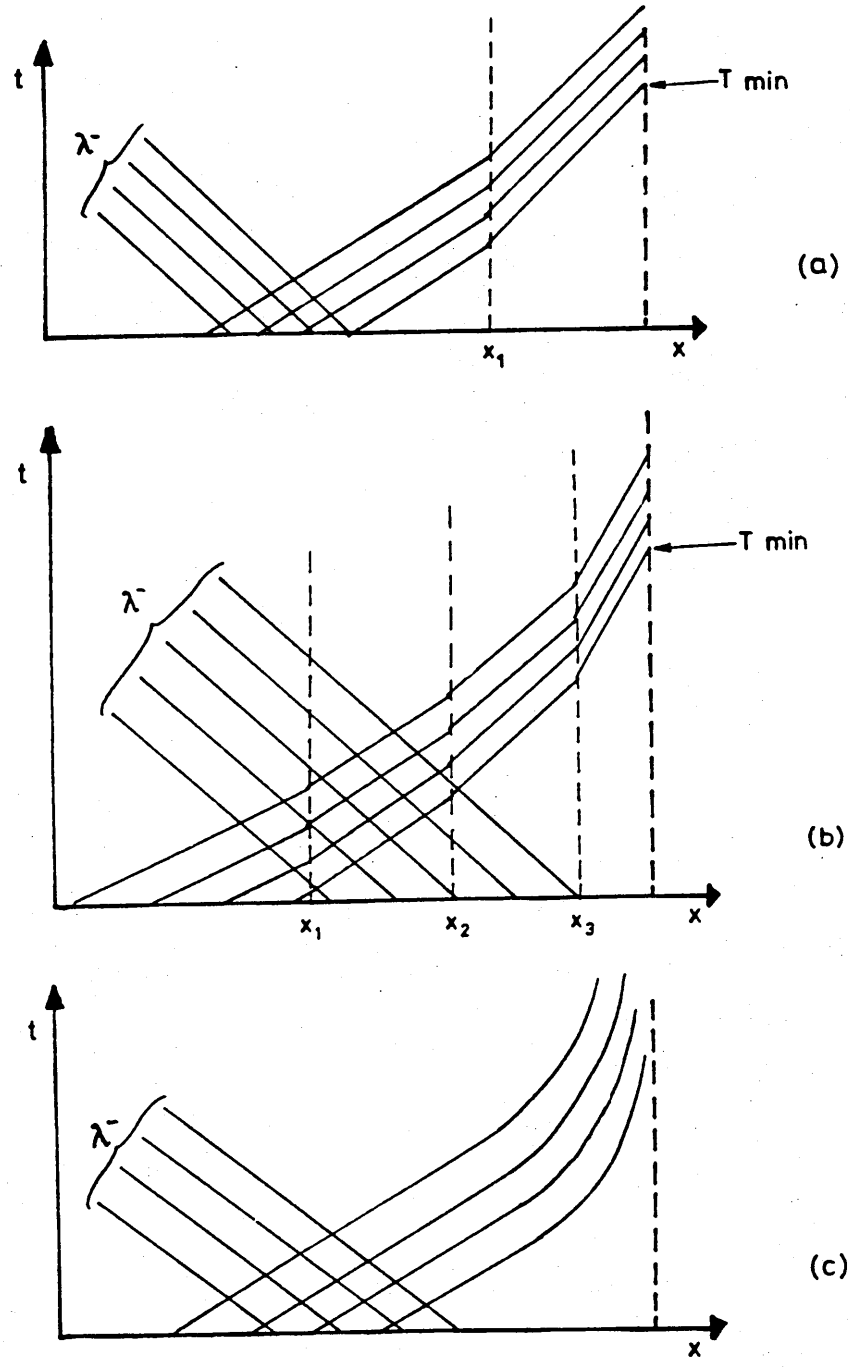

Ill. (III.2) - Pattern of wave propagation (a) & (b) Piecewise constant and (c) Smoothly varying coefficients.

In two space dimensions, the wave equation reads

$$\varphi_{tt} - \lambda^2(\varphi_{xx} + \varphi_{yy}) = 0 \qquad (3.1.2)$$

The domain of influence of every point (x_0,y_0) is enclosed by a characteristic cone whose radius grows like λt. Projecting the characteristic cone into the X-Y plane, we obtain the envelope of wave fronts emerging from (x_0,y_0). (Ill. (III.3)). In each direction $\vartheta\in[0,\pi)$ there are two wave speeds $\pm\lambda$ at which signals may or may not travel, depending on initial and boundary data. The range of angles $\vartheta\in[\pi,2\pi)$ does not have an independent meaning. That the envelope of wave fronts form a circle, reflects the isotropic nature of (3.1.2), i.e. that waves propagate at the same speed λ in all directions. Non-isotropic cases are illustrated in Ill. (III.4): In (a), waves travel at a speed λ in the positive x-direction, but at a reduced speed $a\lambda$ $0<a<1$ in the negative x direction. Similarly in (b) and (c) waves are being slowed down in the negative y direction and in the negative ϑ direction.

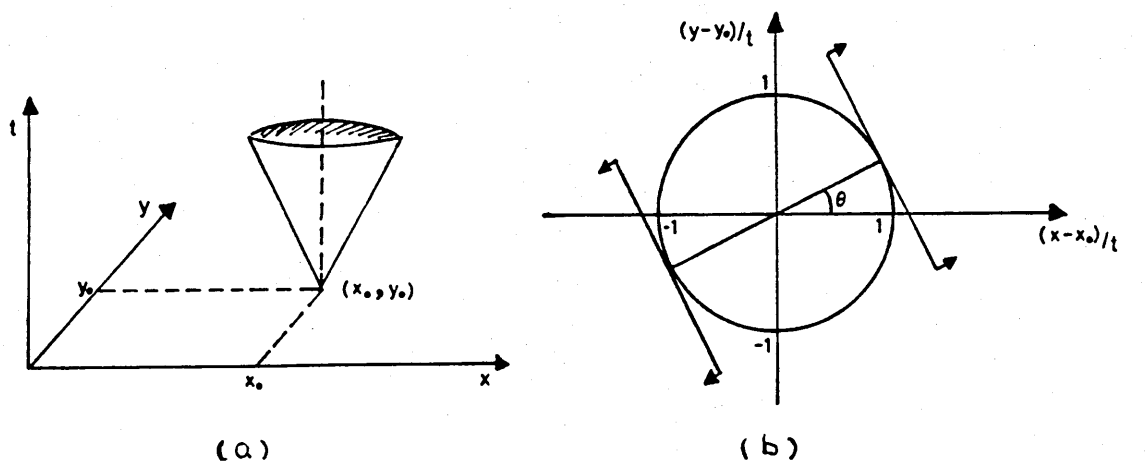

Ill. (III.3) - (a) The domain of influence of (x_0,y_0), (b) The envelope of wave fronts emerging from (x_0,y_0).

Identifying the outgoing waves is evidently dependent on the geometry of the problem. In fully exterior problems, disturbance in the far field travel very nearly radially, hence wave speeds may be modified in the radial direction. The match of wave fronts of both original and modified equations in the inward radial direction indicates that incoming wave propagation is unaltered.

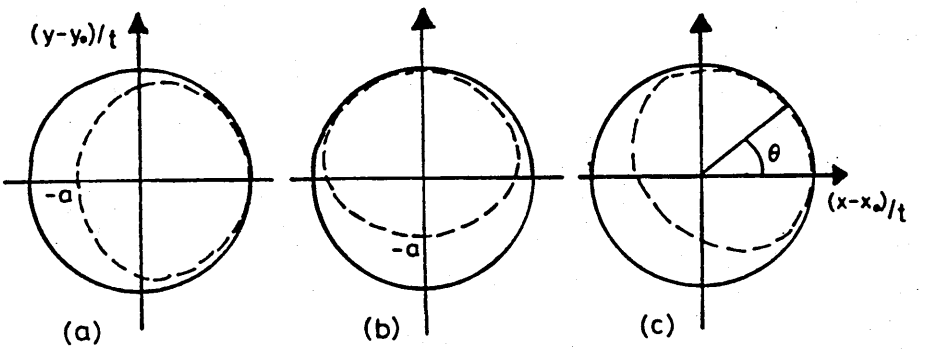

Ill. (III.4) - Non-isotropic envelopes of wave fronts.

A gradual slowing down process as a function of, say, radial distance results in the Mach Cone becoming increasingly 'squashed', and may end up totally one sided, corresponding to $T_{min} \longrightarrow \infty$ (Ill. (III.6)).

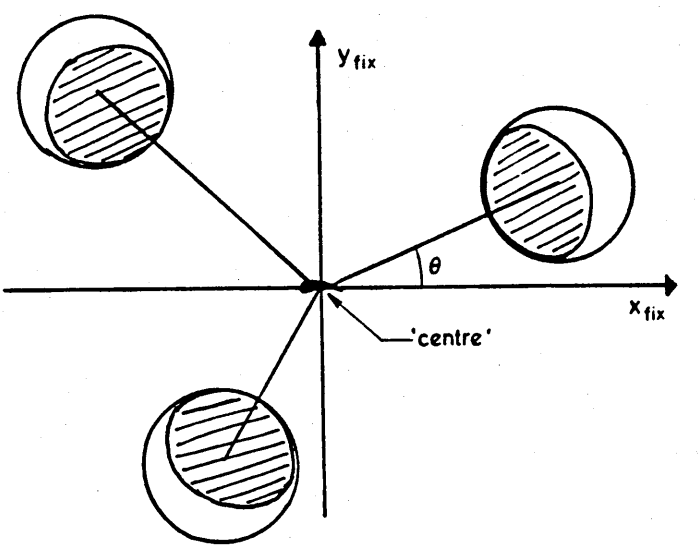

Ill. (III.5) - Modified pattern of wave fronts in circular geometry.

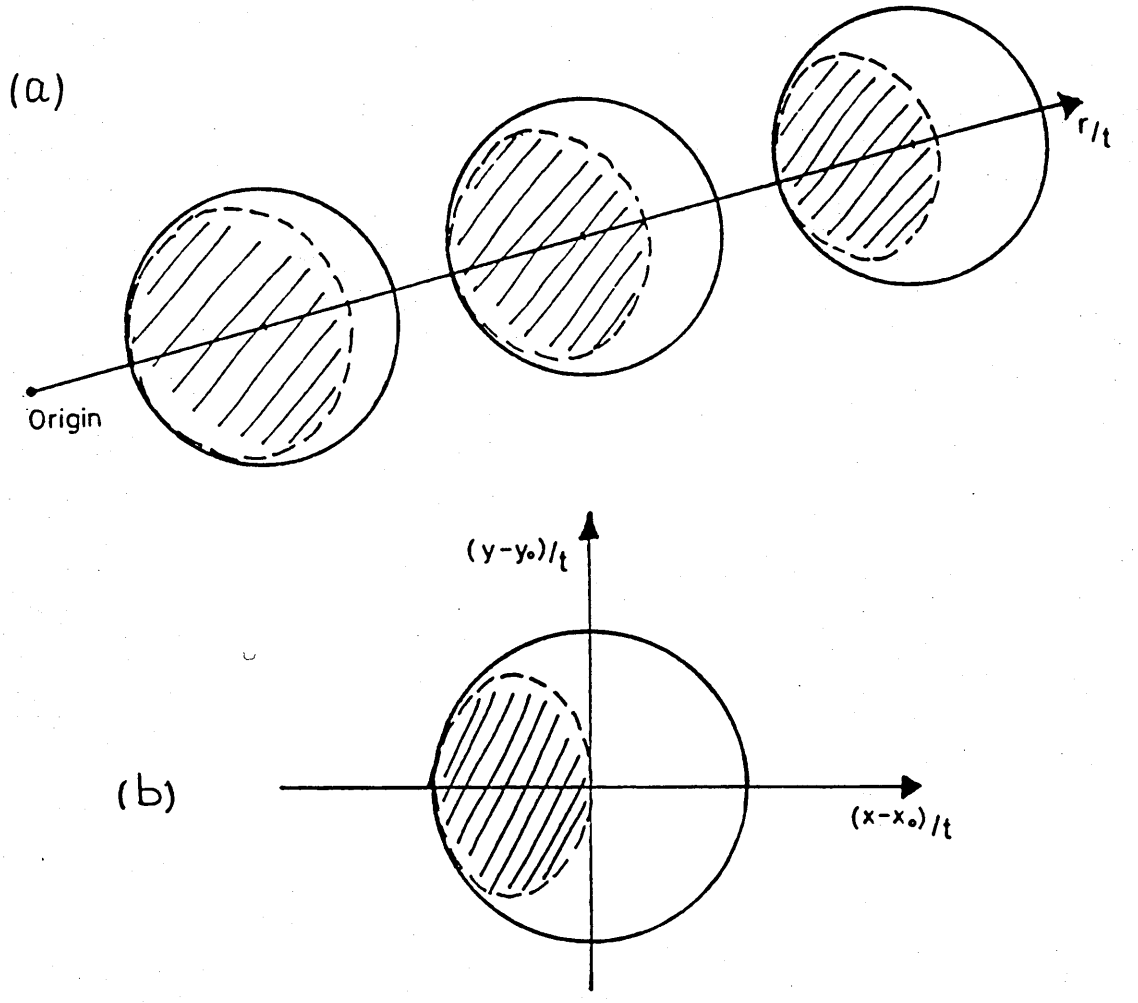

III. (III.6) - Envelope of wave fronts - (a) The outgoing speed is a decaying function of r. (b) Totally one sided wave propagation.

(3.2) Slowing Down Waves in 1D - The Continuous Level

The 1D wave equation with characteristic speeds $\pm\lambda_1$, can be written in operator form

$$\left(\frac{\partial}{\partial t} - \lambda_1 \frac{\partial}{\partial x}\right)\left(\frac{\partial}{\partial t} + \lambda_1 \frac{\partial}{\partial x}\right)\varphi = 0 \qquad (3.2.1)$$

Slowing down the right going waves on, say, x>0 is accomplished by replacing (3.2.1) with the interface problem

$$\left(\frac{\partial}{\partial t} - \lambda_1 \frac{\partial}{\partial x}\right)\left(\frac{\partial}{\partial t} + \lambda_1 \frac{\partial}{\partial x}\right)\varphi = 0 \qquad x<0$$

$$\left(\frac{\partial}{\partial t} - \lambda_1 \frac{\partial}{\partial x}\right)\left(\frac{\partial}{\partial t} + \lambda_2 \frac{\partial}{\partial x}\right)\varphi = 0 \qquad x>0 \qquad (3.2.2)$$

$$[\varphi]_{x=0} = [\partial\varphi/\partial x]_{x=0} = 0$$

with $0 \le \lambda_2/\lambda_1 \le 1$. Single frequency solutions read

$$\varphi(x,t) = \alpha_1 e^{i\omega(t+x/\lambda_1)} + \beta_1 e^{i\omega(t-x/\lambda_1)} \qquad x<0$$

$$\varphi(x,t) = \alpha_2 e^{i\omega(t+x/\lambda_1)} + \beta_2 e^{i\omega(t-x/\lambda_2)} \qquad x>0 \qquad (3.2.3)$$

Continuity requirements across x=0 implies

$$\alpha_1 + \beta_1 = \alpha_2 + \beta_2$$

$$\alpha_1 - \beta_1 = \alpha_2 - \frac{\lambda_1}{\lambda_2}\beta_2 \qquad (3.2.4)$$

and the following hold

$$\begin{bmatrix} \alpha_1 \\ \beta_1 \end{bmatrix} = \begin{bmatrix} 1 & \frac{\lambda_2-\lambda_1}{2\lambda_2} \\ 0 & \frac{\lambda_1+\lambda_2}{2\lambda_2} \end{bmatrix} \begin{bmatrix} \alpha_2 \\ \beta_2 \end{bmatrix} \qquad (3.2.5)\,a$$

$$\begin{bmatrix} \alpha_2 \\ \beta_2 \end{bmatrix} = \begin{bmatrix} 1 & \frac{\lambda_1-\lambda_2}{\lambda_1+\lambda_2} \\ 0 & \frac{2\lambda_2}{\lambda_1+\lambda_2} \end{bmatrix} \begin{bmatrix} \alpha_1 \\ \beta_1 \end{bmatrix} \qquad (3.2.5)\,b$$

A wave approaching the interface from the right

$$\beta_1 = 0 \qquad \alpha_2 = 1 \qquad (3.2.6)\,a$$

passes through the interface without reflections (Ill. (III.7) a)

$$\beta_2 = 0 \qquad \alpha_1 = 1 \qquad (3.2.6)\,b$$

However, a wave approaching the interface from the left

$$\beta_1 = 1 \qquad \alpha_2 = 0 \qquad (3.2.6)\,c$$

is partially reflected and partially transmitted (Ill. (III.7) b)

$$\beta_2 = \frac{2\lambda_2}{\lambda_1+\lambda_2} < 1 \qquad \alpha_1 = \frac{\lambda_1 - \lambda_2}{\lambda_1 + \lambda_2} < 0 \qquad (3.2.6)\,d$$

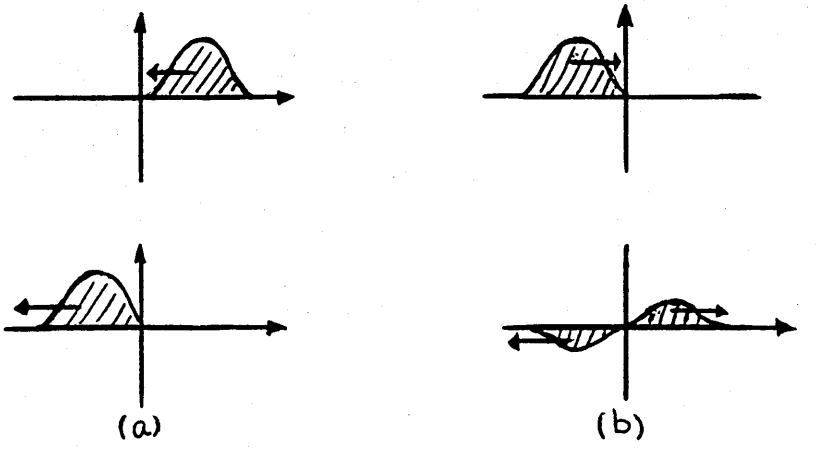

Ill. (III.7) - (a) Full transmition of left going wave
(b) Partial reflection of right going wave at x=0.

As expected, if $|\lambda_2-\lambda_1|<<1$, reflections are very weak. Gradual slowing down process can be thought of as taking λ_2 to be a piecewise constant monotonically decreasing function of x, with jumps at nodes x_k. At each interface x_k, partial reflection takes place with amplitude

$$R = \frac{(\lambda_2)_R - (\lambda_2)_L}{(\lambda_2)_R + (\lambda_2)_L}$$

with R and L denoting conditions to the right and to the left of the interface respectively. This modification, illustrated in Ill. (III.8), is not a very attractive far field boundary treatment.

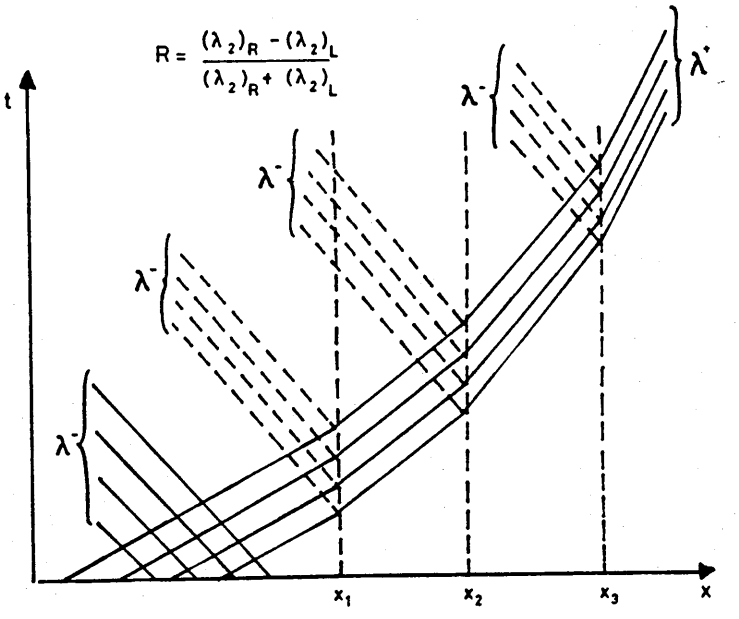

Ill. (III.8) - Partial reflection at interface points x_k in a gradual slowing down process.

Why do we get reflections?

An insight is gained by transforming the second order scalar wave equation into a first order system through the transformation

$$\varphi_t = p \qquad \varphi_x = -u \tag{3.2.7}$$

The interface problem then reads

$$\begin{aligned} \underline{w}_t + A_1 \underline{w}_x &= 0 \qquad x<0 \\ \underline{w}_t + A_2 \underline{w}_x &= 0 \qquad x>0 \\ [\underline{w}]_{x=0} &= 0 \end{aligned} \tag{3.2.8}$$

with

$$\underline{w} = \begin{pmatrix} p \\ u \end{pmatrix} \qquad A_1 = \begin{pmatrix} 0 & \lambda_1^2 \\ 1 & 0 \end{pmatrix} \qquad A_2 = \begin{pmatrix} \lambda_2 - \lambda_1 & \lambda_1 \lambda_2 \\ 1 & 0 \end{pmatrix}$$

The eigenstructure of A_1 and A_2 is respectively

$$\begin{aligned} R_1 &= (\underline{r}_1^1, \underline{r}_2^1) = \begin{pmatrix} 1 & 1 \\ -1/\lambda_1 & 1/\lambda_1 \end{pmatrix} \qquad \Lambda_1 = \mathrm{diag}(-\lambda_1, \lambda_1) \\ R_2 &= (\underline{r}_1^2, \underline{r}_2^2) = \begin{pmatrix} 1 & 1 \\ -1/\lambda_1 & 1/\lambda_2 \end{pmatrix} \qquad \Lambda_2 = \mathrm{diag}(-\lambda_1, \lambda_2) \end{aligned} \tag{3.2.9}$$

with single frequency solutions

$$\begin{aligned} \underline{w} &= \alpha_1 e^{i\omega(t+x/\lambda_1)} \underline{r}_1^1 + \beta_1 e^{i\omega(t-x/\lambda_1)} \underline{r}_2^1 \qquad x<0 \\ \underline{w} &= \alpha_2 e^{i\omega(t+x/\lambda_1)} \underline{r}_1^2 + \beta_2 e^{i\omega(t-x/\lambda_2)} \underline{r}_2^2 \qquad x>0 \end{aligned} \tag{3.2.10}$$

Continuity reads

$$\alpha_1 \begin{pmatrix} 1 \\ -\frac{1}{\lambda_1} \end{pmatrix} + \beta_1 \begin{pmatrix} 1 \\ \frac{1}{\lambda_1} \end{pmatrix} = \alpha_2 \begin{pmatrix} 1 \\ -\frac{1}{\lambda_1} \end{pmatrix} + \beta_2 \begin{pmatrix} 1 \\ \frac{1}{\lambda_2} \end{pmatrix} \tag{3.2.11}$$

(3.2.11) is identical to (3.2.4), hence (3.2.6) are solutions.

The reason for reflections has now become clear - the set of eigenvectors is not preserved across the interface. The matrix A_2 in (3.2.8)b should possess the same eigenvectors as A_1, with respective eigenvalues $\Lambda_2 = \mathrm{diag}(-\lambda_1, \lambda_2)$. Such a matrix is easily constructed

$$A_2 = R_1 \Lambda_2 R_1^{-1} = \begin{bmatrix} \frac{\lambda_2 - \lambda_1}{2} & \lambda_1 \frac{\lambda_2 + \lambda_1}{2} \\ \frac{\lambda_1 + \lambda_2}{2\lambda_1} & \frac{\lambda_2 - \lambda_1}{2} \end{bmatrix} \tag{3.2.12}$$

and reduces to A_1 upon the choice $\lambda_1 = \lambda_2$.

A count of degrees of freedom confirms that a modified wave equation (3.2.2)b has two free coefficients to completely determine the wave motion, while the modified first order system (3.2.8)b has four free entries in the matrix A_2 to be specified. The modification which preserves the eigenvectors is 'beyond the reach' of the second order scalar.

In the general case, consider the N x N interface problem

$$\begin{aligned} &\underline{w}_t + A\underline{w}_x = 0 && x < 0 \\ &\underline{w}_t + A^*\underline{w}_x = 0 && x > 0 \\ &[\underline{w}]_{x=0} = 0 \end{aligned} \tag{3.2.13}$$

A necessary and sufficient condition for full transmission of all waves across the interface is that A and A^* possess the same set of eigenvectors, or equivalently that A and A^* commute. Indeed, let $\underline{r}_k$ be the eigenvectors shared by A and A^*, and let λ_k and λ_k^* be the eigenvalues of A and A^* respectively. Solutions of (3.2.13) are

$$\underline{w}(x,t) = \sum_{k=1}^{N} \alpha_k(t-x/\lambda_k)\underline{r}_k \qquad x<0$$

$$\underline{w}(x,t) = \sum_{k=1}^{N} \beta_k(t-x/\lambda_k^*)\underline{r}_k \qquad x>0 \tag{3.2.14}$$

continuity reads

$$\sum_{k=1}^{N} \alpha_k(t)\underline{r}_k = \sum_{k=1}^{N} \beta_k(t)\underline{r}_k \tag{3.2.15}$$

$\{\underline{r}_k\}$ is a complete set with respect to which the representation of any vector is unique, hence

$$\alpha_k(t) = \beta_k(t) \qquad k=1,\ldots,N \tag{3.2.16}$$

implying full transmission of all waves.

(3.3) Slowing Down the Waves in 1D - The Discrete Level

Preservation of the eigenvectors is essential for full transmission of waves at the differential equation level. Numerical solutions, however, are not merely a discrete image of the continuous solutions. They tend to display additional features which cannot be directly associated with any analytic behaviour. Consequently, analytic properties do not automatically carry over to the discrete level.

Consider the linear advection equation

$$w_t + w_x = 0 \tag{3.3.1}$$

with the analytic dispersion relation

$$\omega = - \xi \tag{3.3.2}$$

A general 2-level explicit scheme to approximate (3.3.1) has the form

$$w_j^{n+1} = \sum_{k=-l}^{r} a_k w_{j+k}^n \tag{3.3.3}$$

with the discrete dispersion relation

$$Z = \sum_{k=-l}^{r} a_k \varkappa^k \tag{3.3.4}$$

For a fixed frequency ω, Z is fixed, and relation (3.3.4) is a polynomial of degree r+1 in the variable $\varkappa$ admitting r+1 solutions. Although not all solutions are necessarily different from one another (ie simple roots) we shall assume that to be the case, and denote the roots by

$$\varkappa_1, \varkappa_2, \ldots, \varkappa_{r+1} \tag{3.3.5}$$

A general single frequency numerical solution is given by

$$w_j^n = Z^n \left(\sum_{k=1}^{r+1} \alpha_k \varkappa_k^j \right) \tag{3.3.6}$$

In contrast to the analytic dispersion relation (3.3.2), where each ω admits a single wave number ξ, the discrete dispersion relation admits r+1 wave numbers ξ_k, each of which travels at a possibly different speed. The number of admissible modes is directly related to the width of the stencil of the numerical scheme. Paradoxically, the more accurate the scheme, the larger the stencil it uses, and the more non-physical modes $\varkappa_k$ it admits.

It can be shown [47,27,76], that for a fixed Z with $|Z|>1$, the

roots $\varkappa$ split into two well defined groups. There are precisely l modes with $|\varkappa|<1$ and r modes with $|\varkappa|>1$. Furthermore, if the scheme is dissipative the inequalities remain strict in the limit $|Z| \to 1$, $Z \neq 1$ (ie real non-zero frequency).

The discrete interface problem reads

$$
\begin{aligned}
w_j^{n+1} &= \sum_{k=-l}^{r} a_k w_{j+k}^n && j \leq 0 \\
v_j^{n+1} &= \sum_{k=-L}^{R} b_k v_{j+k}^n && j > 0 \qquad (3.3.7) \\
w_j^n &= v_j^n && j = -L+1, \ldots, r
\end{aligned}
$$

with (3.3.7)c expressing the identification of w_j^n and v_j^n in the overlapping region. (see Ill. (III.9)).

Two questions have to be addressed. First, is (3.3.7) stable, and second are discrete waves fully transmitted across the interface?

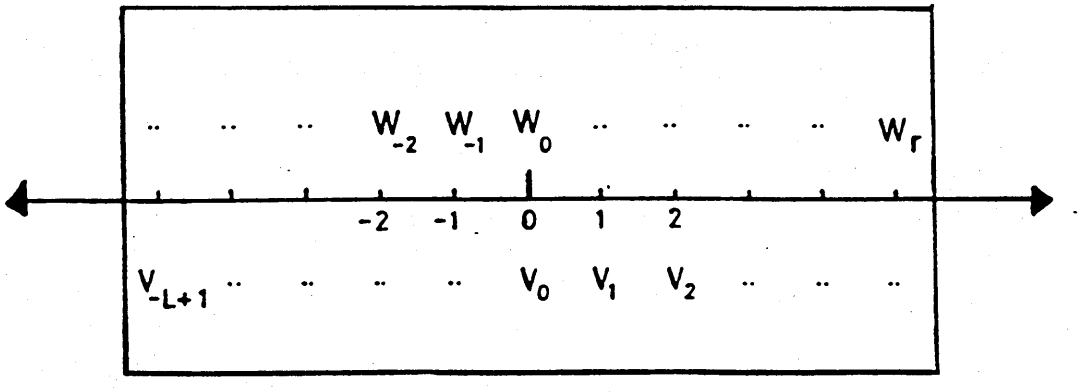

Ill. (III.9) - The overlapping region for the interface problem (3.3.7).

Let w_j^n and v_j^n possess solutions

$$\begin{aligned} w_j^n &= Z^n x^j && j\le 0 \\ v_j^n &= Z^n \mu^j && j>0 \end{aligned} \tag{3.3.8}$$

Assume (3.3.7) is dissipative. Let $|Z|\ge 1$ and assume that

$$\begin{aligned} &|x_k|<1 && k=1,\ldots,l \\ &|x_k|>1 && k=l+1,\ldots,l+r \\ &|\mu_k|<1 && k=1,\ldots,L \\ &|\mu_k|>1 && k=L+1,\ldots,L+R \end{aligned} \tag{3.3.9}$$

Admissible solutions of bounded ℓ_2 norm are of the form

$$\begin{aligned} \Phi_1(j) &= \sum_{k=l+1}^{l+r} \alpha_k x_k^j && j\le 0 \\ \Phi_2(j) &= \sum_{k=1}^{L} \beta_k \mu_k^j && j>0 \end{aligned} \tag{3.3.10}$$

Stability of the interface problem follows if it possesses *no* solutions of the form

$$\begin{aligned} w_j^n &= Z^n \Phi_1(j) && j\le 0 \\ v_j^n &= Z^n \Phi_2(j) && j>0 \end{aligned} \tag{3.3.11}$$

$$w_j^n = v_j^n \qquad j=-L+1,\ldots,r$$

with $|Z|\ge 1$.

It was shown [10] that if the schemes to both sides of the interface are dissipative, (3.3.7) is stable. Crucial to the proof is that the inequalities in (3.3.9) remain strict in the limit $|Z| \to 1$, $Z \neq 1$. To put the proof in the relevant context, let us assume (3.3.7) represents two LW schemes under a sudden change of CFL number. In this case L=R=l=r=1, and if $|Z| \geq 1$ there is only one admissible mode to either side of the interface.

$$w_j^n = \alpha Z^n \varkappa^j \qquad |\varkappa| > 1 \qquad j \leq 0$$

$$v_j^n = \beta Z^n \mu^j \qquad |\mu| < 1 \qquad j > 0 \qquad (3.3.12)$$

$$w_j^n = v_j^n \qquad j = 0,1$$

(3.3.12)$_c$ becomes

$$\alpha = \beta \qquad \alpha\varkappa = \beta\mu$$

leading to a contradiction $\varkappa = \mu$, since by assumption $|\varkappa| > 1$ and $|\mu| < 1$. Equation (3.3.12), thus, possesses no solutions with $|Z| \geq 1$ except for the trivial solution and stability is established. In the general case, (3.3.12)$_c$ is written as a homogeneous system of Vandermonde type, to be solved for the coefficients α_k and β_k, which again possesses only the trivial solution.

The stability of interface problems is closely linked to the stability of IBVPs, whereby a folding principle may be used to convert the two semi-infinite regions joined by an interface, to a single semi-infinite region of twice the number of variables. The conditions at the interface become BCS for the converted problem. These types of problems have been studied by Trefethen [77]. See also [26,22].

Transmission and reflection analysis gets more complicated with the increased number of admissible modes. Obviously, the more admissible modes, the more (3.3.7) is prone to partial reflections. Bearing with the example of the LW scheme under a sudden change of CFL

number, we show in Appendix C that a right going wave is partially reflected from the interface, and in fact

$$R = 0([\nu]) \qquad T = 1 + 0([\nu])$$

where $[\nu] = \frac{\Delta t}{\Delta x}(\lambda^* - \lambda)$ is the jump in the CFL number. If the change in ν is gradual, $[\nu]$ is small and reflections are weak. In addition, the natural dissipation of the scheme rapidly damps out the reflections. If the scheme used is non-dissipative, the reflected waves persist. This can be observed in Ill. (III.10), taken from Trefethen [74], where a wave of given time frequency fed through the LHB propagates through an abrupt change of grid size.

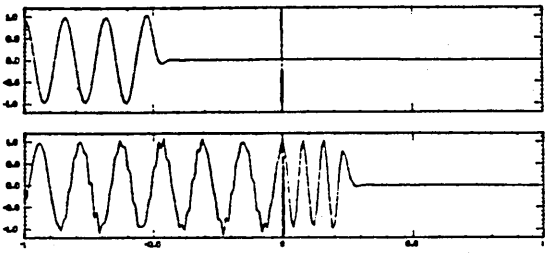

Ill. (III.10) - Undamped reflections under non-dissipative scheme (Trefethen [74]).

In summary, although the conditions derived in section (3.2) ensure full transmission of *continuous* waves, reflections of *discrete* waves may occur, due to approximating the $\partial/\partial x$ term in (3.3.1) using more than the 2 necessary grid points. In practice, owing to dissipativity, the weak reflections are damped out very rapidly.

(3.4) Slowing Down Waves in 2D

As a model system, consider the 2D Euler equations, linearised about a state of rest $u = v = 0$, and $\rho = 1$, $c = 1$

$$\underline{w}_t + A\underline{w}_x + B\underline{w}_y = 0 \qquad (3.4.1)$$

$$\underline{w} = \begin{pmatrix} p \\ u \\ v \end{pmatrix} \qquad A = \begin{pmatrix} 0 & 1 & 0 \\ 1 & 0 & 0 \\ 0 & 0 & 0 \end{pmatrix} \qquad B = \begin{pmatrix} 0 & 0 & 1 \\ 0 & 0 & 0 \\ 1 & 0 & 0 \end{pmatrix}$$

The transformation which recovers the Euler equations, given in Appendix D, allows far field modifications of (3.4.1) to automatically carry over to the Euler equations.

In a transformed set of coordinates (x',y'), rotated at an angle ϑ about (x,y), (3.4.1) takes the form

$$\underline{w}_t + (A\cos\vartheta + B\sin\vartheta)\underline{w}_{x'} + (-A\sin\vartheta + B\cos\vartheta)\underline{w}_{y'} = 0 \qquad (3.4.2)$$

$$x' = x\cos\vartheta + y\sin\vartheta$$
$$y' = -x\sin\vartheta + y\cos\vartheta$$

Plane waves in an arbitrary direction ϑ satisfy $\partial/\partial y' \equiv 0$, yielding

$$\underline{w}_t + M(\vartheta)_{x'} = 0 \qquad (3.4.3)$$

$$M(\vartheta) = A\cos\vartheta + B\sin\vartheta = \begin{pmatrix} 0 & \cos\vartheta & \sin\vartheta \\ \cos\vartheta & 0 & 0 \\ \sin\vartheta & 0 & 0 \end{pmatrix}$$

The eigenstructure of $M(\vartheta)$ is

$$\Lambda = \text{diag}\,(-1,0,1) \qquad R(\vartheta) = \begin{pmatrix} -1 & 0 & 1 \\ \cos\vartheta & -\sin\vartheta & \cos\vartheta \\ \sin\vartheta & \cos\vartheta & \sin\vartheta \end{pmatrix} \qquad (3.4.4)$$

By construction (3.4.4) recovers the eigenstructure of A for $\vartheta=0$, and that of B for $\vartheta=\pi/2$.

In the far field (3.4.1) is to be replaced by

$$\underline{w}_t + M^*(\vartheta)\underline{w}_x = 0 \qquad (3.4.5)$$

$$M^*(\vartheta) = A^*\cos\vartheta + B^*\sin\vartheta$$

A^* and B^* are constant matrices chosen to yield the desired pattern of wave fronts (Ills. (III.5),(III.6)). Following the 1D analysis, the condition for full transmission of plane waves is that $M^*(\vartheta)$ and $M(\vartheta)$ share the set of eigenvectors. The modified set of eigenvalues is

$$\Lambda^* = \mathrm{diag}(-1,0,a) \qquad 0\le a\le 1. \qquad (3.4.6)$$

$M^*(\vartheta)$ is obtained from the matrix product

$$M^*(\vartheta) = R(\vartheta)\Lambda^* R^{-1}(\vartheta) =$$

$$\begin{pmatrix} \frac{a-1}{2} & \frac{a+1}{2}\cos\vartheta & \frac{a+1}{2}\sin\vartheta \\ \frac{a+1}{2}\cos\vartheta & \frac{a-1}{2}\cos^2\vartheta & \frac{a-1}{2}\cos\vartheta\sin\vartheta \\ \frac{a+1}{2}\sin\vartheta & \frac{a-1}{2}\cos\vartheta\sin\vartheta & \frac{a-1}{2}\sin^2\vartheta \end{pmatrix} \qquad (3.4.7)$$

If A^* and B^* in (3.4.5) are to be constant coefficient ϑ-independent matrices, $M^*(\vartheta)$ should only have linear entries in $\cos\vartheta$ and $\sin\vartheta$. This implies $a\equiv 1$ and we are back to square one.

Conclusion

A general far field modification of the form (3.4.5) with A^* and B^* constant coefficient ϑ-independent matrices cannot preserve the eigenvectors in all directions ϑ.

A sensible alternative is to drop the requirement that eigenvectors are preserved in *all* directions, and to settle for eigenvectors being preserved in one preferred direction, say the x direction. By using a rotating system of coordinates this direction can be made to coincide with the outward direction. In semi-bounded channel flows, no rotation is needed, while in fully exterior problems, the x-direction can be matched with the radial direction since waves in the far field travel very nearly radially.

We return to system (3.4.1) and modify it by preserving the eigenvectors in the x-direction, leaving B unchanged for the time being

$$\underline{w}_t + A^* \underline{w}_x + B\underline{w}_y = 0 \tag{3.4.8}$$

$$A^* = R(0)\Lambda^* R^{-1}(0) = \begin{pmatrix} \frac{a-1}{2} & \frac{a+1}{2} & 0 \\ \frac{a+1}{2} & \frac{a-1}{2} & 0 \\ 0 & 0 & 0 \end{pmatrix}$$

The characteristic polynomial of (3.4.8), $\det\left(\lambda I - M^*(\vartheta)\right)=0$ reads

$$\lambda^3 - \lambda^2(a-1)\cos\vartheta - \lambda(\sin^2\vartheta + a\cos^2\vartheta) + \frac{a-1}{2}\cos\vartheta\sin^2\vartheta = 0 \tag{3.4.9}$$

An immediate result is that $\lambda=0$ is no longer an eigenvalue of the system except in the main directions. In terms of propagation pattern, the speed of the central wave $\lambda=0$ (the shear wave in the case of the Euler equations) depends on the speed of the deformed acoustic envelope. Ill. (III.11) shows a typical pattern of such a wave system.

To avoid such a coupling, the matrix B has to be modified as well. Note that preservation of the eigenstructure of B is unimportant, since this is the direction which is least likely to propagate information at all.

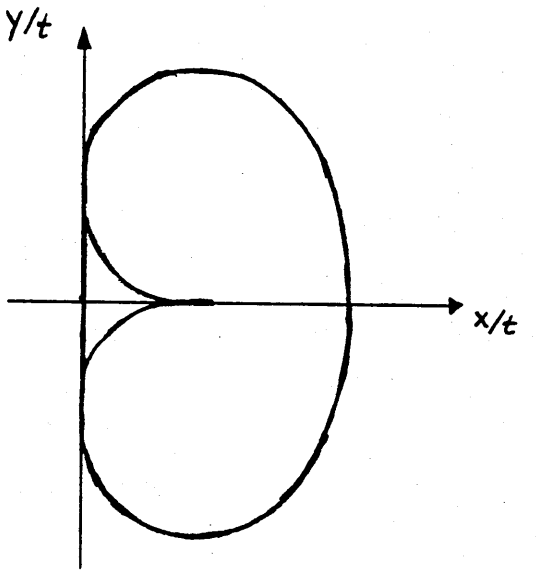

Ill. (III.11) - Typical envelope of wave fronts of (3.4.8) with a=0 (Roe, private communication)

Considering a reduced quadratic characteristic polynomial

$$\lambda^2 - \lambda(a-1)\cos\vartheta - (a\cos^2\vartheta + p^2\sin^2\vartheta) = 0 \qquad (3.4.10)$$

The relation between a general quadratic characteristic polynomial and the conic it describes, given in Appendix E, confirms that (3.4.10) represents an ellipse

$$\frac{\left(x-\frac{a-1}{2}\right)^2}{\left(\frac{a+1}{2}\right)^2} + \frac{y^2}{p^2} = 1 \qquad (3.4.11)$$

centred at $\left(\frac{a-1}{2},0\right)$ with axes $\frac{a+1}{2}$ and p respectively. Different values of p imply different stretching rates in the y-direction, and in particular different curvature in the incoming direction. For the modified curvature to match that of the unmodified circle at (-1,0),

$$p^2 = \frac{a+1}{2} \tag{3.4.12}$$

The importance of this second order match of incoming waves shall become clearer when the eigenvectors are Taylor expanded about the preferred direction. With this choice of p, (3.4.10) reads

$$\lambda^2 - \lambda(a-1)\cos\vartheta - (a\cos^2\vartheta + \frac{a+1}{2}\sin\vartheta) = 0 \tag{3.4.13}$$

Returning to equation (3.4.1) we seek a modification

$$\underline{w}_t + A^*\underline{w}_x + B^*\underline{w}_y = 0 \tag{3.4.14}$$

where A^* is given by (3.4.8) and B^* is such that when combined with A^* yields the characteristic polynomial

$$\lambda\left[\lambda^2 - \lambda(a-1)\cos\vartheta - (a\cos^2\vartheta + \frac{a+1}{2}\sin\vartheta)\right] = 0 \tag{3.4.15}$$

Equation 3.4.15) describes a wave system consisting of a central wave $\lambda=0$ and an elliptic acoustic envelope (compare (3.4.13)). Let B^* be symmetric, then the problem has a unique solution,

$$\underline{w}_t + A^*\underline{w}_x + B^*\underline{w}_y = 0 \tag{3.4.16}$$

$$A^* = \begin{pmatrix} \frac{a-1}{2} & \frac{a+1}{2} & 0 \\ \frac{a+1}{2} & \frac{a-1}{2} & 0 \\ 0 & 0 & 0 \end{pmatrix} \qquad B^* = \begin{pmatrix} 0 & 0 & \frac{\sqrt{a}+1}{2} \\ 0 & 0 & \frac{\sqrt{a}-1}{2} \\ \frac{\sqrt{a}+1}{2} & \frac{\sqrt{a}-1}{2} & 0 \end{pmatrix}$$

The envelope of wave fronts of (3.4.16) for various choices of slowing down parameter 'a' is illustrated in Ill. (III.12).

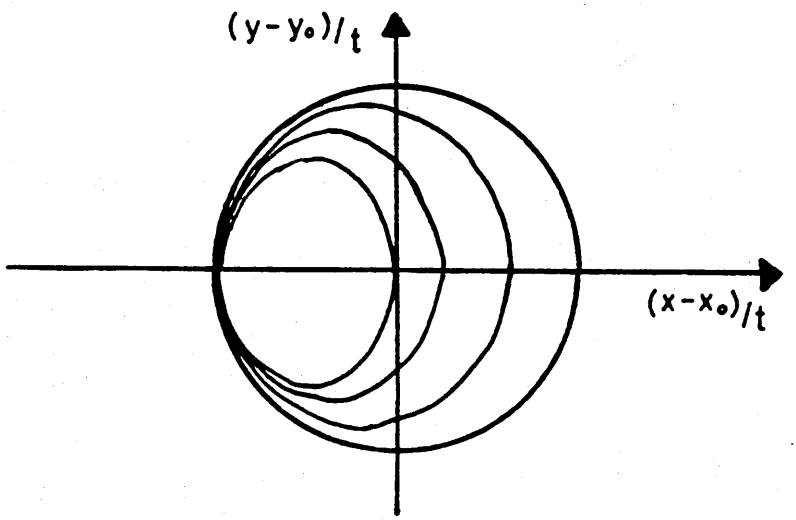

III. (III.12) - Envelope of wave fronts of (3.4.16) for $0 \le a \le 1$.

The complete eigenstructure of (3.4.16) is

$$\underline{r}_1^*(\vartheta) = \begin{pmatrix} \varepsilon \frac{a+1}{2}\cos\vartheta - \gamma\Delta \\ \gamma \frac{a+1}{2}\cos\vartheta - \varepsilon\Delta \\ \frac{a+1}{2}\sin\vartheta \end{pmatrix} \qquad \lambda_1^* = \frac{a-1}{2}\cos\vartheta - \Delta$$

$$\underline{r}_2^*(\vartheta) = \begin{pmatrix} \varepsilon \sin\vartheta \\ -\gamma \sin\vartheta \\ \sqrt{a}\cos\vartheta \end{pmatrix} \qquad \lambda_2^* = 0 \qquad (3.4.17)$$

$$\underline{r}_3^*(\vartheta) = \begin{pmatrix} \varepsilon \frac{a+1}{2}\cos\vartheta + \gamma\Delta \\ \gamma \frac{a+1}{2}\cos\vartheta + \varepsilon\Delta \\ \frac{a+1}{2}\sin\vartheta \end{pmatrix} \qquad \lambda_3^* = \frac{a-1}{2}\cos\vartheta + \Delta$$

with

$$\gamma = \frac{\sqrt{a}+1}{2} \qquad \varepsilon = \frac{\sqrt{a}-1}{2} \qquad \Delta^2 = \left(\frac{a+1}{2}\right)^2 \cos^2\vartheta + \frac{a+1}{2}\sin^2\vartheta$$

Setting a=1 recovers the unmodified eigenstructure (3.4.4).

Finally, (3.4.16) is assumed to hold in a rotated system of coordinates (x′,y′), inclined at an angle ϑ to the fixed set of coordinates (x,y). Let u' and v' denote the velocity components in the x′ and y′ directions, and let u and v denote those in the fixed directions, then the following relations hold

$$\underline{w}' = T\underline{w} \qquad \begin{pmatrix} x' \\ y' \end{pmatrix} = \begin{pmatrix} \cos\vartheta & \sin\vartheta \\ -\sin\vartheta & \cos\vartheta \end{pmatrix} \begin{pmatrix} x \\ y \end{pmatrix}$$

$$\underline{w}' = \begin{pmatrix} p \\ u' \\ v' \end{pmatrix} \qquad \underline{w} = \begin{pmatrix} p \\ u \\ v \end{pmatrix} \qquad T = \begin{pmatrix} 1 & 0 & 0 \\ 0 & \cos\vartheta & \sin\vartheta \\ 0 & -\sin\vartheta & \cos\vartheta \end{pmatrix} \tag{3.4.18}$$

The modified equations in the fixed system read

$$\underline{w}_t + A^{**}\underline{w}_x + B^{**}\underline{w}_y = 0 \tag{3.4.19}$$

$$A^{**} = T^{-1}(A^*\cos\vartheta - B^*\sin\vartheta)\ T$$

$$B^{**} = T^{-1}(A^*\sin\vartheta + B^*\cos\vartheta)\ T$$

Specifying the value of ϑ implies slowing down the waves in that preferred direction. A possible recipe for choosing ϑ for the problem of flow past an aerofoil is depicted in Ill. (III.5) p.60.

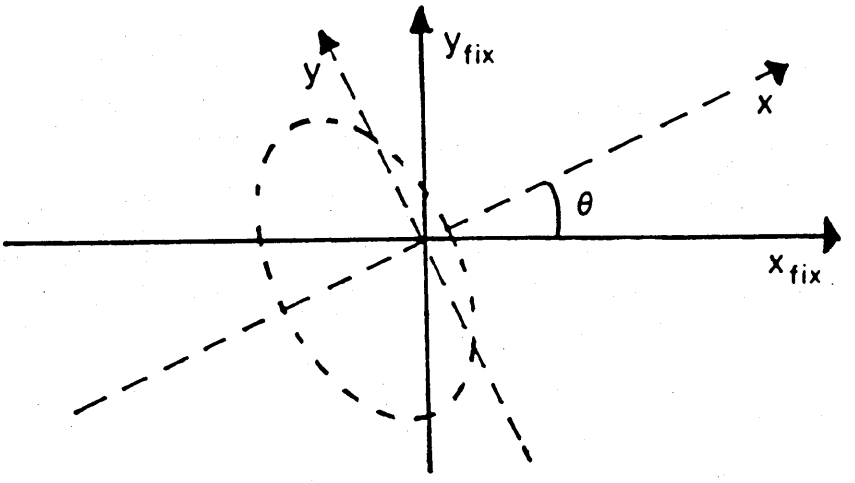

Ill. (III.13) - A rotating set of coordinates (x',y') and an underlying fixed set (x,y).

Asymptotic expansion for small angles ϑ about the preferred direction

By construction, eigenvectors are preserved in the preferred direction. Close to that direction, however, they are not, and it is interesting to see to what order they match. For that purpose we need to compare the eigenvectors in (3.4.4) with those in (3.4.17), expanded for small angle ϑ. For (3.4.4) we find

$$\underline{r}_1 \simeq \begin{pmatrix} -1 \\ 1 - \frac{\vartheta^2}{2} \\ \vartheta \end{pmatrix} \qquad (3.4.20)\,a$$

$$\underline{r}_2 \simeq \begin{pmatrix} 0 \\ -\vartheta \\ 1 - \frac{\vartheta}{2} \end{pmatrix} \qquad (3.4.20)\,b$$

$$\underline{r}_3 \simeq \begin{pmatrix} 1 \\ 1 - \frac{\vartheta^2}{2} \\ \vartheta \end{pmatrix} \qquad (3.4.20)\,c$$

while for (3.4.17) we find

$$\underline{r}_1^* \simeq \begin{pmatrix} -1 - \frac{\vartheta^2}{2}\left[\gamma\left(\frac{a+1}{2}\right)^{-1} + \varepsilon\right] \\ 1 - \frac{\vartheta^2}{2}\left[\varepsilon\left(\frac{a+1}{2}\right)^{-1} + \gamma\right] \\ \vartheta \end{pmatrix}$$

$$\underline{r}_2^* \simeq \begin{pmatrix} \vartheta\varepsilon/\sqrt{a} \\ -\vartheta\gamma/\sqrt{a} \\ 1 - \frac{\vartheta^2}{2} \end{pmatrix} \qquad (3.4.21)$$

$$\underline{r}_3^* \simeq \begin{pmatrix} 1 + \frac{\vartheta^2}{2}\left[\gamma\left(\frac{a+1}{2}\right)^{-1} - \varepsilon\right]/\sqrt{a} \\ 1 + \frac{\vartheta^2}{2}\left[\varepsilon\left(\frac{a+1}{2}\right)^{-1} - \gamma\right]/\sqrt{a} \\ \vartheta/\sqrt{a} \end{pmatrix}$$

and the error for small angle ϑ is

$$\Delta\underline{r}_1(\vartheta) = \begin{pmatrix} 0(\vartheta^2) \\ 0(\vartheta^2) \\ 0 \end{pmatrix} \qquad \text{Incoming waves} \qquad (3.4.22)\,a$$

$$\Delta \underline{r}_2(\vartheta) = \begin{pmatrix} 0(\vartheta) \\ 0(\vartheta) \\ 0 \end{pmatrix} \qquad \text{Stationary waves} \qquad (3.4.22)\,b$$

$$\Delta \underline{r}_3(\vartheta) = \begin{pmatrix} 0(\vartheta^2) \\ 0(\vartheta^2) \\ 0(\vartheta) \end{pmatrix} \qquad \text{Outgoing waves} \qquad (3.4.22)\,c$$

We observe that incoming waves are matched to second order in ϑ, which is a result of the high order match (3.4.12).

Eigenstructure of A^{**} and B^{**} in (3.4.19)

For computational purposes we shall need the eigenstructure of

$$\begin{aligned} A^{**} &= T^{-1}(A^{*}\cos\vartheta - B^{*}\sin\vartheta)\ T \\ B^{**} &= T^{-1}(A^{*}\sin\vartheta + B^{*}\cos\vartheta)\ T \end{aligned} \qquad (3.4.23)$$

Since eigenvalues are preserved under a similarity transformation and eigenvectors are related through the similarity matrix T, all we really need is the eigenstructure of the matrices in brackets in equation (3.4.23)

The eigenstructure of $(A^{*}\cos\vartheta - B^{*}\sin\vartheta)$ is

$$\underline{r}_1(\vartheta) = \begin{pmatrix} \varepsilon\,\frac{a+1}{2}\cos\vartheta - \gamma\Delta \\ \gamma\,\frac{a+1}{2}\cos\vartheta - \varepsilon\Delta \\ -\frac{a+1}{2}\sin\vartheta \end{pmatrix} \qquad \lambda_1 = \frac{a-1}{2}\cos\vartheta - \Delta \qquad (3.4.24)\,a$$

$$\underline{r}_2(\vartheta) = \begin{pmatrix} \varepsilon\sin\vartheta \\ -\gamma\sin\vartheta \\ \sqrt{a}\cos\vartheta \end{pmatrix} \qquad \lambda_2 = 0 \qquad (3.4.24)\,b$$

$$\underline{r}_3(\vartheta) = \begin{pmatrix} \varepsilon \frac{a+1}{2} \cos\vartheta + \gamma\Delta \\ \gamma \frac{a+1}{2} \cos\vartheta + \varepsilon\Delta \\ -\frac{a+1}{2} \sin\vartheta \end{pmatrix} \qquad \lambda_3 = \frac{a-1}{2} \cos\vartheta + \Delta \qquad (3.4.24)c$$

with $\Delta^2 = \left(\frac{a+1}{2}\right)^2 \cos^2\vartheta + \frac{a+1}{2}\sin^2\vartheta$

The eigenvectors of A^{**} are $\underline{r}_k^*(\vartheta) = T^{-1}\underline{r}_k(\vartheta)$.

Similarly, the eigenstructure of $(A^*\sin\vartheta + B^*\cos\vartheta)$ is

$$\underline{r}_1(\vartheta) = \begin{pmatrix} \varepsilon \frac{a+1}{2} \sin\vartheta - \gamma\Delta \\ \gamma \frac{a+1}{2} \sin\vartheta - \varepsilon\Delta \\ \frac{a+1}{2} \cos\vartheta \end{pmatrix} \qquad \lambda_1 = \frac{a-1}{2} \cos\vartheta - \Delta$$

$$\underline{r}_2(\vartheta) = \begin{pmatrix} \varepsilon \cos\vartheta \\ -\gamma \cos\vartheta \\ \sqrt{a} \sin\vartheta \end{pmatrix} \qquad \lambda_2 = 0 \qquad (3.4.26)$$

$$\underline{r}_3(\vartheta) = \begin{pmatrix} \varepsilon \frac{a+1}{2} \sin\vartheta + \gamma\Delta \\ \gamma \frac{a+1}{2} \sin\vartheta + \varepsilon\Delta \\ \frac{a+1}{2} \cos\vartheta \end{pmatrix} \qquad \lambda_3 = \frac{a+1}{2} \cos\vartheta + \Delta$$

with $\Delta^2 = \left(\frac{a+1}{2}\right)^2 \sin^2\vartheta + \frac{a+1}{2}\cos^2\vartheta.$

The eigenvectors of B^{**} are $\underline{r}_k^*(\vartheta) = T^{-1}\underline{r}_k(\vartheta)$.

(3.5) Alternative 2D Far Field Modifications

Two alternative far field modifications have been derived which are given below together with a brief account of their respective attractive features. For convenience of comparison, the far field modification proposed in the last section is repeated here. All systems are of the form

$$\underline{w}_t + A^* \underline{w}_x + B^* \underline{w}_y = 0$$

and shall be referred to as System No. I, II and III.

System No. I

(a)
$$A^* = \begin{pmatrix} \frac{a-1}{2} & \frac{a+1}{2} & 0 \\ \frac{a+1}{2} & \frac{a-1}{2} & 0 \\ 0 & 0 & 0 \end{pmatrix} \qquad B^* = \begin{pmatrix} 0 & 0 & \frac{\sqrt{a}+1}{2} \\ 0 & 0 & \frac{\sqrt{a}-1}{2} \\ \frac{\sqrt{a}+1}{2} & \frac{\sqrt{a}-1}{2} & 0 \end{pmatrix} \qquad (3.5.1)$$

(b) Characteristic polynomial is

$$\lambda\left[\lambda^2 - \lambda(a-1)\cos\vartheta - \left(a\cos^2\vartheta + \frac{a+1}{2}\sin^2\vartheta\right)\right] = 0 \qquad (3.5.2)$$

(c) Eigenvectors in the x-direction are preserved.

$$R = \begin{pmatrix} -1 & 0 & 1 \\ 1 & 0 & 1 \\ 0 & 1 & 0 \end{pmatrix} \qquad \Lambda = \text{diag}\,(-1,0,a) \qquad (3.5.3)$$

(d) Eigenvalues in the y-direction (compare (3.4.12))

$$\Lambda = \text{diag}\left(\sqrt{\frac{a+1}{2}},\ 0,\ \sqrt{\frac{a+1}{2}}\right) \qquad (3.5.4)$$

(e) The acoustic wave fronts form an ellipse centred at $\left(\frac{a-1}{2},\ 0\right)$ with

major and minor axes respectively $\frac{a+1}{2}$ and $\sqrt{\frac{a+1}{2}}$.

(f) The speed of central wave $\lambda=0$ is decoupled from that of the acoustic envelope.

(g) pressure does not satisfy a modified wave equation.

(h) Vorticity is not preserved.

System No. II

(a)
$$A^* = \begin{pmatrix} a-1 & a & 0 \\ 1 & 0 & 0 \\ 0 & 0 & 0 \end{pmatrix} \qquad B^* = \begin{pmatrix} 0 & 0 & \frac{a+1}{2} \\ 0 & 0 & 0 \\ 1 & 0 & 0 \end{pmatrix} \tag{3.5.5}$$

(b) Characteristic polynomial same as for System No. I.

(c) Eigenvectors in the x-direction are not (yet nearly) preserved.

$$R = \begin{pmatrix} -1 & 0 & a \\ 1 & 0 & 1 \\ 0 & 1 & 0 \end{pmatrix} \qquad \Lambda = \text{diag}(-1,0,a) \tag{3.5.6}$$

(d), (e) & (f) Same as system No. I.

(g) Pressure satisfies a modified second order wave equation

$$p_{tt} + (a-1)p_{xt} - ap_{xx} - \frac{a+1}{2}p_{yy} = 0 \tag{3.5.7}$$

(h) Vorticity is preserved

$$(u_y - v_x)_t = 0$$

System No. III

(a)
$$A^* = \begin{pmatrix} \frac{a-1}{2} & \frac{a+1}{2} & 0 \\ \frac{a+1}{2} & \frac{a-1}{2} & 0 \\ 0 & 0 & \frac{a-1}{2} \end{pmatrix} \qquad B^* = \begin{pmatrix} 0 & 0 & \sqrt{\frac{a+1}{2}} \\ 0 & 0 & 0 \\ \sqrt{\frac{a+1}{2}} & 0 & 0 \end{pmatrix} \tag{3.5.8}$$

(b) Characteristic polynomial

$$\left(\lambda-\frac{a-1}{2}\cos\vartheta\right)\left[\lambda^2-\lambda(a-1)\cos\vartheta-\left(a\cos^2\vartheta+\frac{a+1}{2}\sin^2\vartheta\right)\right] = 0 \qquad (3.5.9)$$

(c) Eigenvectors in the x direction are preserved.
Eigenvalues are respectively

$$\Lambda = \left(-1,\ \frac{a-1}{2},\ a\right) \qquad (3.5.10)$$

(d) & (e) Same as System No. I.

(f) The speed of central wave is coupled with that of the acoustic envelope, i.e. 'moves' to the centre of the ellipse.

(g) & (h) Same as System No. I.

Transforming back to the 2D unsteady Euler equations (see Appendix D) we obtain

System No. I

$$A^* = \begin{pmatrix} u+\frac{a-1}{2}c & \frac{a+1}{2}\rho c^2 & 0 \\ \frac{a+1}{2}\frac{1}{\rho} & u+\frac{a-1}{2}c & 0 \\ 0 & 0 & u \end{pmatrix} \qquad (3.5.11)\,a$$

$$B^* = \begin{pmatrix} v & 0 & \frac{\sqrt{a}+1}{2}\rho c^2 \\ 0 & v & \frac{\sqrt{a}-1}{2}c \\ \frac{\sqrt{a}+1}{2}\frac{1}{\rho} & \frac{\sqrt{a}-1}{2}c & v \end{pmatrix} \qquad (3.5.11)\,b$$

$$R = \begin{pmatrix} \rho c & 0 & \rho c \\ -1 & 0 & 1 \\ 0 & 1 & 0 \end{pmatrix} \qquad R^{-1} = \frac{1}{2\rho c}\begin{pmatrix} 1 & -\rho c & 0 \\ 0 & 0 & 2\rho c \\ 1 & \rho c & 0 \end{pmatrix} \qquad (3.5.12)$$

System No. II

$$A^* = \begin{pmatrix} u+(a-1)c & a\rho c^2 & 0 \\ \frac{1}{\rho} & u & 0 \\ 0 & 0 & u \end{pmatrix} \qquad (3.5.13)\,a$$

$$B^* = \begin{pmatrix} v & 0 & \frac{a+1}{2}\rho c^2 \\ 0 & v & 0 \\ \frac{1}{\rho} & 0 & v \end{pmatrix} \qquad (3.5.13)\,b$$

$$R = \begin{pmatrix} \rho c & 0 & a\rho c \\ -1 & 0 & 1 \\ 0 & 1 & 0 \end{pmatrix} \quad R^{-1} = \frac{1}{(a+1)\rho c} \begin{pmatrix} 1 & -a\rho c & 0 \\ 0 & 0 & (a+1)\rho c \\ 1 & \rho c & 0 \end{pmatrix} \qquad (3.5.14)$$

System No. III

$$A^* = \begin{pmatrix} u+\frac{a-1}{2}c & \frac{a+1}{2}\rho c^2 & 0 \\ \frac{a+1}{2}\frac{1}{\rho} & u+\frac{a-1}{2}c & 0 \\ 0 & 0 & u+\frac{a-1}{2}c \end{pmatrix} \qquad (3.5.15)\,a$$

$$B^* = \begin{pmatrix} v & 0 & \sqrt{\frac{a+1}{2}}\rho c^2 \\ 0 & v & 0 \\ \sqrt{\frac{a+1}{2}}\frac{1}{\rho} & 0 & v \end{pmatrix} \qquad (3.5.15)\,b$$

R and R^{-1} are the same as in (3.5.12)

Setting a=1, all three systems recover the unmodified system (3.4.2).

(3.6) Well-Posedness of the Far Field Modifications

To establish that hyperbolic systems of the general form

$$\underline{w}_t + A\underline{w}_x + B\underline{w}_y = 0 \tag{3.6.1}$$

are well-posed as IVPs, the matrices A and B in (3.6.1) should be simultaneously symmetrisable by a non-singular similarity transformation [88], ie there should exist a non-singular matrix S such that

$$\begin{aligned} S\ A\ S^{-1} &= \text{symmetric} \\ S\ B\ S^{-1} &= \text{symmetric} \end{aligned} \tag{3.6.2}$$

Obviously, this can only be achieved if A and B can each be separately symmetrised. Hyperbolicity guarranties that this is possible and in fact that A can be *diagonalised* by the similarity transformation

$$R^{-1}AR = \Lambda = \text{diag}\ (\lambda_1,\lambda_2,\lambda_3) \tag{3.6.3}$$

Following a general technique suggested by [23] cited in [82], we start by diagonalizing A using the transformation in (3.6.3). We then consider the transformed B

$$R^{-1}BR \tag{3.6.4}$$

and seek a *diagonal* matrix $D = \text{diag}(d_1,d_2,d_3)$ such that

$$D^{-1}R^{-1}B\ R\ D\ =\ \text{symmetric} \tag{3.6.6}$$

Under this further transformation, the transformed A remains diagonal, hence symmetric and well-posedness is established.

We proceed in two stages. We first establish well-posedness in the rotated system of coordinates. This amounts to proving that Systems I,II and III, all of which have the form

$$\underline{w}_t + A^* \underline{w}_x + B^* \underline{w}_y = 0 \qquad (3.6.7)$$

are simultaneously symmetrisable,

$$\begin{aligned} SA^*S^{-1} &= \text{diagonal} \\ SB^*S^{-1} &= \text{symmetric} \end{aligned} \qquad (3.6.8)$$

Well-posedness in the fixed system of coordinates immediately follows on physical grounds. More formally, A^{**} and B^{**} in (3.4.19) can be symmetrised by

$$\begin{aligned} STA^{**}T^{-1}S^{-1} &= SA^*S^{-1}\cos\vartheta - SB^*S^{-1}\sin\vartheta \\ STB^{**}T^{-1}S^{-1} &= SA^*S^{-1}\sin\vartheta + SB^*S^{-1}\cos\vartheta \end{aligned} \qquad (3.6.9)$$

It is therefore sufficient to prove that (3.6.7) is symmetrisable for systems I, II and III.

System No. I

R and R^{-1} are given by (3.5.12)

$$R^{-1}B^*R = \begin{pmatrix} v & \frac{1}{2}(\gamma-\varepsilon)c & 0 \\ (\gamma-\varepsilon)c & v & (\gamma+\varepsilon)c \\ 0 & \frac{1}{2}(\gamma+\varepsilon)c & v \end{pmatrix} \qquad (3.6.11)$$

$$D^{-1}R^{-1}B^*RD = \begin{pmatrix} v & \frac{1}{2}(\gamma-\varepsilon)c\frac{d_2}{d_1} & 0 \\ (\gamma-\varepsilon)c\frac{d_1}{d_2} & v & (\gamma+\varepsilon)c\frac{d_3}{d_2} \\ 0 & \frac{1}{2}(\gamma+\varepsilon)c\frac{d_2}{d_3} & v \end{pmatrix}$$

is symmetric if

$$\left(\frac{d_1}{d_2}\right)^2 = \left(\frac{d_3}{d_2}\right)^2 = \frac{1}{2} \tag{3.6.12}$$

System No. II

R and R^{-1} are given by (3.5.14)

$$R^{-1}B^*R = \begin{pmatrix} v & \frac{1}{2}c & 0 \\ c & v & ac \\ 0 & \frac{1}{2}c & v \end{pmatrix} \tag{3.6.13}$$

and $D^{-1}R^{-1}B^*RD$ is symmetric if

$$\left(\frac{d_1}{d_2}\right)^2 = \frac{1}{2} \qquad \left(\frac{d_3}{d_2}\right)^2 = \frac{1}{2a} \tag{3.6.14}$$

System No. III

R and R^{-1} are given by (3.5.12)

$$R^{-1}B^*R = \begin{pmatrix} v & \frac{1}{2}\sqrt{\frac{a+1}{2}}\,c & 0 \\ \sqrt{\frac{a+1}{2}}\,c & v & \sqrt{\frac{a+1}{2}}\,c \\ 0 & \frac{1}{2}\sqrt{\frac{a+1}{2}}\,c & v \end{pmatrix} \tag{3.6.15}$$

and again $D^{-1}R^{-1}B^*RD$ is symmetric if

$$\left(\frac{d_1}{d_2}\right)^2 = \left(\frac{d_3}{d_2}\right)^2 = \frac{1}{2} \tag{3.6.16}$$

(3.7) Physical Validation of the Far Field Modifications

All three far field modifications proposed in section (3.5) are based on a linearized form of the 2D Euler equations, (3.4.1), stripped of their physical dimensions. The modifications are performed to meet requirements which are purely mathematical, and there is a danger that when carried back to the full 2D Euler equations, the modified systems will lose their physical grounds. In particular it seems wise to establish that the velocity components u and v continue to display a vector-like behaviour with regard to coordinate transformations.

System No. I

Equations (3.5.11) are assumed to hold in the rotated system of coordinates (x',y'). Let the velocity components in those directions be denoted by q^R and q^T respectively and let u and v be the velocity components in the fixed directions. Then

$$\begin{aligned} q^R &= u\cos\vartheta + v\sin\vartheta \\ q^T &= -u\sin\vartheta + v\cos\vartheta \end{aligned} \qquad (3.7.1)$$

To confirm that u and v transform in a vector-like manner, we write (3.4.19) in cylindrical coordinates (r,ϑ). By further assuming axial symmetry we expect to recover the properties of each of the individual modifications in the radial direction. In terms of (r,ϑ), equation (3.4.19) reads

$$\underline{w}_t + (A^{**}\cos\vartheta + B^{**}\sin\vartheta)\underline{w}_r + (-A^{**}\sin\vartheta + B^{**}\cos\vartheta)\frac{1}{r}\underline{w}_\vartheta = 0 \qquad (3.7.2)$$

with

$$A^{**}\cos\vartheta + B^{**}\sin\vartheta = T^{-1}A^{*}T =$$

$$\begin{pmatrix} q^R+\frac{a-1}{2}c & \frac{a+1}{2}\cos\vartheta\rho c^2 & \frac{a+1}{2}\sin\vartheta\rho c^2 \\ \frac{a+1}{2}\cos\vartheta\frac{1}{\rho} & q^R+\frac{a-1}{2}\cos^2\vartheta c & \frac{a-1}{2}\cos\vartheta\sin\vartheta c \\ \frac{a+1}{2}\sin\vartheta\frac{1}{\rho} & \frac{a-1}{2}\cos\vartheta\sin\vartheta c & q^R+\frac{a-1}{2}\sin^2\vartheta c \end{pmatrix} \qquad (3.7.3)\,a$$

$$-A^{**}\sin\vartheta + B^{**}\cos\vartheta = T^{-1}B^{*}T =$$

$$\begin{pmatrix} q^T & \frac{\sqrt{a}+1}{2}\sin\vartheta\rho c^2 & \frac{\sqrt{a}+1}{2}\cos\vartheta\rho c^2 \\ -\frac{\sqrt{a}+1}{2}\sin\vartheta\frac{1}{\rho} & q^T-\frac{\sqrt{a}-1}{2}\sin 2\vartheta c & \frac{\sqrt{a}-1}{2}\cos 2\vartheta c \\ \frac{\sqrt{a}+1}{2}\cos\vartheta\frac{1}{\rho} & \frac{\sqrt{a}+1}{2}\cos 2\vartheta c & q^T+\frac{\sqrt{a}-1}{2}\sin 2\vartheta c \end{pmatrix} \qquad (3.7.3)\,b$$

Using relation (3.7.1) and the symmetry assumption, equations (ii) and (iii) in (3.7.3) can be combined into a single equation in the radial velocity q^R, yielding the reduced 2 × 2 system

$$\begin{pmatrix} p \\ q^R \end{pmatrix}_t + \begin{pmatrix} q^R+\frac{a-1}{2}c & \frac{a+1}{2}\rho c^2 \\ \frac{a+1}{2}\frac{1}{\rho} & q^R+\frac{a-1}{2}c \end{pmatrix} \begin{pmatrix} p \\ q^R \end{pmatrix}_r + \frac{1}{r}\begin{pmatrix} \frac{\sqrt{a}+1}{2}\rho c^2 q^R \\ \frac{\sqrt{a}-1}{2}c \end{pmatrix} = 0 \qquad (3.7.4)$$

The eigenstructure of the matrix in (3.7.4)

$$R = \begin{pmatrix} \rho c & \rho c \\ -1 & 1 \end{pmatrix} \qquad \Lambda = \mathrm{diag}(q^R-c,\ q^R+ac) \qquad (3.7.5)$$

recovers the expected properties, namely reduced outgoing speed and preserved eigenvectors.

<u>System No. II</u> reduces to

$$\begin{pmatrix} p \\ q^R \end{pmatrix}_t + \begin{pmatrix} q^R+(a-1)c & a\rho c^2 \\ \frac{1}{\rho} & q^R \end{pmatrix} \begin{pmatrix} p \\ q^R \end{pmatrix}_r + \frac{1}{r}\begin{pmatrix} \frac{a+1}{2}\rho c^2 q^R \\ 0 \end{pmatrix} = 0 \qquad (3.7.6)$$

System No. III reduces to

$$\begin{pmatrix} p \\ q^R \end{pmatrix}_t + \begin{pmatrix} q^R+\frac{a-1}{2}c & \frac{a+1}{2}\rho c^2 \\ \frac{a+1}{2}\frac{1}{\rho} & q^R+\frac{a-1}{2}c \end{pmatrix} \begin{pmatrix} p \\ q^R \end{pmatrix}_r + \frac{1}{r}\begin{pmatrix} \frac{\sqrt{a}+1}{2}\rho c^2 q^R \\ 0 \end{pmatrix} = 0 \qquad (3.7.7)$$

Both (3.7.6) and (3.7.7) possess the expected eigenstructure in the radial direction, this time with account for the physical dimensions.

(3.8) Numerical Experiments

(3.8.1) One Dimensional Tests

In the following 1D tests, it is assumed that the RHB is the artificial boundary and waves travelling from left to right are accordingly outgoing.

Test A (Figure (III.1)a-d)

The governing equation is the modified 1D wave equation

$$\begin{pmatrix} p \\ u \end{pmatrix}_t + \begin{pmatrix} \frac{a-1}{2} & \frac{a+1}{2} \\ \frac{a+1}{2} & \frac{a-1}{2} \end{pmatrix} \begin{pmatrix} p \\ u \end{pmatrix}_x = 0 \qquad (3.8.1)$$

formulated as a first order system. The parameter 'a' controls the speed of the right moving wave, assuming values between 0 and 1. The eigenvectors and eigenvalues of (3.8.1) are

$$R = \begin{pmatrix} 1 & 1 \\ -1 & 1 \end{pmatrix} \qquad \Lambda = \text{diag}\ (-1,a) \qquad (3.8.2)$$

The numerical method is Roe's field decomposition [61,62] with LW scheme applied to each characteristic field. No flux limiter is used.

Initial data are

$$\begin{pmatrix} p \\ u \end{pmatrix} = \begin{pmatrix} 1 \\ 1 \end{pmatrix} e^{-\sigma(x-x_0)^2} + \begin{pmatrix} 1 \\ -1 \end{pmatrix} e^{-\sigma(x-x_1)^2} \qquad (3.8.3)$$

generating two waves moving in opposite directions with respective speeds -1 and a. Clearly the choice of parameter 'a' does not alter the propagation of the left running wave. The right going wave is propagating at various reduced speeds a=1, 0.8, 0.5 and a=1-x. A slight compression of the slowed down wave can be observed in the last case due to the gradual change in the speed of propagation.

Test B (Figure (III.2)a-d)

The governing equations are the 1D Euler equations given in (2.2.1) with eigenstructure given in (2.2.3). The equation is replaced by the modified equation

$$\underline{w}_t + A^*(\underline{w})\underline{w}_x = 0 \qquad (3.8.4)$$

where $A^* = R\Lambda^* R^{-1}$ $\quad \Lambda^* = \mathrm{diag}(\lambda_1^*, \lambda_2^*, \lambda_3^*)$

$$\lambda_1^* = a_1(u-c)$$

$$\lambda_2^* = a_2 u$$

$$\lambda_3^* = a_3(u+c)$$

The numerical algorithm is again Roe's field decomposition with LW scheme and Superbee flux limiter on each characteristic field [71]. Initial data correspond to the shock tube problem [68]

$$\underline{w}_L = (1,\ 0,\ 2.5)^T \qquad \underline{w}_R = (0.1,\ 0,\ 0.25)^T$$

generating a left running expansion fan and a right running shock followed by a contact discontinuity. Evolution with time of momentum

profiles is shown in figure (III.2), for the choices

$a_1 = a_2 = a_3 = 1$ (unmodified)

$a_1 = 1 \quad a_2 = a_3 = 0.8,\ 0.5,\ 0.2$

Comparison of the figures confirms that the left moving fan is not distorted by the choice of a_2 and a_3. The right moving waves preserve their respective profiles, yet propagate at reduced speeds.

Test C (Figure (III.3)a,b)

The governing equations are the 1D Euler equations, and the test is the one described in Section (2.2.2) Test A, where a high pressure is fed through the LHB, giving rise to right moving shock wave and a contact discontinuity. The method of solution is the same as in Test B. Figure (III.3)a shows the evolution of density profiles under several sudden changes of coefficients. Although theoretical analysis predicts weak reflections from interfaces across which the coefficients change, the natural dissipation of the scheme results in a very rapid decay of the reflected waves, and consequently to a smooth passage of waves.

Finally figure (III.3)b repeats the same test with smoothly varying slowing-down coefficients. The right moving waves are, in fact, brought to a complete rest before reaching the RHB. This is accomplished by letting a_2 and a_3 be a decaying function of x. The gradual slowing down process is the limit of a multiple interface problem, as the interfaces are brought close together. It is known that mild instabilities may be strongly amplified by multiple reflections from either boundaries or interfaces [77]. The problem is particularly acute when the boundaries or interfaces are close to one another, rendering the travelling time between them tend to zero. In the present example, there is no evidence of such a process happening, and the right moving waves are brought to rest gradually, without generating any leftgoing disturbances.

(3.8.2) Two Dimensional Tests

The experiments were conducted using the 2D linearized Euler equations (3.4.1) for which three far field modifications have been derived (3.5.1), (3.5.5) and (3.5.8). The results presented in this section were obtained by (3.5.1). A comparison between the performance of (3.5.1) and (3.5.5) is also presented.

Test A (Figures (III.4)a,b, (III.5)a-d)

Initial data is a Gaussian high pressure distribution centred at the origin

$$p(x,y,0) = e^{\sigma(x^2+y^2)} \tag{3.8.5}$$

$$u(x,y,0) = v(x,y,0) = 0.0$$

Due to symmetry, the problem is solved in the quarter plane ($x \geq 0$, $y \geq 0$) with reflecting conditions on the boundaries $x=0$ and $y=0$.

Second differentiation of the unmodified equations (3.4.1) shows that pressure satisfies the 2D wave equation $p_{tt} - p_{xx} - p_{yy} = 0$, for which an exact solution exists in the integral form

$$p(x,y,t) = \frac{1}{2\pi} \frac{\partial}{\partial t} \iint_{r \leq t} \frac{p(x^*,y^*,0)}{\sqrt{t^2-r^2}} \, dx^* dy^* \tag{3.8.6}$$

Figure (III.4) shows the exact solution for the initial data (3.8.5), obtained by numerically integrating (3.8.6) using Simpson's rule.

The numerical algorithm uses a two stage space operator

splitting

$$\text{(i)}\quad \underline{W}_t + A^{**}\underline{W}_x = 0$$

$$\text{(ii)}\quad \underline{W}_t + B^{**}\underline{W}_y = 0$$

In each direction, Roe's field decomposition is performed and the LW scheme is applied to each characteristic field. The eigenstructure of A^{**} and B^{**} is given in section (3.4). Figure (III.5) presents the numerical solution for various choices of radial speed.

$$a = 1.0,\ 0.8,\ 0.6,\ 1\text{-}r$$

The important feature to note is that the outgoing waves do not generate any incoming disturbances as they propagate. They leave behind a quiet state which asymptotically approaches the undisturbed state. A slight compression of the outgoing wave is observed in Figure (III.5)d, which is due to the non-uniform radial speed (compare Figure (III.1)d). Since our interest does not lie with the precise details of the outgoing flow, this slight distortion does not constitute a problem as long as no incoming waves are generated as a result.

Test B (Figure III.6)a,b)

We repeat the same test and compare the performance of system No. I and II. Recall that in the latter, eigenvectors in the radial directions are not preserved, and as a result incoming waves are generated when the outgoing ones are gradually slowed down.

Test C (Figure (III.7)a-b,Figure (III.8)a,c)

The test is similar to (3.8.5), with the high pressure now centred at $(x,y) = (x_0,y_0)$

$$p(x,y,0) = e^{-\sigma((x-x_0)^2 + (y-y_0)^2)}$$

$$u(x,y,0) = v(x,y,0) = 0.0 \qquad (3.8.7)$$

Under the unmodified equations, the expected solution is a circular pressure wave decaying like $1/\sqrt{r}$ as it moves away from (x_0,y_0) leaving behind a quiet region. Figure (III.7) shows the exact solution. Figure (III.8) shows the numerical solution for a = 1.0, 0.8, 0.6, which slows down the outgoing waves while not altering the incoming ones. In fact what we see is precisely the envelope of wave fronts originated at (x_0,y_0) under different slowing down rates.

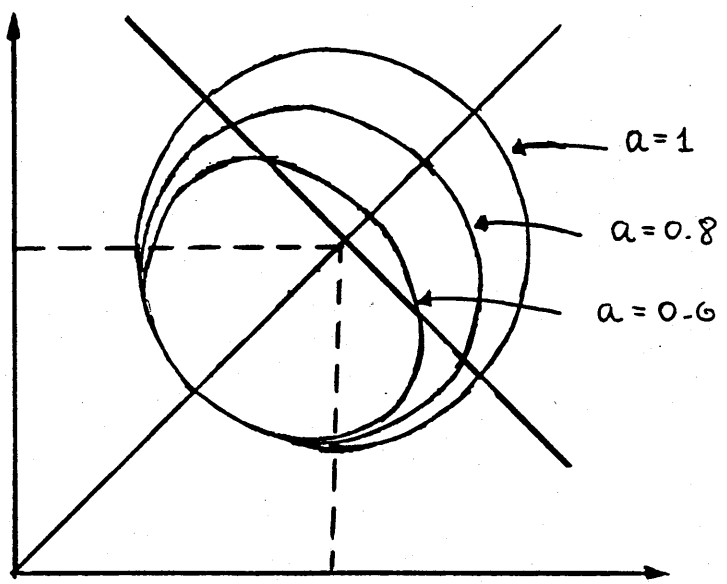

III. (III.14) - Envelope of wave fronts corresponding to figure (III.8).

(3.9) The Proposed Modification and Conservation

It seems only natural to expect that the proposed modified system

$$\underline{w}_t + A^*(\underline{w})\underline{w}_x = 0 \tag{3.9.1}$$

corresponds to a modified set of conservation laws

$$\underline{w}_t + \underline{f}^*(\underline{w})_x = 0 \tag{3.9.2}$$

The question is, can a flux function f^* always be associated with a Jacobian matrix A^* ? In support of this expectation we have Euler's Theorem on *homogeneous functions* ([12], p.108).

Definition

A function f(x,y,z) is homogeneous of degree k in x,y and z if $f(hx,hy,hz) = h^k f(x,y,z)$

Euler's Theorem

f(x,y,z) is homogeneous of degree k iff it satisfies

$$x\frac{\partial f}{\partial x} + y\frac{\partial f}{\partial y} + z\frac{\partial f}{\partial z} = kf \tag{3.9.3}$$

The vector of physical flux functions of the 1D Euler equations is homogeneous of degree k=1 in the conserved variables. When extended to systems, setting k=1, (3.9.3) reads

$$\frac{\partial \underline{f}}{\partial \underline{w}} \cdot \underline{w} = \underline{f} \tag{3.9.4}$$

That is, if $\underline{f}$ is homogeneous of degree k=1 in $\underline{w}$, and $A = \partial\underline{f}/\partial\underline{w}$, then $\underline{f}$ can be reconstructed from its Jacobian matrix A by the product $\underline{f} = A\underline{w}$.

On dimensional grounds, the matrix A^* is homogeneous of degree k=0. Let $\underline{f}^*$ be defined by

$$\underline{f}^* = A^* \underline{w} \tag{3.9.5}$$

which by construction is homogeneous of degree k=1. Is A^* necessarily the Jacobian matrix of $\underline{f}^*$? Let

$$A^{**} = \partial \underline{f} / \partial \underline{w} \tag{3.9.6}$$

by (3.9.4) it follows that

$$f^* = A^{**} \underline{w} \tag{3.9.7}$$

implying

$$A^* \underline{w} = A^{**} \underline{w} \tag{3.9.8}$$

Unfortunately, this does not imply $A^{**} = A^*$, since $\underline{w} = (\rho, \rho u, e)^T$ is *not* an arbitrary vector. The only conclusion from (3.9.8) is

$$\underline{w} \in \ker(A^{**} - A^*)$$

Simple examples can be constructed for which

$$A^* \neq A^{**}$$
$$A^* \underline{w} = A^{**} \underline{w}$$

Since the existence of a modified flux function is not guaranteed, we now turn to the Euler equations and check whether or not the modified equations correspond to a modified conservation law. For simplicity, we consider the Isothermal Euler equations

$$\begin{pmatrix} \rho \\ \rho u \end{pmatrix}_t + \begin{pmatrix} \rho u \\ \rho u^2 + \rho c^2 \end{pmatrix}_x = 0 \tag{3.9.9}$$

the sound speed c is constant. The eigenstructure of the system is

$$\underline{r}_1 = (1,\ u-c) \qquad \lambda_1 = u-c \tag{3.9.10}$$

$$\underline{r}_2 = (1,\ u+c) \qquad \lambda_2 = u+c$$

For general eigenvalues $\Lambda^* = \mathrm{diag}(\lambda_1^*, \lambda_2^*)$

$$A^* = R\Lambda^* R^{-1}$$

with

$$A_{11}^* = \frac{1}{2c}\left[\lambda_1^*(u+c) - \lambda_2^*(u-c)\right]$$

$$A_{12}^* = \frac{1}{2c}\left[-\lambda_1^* + \lambda_2^*\right]$$

$$A_{21}^* = \frac{1}{2c}\left[(\lambda_1^*-\lambda_2^*)(u^2-c^2)\right]$$

$$A_{22}^* = \frac{1}{2c}\left[-\lambda_1^*(u-c) + \lambda_2^*(u+c)\right]$$

For the particular choice

$$\lambda_1^* = a_1(u-c) \qquad \lambda_2^* = a_2(u+c) \tag{3.9.11}$$

with arbitrary constants a_1, a_2 we obtain

$$A_{11}^* = \frac{1}{2c}\left[(a_1 - a_2)(u^2-c^2)\right]$$

$$A_{12}^* = \frac{1}{2c}\left[(a_2 - a_1)u + (a_1 + a_2)c\right] \tag{3.9.12}$$

If A^* is to be a Jacobian matrix we must have

$$\int A_{11}^* d\rho = \int A_{12}^* d(\rho u) = f_1^*$$

Integrating (3.9.12) we find

$$\int A_{11}^{*} d\rho = -\frac{a_1-a_2}{2}\frac{\rho u^2}{c} + \frac{a_1-a_2}{2}\rho c + g(\rho u)$$

$$\int A_{12}^{*} d(\rho u) = -\frac{a_1-a_2}{4}\frac{\rho u^2}{c} + \frac{a_1+a_2}{2}\rho u + h(\rho) \qquad (3.9.13)$$

clearly

$$g(\rho u) = \frac{a_1+a_2}{2}\rho u \qquad h(\rho) = \frac{a_1-a_2}{2}\rho c$$

yet no choice of a_1 and a_2 can match the first term unless $a_1=a_2$ which recovers the unmodified equations up to a scaling factor.

Similar result is obtained if we choose

$$\lambda_1^{*} = u-a_1 c \qquad \lambda_2^{*} = u+a_2 c$$

Conclusion: The modified equations are not modified conservation laws.

This result carries over to more complete formulations of the equations of flow. Indeed if we write System No.II in conserved variable, we obtain

$$\begin{pmatrix}\rho\\ \rho u\\ E\end{pmatrix}_t + \begin{pmatrix}\rho u\\ \rho u^2+p\\ uE+up\end{pmatrix}_x + (a-1)\begin{pmatrix}\rho u_x+(\gamma-1)\frac{1}{c^2}p_x\\ \rho u u_x+Mp_x\\ (e+p)u_x+\frac{c}{\gamma-1}(1+M^2\frac{\gamma-1}{2}p_x)\end{pmatrix} = 0$$

Obviously by setting a=1 we recover the lost conservation.

The loss of conservation chiefly bears on flows which contain shocks, where conservation is essential for accurate predictions. Since the modification is to be applied only in the far field, where the flow is not only smooth but in fact can be regarded as locally linear, this may have only a minor effect, if at all, on the solution in the inner region. From the practical point of view, the additional term in (3.9.14) can be treated as a correction source-like term. Schemes that are based on characteristic field decomposition (eg Roe

[59,60], Van Leer [80], Osher [55]) can absorb the correction term into the decomposition algorithm. Shock fitting techniques [eg The λ-scheme [54]) do not make explicit use of conservation and may also absorb the correction term into a modified set of characteristic equations.

(3.10) The Proposed Modification and Preconditioning

Preconditioning is a technique applied to accelerate the convergence of the transient solution to steady state. Starting from initial conditions, the rate of convergence to steady state is determined by how quickly one can march toward $t \to \infty$, ie by the size of the allowable Δt. Bounded by the CFL condition for stability, it is always the largest wave speed that places the constraint on Δt

$$\frac{\Delta t}{\Delta x} \max_k |\lambda_k| \leq K \tag{3.10.1}$$

with K a scheme dependent constant. In problems involving different time scales, (3.10.1) seems particularly wasteful on the slow waves, which could be advanced a lot faster. Furthermore, with most explicit schemes, small time steps, ie small CFL numbers, imply very weak dissipation and large dispersion errors, which further decreases convergence rate to steady state.

As a remedy, one usually replaces the hyperbolic system

$$\underline{W}_t + A\underline{W}_x = 0 \tag{3.10.2}$$

with (λ_k) the significantly different wave speeds, by

$$P^{-1}\underline{W}_t + A\underline{W}_x = 0 \tag{3.10.3}$$

where P^{-1} is a non singular preconditioner. Clearly (3.10.2) and (3.10.3) possess the same steady state solution, yet the time accuracy

of (3.10.3) is destroyed by the introduction of additional time derivatives. The rate of convergence to steady state of (3.10.3) now is determined by

$$\underline{w}_t + PA\underline{w}_x = 0 \qquad (3.10.4)$$

and P is chosen so that the eigenvalues of PA are of a comparable size, ie that PA has a condition number of unity and $|\lambda_k^*|=1$ for all k. If, for example, all the eigenvalues of A are positive,

$$P = R\Lambda^{-1}R^{-1} = A^{-1} \qquad (3.10.5)$$

The modification proposed in section (3.2) can be viewed as a preconditioned system in that

$$\underline{w}_t + A^*\underline{w}_x = 0 \qquad (3.10.6)$$

is equivalent to

$$P^{-1}\underline{w}_t + A\underline{w}_x = 0 \qquad (3.10.7)$$

where $PA = A^*$. P is a non singular matrix and in fact

$$P= R\Lambda^*\Lambda^{-1}R^{-1} \qquad (3.10.8)$$

with $\Lambda = \mathrm{diag}(\lambda_k)$ the original wave speeds and $\Lambda^*=\mathrm{diag}\ (\lambda_k^*)$ are the modified ones.

In 2D, the preconditioned system takes the form

$$P^{-1}\underline{w}_t + A\underline{w}_x + B\underline{w}_y = 0$$

$$\underline{w}_t + PA\underline{w}_x + PB\underline{w}_y = 0 \qquad (3.10.9)$$

Choosing a matrix P such that $PA= A^*$ possesses certain features, eg a desirable eigenstructure, completely determines B^*, $B^*=PB$. Upon the

one-dimensional choice (3.10.5) $P=A^{-1}$

$$B^{*} = A^{-1}B \tag{3.10.10}$$

The modifications proposed in section (3.5) are in a sense more general than the class of preconditioned system of the form (3.10.9), and are equivalent to

$$\underline{w}_t + P_1 A \underline{w}_x + P_2 B \underline{w}_y = 0 \tag{3.10.11}$$

where P_1 and P_2 are not necessarily identical. Obviously choosing $P_1=P_2$ ensures that in the steady state, the system is fully conservative. This property is lost under the present modifications (see section (3.9)), which take care of the details of the transient phase ie conforming to a strict physically 'realistic' wave pattern, at the expense of not maintaining conservation.

(4.1) Gradual Wave Attenuation in 1D - The Continuous Level

One dimensional disturbances maintain a constant profile as they propagate, unless they interact with one another (eg a rarefaction fan overtaking a shock wave). In contrast, multi-dimensional disturbances decay as they move away from the origin (like $r^{-1/2}$ in 2D and r^{-1} in 3D) and tend to zero strength as they approach infinity. Placing the far field boundaries at a large distance usually renders all boundary statements more accurate and results in weaker reflections. An attractive far field modification is to force the waves to decay to their far field values more rapidly than they naturally do, thus avoiding the need for large computational domains and excessive costs.

If the 1D wave equation

$$\varphi_{tt} - \lambda^2 \varphi_{xx} = 0 \tag{4.1.1}$$

with solutions

$$\varphi(x,t) = \alpha e^{i\omega(t+x/\lambda)} + \beta e^{i\omega(t-x/\lambda)} \tag{4.1.2}$$

is replaced in the far field by

$$\varphi_{tt} - \lambda^2 \varphi_{xx} + 2c\varphi_t + c^2\varphi = 0 \tag{4.1.3}$$

it now possesses solutions

$$\varphi(x,t) = \alpha e^{cx/\lambda} e^{i\omega(t+x/\lambda)} + \beta e^{-cx/\lambda} e^{i\omega(t-x/\lambda)} \tag{4.1.4}$$

representing one dimensional waves exponentially attenuated in space. The rate of attenuation, determined by the value of c, is the same for all frequencies ω, so that the propagating wave does not distort or disperse. The resulting interface problem is

$$\varphi_{tt} - \lambda^2\varphi_{xx} + 2c_1\varphi_t + (c_1)^2\varphi = 0 \qquad x<0$$

$$\varphi_{tt} - \lambda^2\varphi_{xx} + 2c_2\varphi_t + (c_2)^2\varphi = 0 \qquad x>0 \qquad (4.1.5)$$

$$[\varphi]_{x=0} = [\partial\varphi/\partial x]_{x=0} = 0$$

Respective solutions are

$$\varphi(x,t) = \alpha_1 e^{c_1 x/\lambda}\, e^{i\omega(t+x/\lambda)} + \beta_1 e^{-c_1 x/\lambda}\, e^{i\omega(t-x/\lambda)} \qquad x<0$$

$$\varphi(x,t) = \alpha_2 e^{c_2 x/\lambda}\, e^{i\omega(t+x/\lambda)} + \beta_2 e^{-c_2 x/\lambda}\, e^{i\omega(t-x/\lambda)} \qquad x>0 \qquad (4.1.6)$$

Continuity at the interface reads

$$\alpha_1 + \beta_1 = \alpha_2 + \beta_2$$

$$\alpha_1 - \beta_1 = \frac{c_2 + i\omega}{c_1 + i\omega}\ (\alpha_2 - \beta_2) \qquad (4.1.7)$$

A right running wave approaching x=0 from the left has

$$\alpha_1 = R \qquad \alpha_2 = 0$$
$$\beta_1 = 1 \qquad \beta_2 = T$$

Solving for T and R we obtain

$$T = \frac{2(c_1 + i\omega)}{c_1 + c_2 + 2i\omega}$$

$$R = \frac{c_1 - c_2}{c_1 + c_2 + 2i\omega} \qquad (4.1.8)$$

If $c_1 \neq c_2$, T and R are both complex expressions indicating that right moving waves undergo a change of phase across the interface. Note also that

$$|T|^2 = \frac{4(c_1)^2 + 4\omega^2}{(c_1+c_2)^2+4\omega^2} \tag{4.1.9}$$

and for $c_1 < c_2$, $|T| < 1$ consistent with the choice of attenuation rates. By symmetry we have for left running waves

$$T = \frac{2(c_2 + i\omega)}{c_1 + c_2 + 2i\omega}$$
$$R = \frac{c_2 - c_1}{c_1 + c_2 + 2i\omega} \tag{4.1.10}$$

Allowing c to vary with the space coordinate x in a, say, piecewise constant manner, gradually increases the rate of decay but at the same time creates more interfaces across each of which partial reflections occurs.

This was the approach taken by Kosloff and Kosloff in [46], and its main drawbacks are:(a) Waves are not fully transmitted across interfaces, (b) As the distinction is not made between incoming and outgoing waves, the same attenuation rate is applied to both, which immediately renders this modification inapplicable to a certain class of time dependent problems as discussed in the introduction to Part II. In the next section an alternative modification is proposed which is advantageous in both those respects.

(4.2) A Remedy to Partial Reflections at Interfaces

As seen in Chapter III, a better way to go about the problem of partial reflections is by considering first order systems instead of second order scalars.

If the advection equation (1.2.1) with solution (1.2.2) is replaced by

$$w_t + \lambda w_x + c\lambda w = 0 \tag{4.2.1}$$

it now possesses solutions

$$w(x,t) = e^{-cx} f(x-\lambda t) \tag{4.2.2}$$

This readily generalizes to first order systems. The system

$$\underline{w}_t + A\underline{w}_x = 0$$

with solutions

$$\underline{w}(x,t) = \sum_{k=1}^{N} \alpha_k e^{i\omega(t-x/\lambda_k)} \underline{r}_k \tag{4.2.3}$$

is replaced by

$$\underline{w}_t + A\underline{w}_x + C\underline{w} = 0 \tag{4.2.4}$$

The matrix C is chosen so that solutions are now of the form

$$\underline{w}(x,t) = \sum_{k=1}^{N} \alpha_k e^{-c_k x} e^{i\omega(t-x/\lambda_k)} \underline{r}_k \tag{4.2.5}$$

By considering simple wave solutions it is found that C should possess same eigenvectors as A, with respective eigenvalues $\Delta = \mathrm{diag}(c_k\lambda_k)$. It can thus be easily constructed

$$C = R\Delta R^{-1} \tag{4.2.6}$$

with R the matrix of eigenvectors of A. The resulting interface problem reads

$$\begin{aligned} &\underline{w}_t + A\underline{w}_x + C_1\underline{w} = 0 && x<0 \\ &\underline{w}_t + A\underline{w}_x + C_2\underline{w} = 0 && x>0 \\ &[\underline{w}]_{x=0} = 0 \end{aligned} \qquad (4.2.7)$$

with

$$C_1 = R\Delta_1 R^{-1} \qquad \Delta_1 = \text{diag}\,(c_k\lambda_k)$$

$$C_2 = R\Delta_2 R^{-1} \qquad \Delta_2 = \text{diag}\,(d_k\lambda_k)$$

The respective solutions are

$$\begin{aligned} \underline{w}(x,t) &= \sum_{k=1}^{N} e^{-c_k x}\, \alpha_k(t-x/\lambda_k)\, \underline{r}_k && x<0 \\ \underline{w}(x,t) &= \sum_{k=1}^{N} e^{-d_k x}\, \beta_k(t-x/\lambda_k)\, \underline{r}_k && x>0 \end{aligned} \qquad (4.2.8)$$

Continuity requirement becomes

$$\sum_{k=1}^{N} \alpha_k(t)\, \underline{r}_k = \sum_{k=1}^{N} \beta_k(t)\, \underline{r}_k \qquad (4.2.9)$$

Uniqueness of representation again implies

$$\alpha_k(t) = \beta_k(t) \qquad k = 1,\ldots,N$$

and full transmission of all waves is established.

Like in the previous chapter, formulating the problem as a first order system rather than as a second order scalar, offers a wider choice of far field modifications as a count of degrees of freedom will confirm. Some of these modifications are no longer equivalent to

a modified wave equation, including the one presented here. The proposed modification appears advantageous to the one in [46] in two respects:

(a) Full transmission of the analytic solution is guaranteed by construction.

(b) Different attenuation rates may be chosen for different simple waves, including the choice of not attenuating certain waves at all. Thus we can identify and selectively damp the outgoing waves only.

(4.3) Gradual Wave Attenuation in 1D - The Discrete Level

The analysis required in this section is nearly identical to the one carried out in section (3.3), and will therefore be discussed very briefly. The problem to analyse is

$$\begin{aligned} &u_t + \lambda u_x + \lambda c_1 u = 0 && x<0 \\ &u_t + \lambda u_x + \lambda c_2 u = 0 && x>0 \\ &[u]_{x=0} = 0 \end{aligned} \qquad (4.3.1)$$

which is approximated by

$$\begin{aligned} &u_j^n = \sum_{k=-l}^{r} \alpha_k u_{j+k}^n && j\le 0 \\ &v_j^n = \sum_{k=-L}^{R} \beta_k v_{j+k}^n && j>0 \\ &u_j^n = v_j^n && j = -L+1,\ldots,r \end{aligned} \qquad (4.3.2)$$

First and foremost stability of (4.3.2) needs to be established. Only then the question of reflections may be addressed. As pointed out, full transmission of discrete waves across an interface does not automatically follow from full transmission of continuous waves, and in fact in most circumstances, discrete waves do suffer partial, though weak, reflections. This is due to the increased number of modes admitted by the discrete dispersion relation.

As shown in section (3.3), if $(4.3.2)_a$ and $(4.3.2)_b$ are both dissipative, their match across the interface is stable [10]. In Appendix C, we show that for a particular 3-point approximation to (4.3.1), both $(4.3.2)_{ab}$ are dissipative hence stability follows. We also show that for the same approximation, transmission and reflection coefficients are respectively

$$T = 1 + 0([c]) \qquad (4.3.3)$$

$$R = 0([c])$$

where $[c] = c_2 - c_1$ is the jump in the attenuation rate across the interface.

In practice, however, the reflected part is of small amplitude and of high wave number and is very rapidly damped out. In the numerical results, presented in section (4.6), there is no evidence of any noticeable reflections at all.

(4.4) Gradual Wave Attenuation in 2D

Consider the 2D linearised isentropic Euler equations

$$\underline{w}_t + A\underline{w}_x + B\underline{w}_y = 0 \qquad (4.4.1)$$

$$\underline{w} = \begin{pmatrix} p \\ u \\ v \end{pmatrix} \qquad A = \begin{pmatrix} 0 & 1 & 0 \\ 1 & 0 & 0 \\ 0 & 0 & 0 \end{pmatrix} \qquad B = \begin{pmatrix} 0 & 0 & 1 \\ 0 & 0 & 0 \\ 1 & 0 & 0 \end{pmatrix}$$

Following the derivation in section (3.4), plane wave disturbances in a direction x′ inclined at an angle ϑ to the positive x direction, are governed by the equation

$$\underline{w}_t + M(\vartheta)\underline{w}_{x'} = 0 \tag{4.4.2}$$

$$M(\vartheta) = A\cos\vartheta + B\sin\vartheta = \begin{pmatrix} 0 & \cos\vartheta & \sin\vartheta \\ \cos\vartheta & 0 & 0 \\ \sin\vartheta & 0 & 0 \end{pmatrix}$$

The eigenvectors and eigenvalues of $M(\vartheta)$

$$R(\vartheta) = (\underline{r}_1, \underline{r}_2, \underline{r}_3) = \begin{pmatrix} -1 & 0 & 1 \\ \cos\vartheta & -\sin\vartheta & \cos\vartheta \\ \sin\vartheta & \cos\vartheta & \sin\vartheta \end{pmatrix} \tag{4.4.3}$$

$$\Lambda = \text{diag } (-1,\ 0,\ 1)$$

which by construction recovers the eigenstructure of A for ϑ=0, and that of B for $\vartheta = \frac{\pi}{2}$. Equation (4.4.2) possesses exact solution of the form

$$\underline{w}(x,t) = \sum_{k=1}^{3} \alpha_k e^{i\omega(t-x'(\vartheta)/\lambda_k)} \underline{r}_k(\vartheta) \tag{4.4.4}$$

with $x'(\vartheta) = x\cos\vartheta + y\sin\vartheta$, $\underline{r}_k$ and λ_k given by (4.4.3). In the far field (large x′), (4.4.2) is replaced by

$$\underline{w}_t + M(\vartheta)\underline{w}_{x'} + C(\vartheta)\underline{w} = 0 \tag{4.4.5}$$

and by the one dimensional analysis of section (4.2)

$$C(\vartheta) = R(\vartheta)\Delta R^{-1}(\vartheta) \qquad \Delta = \mathrm{diag}(\lambda_k c_k) \tag{4.4.6}$$

Exact solutions of the modified system are of the form

$$\underline{w}(x,t) = \sum_{k=1}^{3} \alpha_k e^{-c_k x'} e^{i\omega(t-x'/\lambda_k)} \underline{r}_k(\vartheta) \tag{4.4.7}$$

describing plane waves, exponentially attenuated as they propagate in the x′ direction. The matrix $C(\vartheta)$ is given by

$$C(\vartheta) = \begin{pmatrix} \frac{c_3-c_2}{2} & \frac{c_3+c_1}{2}\cos\vartheta & \frac{c_3+c_1}{2}\sin\vartheta \\ \frac{c_3+c_1}{2}\cos\vartheta & \frac{c_3c_1}{2}\cos^2\vartheta & \frac{c_3-c_1}{2}\cos\vartheta\sin\vartheta \\ \frac{c_3+c_1}{2}\sin\vartheta & \frac{c_3-c_1}{2}\cos\vartheta\sin\vartheta & \frac{c_3-c_1}{2}\sin^2\vartheta \end{pmatrix} \tag{4.4.8}$$

The presence of entries in (4.4.8) which are not linear in $\cos\vartheta$ and $\sin\vartheta$ imply that $C(\vartheta)$ cannot be of the simple form

$$C(\vartheta) = A_1\cos\vartheta + B_1\sin\vartheta \tag{4.4.9}$$

unless we choose $c_1=c_2=c$, ie same decay rate for both incoming and outgoing waves. The far field modification in that case reduces to

$$\underline{w}_t + A\underline{w}_x + B\underline{w}_y + c(A\cos\vartheta + B\sin\vartheta)\underline{w} = 0 \tag{4.4.10}$$

However, there is no need to restrict all waves to the same rate of decay and $C(\vartheta)$ can remain in its general form, yielding

$$\underline{w}_t + A\underline{w}_x + B\underline{w}_y + C(\vartheta)\underline{w} = 0 \tag{4.4.11}$$

The choice of ϑ is again problem dependent, and is to coincide with the direction of the main disturbance at each position. (See section (3.1) for details).

It is interesting to note, though perhaps not surprising, that (4.4.11) emerges again, if the equations are modified in one preferred direction, say the x-direction, and then rotated so that the preferred direction coincides with a general direction indicated by ϑ. The modification then takes the form

$$\underline{w}_t + A\underline{w}_x + B\underline{w}_y + T^{-1}C(0)T\underline{w} = 0 \qquad (4.4.12)$$

T is the rotation transformation (3.4.18), $C(0) = R(0)\Delta R^{-1}(0)$ with R(0) given by (4.4.3) setting $\vartheta = 0$, and $\Delta = \text{diag}\,(c_k\lambda_k)$. Explicitly

$$C(0) = \begin{pmatrix} \frac{c_3-c_1}{2} & \frac{c_3+c_1}{2} & 0 \\ \frac{c_3+c_1}{2} & \frac{c_3-c_1}{2} & 0 \\ 0 & 0 & 0 \end{pmatrix} \qquad (4.4.13)$$

and it can be verified that

$$C(\vartheta) = T^{-1}C(0)T \qquad (4.4.14)$$

Finally, since the modification is based on a 1-dimensional argument, we verify that properties are recovered in genuinely quasi one dimensional problems. Indeed, transforming (4.4.11) into cylindrical coordinates (r,ϑ) and assuming axial symmetry, we obtain

$$\begin{pmatrix} p \\ q \end{pmatrix}_t + \begin{pmatrix} 0 & 1 \\ 1 & 0 \end{pmatrix} \begin{pmatrix} p \\ q \end{pmatrix}_r + \begin{pmatrix} \frac{c_3-c_1}{2} & \frac{c_3+c_1}{2} + \frac{1}{r} \\ \frac{c_3+c_1}{2} & \frac{c_3-c_1}{2} \end{pmatrix} \begin{pmatrix} p \\ q \end{pmatrix} = 0 \qquad (4.4.15)$$

here $q = u\cos\vartheta + v\sin\vartheta$ is the velocity in the radial direction. Equation (4.4.14) has general solutions of the form

$$\begin{pmatrix} p \\ q \end{pmatrix} = \alpha_1 e^{-c_1 r} \frac{f(t+r)}{\sqrt{r}} \begin{pmatrix} 1 \\ -1 \end{pmatrix} + e^{-c_3 r} \frac{f(t-r)}{\sqrt{r}} \begin{pmatrix} 1 \\ 1 \end{pmatrix} + O\begin{pmatrix} 1 \\ \overline{r^2} \end{pmatrix}$$

representing travelling waves in the positive and negative radial direction which, which in addition to their natural decay, are further exponentially attenuated with decay rates c_1 and c_3.

(4.5) Combination of the Two Approaches

The two proposed far field modifications (a) slowing down and (b) gradually attenuating the outgoing waves, are clearly closely linked to one another. The respective modifications are constructed to conform to a desirable far field wave structure. In both cases the outgoing waves are identified using characteristic field decomposition. Preservation of simple wave structure ensures full transmission of all waves across interfaces. Both approaches can be combined into a single far field modification under which the outgoing waves are slowed down and attenuated at the same time.

Indeed, the 1D system

$$\underline{w}_t + A^* \underline{w}_x + C^* \underline{w} = 0 \qquad (4.5.1)$$

$$A^* = R\Lambda^* R^{-1} \qquad \Lambda^* = \mathrm{diag}(\lambda_k^*)$$

$$C^* = R\Delta^* R^{-1} \qquad \Delta^* = \mathrm{diag}(c_k \lambda_k^*)$$

where the λ_k^* are the modified speeds and c_k are the attenuation rates, possesses exact solutions

$$\underline{w}(x,t) = \sum_{k=1}^{N} e^{-c_k x} \alpha_k(t-x/\lambda^*)\ \underline{r}_k \qquad (4.5.2)$$

and full transmission of all waves is easily verified. In two space dimensions, consider the system

$$\underline{w}_t + A^*\underline{w}_x, + B^*\underline{w}_y, + C^*\underline{w} = 0 \qquad (4.5.3)$$

with A^* and B^* given by any of the modifications of section (3.5), R, λ_k^* and c_k are the eigenvectors, the modified speeds and the attenuation rates in the x'-direction respectively and

$$C^* = R\Delta^* R^{-1} \qquad \Delta^* = \text{diag}\ (c_k\lambda_k^*)$$

Viewed from the x and y fixed set of coordinates, equations (4.5.3) take the form

$$\underline{w}_t + A^{**}\underline{w}_x + B^{**}\underline{w}_y + C^{**}\underline{w} = 0 \qquad (4.5.4)$$

$$A^{**} = T^{-1}(A^*\cos\vartheta - B^*\sin\vartheta)T$$

$$B^{**} = T^{-1}(A^*\sin\vartheta + B^*\cos\vartheta)T$$

$$C^{**} = T^{-1}C^*T$$

T is given by (3.4.18). Numerical results for the combined far field modification in both one and two space dimensions are presented in the next section.

(4.6) Numerical Experiments

(4.6.1) One Dimensional Tests

In the following one dimensional tests, it is assumed that the RHB is the artificial boundary and waves travelling from left to right are accordingly outgoing.

Test A (Figure (IV.1)a-c)

The governing equation is the advection equation (4.2.1) with initial data

$$w(x,0) = e^{-\sigma(x-x_0)^2} \tag{4.6.1}$$

The numerical scheme is a LW adaptation to (4.2.1)

$$w_j^{n+1} = w_j^n - \frac{\nu}{2}\left(w_{j+1}^n - w_{j-1}^n\right) + \frac{\nu^2}{2}\left(w_{j+1}^n - 2w_j^n + w_{j-1}^n\right)$$

$$- c\Delta t\left(1 - \frac{1}{2}\Delta tc\right)w_j^n + \nu c\Delta t\left(w_{j+1}^n - w_{j-1}^n\right) \tag{4.6.2}$$

The interface is located at a given grid point $j=j_0$ to the right of which waves are attenuated. Results are for $c = 0.00, 0.01, 0.02$. Reflections from the interface, although theoretically present, are unnoticeable. By the time the wave has reached the RHB, it is of practically zero strength.

Test B (Figure (IV.2))

The governing equations are the 1D wave equation written as a first order system

$$\underline{w}_t + A\underline{w}_x + C\underline{w} = 0$$

$$C = R\Delta R^{-1} \qquad \Delta = \mathrm{diag}(c_k\lambda_k) \tag{4.6.3}$$

The method of solution is Roe's field decomposition, with LW scheme applied to each characteristic field. The non-homogeneous term in (4.6.3) is projected onto the eigenvectors of A, generating waves of strengths

$$\beta_1 = -c_1\frac{p-u}{2} \qquad \beta_2 = c_2\frac{p+u}{2}$$

Initial data is

$$\begin{pmatrix} p \\ u \end{pmatrix} = e^{-\sigma(x-x_0)^2}\begin{pmatrix} 1 \\ 1 \end{pmatrix} + e^{-\sigma(x-x_1)^2}\begin{pmatrix} 1 \\ -1 \end{pmatrix} \tag{4.6.4}$$

The left running wave is undamped c_1=0.0, while the damping coefficient for the right moving wave is c_2 = 0.02.

Test C (Figure (IV.3)a,b)

The governing equations are the modified 1D isothermal Euler equations (3.9.9)

$$\underline{w}_t + A(\underline{w})\underline{w}_x + C(\underline{w})(\underline{w}-\underline{w}_\infty) = 0 \tag{4.6.5}$$

The method of solution is the same as in Test B, for which

$$\beta_1 = c_1(u-c)[(\rho-\rho_\infty)c - \rho_\infty(u-u_\infty)]/2c$$

$$\beta_2 = c_2(u+c)[(\rho-\rho_\infty)c + \rho_\infty(u-u_\infty)]/2c \tag{4.6.6}$$

Initial data is

$$\rho(x,0) = \rho_\infty + e^{-\sigma(x-x_0)^2}$$

$$u(x,0) = \pm\, c\cdot\log(\rho/\rho_\infty)$$

giving rise to a right (left) running compression wave gradually steepening up to form a shock wave. Damping coefficients are

$$c_1 = 0.00,\ c_2 = 0.03.$$

Consequently, the right moving wave (figure (IV.3)a) is damped out before the shock wave has been formed. Note that the steepening up and propagation of the left moving wave (figure (IV.3)b) is not affected by the far field modification.

(4.6.2) Two Dimensional Tests

Test D (figures (IV.4)a-d, (IV.5)a,b)

The governing equations are the 2D linearised Euler equations (4.4.11) with initial data (compare section (3.8.2) Test A)

$$p(x,y,0) = e^{-\sigma(x^2+y^2)}$$

$$u(x,y,0) = v(x,y,0) = 0.0$$

The numerical algorithm uses a two stage space operator splitting. In each direction Roe's field decomposition is performed. The rate of attenuation of the outgoing waves is

$$c_3 = 0.0,\ 0.01,\ 0.02,\ 0.03$$

resulting (figure (IV.4)) in strong decay of the outgoing wave. Figure (IV.5) shows the evolution with time of pressure profiles along the main diagonal for the same problem, with $c_3 = 0.00,\ 0.03$.

Test E (Figure (IV.6)a,d)

The two far field modifications are combined. The same test problem is repeated with

slowing down coefficient	$a = 0.8$
attenuation rates	$c_3 = 0.0, 0.01, 0.02, 0.03$

Test F (Figures (IV.7),(IV.8))

In this test, the steady state solution for flow past a circular arc in sought by means of integrating the 2D unsteady Euler equations until convergence is obtained (nodal changes $\leq 10^{-6}$). The circular arc is of normalised 1 unit length and of 10% thickness.

Grid features: The numerical grid is aligned with the arc with 32 evenly spaced cells on the bump and 16 linearly stretching cells over one chord length to either side of the bump and in the vertical direction, at a stretching ratio of 3. This part of the grid remains unchanged. To obtain a larger domain of computation, additional points are inserted, using geometric expansion at a rate of 10% on either side of the basic grid and in the vertical direction (See Ill. (IV.1)).

The method of solution and BCS: The method of solution is Hall's variation of Ni's scheme [29], which is a cell vertex scheme with LW time integration. In all tests, the far field boundaries are subsonic. The boundary procedures used are the ones recommended by Hall, adapted to the extended 4×4 system. At inflow, tangential velocity, entropy and specific enthalpy are specified and normal velocity is extrapolated using one-sided version of the interior scheme. At outflow, velocity components and enthalpy are extrapolated using the interior scheme and pressure in specified. On the solid wall, a simple tangency condition is applied [29].

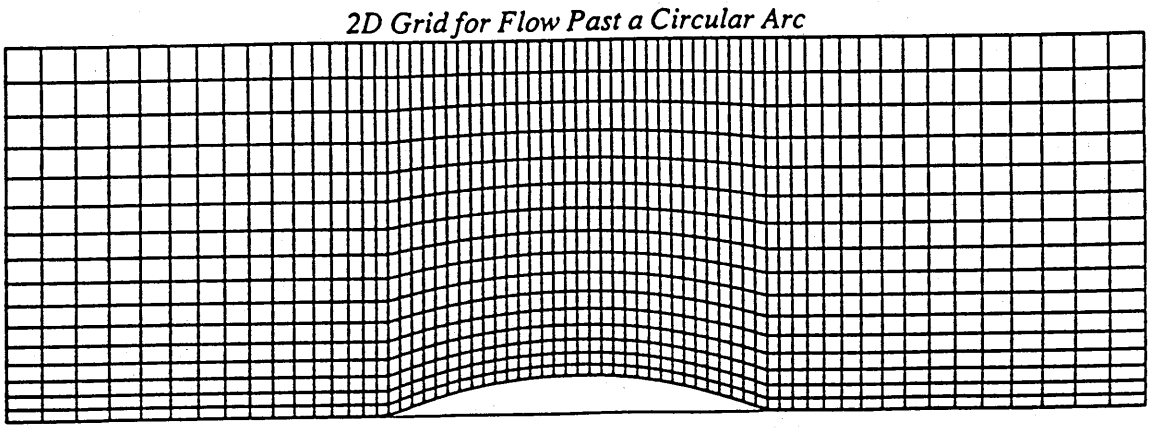

111. (IV.1) - Numerical grid for 2D flow past a circular arc

'Accuracy' study: To assess the effect of the far field boundary procedures on the accuracy of the converged solution, a series of tests were conducted with varying boundary distances. The solution is considered 'accurate' when further enlargement of the domain gives rise only to small changes (of order 10^{-4}) in the converged values of the computed drag and lift coefficients

$$C_D = \sum_i \frac{(p_i - p_\infty)\Delta y_i}{\rho_\infty u_\infty^2}$$

$$C_L = \sum_i \frac{(p_i - p_\infty)\Delta x_i}{\rho_\infty u_\infty^2}$$

Numerical tests: Fully subsonic (M_∞= 0.5) and transonic (M_∞= 0.75) tests were conducted. The results are summarised in the table below. Note that the overall number of iterations increases with the grid size. This is due to the increased number of error modes that need to be damped before steady state can be reached. Yet, the amount of work per node decreases, which is partly a result of the far field BCS becoming more accurate as the boundaries are moved further out.

Solution of tests (5) and (11) were considered accurate and are depicted in figures (IV.1) and (IV.2) respectively.

Test Number	Boundary distance	Numerical grid size	C_L	C_D	No. of iterations to steady state
M_∞= 0.5					
1	1.0	65×17	-0.281787	0.001360	5390
2	2.64355	85×27	-0.313781	0.000478	5168
3	4.70732	97×33	-0.317904	0.000363	6358
4	6.90649	105×37	-0.318964	0.000353	6503
5	10.12629	113×41	-0.319406	0.000358	6418
6	12.25938	117×43	-0.319529	0.000342	6289
M_∞= 0.75					
7	1.0	65×17	-0.355310	0.005332	1673
8	2.64355	85×27	-0.437400	0.012209	3919
9	4.70732	97×33	-0.450744	0.013626	4540
10	6.90649	105×37	-0.460982	0.014580	5342
11	10.12629	113×41	-0.462811	0.014788	5528
12	12.25938	117×43	-0.463335	0.014851	5879

Tabel (4.6.1) - Converged values against boundary distance

Gradual far field damping was applied to tests (5) and (11), and the influence of boundary thickness and rate of attenuation was studied (See Tables (4.6.2)a,b). In the tables, Boundary Thickness indicates the number of points across the modified region; Direction of Modification indicates the direction in which waves were damped (X for inflow and outflow boundaries and Y for top boundary). Table (4.6.2)a is for the transonic case, M_∞= 0.75, and Table (4.6.2)b is for the subsonic case, M_∞= 0.5. The first line in each table refers to the case where no far-field damping was applied, and should serve to assess the performence of the far-field boundary treatment. In all cases, the far field damping accelerates convergence to steady state. Comparison of Test (1) and Test (6) in Table (a) reveals that in the transonic case the Number of Iterations to steady state was considerably reduced by some 35%. Relative changes in c_N were far less than 1% and those in c_D were within 2%. Absolute changes in both

were far less than 1%. These very small changes in the solution may be attributed to very weak reflection mechanisms due to change of coefficients in the far field. In the fully subsonic case, the number of iterations dropped quite dramatically by over 60% (compare Test (1) and Tests (3) and (4) in Table (b)), while the normal force and drag coefficients changed by less than 1%. While far-field damping is relatively insensitive to the damping strength and to the boundary thickness, its efficiency in accelerating convergence depends strongly on the direction of modification. The results indicate that it is mostly reflections from the top boundary that inhibit convergence while inflow and outflow boundaries generate weaker reflection mechanisms. Applying far-field damping in both X-Y directions proved best in both transonic and subsonic cases. An explanation as to why far-field damping is more efficient in the subsonic case than it is in the transonic case, is provided by noting that reflections from far-field boundaries are only one of the mechanisms that inhibit convergence to steady state. The formation of shock waves is another such mechanism. Convergence rate in the transonic case is influenced by both mechanisms, hence the reduced effect of far-field damping.

Test No.	Damping Coef.	Boundary Thickness	Dir. of Mod.	Number of Iterations	C_N	C_D
1	0.0	0	-	5528	-.46281	.01479
2	0.5	6	X	5886	-.46443	.01515
3	0.5	6	Y	4799	-.46116	.01462
4	0.4	5	Y	4926	-.46158	.01466
5	0.6	5	Y	4884	-.46144	.01465
6	0.5	6	X-Y	3621	-.46355	.01510
7	0.4	6	X-Y	3646	-.46355	.01510

Table (4.6.2)a - Parameter study of far-field damping
Transonic case.

Test No.	Damping Coef.	Boundary Thickness	Dir. of Mod.	Number of Iterations	C_N	C_D
1	0.0	0	-	6418	-.31941	.00036
2	0.5	6	X	5573	-.31976	.00036
3	0.5	6	X-Y	2404	-.32007	.00036
4	0.4	6	X-Y	2418	-.32005	.00036
5	0.5	6	Y	3192	-.31985	.00036
6	0.4	5	Y	3383	-.31995	.00036
7	0.5	5	Y	3352	-.31997	.00037

Table (4.6.2)b - Parameter study of far-field damping
Subsonic case.

CONCLUSIONS

This work was devided into two parts.

In PART I, the problem of far-field artificial boundaries, arising in external flow calculation, was introduced and discussed. The conventional approach for treating far-field boundaries, namely deriving BCS of absorbing type, was presented. Mathematical backgroung in the theories of *Well-Posedness* and *Stability* of mixed IBVPs was also presented, familiarity with which is necessary for understanding the philosophy in constructing such BCS. A survey of existing recipes for absorbing BCS was conducted. PART I concluded with a thorough numerical study of the efficiency of several, widely used, BCS, in absorbing outgoing disturbances. The performance of these BCS strongly depends on key numerical parameters such as local CFL number, local wave number and grid stretching. This dependence was theoretically analysed and computationally studied. The limitations of all boundary recipes were exposed. It was found that under conditions prevailing in the far-field, ie small CFL numbers and small local wave numbers, strong reflections may occur and that grid stretching tends to enhance reflection mechanisms. Although classified as higher-order effects, these reflections may reach intolerable levels as demonstrated by the numerical results.

In view of these results, PART II presented a less conventional approach for treating reflections from artificial boundaries, which to some extent circumvents the problem of reflections from the boundary itself. It was proposed to introduce an outer 'sponge' layer of one-way absorbing character, in which the governing equations are modified to conform to a desirable far-field behaviour. Two such far-field modifications were presented: (a) Slowing down the outgoing waves and (b) Damping the outgoing waves. The two are closely related in that both require very similar chracteristic field analysis and make use of simply wave theory. Under the proposed modifications, the propagation of the incoming waves is unaltered while the outgoing

waves either do not reach the boundary (a), or by the time they do so, they are of practically zero strength (b). Reflections from the actual boundaries are thus avoided. Conditions were derived to ensure that no reflections are generated at interfaces due to change of coefficients in the governing equations. The modifications were analysed and were shown to be mathematically well-posed and numerically stable. They were extended to 2D and tested in a variety of 1D and 2D time-dependent test problems. Both were found to offer gains in accuracy of transient solutions, due to reduced levels of reflections from far-field boundaries. Although originally designed for time-dependent problems, far-field damping was successfully applied to 2D steady-state Euler calculations and was found to dramatically accelerate convergence of transient solutions to steady-state leading to costs reductions of between 35%-60%. Far-field damping is expected to accelerate convergence to steady-state, probably in a less dramatic way, when combined with other acceleration strategies such as multigrid and enthalpy damping. Finally, the proposed modifications can be extended to 3D along very similar lines to the 2D extentions and if fact retain a very similar structure.

LIST OF REFERENCES

(1) Bamberger A.,Engquist B., Halpern L. and Joly P., (1988) *SIAM J Appl. Maths.*, 48, p. 99, "Parabolic wave equation approximations in heterogeneous media".

(2) Bamberger A.,Engquist B., Halpern L. and Joly P., (1988) *SIAM J Appl. Maths.*, 48, p. 129, " Higher order paraxial wave equation approximations in heterogeneous media".

(3) Barry A., Bielak J. and MacCamey R.C., (1988), *J Comp Phys*, 79, pp. 449-468, " On absorbing boundary conditions for wave propagation".

(4) Bayliss A. and Turkel E., (1980), *Comm Pure Appl Maths*, 33, pp. 707-725, " Radiation boundary conditions for wave-like equations".

(5) Bayliss A. and Turkel E., (1982), *J Comp Phys*, 48, pp. 182-199, " Far field boundary conditions for compressible flows".

(6) Bayliss A., Gunzburger M. and Turkel E., (1982), *SIAM J Appl Maths*, 42, pp. 430-451, " Boundary conditions for the numerical solution of elliptic equations in exterior regions".

(7) Brillouin L., (1960), " Wave Propagation and Group Velocity", Academic Press, New York and London.

(8) Brown D.L., (1984), *Maths of Comp*, 42, pp. 369-391, " A note on the numerical solution of the wave equation with piecewise smooth coefficients".

(9) Burgess N.A., (1986), Oxford University Computing Laboratory, Report No. 86/2. " The stability of a simple IBVP".

(10) Ciment M., (1972), *SIAM J Num Anal*, 9, pp. 695-701, " Stable matching of difference schemes".

(11) Clayton R. and Engquist B., (1977), *Bull Seism Soc of America*, 67, pp. 1529-1540, " Absorbing boundary conditions for acoustic and elastic wave equations".

(12) Courant R., (1936), Differential and Integral Calculus, Vol. 2, Blackie and Sons Ltd.

(13) Emerman S.H. and Stephen R.A., (1983), *Bull Seism Soc of America*, 73, pp. 661-665, " Comment on 'Absorbing boundary conditions for acoustic and elastic wave equations' by Clayton and Engquist".

(14) Engquist B. and Majda A., (1977), *Maths of Comp*, 31, pp. 629-651, " Absorbing boundary conditions for the numerical simulation of waves".

(15) Engquist B. and Majda A., (1979), *Comm Pure Appl Maths*, 32, pp. 313-357, " Radiation boundary conditions for acoustic and elastic wave calculations".

(16) Engquist B. and Majda A., (1981), *J Comp Phys*, 40, pp. 91-103, " Numerical radiation boundary conditions for unsteady transonic flow".

(17) Ferm L., (1988), *J Comp Phys*, 78, pp. 94-113, " Open boundary conditions for stationary inviscid flow problems".

(18) Ferm L. and Gustafsson B., (1982), *Computers and Fluids*, 10, pp. 261-276, " A downstream boundary procedure for the Euler equations".

(19) Fix G.J. and Marin S.P., (1978), *J Comp Phys*, 28, pp. 253-270, " Variational methods for underwater acoustic problems".

(20) Giles M., (1988), MIT CFD Laboratory, CFDL-TR-88-1,

" Nonreflecting boundary conditions for the Euler equations".

(21) Giles M. and Thompkins K.W., (1984), *Adv Comput Meth for PDE's*, (R. Vicnevetsky and R.S. Stepleman eds), V Pub. IMACS, pp. 322-328, " Internal reflections due to nonuniform grids".

(22) Goldberg M. and Tadmor E., (1981), *Maths of Comp*, **36**, pp. 603-626, " Scheme independent stability creteria for difference approximations of hyperbolic IBVP's II".

(23) Gottlieb D. and Gustafsson B., (1976), *Stud in Appl Maths*, **11**, p. 167.

(24) Grosch C.E. and Orszag S.A. (1977), *J Comp Phys*, **25**, pp. 273-296, " Numerical solution of problems in unbounded regions: Coordinate transforms".

(25) Gustafsson B., (1988), *Appl Num Maths*, **4**, pp. 3-19, " Inhomogeneous conditions at open boundaries for wave propagation problems".

(26) Gustafsson B. and Kreiss H-O, (1979), *J Comp Phys*, **30**, pp. 333-351, " Boundary conditions for time dependent problems with artificial boundaries".

(27) Gustafsson B. Kreiss H-O and Sundström A., (1972), *Maths of Comp*, **26**, pp. 649-686, " Stability theory of difference approximations for mixed IBVP's II ".

(28) Hagstrom T. and Hariharan S.I., (1988), *Maths of Comp*, **51**, pp. 581-597, " Accurate boundary conditions for exterior problems in gas dynamics".

(29) Hall M.G. (1985), Numerical Methods for Fluid Dynamics II, K.W. Morton and M.J. Baines eds., Oxford University Press, pp. 303-345, " Cell-vertex multigrid schemes for solutions of the Euler equations".

(30) Halpern L., (1982), *Maths of Comp*, 38, pp. 415-429, " Absorbing boundary conditions for the discretization schemes of one dimensional wwave equations".

(31) Halpern L. and Trefethen L.N., (1986), MIT Numerical Analysis Reprort No. 86-5, " Wide-angle one way wave equations". (Also in *J Acous Soc of America*).

(32) Harten A., (1983), *J Comp Phys*, **49**, pp. 357-393, " High resolution schemes for hyperbolic conservation laws"

(33) Hedstrom G.W., (1979), *J Comp Phys*, 30, pp. 222-237, " Nonreflecting boundary conditions for nonlinear hyperbolic systems".

(34) Higdon R.L., (1986), *SIAM Review*, 28, pp. 177-217, " Initial boundary value problems for hyperbolic systems".

(35) Higdon R.L., (1986), *Maths of Comp*, **47**, pp. 437-459, " Absorbing boundary conditions for difference approximations to the multidimensional wave equation".

(36) Higdon R.L., (1987), *Maths of Comp*, **49**, pp. 65-90, " Numerical absorbing boundary conditions for the wave equation".

(37) If F., Berg P., Christiansen P.L. and Skovgaard O., (1987), *J Comp Phys*, 72, pp. 501-503, " Split-step spectral method for nonlinear Schrödinger equation with absorbing boundaries".

(38) Iserles A., (1986), *IMA J Num Anal*, 6, pp. 381-392, " Generalized Leap-Frog methods".

(39) Jameson A., (1982), Numerical Methods in Aeronautical Fluid Dynamics (P.L. Roe ed), Accademic Press, pp. 289-308, " Transonic Aerofoil calculations using the Euler equations".

(40) Jameson A., Schmidt W. and Turkel E., (1981), AIAA Paper No. 81-1259, " numerical solution of the Euler equations by finite volume methods using Runge-Kutta time stepping schemes".
(41) Jespersen D.C., (1985), *Appl Num Maths*, 1, pp. 363-456, " Enthalpy damping for the steady Euler equations".
(42) Jiang H. and Wong Y.S., (1989), NASA Technical Memorandum 102009, ICOMP-89-7, " Absorbing boundary conditions for second order hyperbolic equations".
(43) Karni S., (1987), Cranfield Institute of Technology, CoA Report No. 8711, " Far field behaviour and far field boundary conditions - A numerical study".
(44) Karni S., (1987), Cranfield Institute of Technology, CoA Report No. 8721, " The problem of far field boundaries - Slowing down the outgoing waves".
(45) Karni S., (1988), Cranfield Institute of Technology, CoA Report No. 8816, "One way absorbing boundaries by gradual wave attenuation".
(46) Kosloff R. and Kosloff D., (1986), *J Comp Phys*, 63, pp. 363-376, " Absorbing boundaries for wave propagation problems".
(47) Kreiss H-O, (1968), *Maths of Comp*, 22, pp. 703-714, " Stability theory for difference approximations of IBVP's I ".
(48) Kreiss H-O, (1970), *Comm Pure Appl Maths*, 23, pp. 277-298, " IBVP's for hyperbolic systems".
(49) Kwak D., (1980), AIAA Paper No. 80-1393, " Nonreflecting far field boundary conditions for unsteady transonic flow".
(50) Kwak D. (1981), Symposium on Numerical Boundary Condition Procedures NASA Ames Research Centre, pp. 21-44, " A comparative study of nonreflecting far field boundary conditions for unsteady transonic flow computations".
(51) Lindman E.L., (1975), *J Comp Phys*, 18, pp. 66-78, " 'Free-space' boundary conditions for the time dependent wave equation".
(52) MacCormack R.W., (1969), *AIAA Paper 69-354*, " The effect of viscosity in hypervelocity impact cratering".
(53) Mahrer K., (1986), *Geophysics*, 51, pp. 1499-1501, " An empirical study of instability and improvement of absorbing boundary conditions for the elastic wave equation".
(54) Moretti G., (1979), *Computers and Fluids*, 7, p. 191, " The λ-scheme".
(55) NI R-H, (1981), AIAA Paper No. 81-1025, " A multiple grid scheme for solving the Euler equations".
(56) Orlanski I., (1976), *J Comp Phys*, 21, pp. 251-269, " A simple boundary condition for unbounded hyperbolic flows".
(57) Osher S. and Solomon F., (1982), *Maths Comp*, 38, p.339, " Upwind difference schemes for hyperbolic systems of conservation laws".
(58) Paisley M.F., (1986), Oxford University Computing Laboratory, Report No. 86/1, " A comparison of the cell-centre and cell-vertex scheme for the steady Euler equations".
(59) Pike J., (1984), Royal Aircraft Establishment Technical Report No. TR 84104, " Grid-adapted algorithms for the solution of the Euler equations on irregular grids".
(60) Richtmeyer R.D. and Morton K.W., (1967), *Difference Methods for Initial-Value Problems*, second edition, Interscience.
(61) Roe P.L., (1981), *J Comp Phys*, 43, pp. 357-372, " Approximate Riemann solvers, parameter vectors and difference schemes".
(62) Roe P.L., (1982), Numerical Methods for Fluid Dynamics (K.W.

Morton and M.J. Baines eds.), Accademic Press, New York, 219-257, " Fluctuations and signals, a framework for numerical evolution problms".

(63) Roe P.L., (1987), ICASE Reprort No. 87-6, " Error estimates for cell-vertex solutions of the compressible Euler equations".

(64) Roe P.L., (1989), *Computers and Fluids*, 17, pp. 221-231, " Remote boundary conditions for unsteady multidimensional aerodynamic calculations".

(65) Rudy D.H. and Strikwerda J.C., (1980), *J Comp Phys*, 36, pp. 55-70, " A nonreflectinf outflow boundary condition for subsonic N-S calculations".

(66) Rudy D.H. and Strikwerda J.C., (1981), *Computers and Fluids*, 9, pp. 327-338, " Boundary conditions for subsonic compressible N-S calculations".

(67) Smith W.D., (1974), *J Comp Phys*, 15, pp. 492-503, " A nonreflecting plane boundary for wave propagation problems".

(68) Sod G.A., (1978), *J Comp Phys*, 27, p. 1, " A survey of several finite difference methods for systems of non-linear hyperbolic conservation laws".

(69) Sommerfeld A., (1964), " Partial Differential Equations in Physics", Academic Press, New York.

(70) Sommerville D.M.Y., (1946), Analytic Conics, Bell's Mathematical Series, London, G. Bell and Sons (p. 130).

(71) Sweby P.K., (1982), *PhD Thesis*, University of Reading.

(72) Tadmor E., (1983), *Maths of Comp*, 41, pp. 309-319, " The unconditional instability of inflow-dependent boundary conditions in difference approximations to hyperbolic systems".

(73) Thompson K.W., (1987), *J Comp Phys*, 68, pp. 1-24, " Time dependent boundary conditions for hyperbolic systems".

(74) Trefethen L.N., (1982), *SIAM Review*, 24, pp. 113-135, " Group velocity in finite difference schemes".

(75) Trefethen L.N., (1983), *J Comp Phys*, 49, pp. 199-217, " Group velocity interpretation of the stability theory of Gustafsson, Kreiss and Sunström".

(76) Trefethen L.N., (1984), *Comm Pure Appl Maths*, 37, pp. 329-367, " Instability of difference models for hyperbolic IBVP's".

(77) Trefethen L.N., (1985), *Maths of Comp*, 45, pp. 279-300, " Stability of finite difference models containing two boundaries or interfaces".

(78) Trefethen L.N., Pitman Research Notes in Maths Series, No. 140, D.F. Griffiths and G.A. Watson eds, pp. 200-220, " Dispersion, dissipation and stability".

(79) Trefethen L.N. and Halpern L., ( ), " Well-posedness of one way wave equations and absorbing boundary conditions".

(80) Trefethen L.N. and Halpern L., ( ), " New families of one way wave equations and absorbing boundary conditions".

(81) Turkel E., (1985), ICASE Report No. 85-43, " Accuracy of schemes with non uniform meshes for compressible fluid flows".

(82) Turkel E., (1987), *J Comp Phys*, 72, pp. 277-298, " Preconditioned methods for solving the incompressible and low-speed compressible equations".

(83) Van-leer B., (1979), *J Comp Phys*, 32, pp. 101-136, " Towards the ultimate conservative differencing scheme V ".

(84) Vichnevetsky R., (1987), *Intl J Num Meths in Fluids*, 7, pp. 409-452, " Wave propagation analysis of difference schemes for

hyperbolic equations: A review".

(85) Vichnevetsky R. and Pariser E.C., (1985), *Comp & Maths with Appls*, 11, Nos. 1-3, pp. 67-78, " High order numerical Sommerfeld boundary conditions: Theory and experiments".

(86) Vichnevetsky R. and Pariser E.C., (1986), *Num Meths for PDE's*, 2, pp. 1-12, " Nonreflecting upwind boundaries for hyperbolic equations".

(87) Whitham G.B., (1974), Linear and Nonlinear Waves, Wiley Interscience, New York.

(88) Friedrics K.O., (1985), *Comm Pure Appl Maths*, 11, "Symmetric Positive Linear Differential Equations".

Appendix A: Roe's Boundary Conditions

Roe's far field BCS are demonstrated in two simple cases. The reader is referred to [64] for extensions to 2D and 3D Euler equations. The strategy is to obtain one outgoing characteristic equation from global considerations and to substitute it into the governing equations to yield another outgoing characteristic equation. In the case of the 1D wave equation

$$\begin{pmatrix} p \\ u \end{pmatrix}_t + \begin{pmatrix} 0 & 1 \\ 1 & 0 \end{pmatrix} \begin{pmatrix} p \\ u \end{pmatrix}_x = 0 \qquad \text{(A1)}$$

Second differentiation yields $p_{tt} - p_{xx} = 0$. Hence a right moving pressure wave approaching the RHB must be of the form

$$p(x,t) = f(x-t) \qquad \text{(A2)}$$

satisfying

$$p_t + p_x = 0 \qquad \text{(A3)a}$$

Substituting (A3)a into (A1) gives

$$u_t + u_x = 0 \qquad \text{(A3)b}$$

Both (A3)ab are outgoing characteristic equations. Generalized to the 1D Euler equations, (A3) reads

$$\begin{aligned} p_t + (u+c)\,p_x &= 0 \\ u_t + (u-c)\,u_x &= 0 \end{aligned} \qquad \text{(A4)}$$

The 2D linearised Euler equations with axial symmetry read

$$\begin{pmatrix} p \\ q \end{pmatrix}_t + \begin{pmatrix} 0 & 1 \\ 1 & 0 \end{pmatrix} \begin{pmatrix} p \\ q \end{pmatrix}_r + \begin{pmatrix} q/r \\ 0 \end{pmatrix} = 0 \qquad \text{(A5)}$$

Second differentiation shows that

$$p_{tt} - p_{rr} - \frac{1}{r} p_r = 0 \qquad \text{(A6)}$$

An outwardly radiating wave satisfies (to order $(r^{-5/2})$)

$$p_t + p_r + \frac{p-p_\infty}{2r} = 0 \qquad \text{(A8)}_a$$

Substituting into (A5) gives

$$q_t + q_r + \frac{2q - (p-p_\infty)}{2r} = 0 \qquad \text{(A7)}_b$$

Both (A7)_{ab} are outgoing characteristic equations.

Discrete one-sided approximations to either (A3) or (A7) should be stable since they use the correct domain of dependence. No assumptions are required on the state prevailing outside the computational domain.

Appendix B: Adaptation of the LW Scheme to Non Uniform Grids

Let a non-uniform grid be defined by $\Delta x_{j+1} = x_{j+1} - x_j$ and assume that w_j occupies the interval

$$I_j = \frac{\Delta x_{j-1} + \Delta x_j}{2} \tag{B1}$$

Consider the LW approximation to the advection equation (2.2.1)

$$w_j^{n+1} = w_j^n - (\lambda\Delta t/I_j)\left[\alpha_{j-1}(w_j^n - w_{j-1}^n) + \beta_j(w_{j+1}^n - w_j^n)\right] \tag{B2}$$

$$\alpha_j = \frac{1+\nu_j}{2} \qquad \beta_j = \frac{1-\nu_j}{2} \qquad \nu_j = \lambda\Delta t/\Delta x_j$$

Using the consistency relation $\alpha_j + \beta_j \equiv 1$, equation (B2) can be written in conservation form

$$(w_j^{n+1} - w_j^n)I_j = -\Delta t\left(f_{j+\frac{1}{2}}^n - f_{j-\frac{1}{2}}^n\right) \tag{B3}$$

$$f_{j+\frac{1}{2}}^n = \lambda\left(\alpha_j w_j^n + \beta_j w_{j+1}^n\right)$$

and conservation of the marching procedure immediately follows.

Definition:
The scheme is said to be $p^{\underline{th}}$ order accurate if it recovers polynomials of degree p with an error of order $(\Delta x)^{p+1}$.

Let the data be

$$w^n = (x - x_j)^p \tag{B4}$$

For which the exact solution after one time step is

$$(w_e)_j^{n+1} = (-\lambda\Delta t)^p \tag{B5}$$

Substituting (B4) into (B3) gives

$$w_j^{n+1} = (\lambda\Delta t/L_j)\left[-\alpha_{j-1}(-\Delta x_{j-1})^p + \beta_j(\Delta x_j)^p\right] \tag{B6}$$

For $p^{\underline{th}}$ order of accuracy

$$(w_e)_j^{n+1} - w_j^n = O(\Delta x)^{p+1} \tag{B7}$$

For p=1 (B7) is an identity. For p=2 the error is $\Delta x_j^2 - \Delta x_{j-1}^2$, which for a geometric grid expansion

$$\Delta x_{j+1}/\Delta x_j = 1 + O(\Delta x^2) \tag{B8}$$

is $O(\Delta x)^3$. The present adaptation of the LW scheme is therefore conservative and retains second order accuracy on geometrically expanding grids that satisfy (B8).

Appendix C The Discrete Interface Problem

I. Slowing down the outgoing waves

Consider the discrete interface problem

$$w_j^{n+1} = w_j^n - \frac{\nu}{2}\left(w_{j+1}^n - w_{j-1}^n\right) + \frac{\nu^2}{2}\left(w_{j+1}^n - 2w_j^n + w_{j-1}^n\right) \qquad j\le 0$$

$$v_j^{n+1} = v_j^n - \frac{\nu_1}{2}\left(v_{j+1}^n - v_{j-1}^n\right) + \frac{\nu_1^2}{2}\left(v_{j+1}^n - 2v_j^n + v_{j-1}^n\right) \qquad j>0 \tag{C1}$$

$$w_j^n = v_j^n \qquad j=0,1$$

ν and ν_1 are the possibly different CFL numbers to both sides of the interface. A single frequency mode is of the form (3.3.11)

$$w_j^n = Z^n\,(A^- x_1^j + B^- x_2^j) \qquad j\le 0$$

$$v_j^n = Z^n\,(A^+ \mu_1^j + B^+ \mu_2^j) \qquad j>0 \tag{C2}$$

with

$$x_1 = \frac{1}{\nu(\nu+1)}\left[\nu^2 + Z - 1 - \Delta^-\right]$$

$$x_2 = \frac{1}{\nu(\nu+1)}\left[\nu^2 + Z - 1 + \Delta^-\right]$$

$$\mu_1 = \frac{1}{\nu_1(\nu_1+1)}\left[\nu_1^2 + Z - 1 - \Delta^+\right] \tag{C3}$$

$$\mu_2 = \frac{1}{\nu_1(\nu_1+1)}\left[\nu_1^2 + Z - 1 + \Delta^+\right]$$

$$(\Delta^-)^2 = (1-Z)^2 + (2Z-1)\nu^2$$

$$(\Delta^+)^2 = (1-Z)^2 + (2Z-1)\nu_1^2$$

It follows from (C1)3 that

$$\begin{aligned} A^- + B^- &= A^+ + B^+ \\ A^-\varkappa_1 + B^-\varkappa_2 &= A^+\mu_1 + B^+\mu_2 \end{aligned} \tag{C4}$$

A right moving $\varkappa$ mode

$$\begin{aligned} A^- &= R & A^+ &= 0 \\ B^- &= 1 & B^+ &= T \end{aligned} \tag{C5}$$

gives

$$T = \frac{\varkappa_1-\varkappa_2}{\varkappa_1-\mu_2} \qquad R = -\frac{\mu_2-\varkappa_2}{\mu_2-\varkappa_1} \tag{C6}$$

Denote by $[\nu] = \nu_1-\nu$. To first order it follows from (C3) that

$$\mu_2/\varkappa_2 = 1 + c[\nu] + O([\nu])^2$$

$$c = \frac{2\nu+1}{\nu(\nu+1)} - \frac{1+(2Z-1)/2\Delta^-}{\nu^2+Z-1+\Delta^-}$$

Also

$$\begin{aligned} T = \frac{k_1-k_2}{k_1-\mu_2} &= \frac{k_1-k_2}{k_1-(\mu_2/k_2)k_2} \\ &\simeq \frac{\varkappa_1-\varkappa_2}{\varkappa_1-\varkappa_2-c\varkappa_2\Delta[\nu]} \\ &= \left(1-c\,\frac{\varkappa_2}{\varkappa_1-\varkappa_2}\,[\nu]\right)^{-1} \\ &\simeq 1 + c\,\frac{\varkappa_2}{\varkappa_1-\varkappa_2}\,[\nu] \end{aligned} \tag{C7}$$

It follows from (C4)

$$1 + R = T$$

$$R = T-1 = c\,\frac{\varkappa_2}{\varkappa_1-\varkappa_2}\,[\nu] \tag{C8}$$

II Gradual Attenuation of Outgoing Waves

Assume that the finite difference approximation to solve the interface problem (4.3.1) is using time operator splitting with the following two half steps

$$\left.\begin{aligned} &\text{(I)} \quad u_t + \lambda u_x = 0 \\ &\text{(II)} \quad u_t + \lambda c_1 u = 0 \end{aligned}\right\} \qquad x<0$$

$$\left.\begin{aligned} &\text{(I)} \quad v_t + \lambda v_x = 0 \\ &\text{(II)} \quad v_t + \lambda c_2 v = 0 \end{aligned}\right\} \qquad x>0 \tag{C9}$$

Assume further that (I) is approximated by the LW scheme and (II) by the first order forward differencing. The discrete interface problem then reads

$$u_j^{n+1} = C_1\left[u_j^n - \frac{\nu}{2}\left(u_{j+1}^n - u_{j-1}^n\right) + \frac{\nu^2}{2}\left(u_{j+1}^n - 2u_j^n + u_{j-1}^n\right)\right] \qquad j\le 0$$

$$v_j^{n+1} = C_2\left[v_j^n - \frac{\nu}{2}\left(v_{j+1}^n - v_{j-1}^n\right) + \frac{\nu^2}{2}\left(v_{j+1}^n - 2v_j^n + v_{j-1}^n\right)\right] \qquad j>0$$

$$u_j^n = v_j^n \qquad j=0,1$$

with $C_1 = (1 - c_1\Delta t)$ and $C_2 = (1 - c_2\Delta t)$. Since $|C_1|\le 1$ and $|C_2|\le 1$, both schemes in (C10) are dissipative and stability of the interface problem follows. Single frequency modes are of the form (C2) with

$$x_1 = \frac{Z - C_1(1-\nu^2) - \Delta^-}{C_1\nu(\nu+1)}$$

$$x_2 = \frac{Z - C_1(1-\nu^2) + \Delta^-}{C_1\nu(\nu+1)}$$

(C11)

$$\mu_1 = \frac{Z - C_2(1-\nu^2) - \Delta^+}{C_2\nu(\nu+1)}$$

$$\mu_1 = \frac{Z - C_2(1-\nu^2) + \Delta^+}{C_2\nu(\nu+1)}$$

$$(\Delta^-)^2 = (Z - C_1)^2 + C_1\nu^2(2Z - C_1)$$

$$(\Delta^+)^2 = (Z - C_2)^2 + C_2\nu^2(2Z - C_2)$$

Continuity requirements imply (C4) with (C5) and (C6) to follow. Denote by $[C] = C_2 - C_1$. To first order it follows from (C11) that

$$\mu_2/x_2 \simeq 1 + d[C] + O([C])^2$$

$$d = \frac{(Z-C_1)(\nu^2-1) - (1-\nu^2)\Delta^-}{(Z-C_1(1-\nu^2))\Delta^- + (\Delta^-)^2} - \frac{1}{C_1}$$

Following (C7) and (C8)

$$T = 1 + O([C])$$

$$R = O([C])$$

Appendix D: Linearizing the Euler Equations

The 2D linearized Euler equations in primitive variables (p,u,v,s) is

$$\begin{pmatrix} p \\ u \\ v \end{pmatrix}_t + \begin{pmatrix} u_\infty & \rho_\infty c_\infty^2 & 0 \\ \rho_\infty^{-1} & u_\infty & 0 \\ 0 & 0 & u_\infty \end{pmatrix} \begin{pmatrix} p \\ u \\ v \end{pmatrix}_x + \begin{pmatrix} v_\infty & 0 & \rho_\infty c_\infty^2 \\ 0 & v_\infty & 0 \\ \rho_\infty^{-1} & 0 & v_\infty \end{pmatrix} \begin{pmatrix} p \\ u \\ v \end{pmatrix}_y = 0 \qquad \text{(D1)}$$

with the entropy equation completely decoupled.

$$s_t + u_\infty s_x + v_\infty s_y = 0 \qquad \text{(D2)}$$

under the coordinate transformation

$$\begin{aligned} \xi &= x - u_\infty t \\ \eta &= y - v_\infty t \\ \tau &= c_\infty t \end{aligned} \qquad \text{(D3)}$$

equation (D1) becomes

$$\begin{pmatrix} p \\ u \\ v \end{pmatrix}_\tau + \begin{pmatrix} 0 & A & 0 \\ A^{-1} & 0 & 0 \\ 0 & 0 & 0 \end{pmatrix} \begin{pmatrix} p \\ u \\ v \end{pmatrix}_\xi + \begin{pmatrix} 0 & 0 & A \\ 0 & 0 & 0 \\ A^{-1} & 0 & 0 \end{pmatrix} \begin{pmatrix} p \\ u \\ v \end{pmatrix}_\eta = 0 \qquad \text{(D4)}$$

with $A = \rho_\infty c_\infty$. By further transformation of the dependent variables

$$\begin{pmatrix} \bar{p} \\ \bar{u} \\ \bar{v} \end{pmatrix} = \begin{pmatrix} 1 & 0 & 0 \\ 0 & A & 0 \\ 0 & 0 & A \end{pmatrix} \begin{pmatrix} p \\ u \\ v \end{pmatrix}$$

we obtain system (3.4.1). Far field modifications of (3.4.1) can be carried over to the Euler equations by the inverse of the present transformation, and systems I, II and III are easily obtained.

Appendix E: Point Equation and Line Equation of a Conic

The line equation of a conic is a representation of the conic in terms of the envelope formed by its tangents. Let a general line be described by

$$nx + my + 1 = 0 \tag{E1}$$

and consider the family of such lines that satisfy

$$An^2 + 2Hnm + Bm^2 + 2Gn + 2Fm + C = 0 \tag{E2}$$

The envelope formed by these lines is a conic whose point equation is given by [70]

$$ax^2 + 2hxy + by^2 + 2gx + 2fy + c = 0 \tag{E3}$$

where a,b,c etc are the A,B,C etc. minors of the matrix

$$M = \begin{pmatrix} A & H & G \\ H & B & F \\ G & F & C \end{pmatrix} \tag{E4}$$

Consider now the characteristic polynomial (3.4.10)

$$\lambda^2-\lambda(a-1)\cos\vartheta-(a\cos^2\vartheta + p^2\sin^2\vartheta) = 0 \tag{E5}$$

In terms of the intersection points with the x and y axes

$$X = \lambda/\cos\vartheta \qquad Y = \lambda/\sin\vartheta \tag{E6}$$

Equation (E5) reads

$$XY - (a-1)Y - aY/X - p^2X/Y = 0 \tag{E7}$$

For the line described by (E1), X = -1/n, Y = -1/m, and (E7) becomes

$$an^2 - (a-1)n + p^2m^2 = 0 \tag{E8}$$

for which the point equation, using minors of (E4), is

$$\frac{\left(x - \frac{a-1}{2}\right)^2}{\left(\frac{a+1}{2}\right)^2} + \frac{y^2}{p^2} = 0$$

representing an ellipse centred at $\left(\frac{a-1}{2}, 0\right)$ with respective axes $\frac{a+1}{2}$ and p.

Appendix F: On the Group Velocity of Symmetric and Upwind Schemes

Consider the 2-level explicit model to approximate (1.2.1)

$$u_j^{n+1} = \sum_{k=-l}^{r} c_k(\nu) u_{j+k}^n \qquad \text{(F1)}$$

Let $Z = e^{i\omega k}$ and substitute in (F1) a trial solution $u_j^n = Z^n \exp(i\xi jh)$. The amplification factor Z is given by

$$Z = \sum_{k=-l}^{r} c_k(\nu)\, e^{i\xi kh} \qquad \text{(F2)}$$

and for Cauchy stability the model must satisfy $|Z| \leq 1$ for all $\xi \in \mathbb{R}$. Where applicable, the group velocity is given by

$$G = -\frac{d\omega}{d\xi} = -\frac{a}{\nu Z} \sum_{k=-l}^{r} k c_k(\nu)\, e^{i\xi kh} \qquad \text{(F3)}$$

Symmetric Schemes

In the symmetric case we have $l=r\equiv s$ and the stencil of (F1) stretches over 2s+1 grid points. The maximal order of accuracy is 2s and is attained by choosing c_k that satisfy

$$\sum_{k=-s}^{s} k^p c_k(\nu) = \nu^p \qquad p = 0,1,\ldots,2s \qquad \text{(F4)}$$

Equation (F4) is a linear non-homogeneous system of Vandermonde type which can be solved using Cramer's rule

$$c_k(\nu) = \prod_{\substack{j=-s \\ j\neq k}}^{s} \frac{(\nu-j)}{(k-j)} \qquad \text{(F5)}$$

Using the generalised factorial notation

$$(\nu-j)_{n+1} = (\nu-j)(n-j+1)\cdots(\nu-j+n)$$

equation (F5) simplifies to read

$$c_k(\nu)=(-1)^{s+k}\frac{(\nu-s)_{2s+1}}{(s-k)!\,(s+k)!\,(\nu-k)} \tag{F6}$$

It follows from (7) that:

(a) $c_k(\nu) = c_{-k}(-\nu)$

(b) The amplification factor, defined in (3), for $\xi h=\pi$ $Z = \sum_{k=-s}^{s} (-1)^k c_k(\nu)$ is a symmetric function in the CFL number ν.

(c) Assuming Cauchy stability, then for ν sufficiently small

$$Z \simeq 1-c\nu^2 \tag{F7}$$

for some positive constant c.

(d) The group velocity for $\xi h=\pi$ reads $G = -\frac{a}{\nu Z}\sum_{k=-s}^{s}(-1)^k kc_k(\nu)$. Substituting (F6) and rearranging we obtain

$$G = \frac{a}{Z}\frac{(1-\nu)_s(\nu+1)_s}{(2s)!}\sum_{k=1}^{s}\binom{2s}{s+k}\frac{2k^2}{k^2-\nu^2} \tag{F8}$$

It follows from (F7) that for sufficiently small ν, Z is positive. For $|\nu|\leq 1$, all the ν-dependent terms in (F8) are positive, leading to group velocity that points in the wrong direction.

(e) Since at small CFL numbers, waves propagate through fewer grid cells, the true implication of (F8) has to be assessed in the double limit $|\nu|\to 0$, $N\to\infty$ so that $T=Nk=N\nu h/a$ is fixed. After a fixed time T, assuming a=1 and h=1, a mode with $\xi h=\pi$ will have dissipated by

$$\begin{aligned} Z^{T/\nu} &\simeq (1-c\nu^2)^{T/\nu} \simeq (1-c\nu^2)^{(1/c\nu^2)\cdot c\nu T} \\ &\simeq e^{-c\nu T} \xrightarrow[|\nu|<<1]{} 1 \end{aligned} \tag{F9}$$

and in the limit of small ν the mode is not dissipated at all. An example of a scheme in this class is the LW scheme (2.1.1)

Upwind Schemes

Even Order Schemes

These have the general form

$$u_j^{n+1} = \sum_{k=-s+s_0}^{s+s_0} c_k(\nu) u_{j+k}^n \qquad \text{(F10)}$$

and of which the symmetric schemes are a particular case $s_0=0$. In order for $\nu=0$ to be inside the stability region $s_0=0,1$[88], but we shall keep the general notation s_0. Let $c_k^u(\nu)$ and $c_k^c(\nu)$ denote the coefficients in the upwind and central (symmetric) cases respectively. For optimal accuracy

$$c_k^u(\nu) = \prod_{j \neq k-s+s_0}^{s+s_0} \frac{(\nu-j)}{(k-j)} = \prod_{j \neq k-s}^{s} \frac{(\nu-s_0-j)}{(k-s_0-j)} = c_{k-s_0}^c(\nu-s_0) \qquad \text{(F11)}$$

where $c_k^c(\nu)$ are given by (F6). The coefficients are thus related through a simple shift operator. It can be shown that:

(a) $c_{s_0+k}^u(s_0+\nu) = c_{s_0-k}^u(s_0-\nu)$.

(b) The amplification factor of the mode $\xi h=\pi$ is not symmetric in ν hence for sufficiently small ν inside the stability region

$$Z^u \simeq 1 - c\nu + O(\nu^2) \qquad \text{(F12)}$$

where c is a positive constant. In general there is no reason to assume c=0 although if the requirement for optimal accuracy is dropped, the resulting degrees of freedom can be used to construct schemes for which c=0, leading to amplification factor of the form (F7). A simple relation holds between the amplification factors in the upwind and symmetric cases. Let $\mu=\nu-s_0$

$$Z^u(\nu) = \sum_{k=-s+s_0}^{s+s_0} (-1)^k c_k^u(\nu) = (-1)^{s_0} \sum_{k=-s}^{s} (-1)^k c_k^c(\mu)$$

$$= (-1)^{s_0} Z^c(\mu) \tag{F13}$$

It follows from (F7) that Z^u is symmetric in μ. Assuming Cauchy stability, for sufficiently small μ

$$Z^u(\nu) \simeq (-1)^{s_0} (1 - c\mu^2) \tag{F14}$$

for some positive constant c.

(c) It follows from (b) that group velocity analysis is applicable for either $\mu \cong 0$ ($\nu \cong s_0$) or $\nu \cong 0$. The general expression for the group velocity reads

$$G = -\frac{a}{\nu} Z^u (-1)^{s+s_0} \frac{(\mu-s)_{2s+1}}{(2s)!} \sum_{k=-s}^{s} \binom{2s}{s+k} \frac{k+s}{\mu-k}_0 \tag{F15}$$

For $|\mu| \ll 1$, the main contribution to G comes from k=0 leading to

$$G \simeq -\frac{a}{s_0} \frac{s!s!}{(2s)!} \binom{2s}{s} s_0 = -a$$

ie high frequency modes in this range of CFL numbers move in the correct direction.

In the limit of small ν, (F15) takes the form

$$G \simeq \frac{a}{\nu} \sum_{k=-s}^{s} \binom{2s}{s+k} \Big/ \binom{2s}{s+s_0}$$

and is strictly positive. High frequencies in this range of CFL numbers move in the wrong direction.

(d) The fundamental difference between the symmetric and upwind cases lies in their respective long time behaviour. After a fixed time T=Nk, high frequencies will have dissipated by

$$Z \cong (1-c\nu)^{T/\nu} \xrightarrow[|\nu| \ll 1]{} e^{-Tc} \tag{F16}$$

This suggests that in the upwind case, high frequency parasitic modes

do not constitute a severe problem since even at small CFL numbers all waves will eventually be damped out. In the symmetric case the accumulative damping factor tends to 1 in the limit of small ν and waves will persist. This is confirmed by simple numerical tests.

An example of a scheme in this class is the second order upwind scheme with s=1, s_0=1

$$u_j^{n+1} = \frac{(1-\nu)(2-\nu)}{2} u_j^n + \nu(2-\nu) u_{j+1}^n - \frac{\nu(1-\nu)}{2} u_{j+2}^n \qquad \text{(F17)}$$

Odd Order Schemes

These have the general form

$$u_j^{n+1} = \sum_{k=-s+s_0+1}^{s+s_0} c_k(\nu) u_{j+k}^n$$

and we assume $s \geq s_0+1 \geq 1$. For optimal accuracy

$$c_k^u(\nu) = \prod_{\substack{j=-s+s_0+1 \\ j \neq k}}^{s+s_0} \frac{(\nu-j)}{(k-j)} = \prod_{\substack{j=-s+1 \\ j \neq k-s_0}}^{s} \frac{(\nu-s_0-j)}{(k-s_0-j)}$$

$$= \frac{k-s_0+s}{\nu-s_0+s} c_{k-s_0}^c(\nu-s_0) \qquad \text{(F18)}$$

(a) The amplification factor of the mode $\xi h=\pi$ reads

$$Z^u(\nu) = \sum_{k=-s+s_0+1}^{s+s_0} (-1)^k c_k^u(\nu) = (-1)^{s_0} \sum_{k=-s+1}^{s} (-1)^k \frac{k+s}{\mu+s} c_k^c(\mu)$$

$$= (-1)^{s+s_0} \frac{(\mu-s)_{2s}}{(2s)!} \sum_{k=-s+1}^{s} \binom{2s}{s+k} \frac{k+s}{\mu-k}$$

It can be verified that for small μ ($\nu \simeq s_0$)

$$Z \simeq (-1)^{s_0}(1-c\mu)$$

for some positive constant c. Likewise, for small ν inside the stability region

$$Z \simeq 1-c\nu$$

for some other positive constant. Group velocity analysis is thus applicable in those two ranges of CFL numbers.

(b) The expression for the group velocity of the mode $\xi h=\pi$ reads

$$G = -\frac{a}{\nu Z}(-1)^{s+s_0}\frac{(\mu-s)_{2s}}{(2s)!}\sum_{k=-s+1}^{s}\binom{2s}{s+k}\frac{(k+s)(k+s_0)}{(\mu-k)} \qquad \text{(F19)}$$

For $\nu\simeq 0$, the main contribution to G comes from k=0, leading to approximate group velocity which points in the correct direction $G \simeq -a$. For $\nu\simeq 0$, the group speed reads

$$G \simeq \frac{a}{\nu}\frac{1}{s-s_0}\sum_{k=-s+1}^{s}\binom{2s}{s+k}(k+s)\Big/\binom{2s}{s+s_0}$$

which is strictly positive hence points in the wrong direction.

(c) Schemes in this class will display a long time behaviour similar to (F16). An example of a scheme in this class is the first order upwind scheme with s=1, $s_0=0$

$$u_j^{n+1} = (1-\nu)u_j^n + \nu u_{j+1}^n$$

RK Type Schemes

Consider the (s) stage RK algorithm to approximate (1.2.1)

$$u_j^{(1)} = u_j^n + \lambda_s \frac{\nu}{2}(\mathbb{K} - \mathbb{K}^{-1})u_j^n$$

$$u_j^{(2)} = u_j^n + \lambda_{s-1} \frac{\nu}{2}(\mathbb{K} - \mathbb{K}^{-1})u_j^{(1)} \qquad \text{(F20)}$$

$$\vdots \qquad\qquad \vdots$$

$$u_j^{(s)} = u_j^n + \lambda_1 \frac{\nu}{2}(\mathbb{K} - \mathbb{K}^{-1})u_j^{(s-1)}$$

$$u_j^{n+1} = u_j^{(s)}$$

where $\mathbb{K}$ is the shift operator $\mathbb{K}u_j^n = u_{j+1}^n$ and λ_k are arbitrary positive constants. Let $\Lambda_k = \left(\frac{\nu}{2}\right)^k \prod_{l=1}^{k} \lambda_l$, then (F20) may be written explicitly as

$$u_j^{n+1} = \left(I + \sum_{k=1}^{s} \Lambda_k \sum_{m=0}^{k} (-1)^m \mathbb{K}^{k-2m} \right) u_j^n \qquad \text{(F21)}$$

$$= \sum_{k=-s}^{s} c_k(\nu)\, u_{j+k}^n$$

It can be shown that:

(a) $c_k(\nu) = c_{-k}(\nu)$ k=even

$c_k(\nu) = -c_{-k}(\nu)$ k=odd

and for $k \geq 0$

$$c_k(\nu) = \sum_{n=0}^{\left[\frac{s-k}{2}\right]} (-1)^n \Lambda_{k+2n} \binom{k+2n}{n} \qquad \text{(F22)}$$

where [x] denotes the integer part of x.

(b) The amplification factor for $\xi h = \pi$ is Z=1 for which group velocity analysis strictly applies.

(c) Using (a) and (b) the group velocity for high frequency modes reads

$$G = -\frac{a}{\nu} \left(\sum_{\substack{k=-S \\ k=\text{odd}}}^{S} + \sum_{\substack{k=-S \\ k=\text{even}}}^{S} \right) (-1)^k k c_k(\nu)$$

The even order terms cancel out and the odd order terms yield

$$G = \frac{2a}{\nu} \sum_{\substack{k=1 \\ k=\text{odd}}}^{S} k c_k(\nu) \qquad \text{(F23)}$$

with c_k given by (F22). For specific choices of (s) we obtain

(i) s=1 (s=2)

$$G(\pi) = \frac{2a}{\nu} \Lambda_1 \begin{pmatrix} 1 \\ 0 \end{pmatrix}$$

(ii) s=3 (s=4)

$$G(\pi) = \frac{2a}{\nu} \left\{ \Lambda_1 \begin{pmatrix} 1 \\ 0 \end{pmatrix} + \overset{0}{\Lambda_3} \left(3 \begin{pmatrix} 3 \\ 0 \end{pmatrix} - 1 \begin{pmatrix} 3 \\ 1 \end{pmatrix} \right) \right\}$$

(iii) s=5 (s=6)

$$G(\pi) = \frac{2a}{\nu} \left\{ \Lambda_1 \begin{pmatrix} 1 \\ 0 \end{pmatrix} + \overset{0}{\Lambda_3} \left(3 \begin{pmatrix} 3 \\ 0 \end{pmatrix} - 1 \begin{pmatrix} 3 \\ 1 \end{pmatrix} \right) + \overset{0}{\Lambda_5} \left(5 \begin{pmatrix} 5 \\ 0 \end{pmatrix} - 3 \begin{pmatrix} 5 \\ 1 \end{pmatrix} + 1 \begin{pmatrix} 5 \\ 2 \end{pmatrix} \right) \right\}$$

etc. It is claimed that

$$\sum_{k=0}^{m} (-1)^k (2m+1-2k) \binom{2m+1}{k} \equiv 0 \qquad m=1,2,\cdots \tag{F24}$$

The proof is due to P.L. Roe. Consider

$$(1-x)^{2m+1} = \sum_{k=0}^{2m+1} \binom{2m+1}{k} (-x)^k$$

Then

$$\frac{d}{dx}(1-x)^{2m+1} = \sum_{k=0}^{2m+1} (-1)^k k \binom{2m+1}{k} (x)^{k-1} \equiv f(x)$$

and

$$f(1) \equiv 0 = \sum_{k=0}^{2m+1} (-1)^k k \binom{2m+1}{k}$$

Using $\binom{2m+1}{k} \equiv \binom{2m+1}{2m+1-k}$ we get

$$0 \equiv \sum_{k=0}^{m} (-1)^k k \binom{2m+1}{k} + (-1)^{2m+1-k}(2m+1-k) \binom{2m+1}{2m+1-k}$$

$$= \sum_{k=0}^{m} (-1)^{k+1}(2m+1-2k) \binom{2m+1}{k} \qquad \square$$

This implies that the group velocity of high frequency modes under a general (s) stage RK scheme is

$$G = \frac{2a}{\nu} \Lambda_1 \binom{1}{0} = a\lambda_1$$

For consistency of (F20) $\lambda_1=1$ and the group speed always points in the wrong direction. This is confirmed by simple numerical tests.

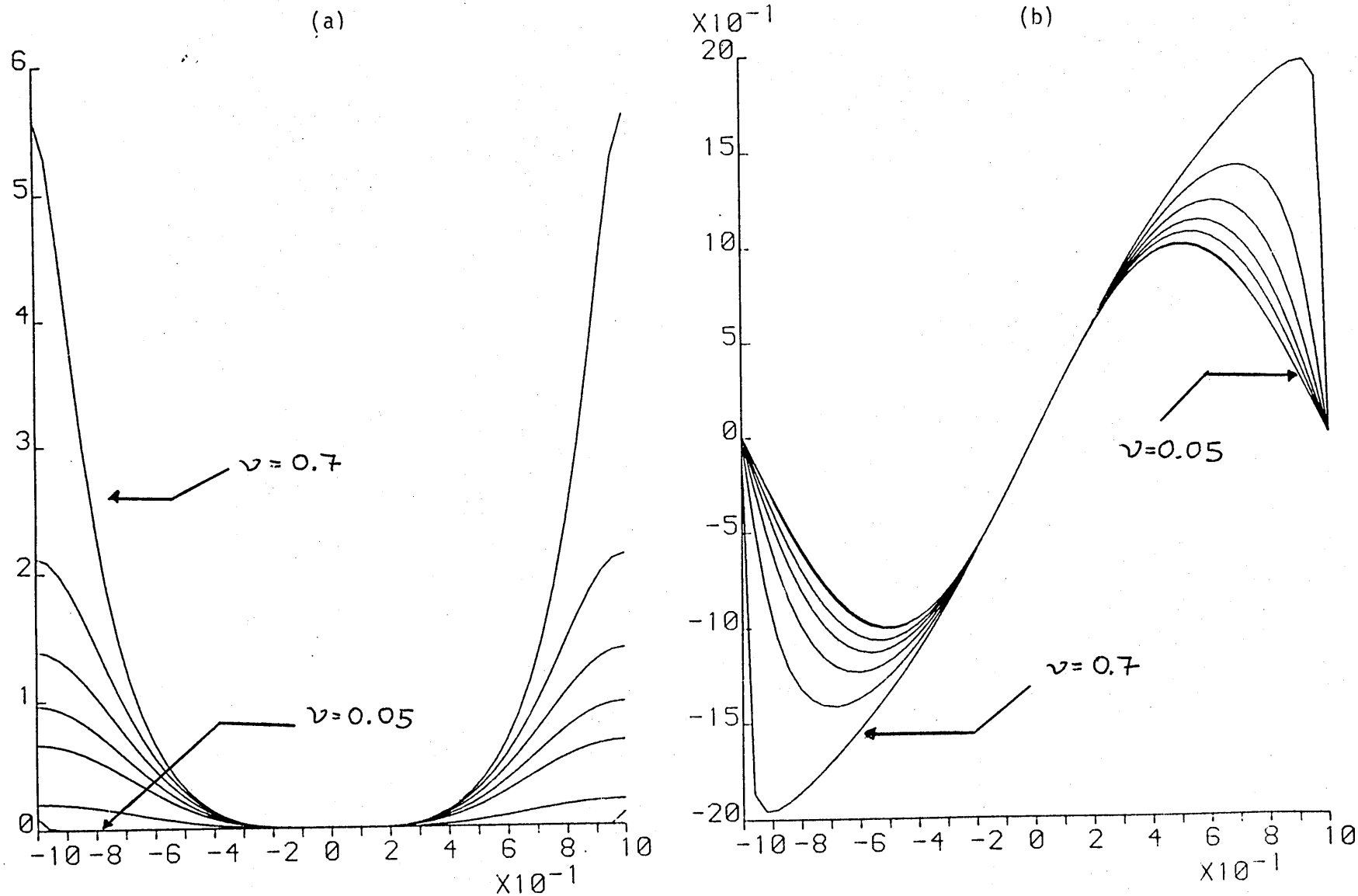

Figure (II.1) - Imaginary and Real parts of dispersion relation (2.1.3): (a) $\omega_I \Delta t$ and (b) $\omega_R \Delta t$ as a function of $\frac{3}{4}\Delta x$ for various CFL numbers.

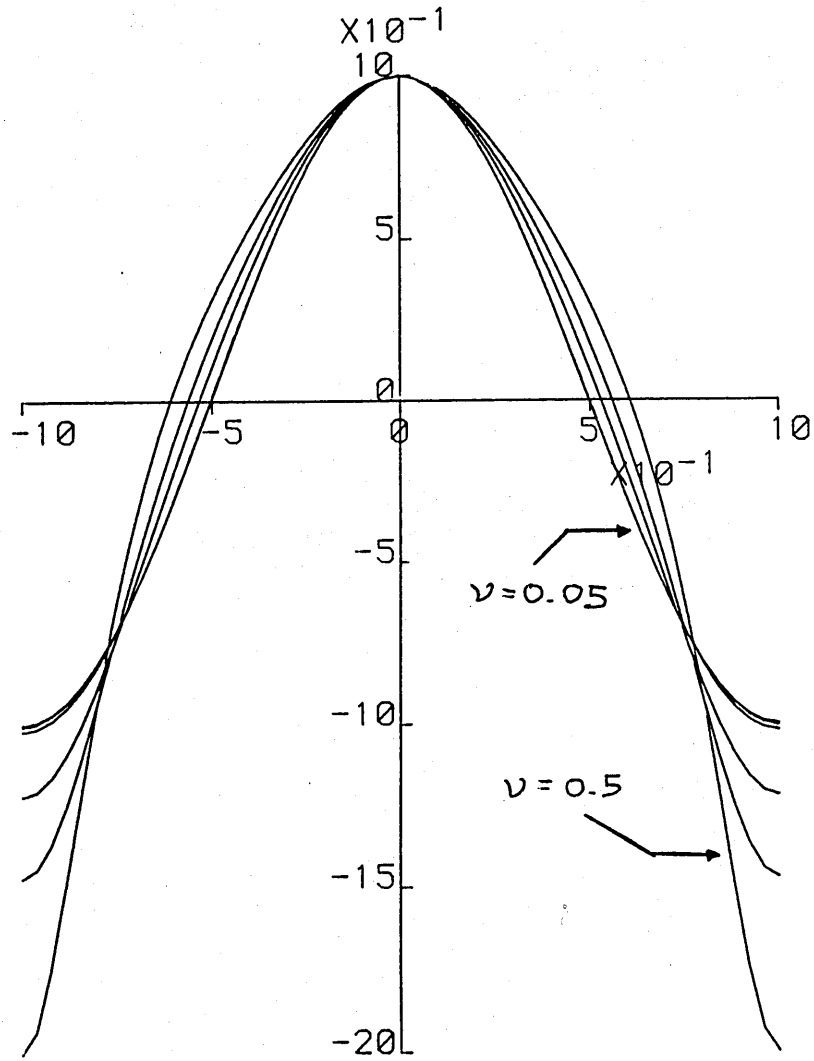

Figure (II.1) - (c) Approximated group velocity as a function of $\xi\Delta x$ for various CFL numbers.

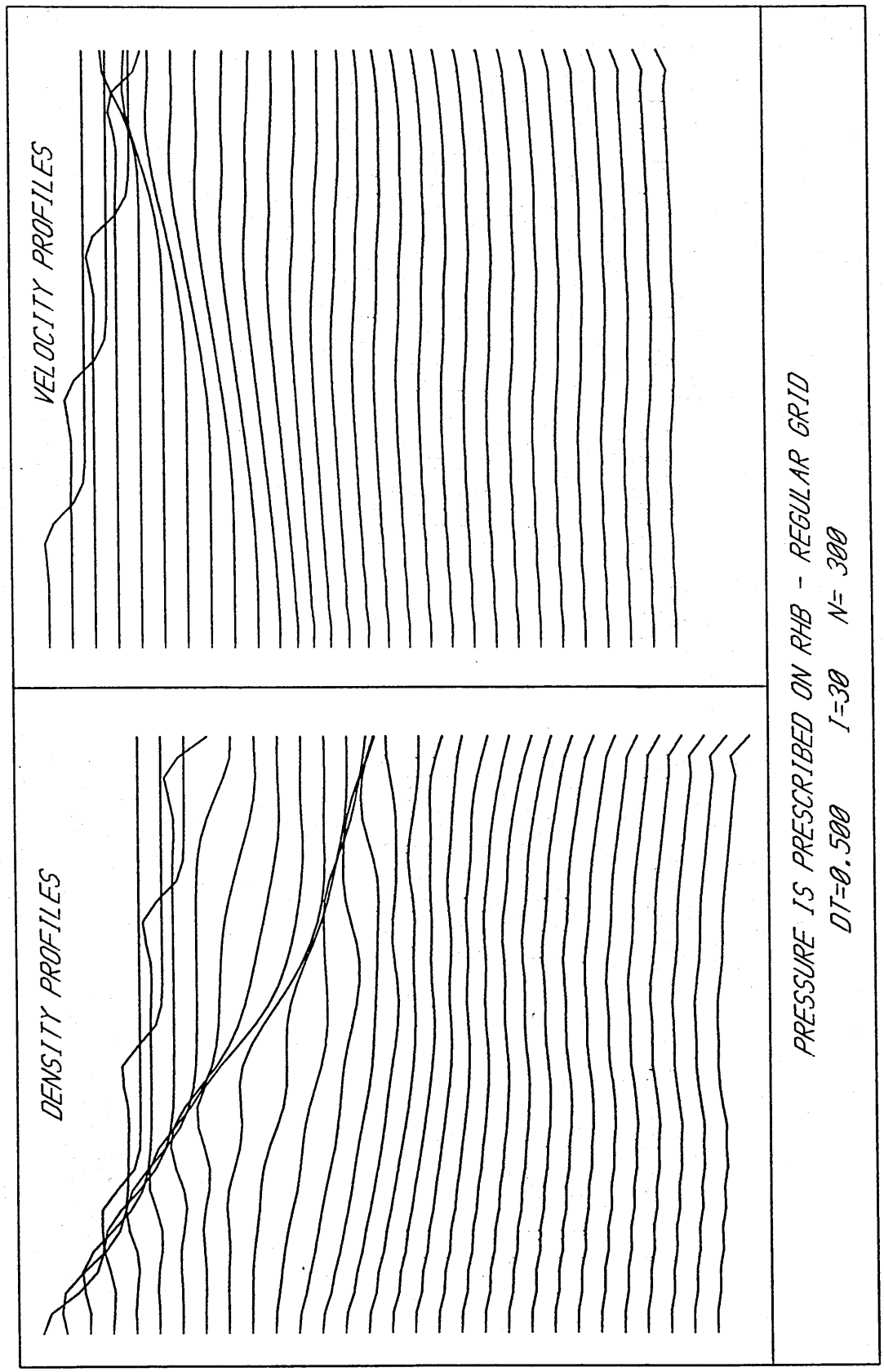

(a)

Figure (II.2) - 1D Euler equations at moderate CFL numbers - A Reflection study with boundary conditions (i)-(v).

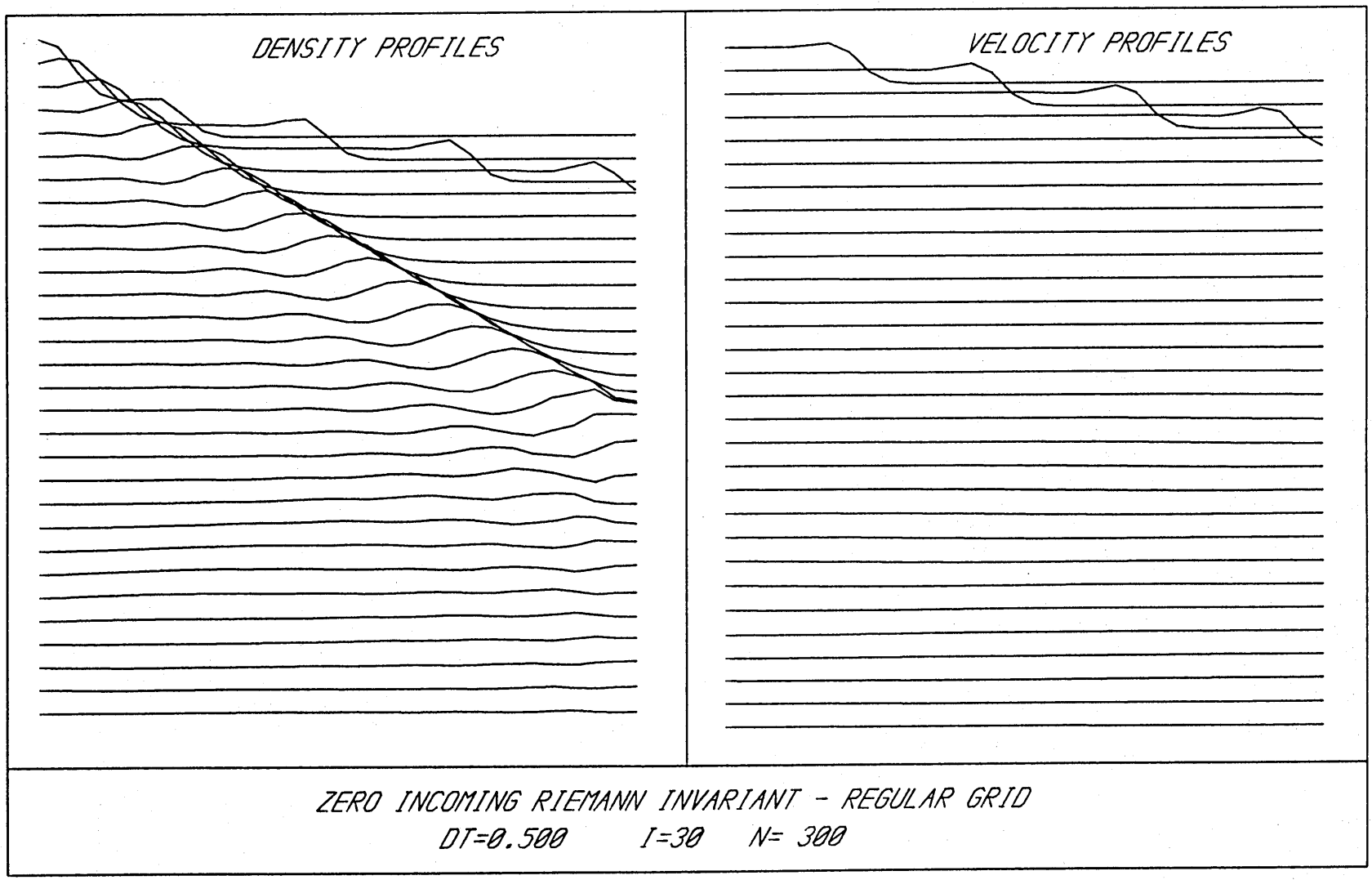
DENSITY PROFILES
VELOCITY PROFILES
ZERO INCOMING RIEMANN INVARIANT - REGULAR GRID
DT=0.500 I=30 N= 300

(b)

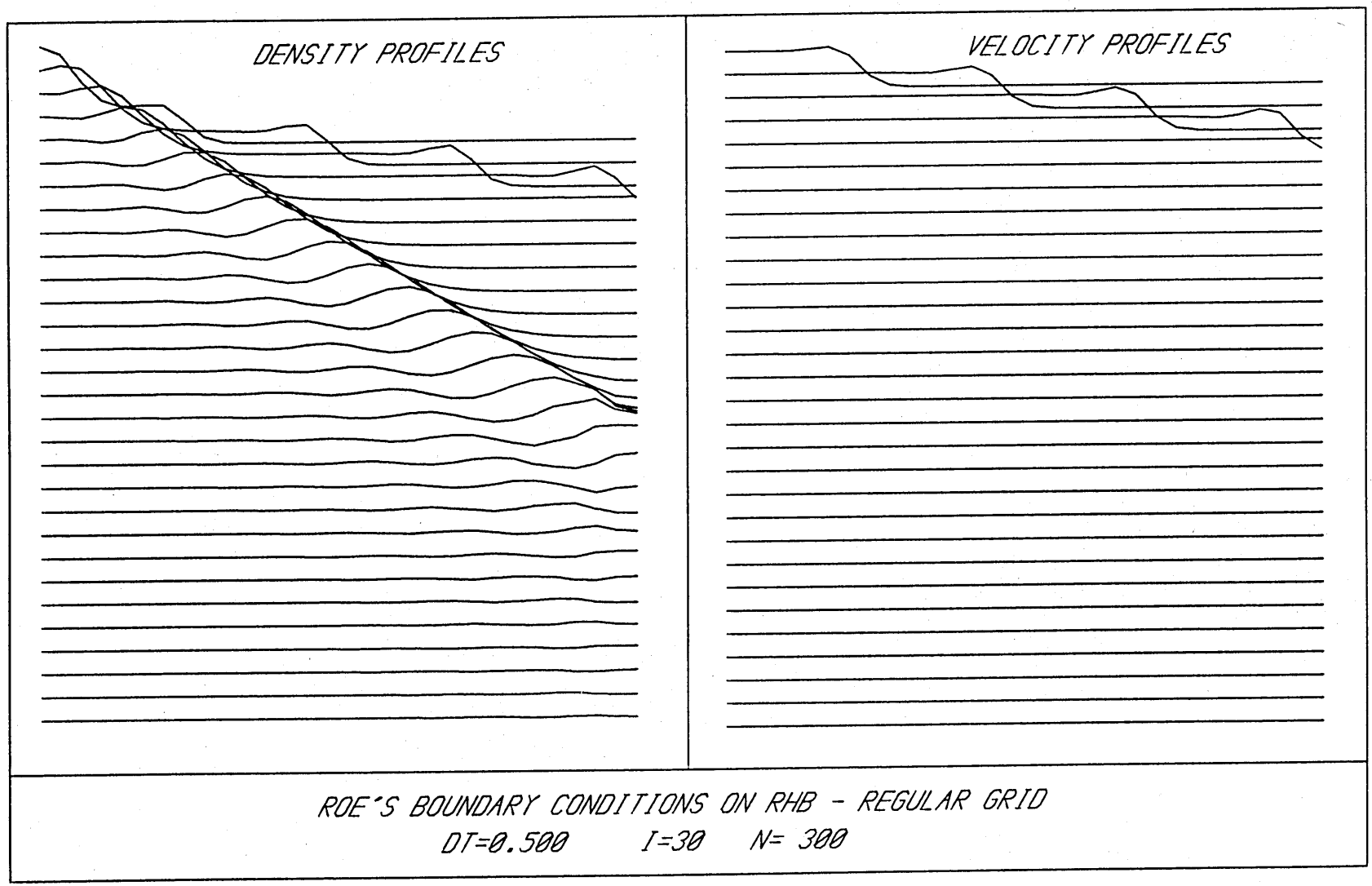
DENSITY PROFILES
VELOCITY PROFILES
ROE'S BOUNDARY CONDITIONS ON RHB - REGULAR GRID
DT=0.500 I=30 N= 300

(c)

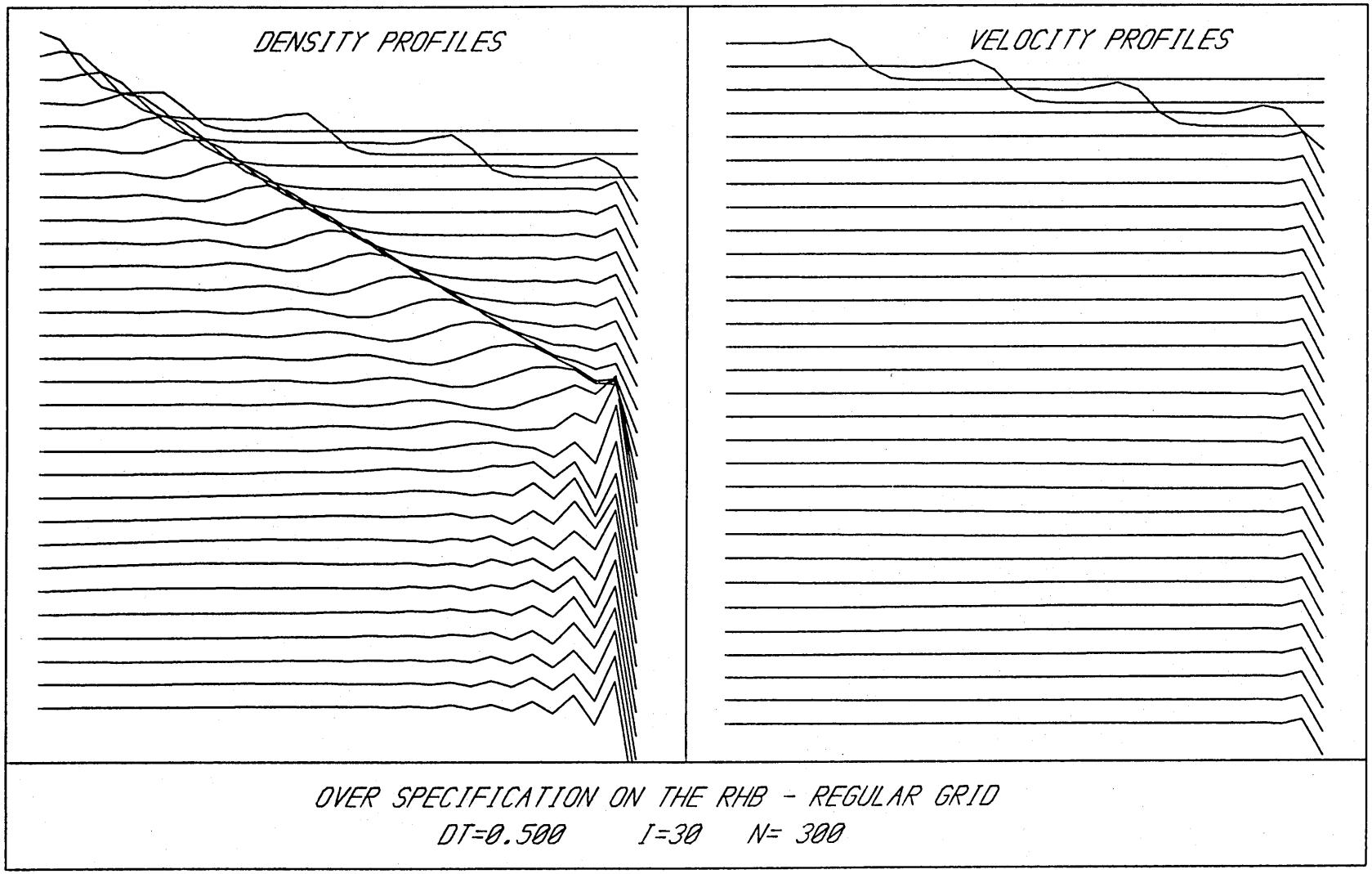
DENSITY PROFILES
VELOCITY PROFILES
OVER SPECIFICATION ON THE RHB - REGULAR GRID
DT=0.500 I=30 N= 300

(d)

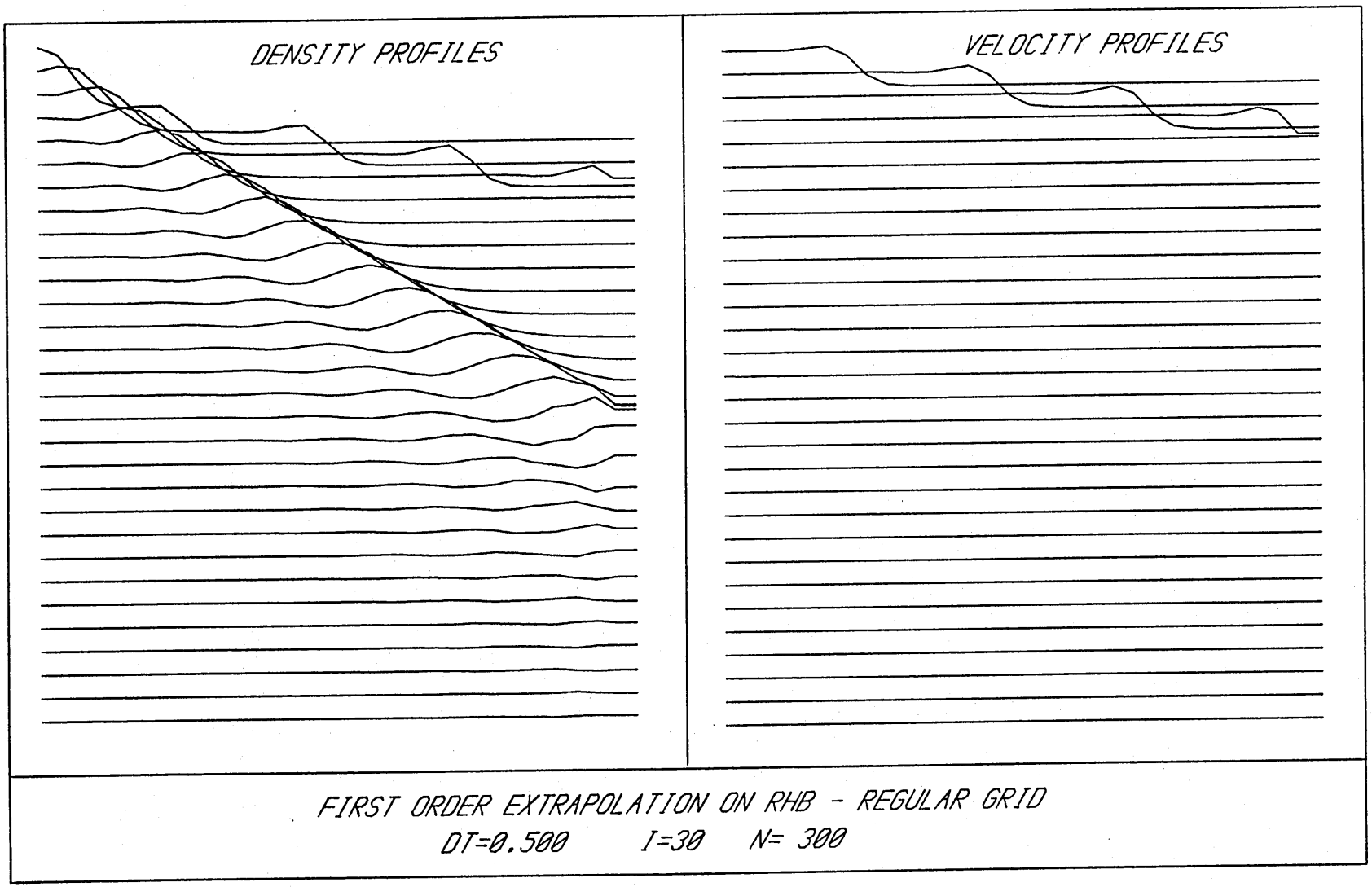
DENSITY PROFILES
VELOCITY PROFILES
FIRST ORDER EXTRAPOLATION ON RHB - REGULAR GRID
DT=0.500 I=30 N= 300

(e)

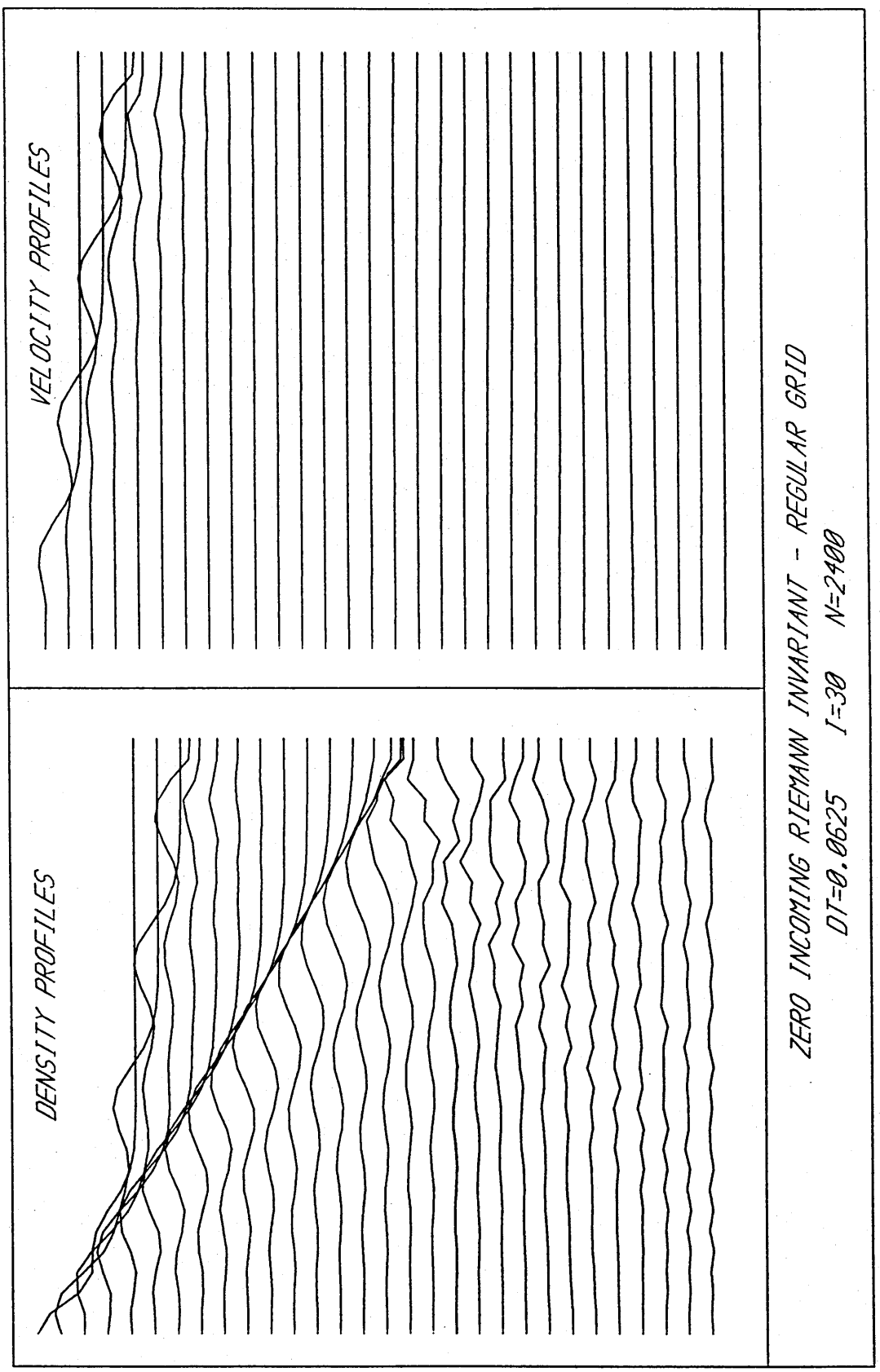

Figure (II.3) - 1D Euler Equations at small CFL numbers - A Reflection study with boundary conditions (ii)-(v).

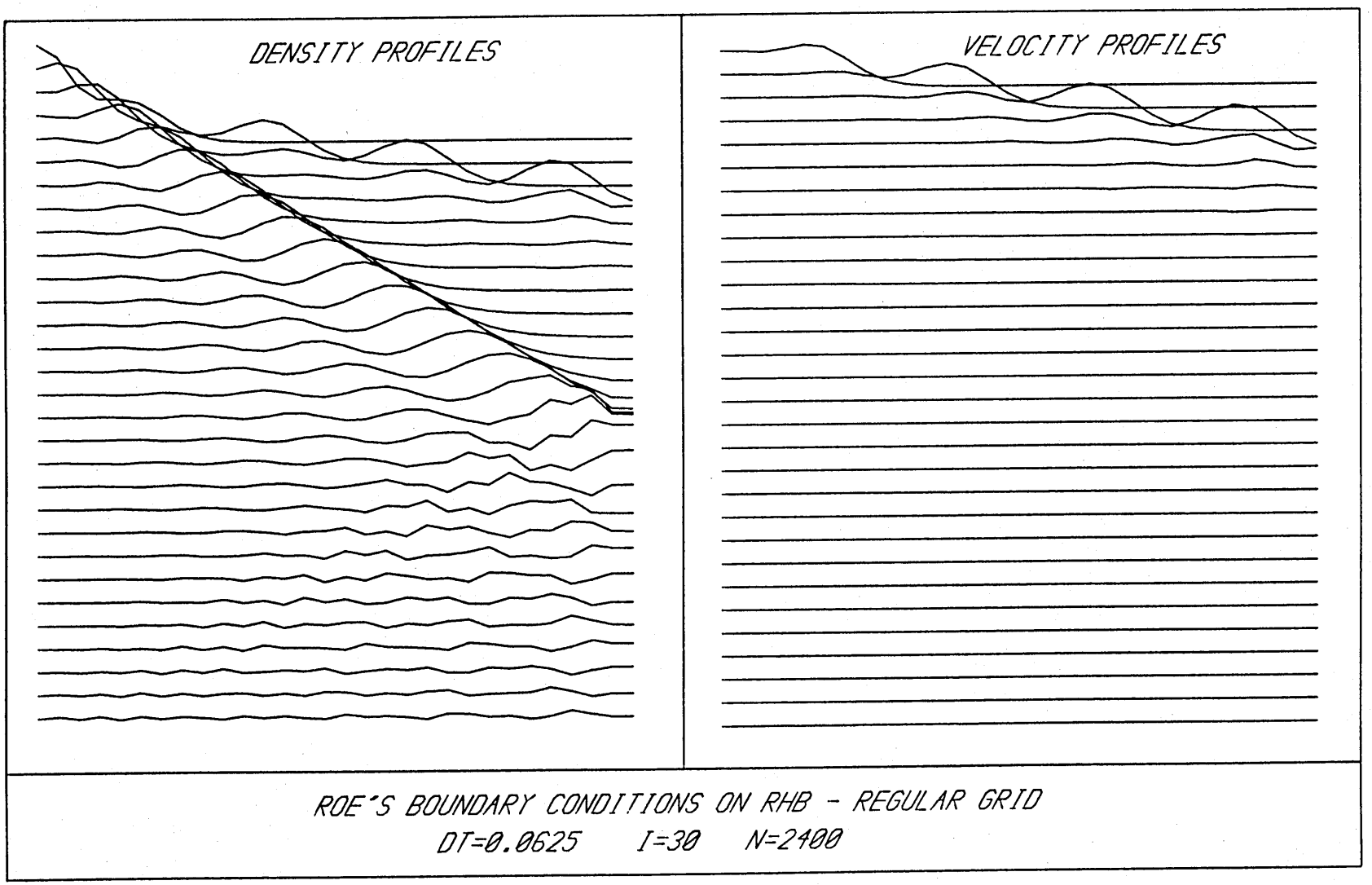
DENSITY PROFILES
VELOCITY PROFILES
ROE'S BOUNDARY CONDITIONS ON RHB - REGULAR GRID
DT=0.0625 I=30 N=2400

(b)

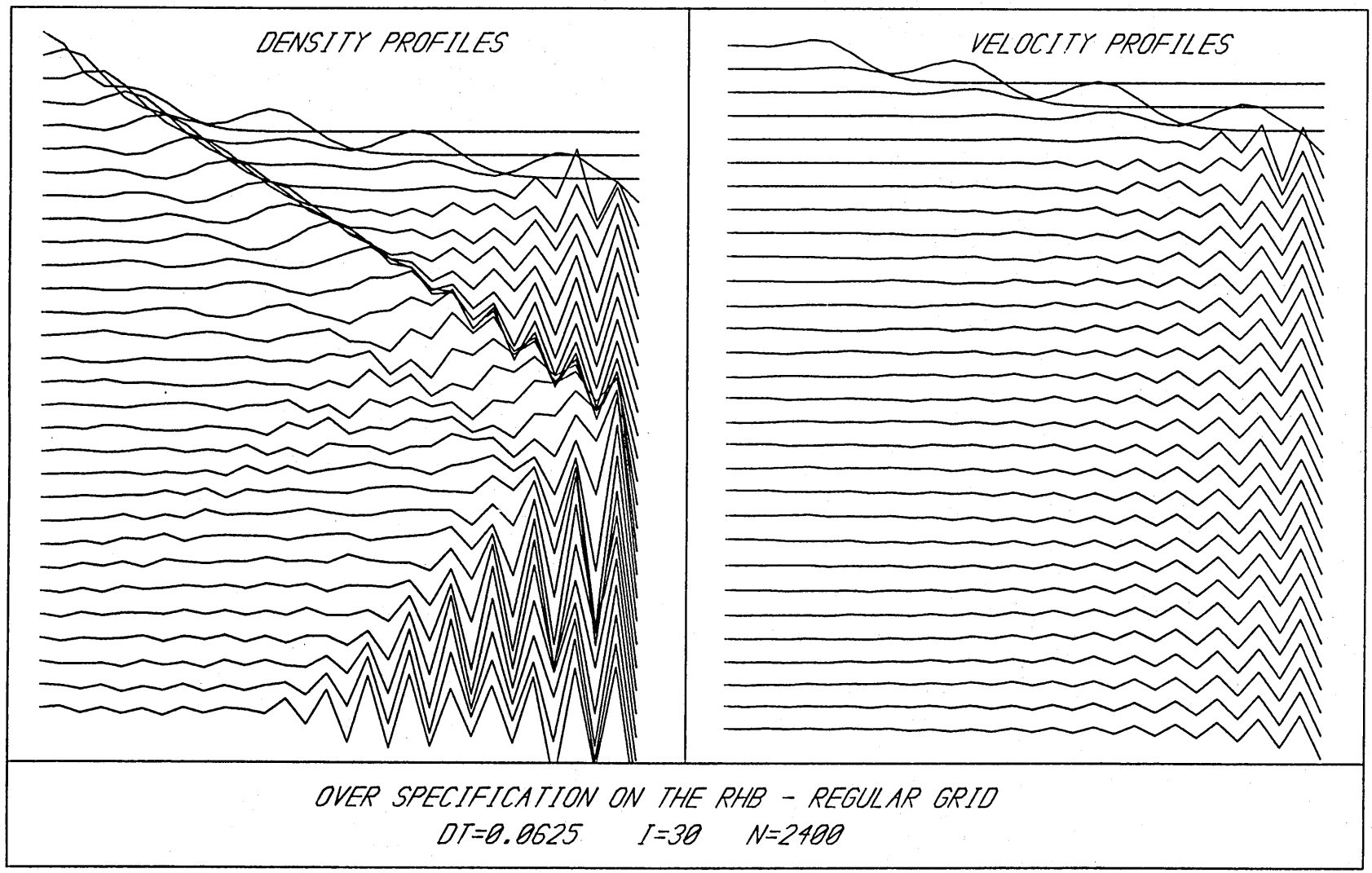
DENSITY PROFILES
VELOCITY PROFILES
OVER SPECIFICATION ON THE RHB - REGULAR GRID
DT=0.0625 I=30 N=2400

(c)

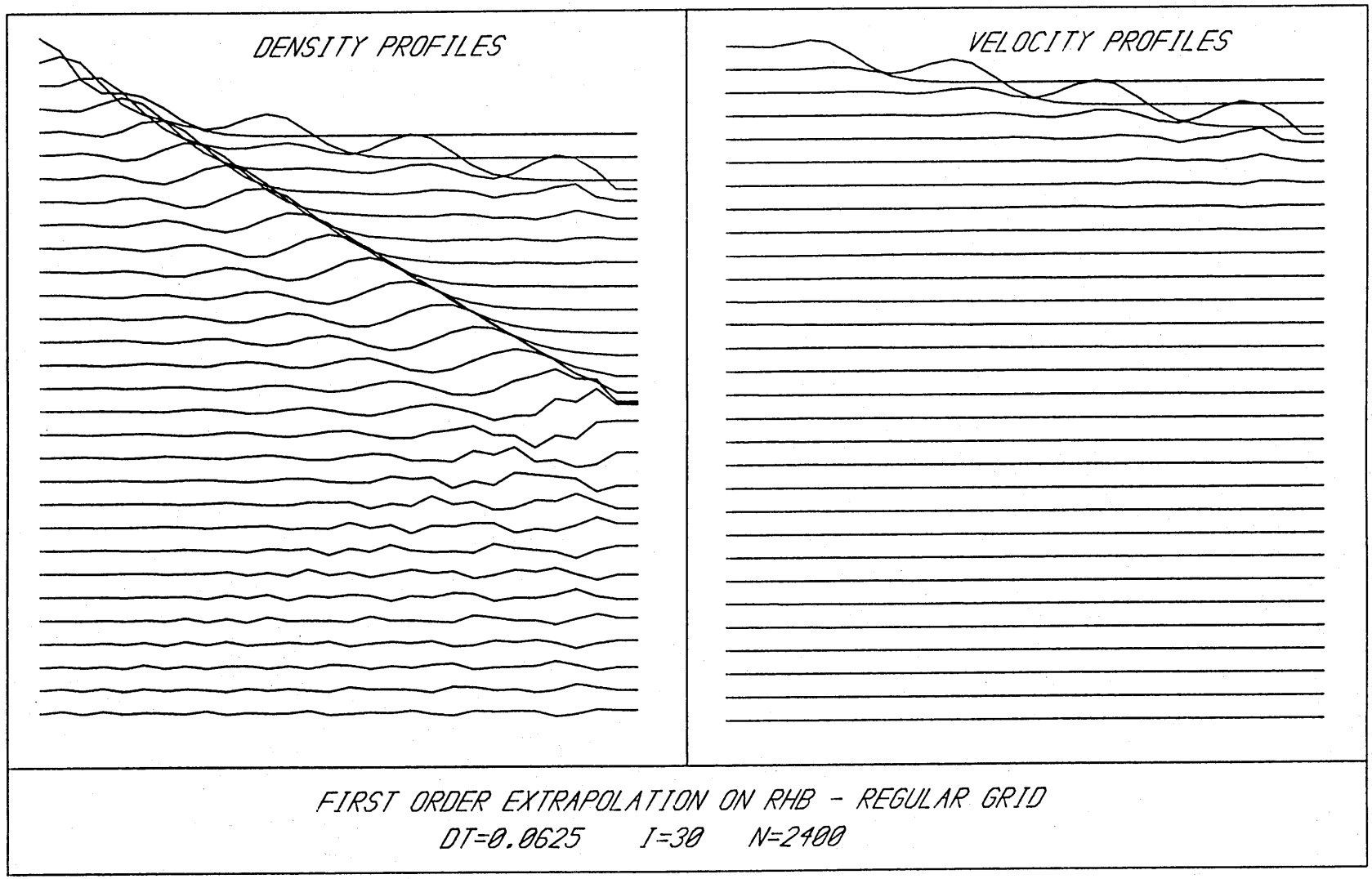
DENSITY PROFILES
VELOCITY PROFILES
FIRST ORDER EXTRAPOLATION ON RHB - REGULAR GRID
DT=0.0625 I=30 N=2400

(d)

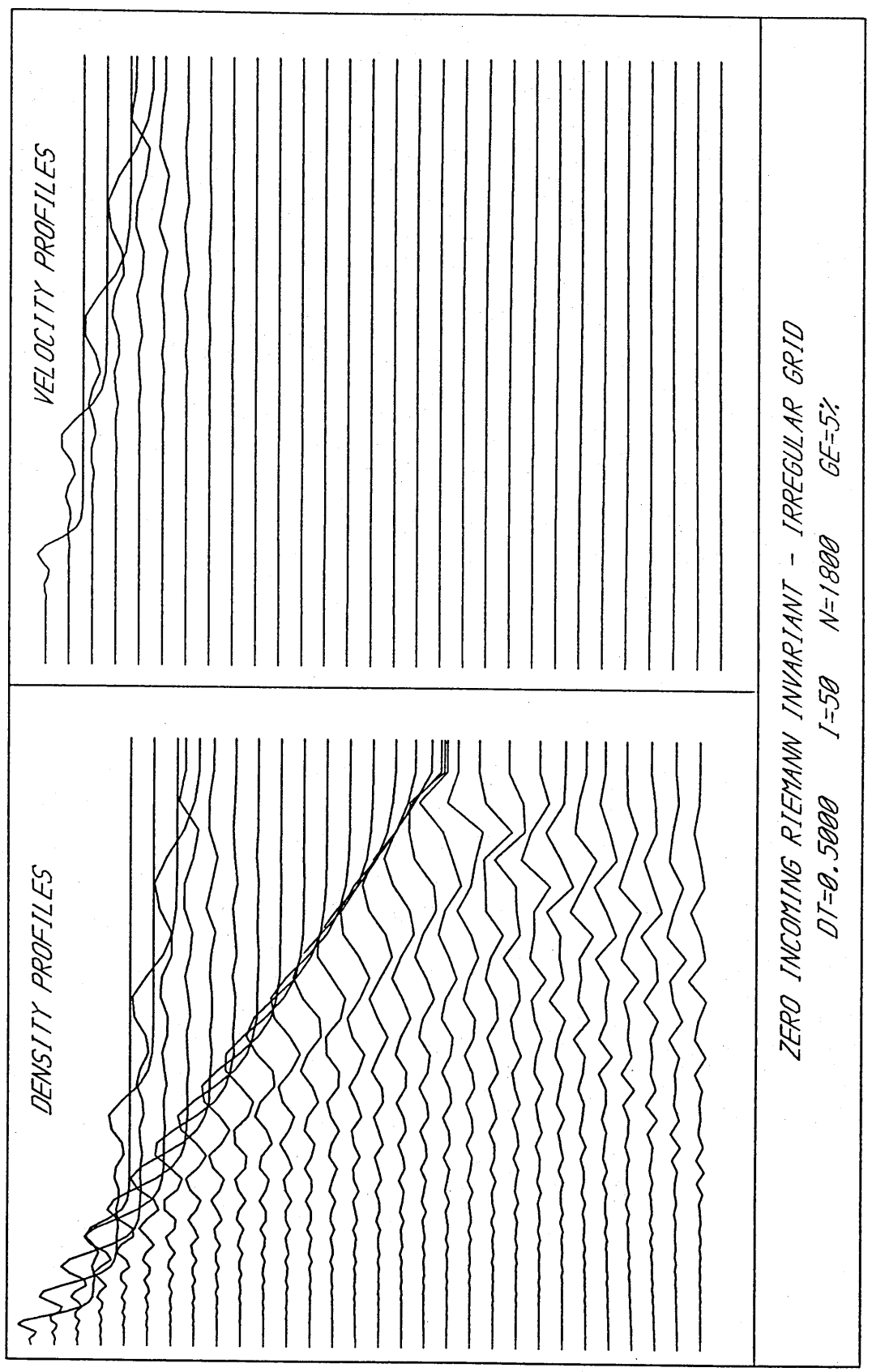

Figure (II.4) - 1D Euler Equations on a mildly expanding grid - A Reflection study with boundary conditions (ii), (iii) and (v).

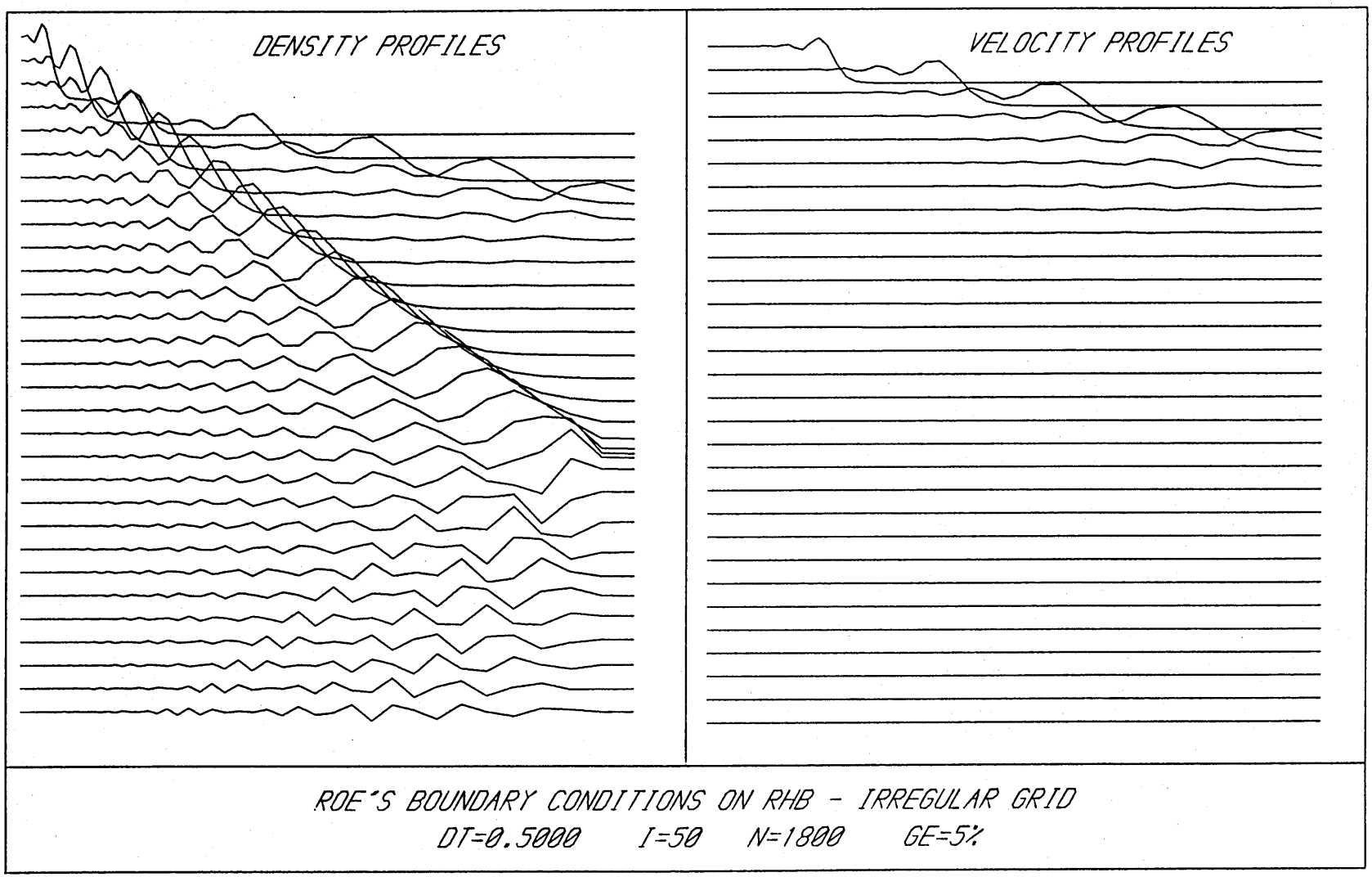
DENSITY PROFILES
VELOCITY PROFILES
ROE'S BOUNDARY CONDITIONS ON RHB - IRREGULAR GRID
DT=0.5000 I=50 N=1800 GE=5%

(b)

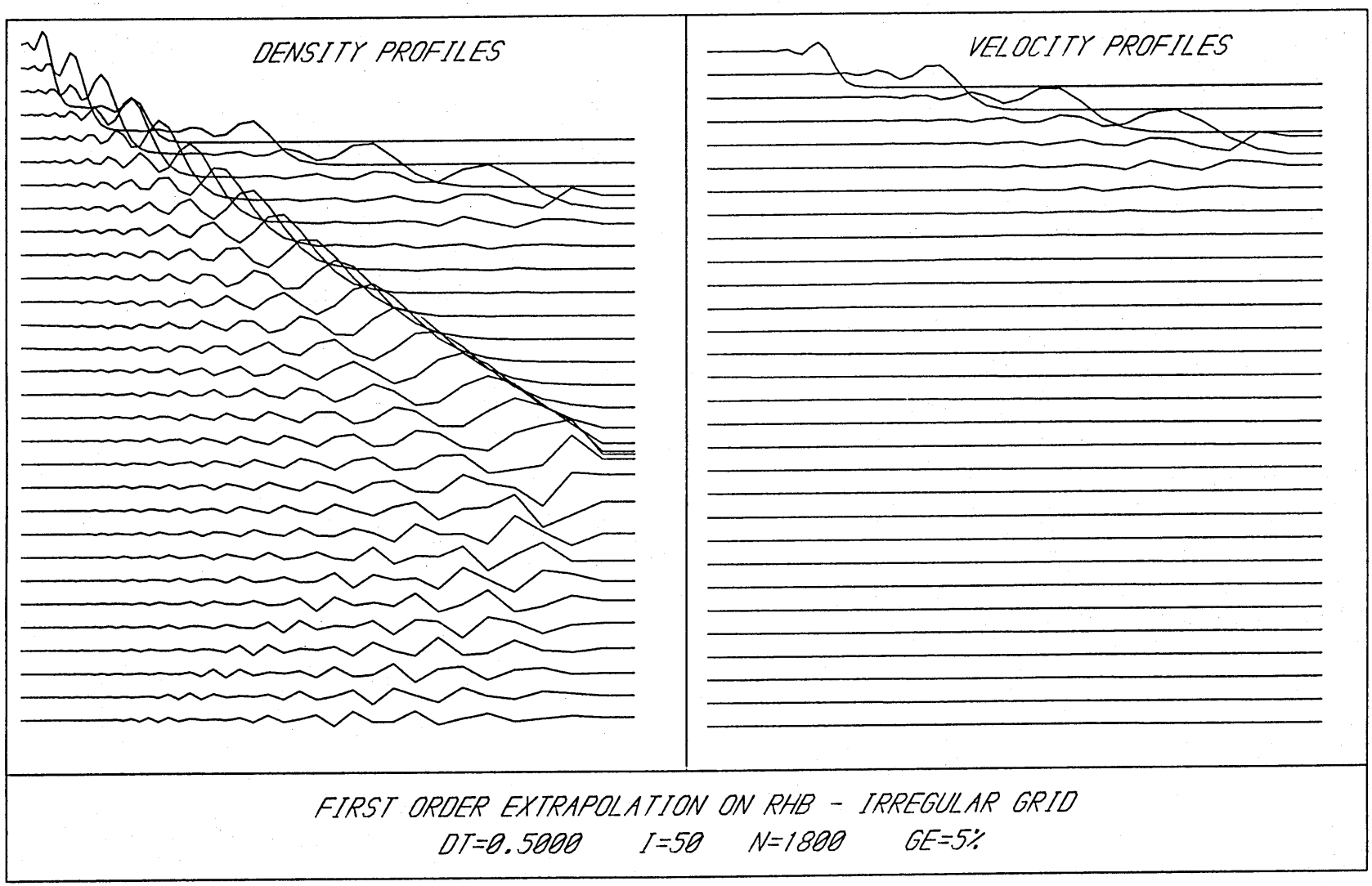
DENSITY PROFILES
VELOCITY PROFILES
FIRST ORDER EXTRAPOLATION ON RHB - IRREGULAR GRID
DT=0.5000 I=50 N=1800 GE=5%

(c)

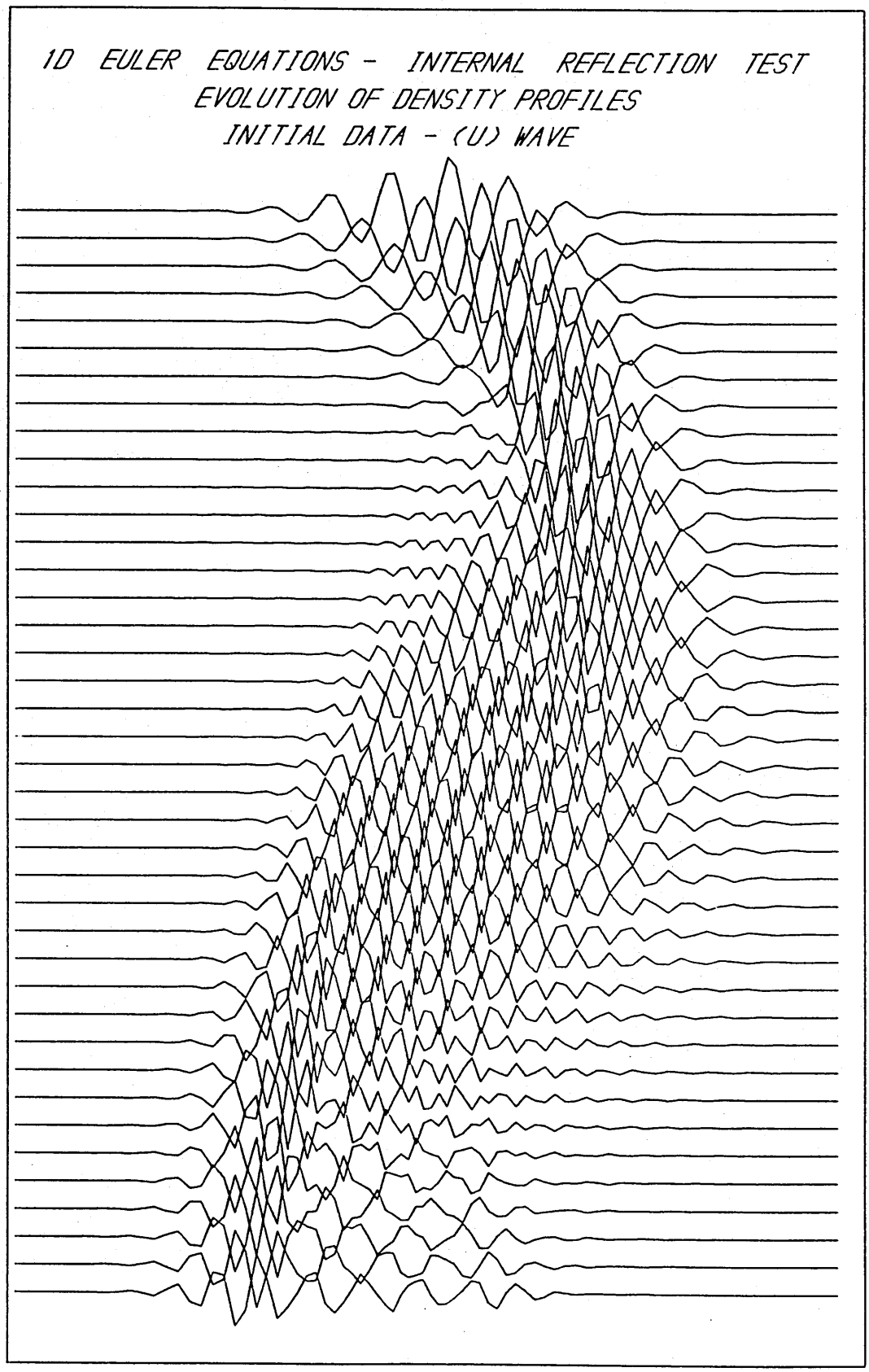
1D EULER EQUATIONS - INTERNAL REFLECTION TEST
EVOLUTION OF DENSITY PROFILES
INITIAL DATA - (U) WAVE

Figure (II.5)a

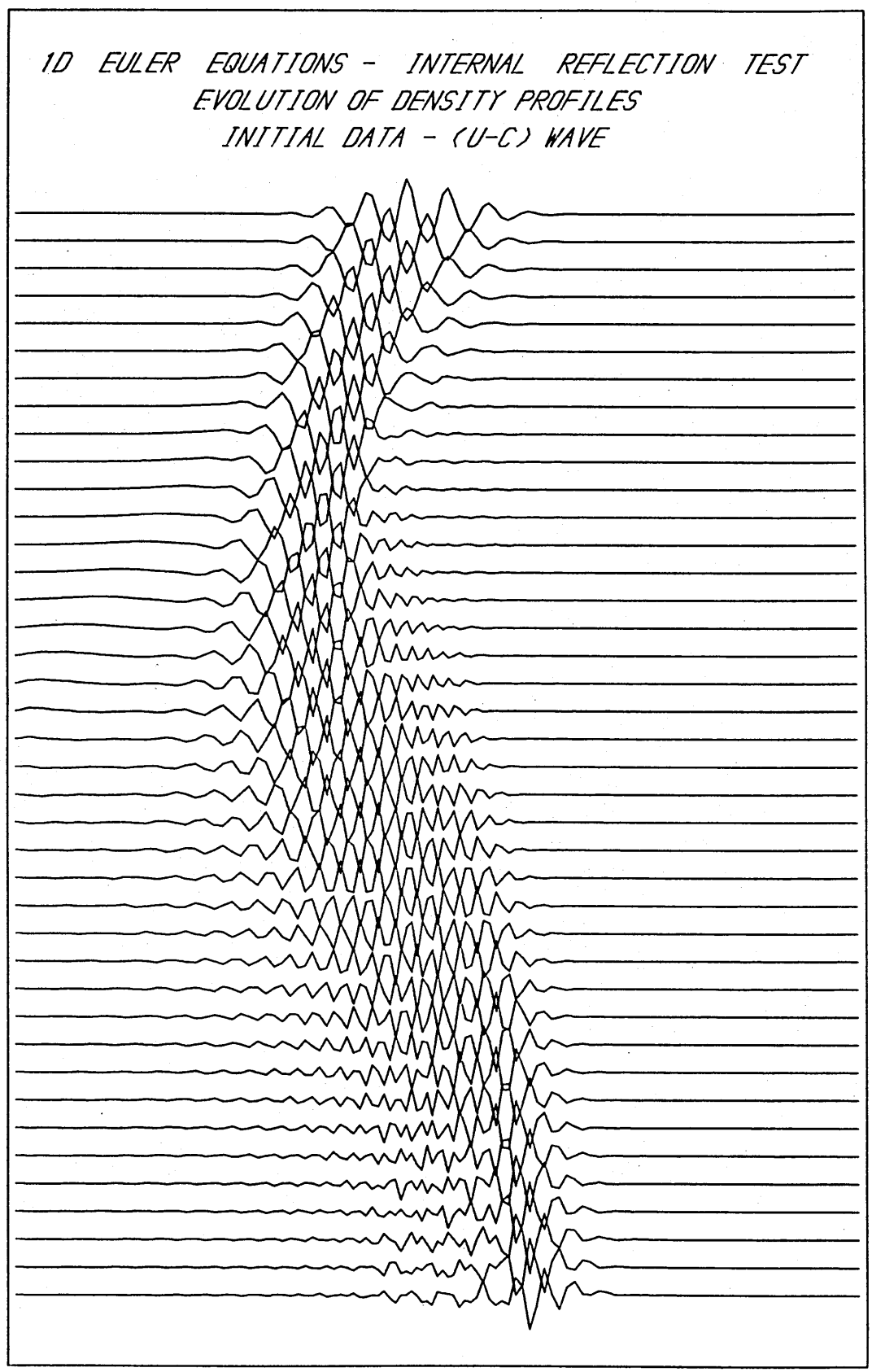
1D EULER EQUATIONS - INTERNAL REFLECTION TEST
EVOLUTION OF DENSITY PROFILES
INITIAL DATA - (U-C) WAVE

Figure (II.5)b

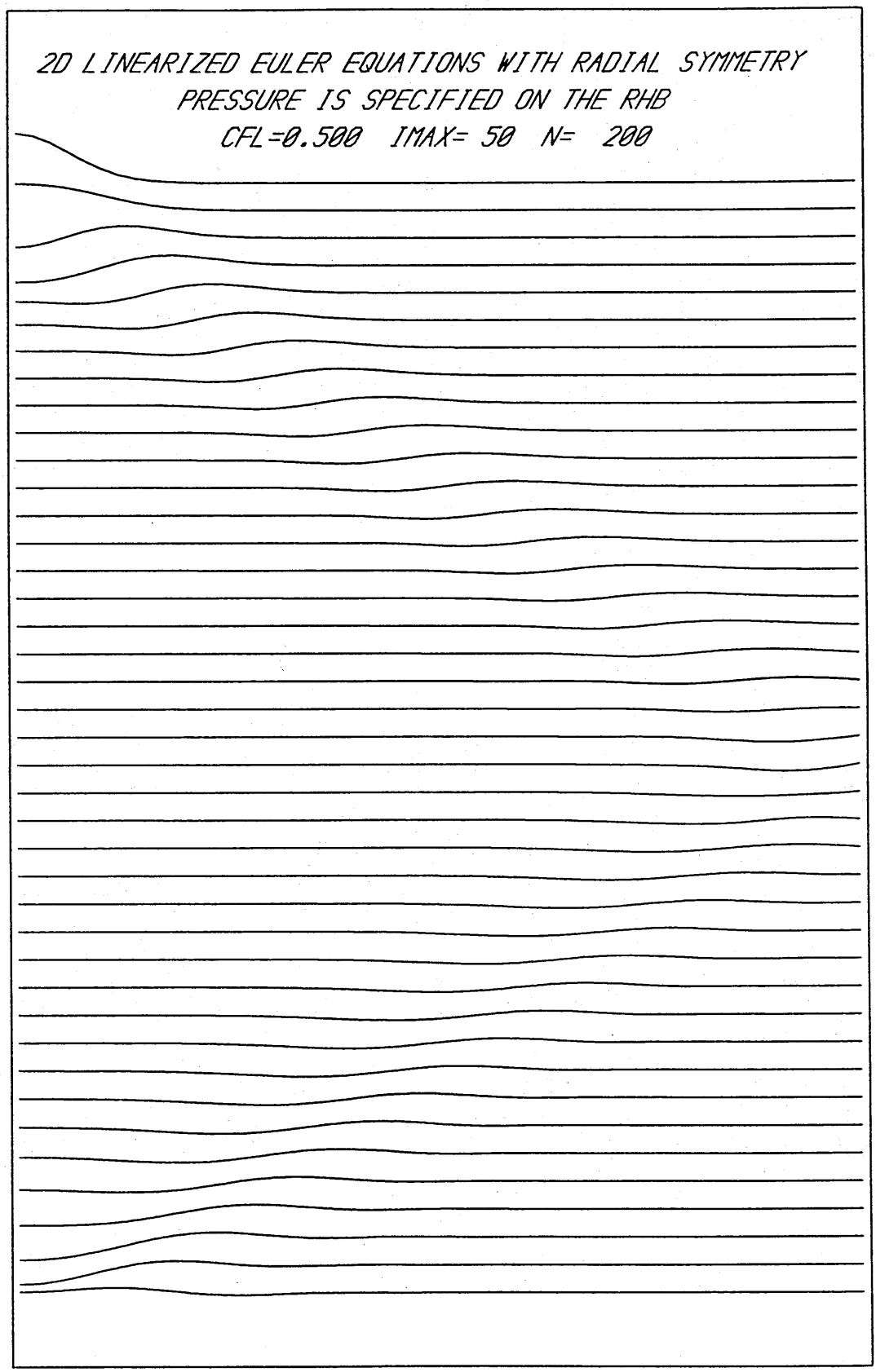

Figure (II.6) - Strong focussing of an error generated at the boundary (a) 2D linearised Euler Equations.

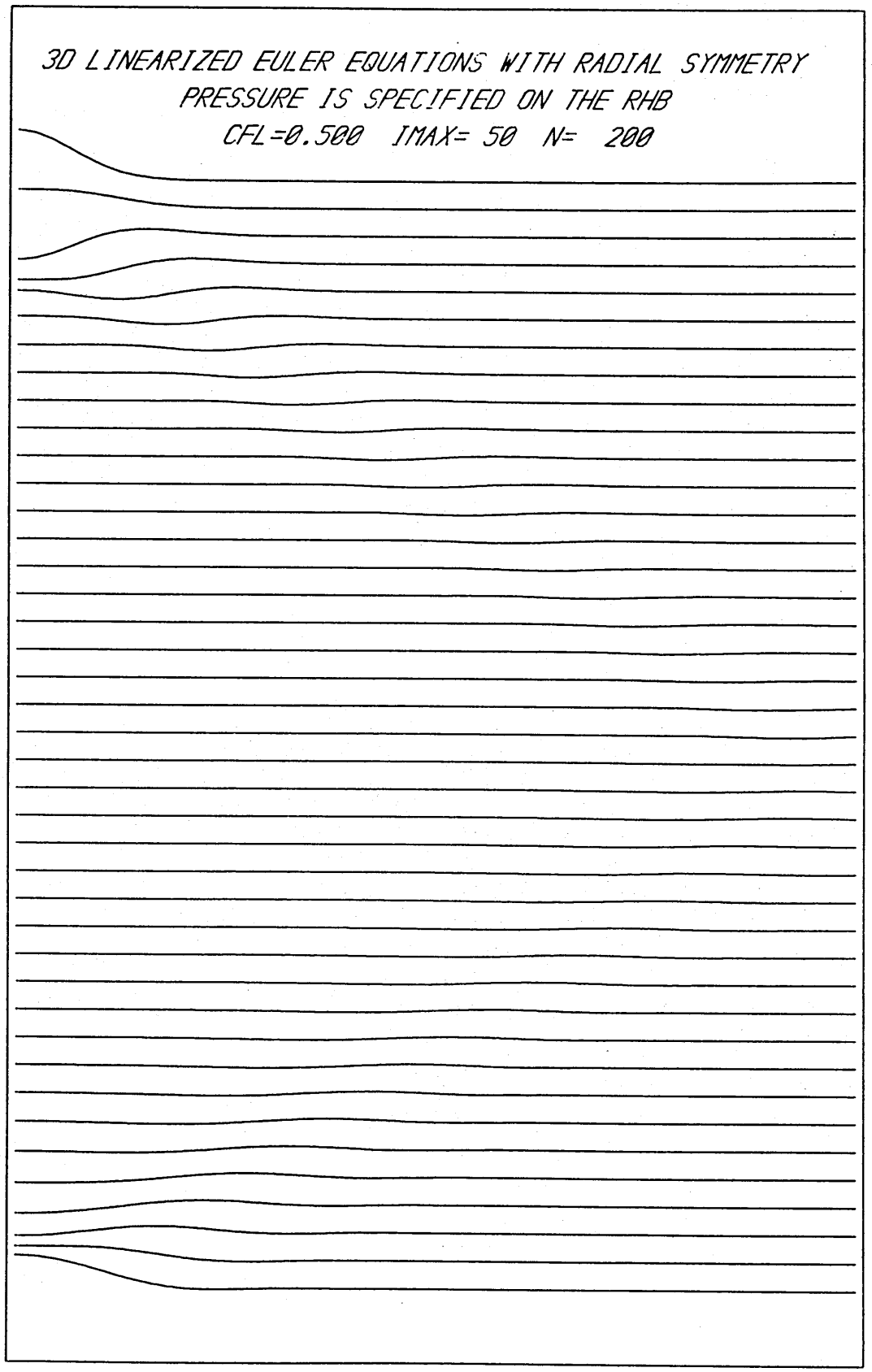

Figure (II.6) - Strong focussing of an error generated at the boundary (b) 3D linearised Euler Equations.

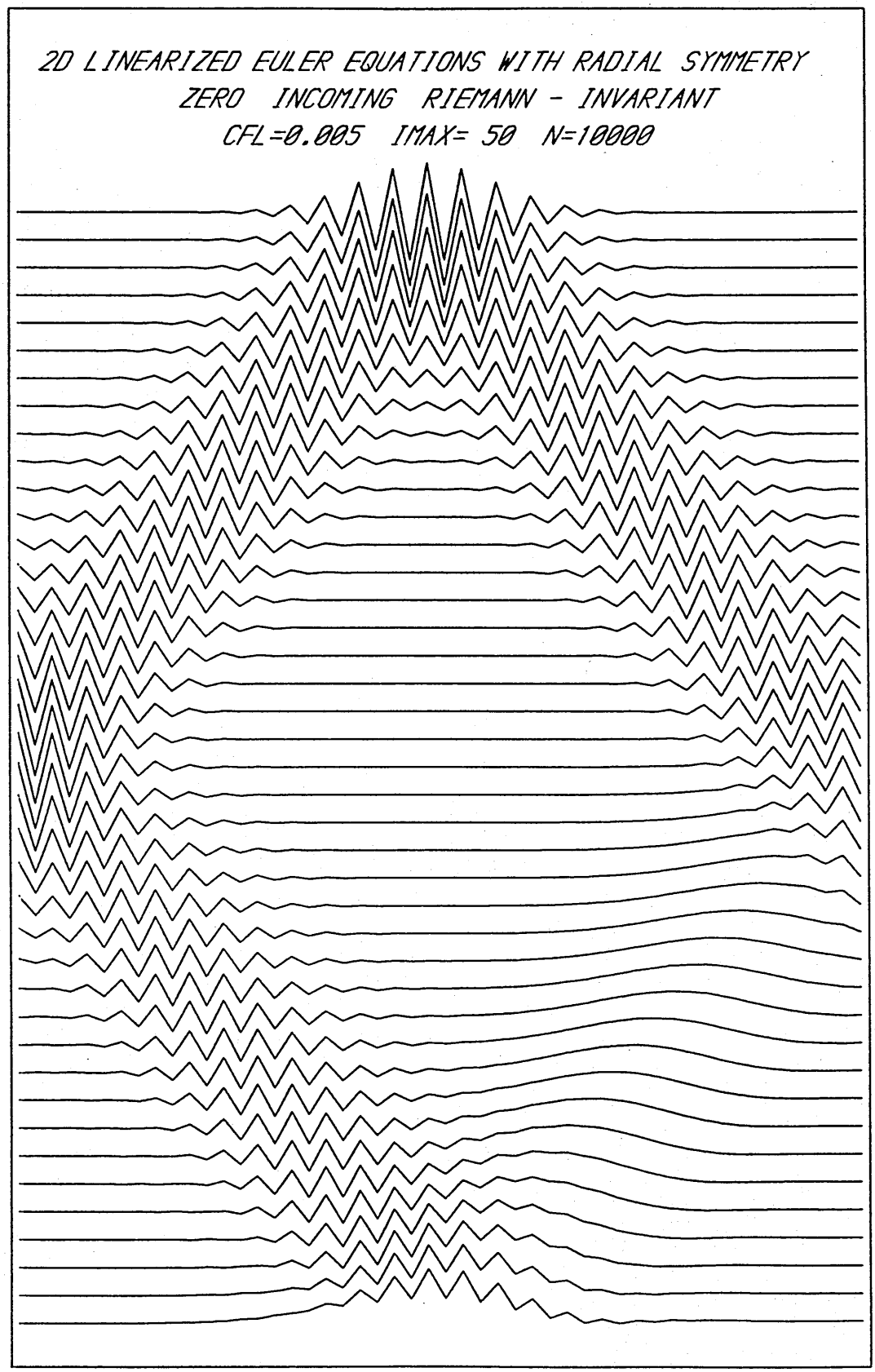

Figure (II.7) - 2D linearised Euler Equations - High frequency initial data : (a) p profiles.

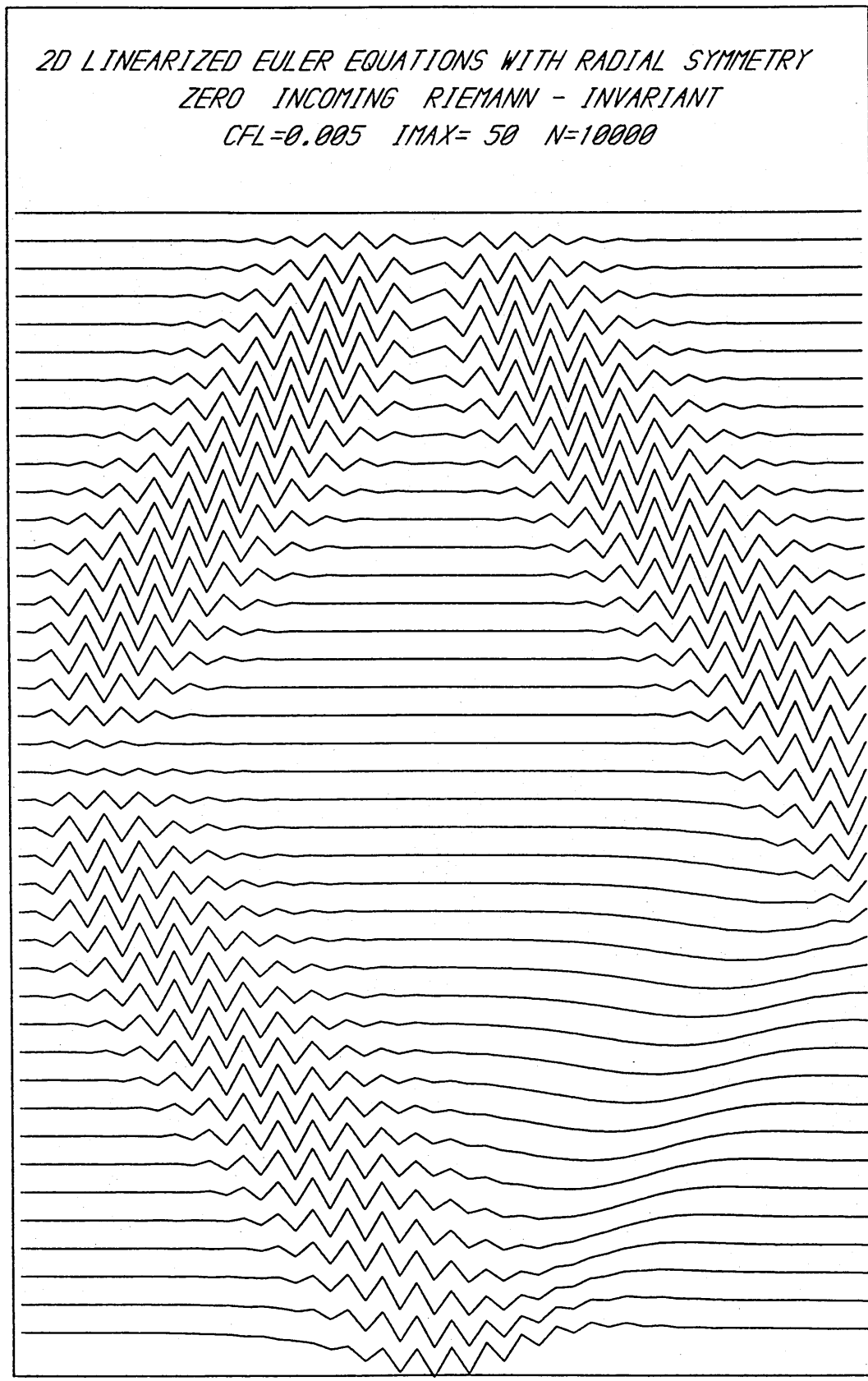

Figure (II.7) - 2D linearised Euler Equations - High frequency initial data (b) : q profiles.

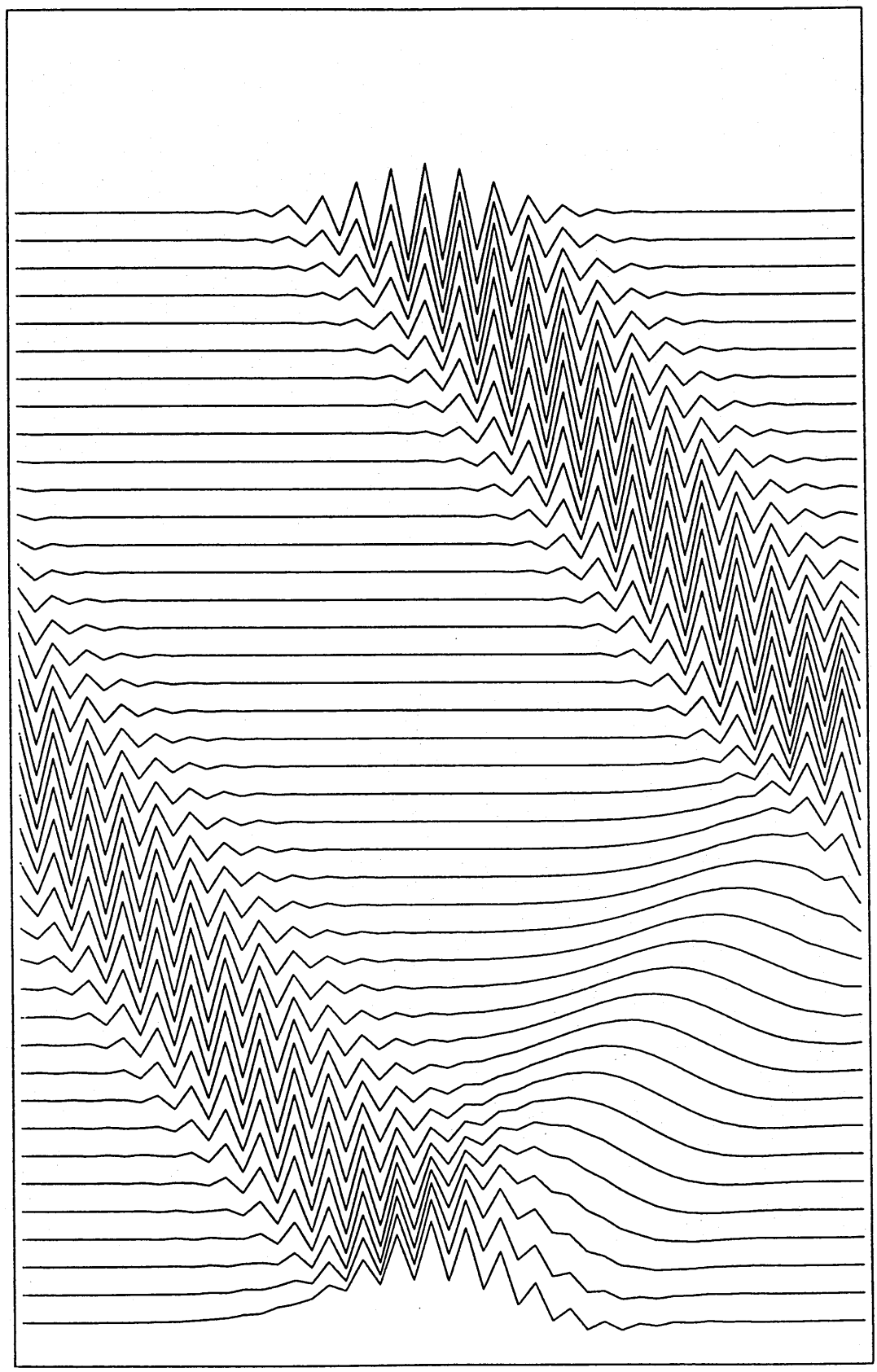

Figure (II.7) - 2D linearised Euler Equations - High frequency initial data: (c) p-q profiles.

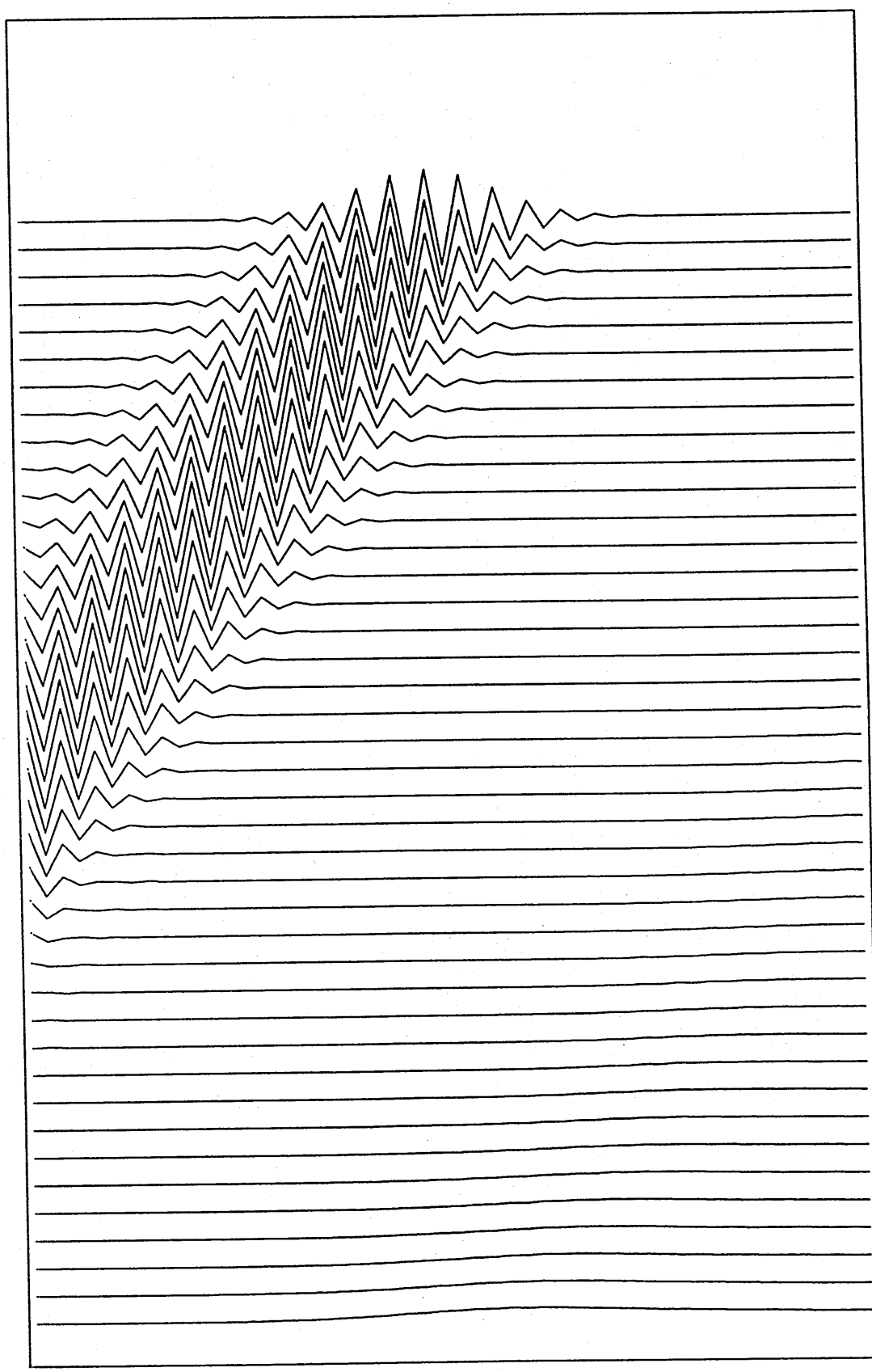

Figure (II.7) - 2D linearisec Euler Equations - High frequency initial data: (d) p+q profiles.

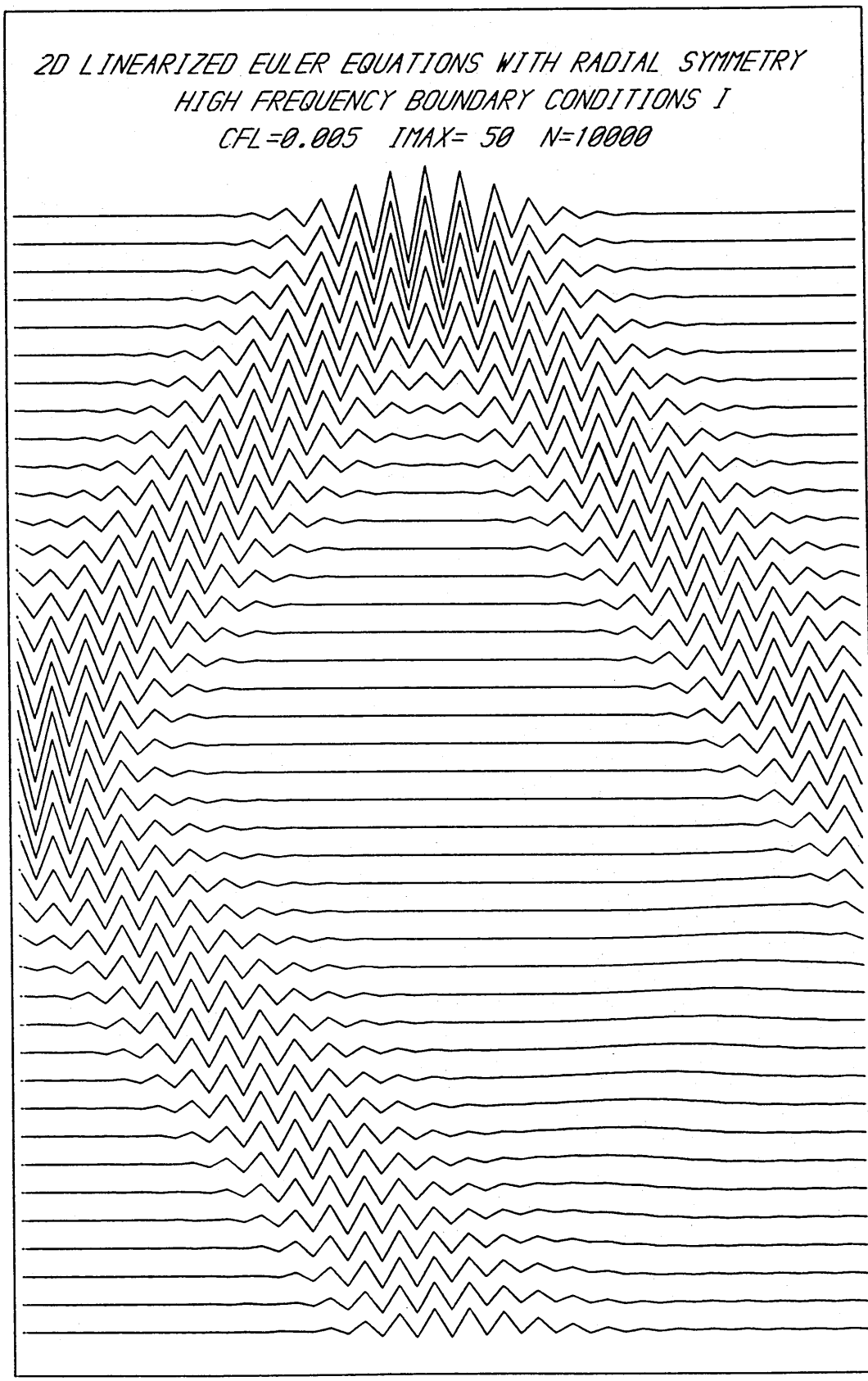

Figure (II.8) - 2D linearisec Euler Equations - High frequency boundary conditions (a).

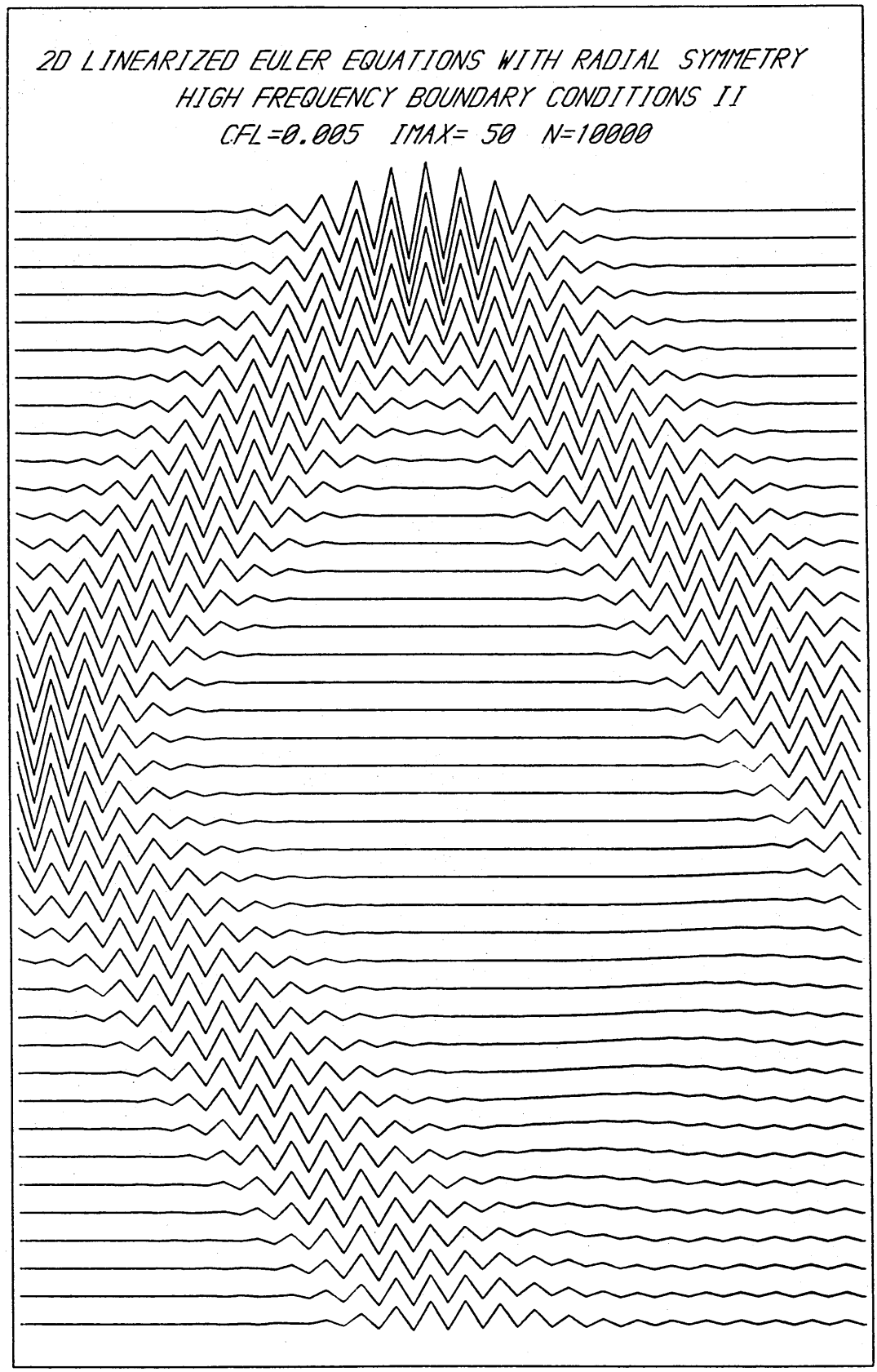

Figure (II.8) - 2D linearised Euler Equations - High frequency boundary conditions (b).

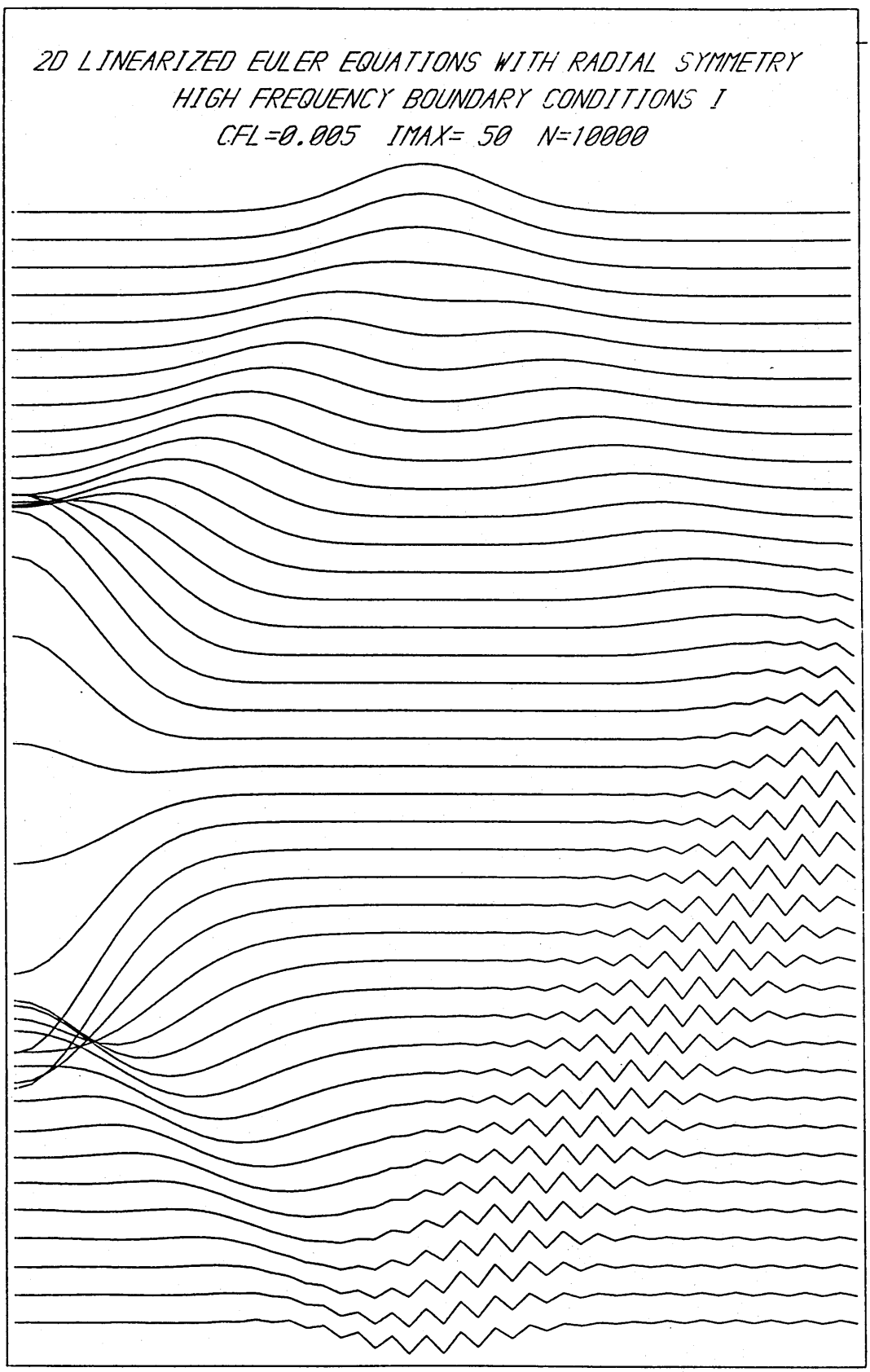

Figure (II.9) - 2D linearised Euler Equations - Reflection of a smooth wave from a high frequency boundary (a).

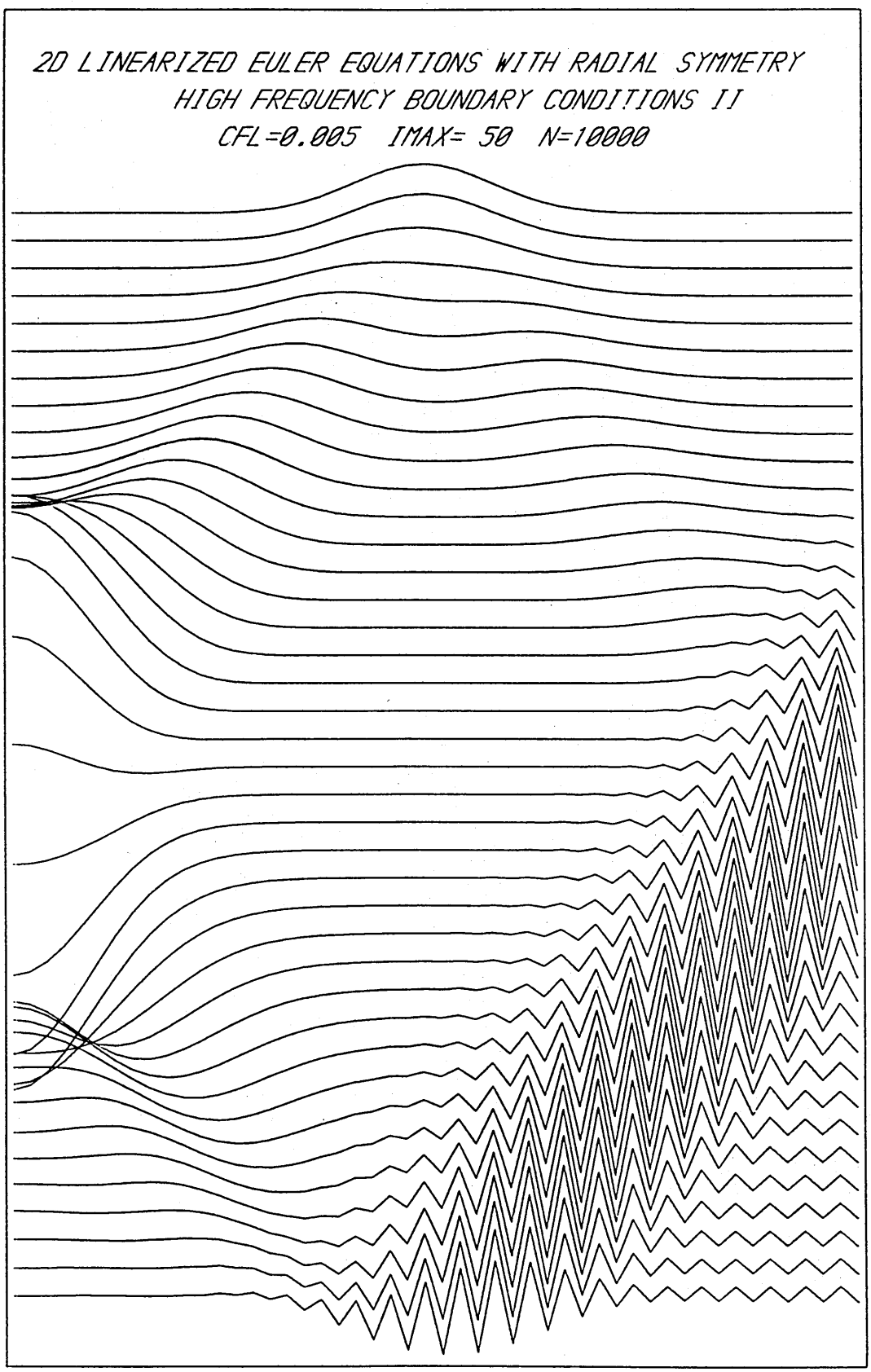

Figure (II.9) - 2D linearised Euler Equations - Reflection of a smooth wave from a high frequency boundary (b).

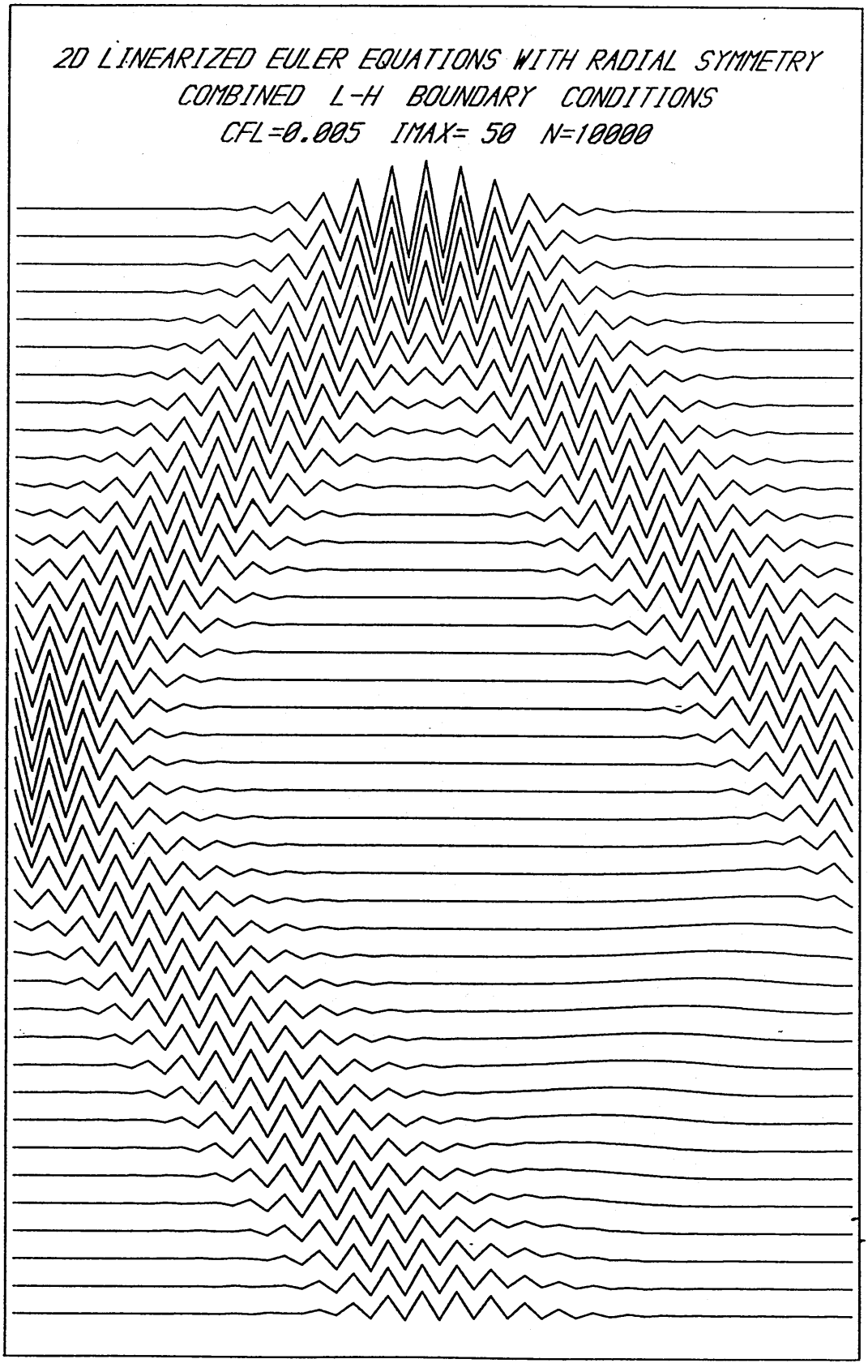

Figure (II.10) - 2D linearised Euler Equations - Combined Low-High frequency boundary conditions. (a)

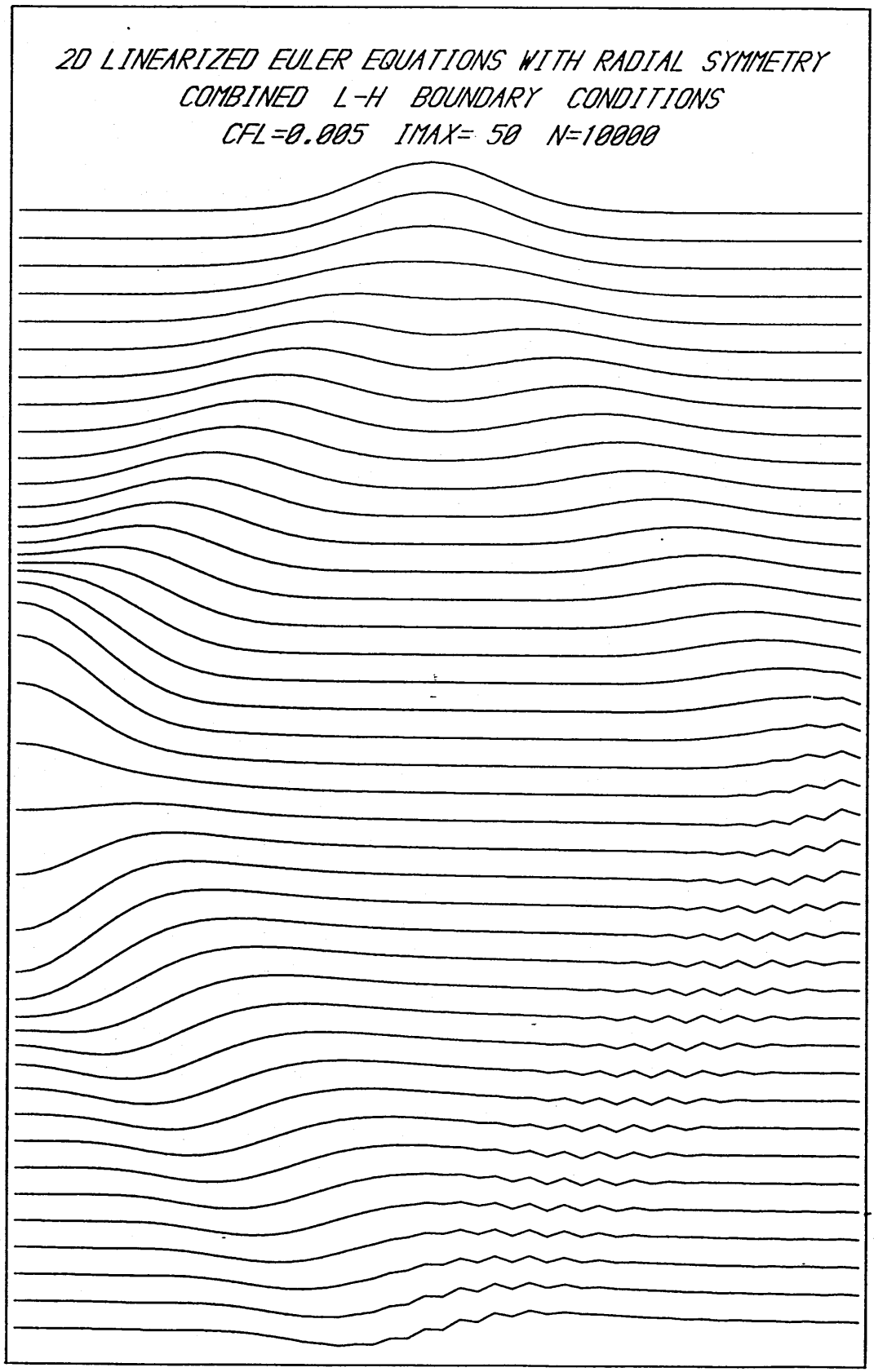
2D LINEARIZED EULER EQUATIONS WITH RADIAL SYMMETRY
COMBINED L-H BOUNDARY CONDITIONS
CFL=0.005 IMAX= 50 N=10000

(b)

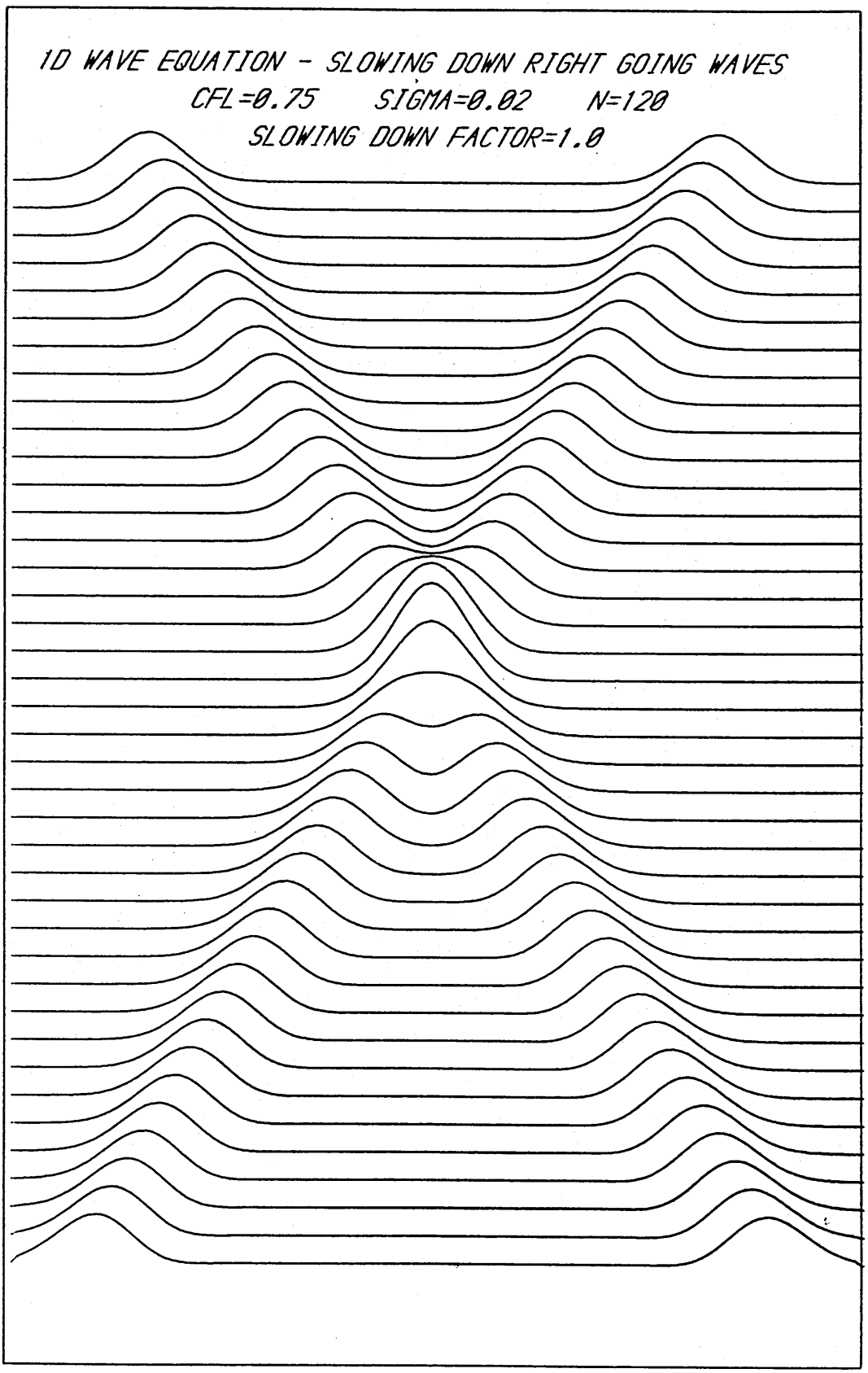

Figure (III.1) - 1D wave equation: (a) Constant slowing down coefficient.

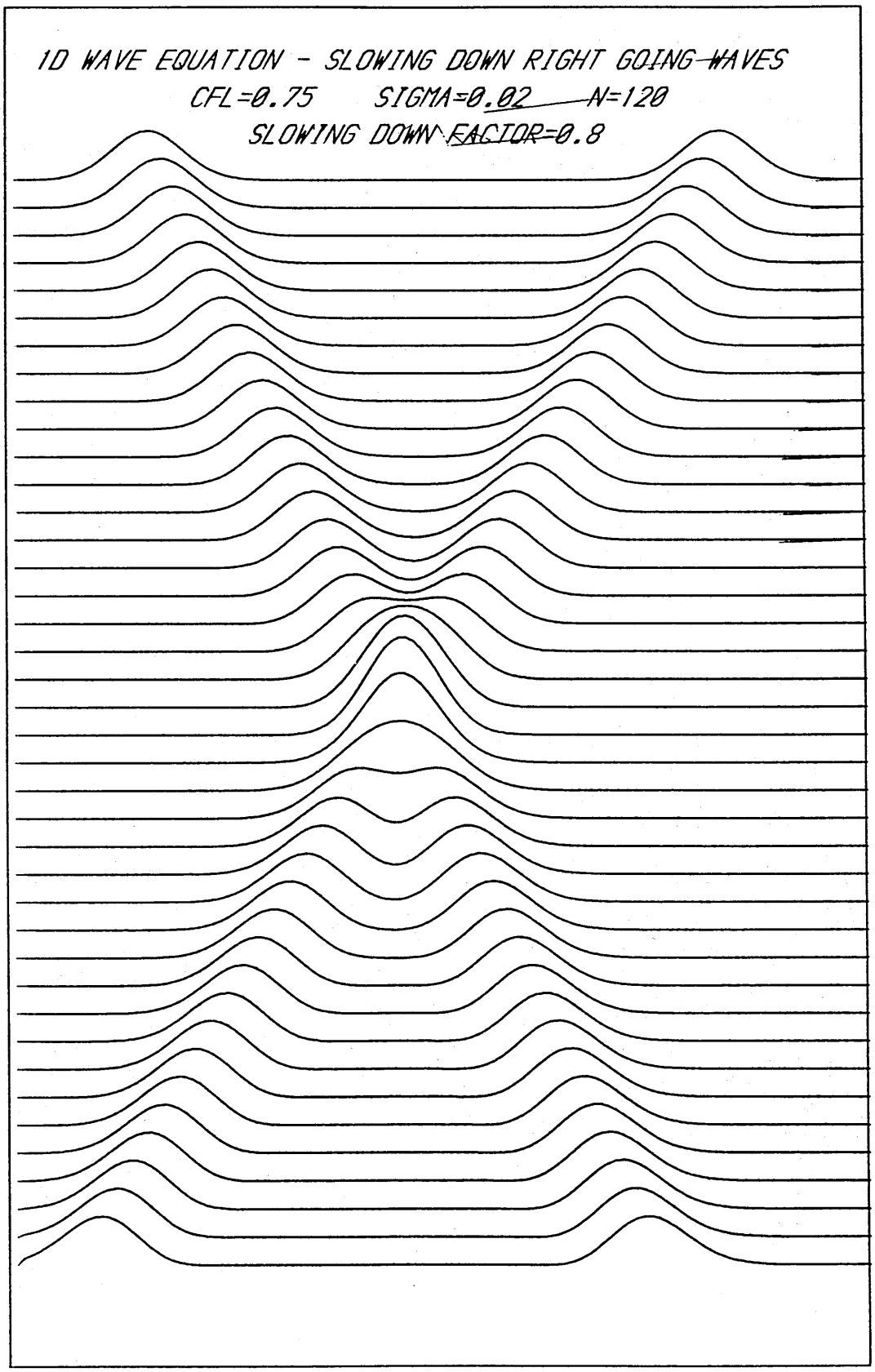

Figure (III.1) - 1D wave equation: (b) Constant slowing down coefficient.

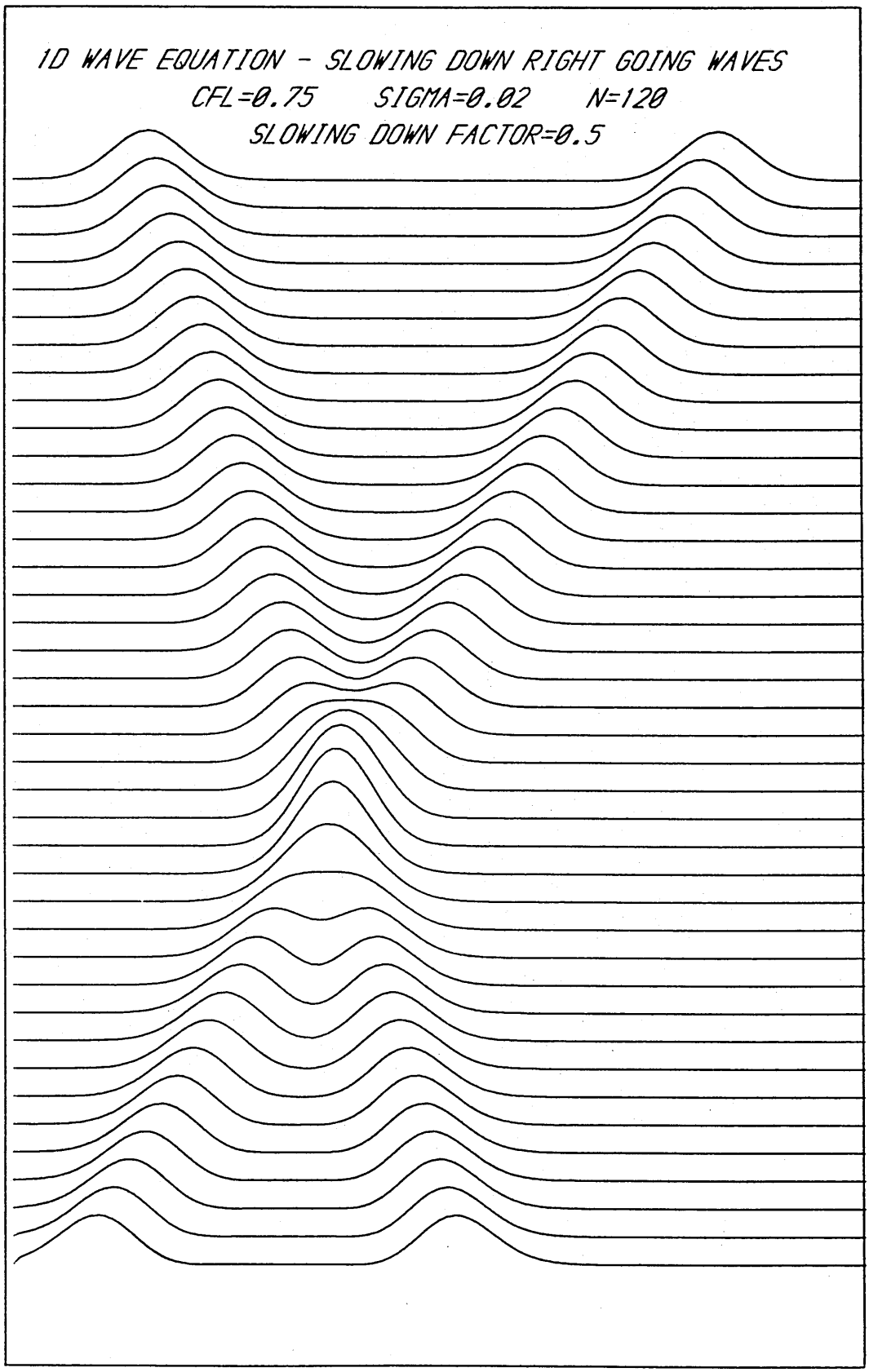

Figure (III.1) - 1D wave equation: (c) Constant slowing down coefficient.

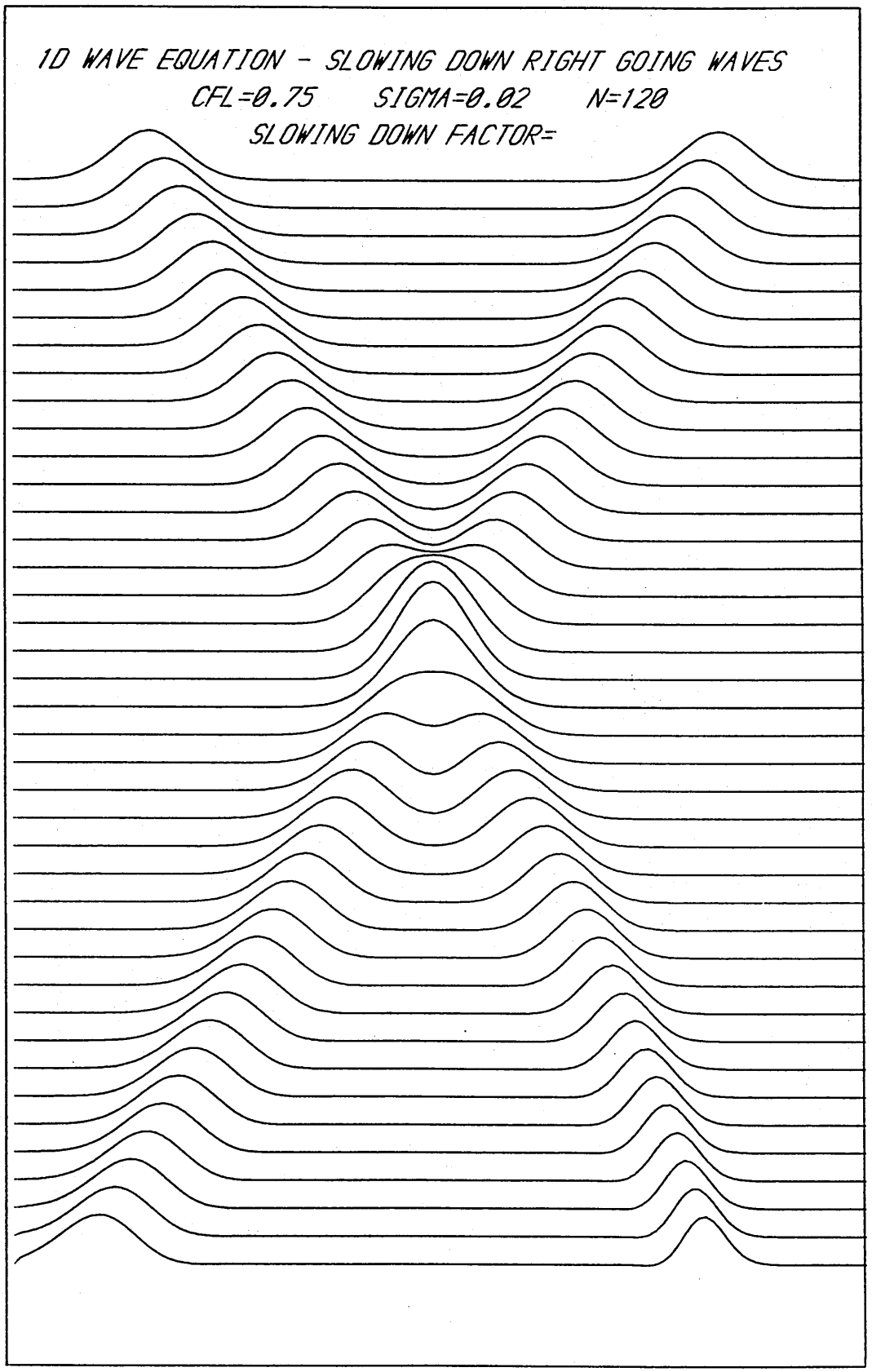

Figure (III.1) - 1D wave equation: (d) Smoothly varying slowing down coefficient.

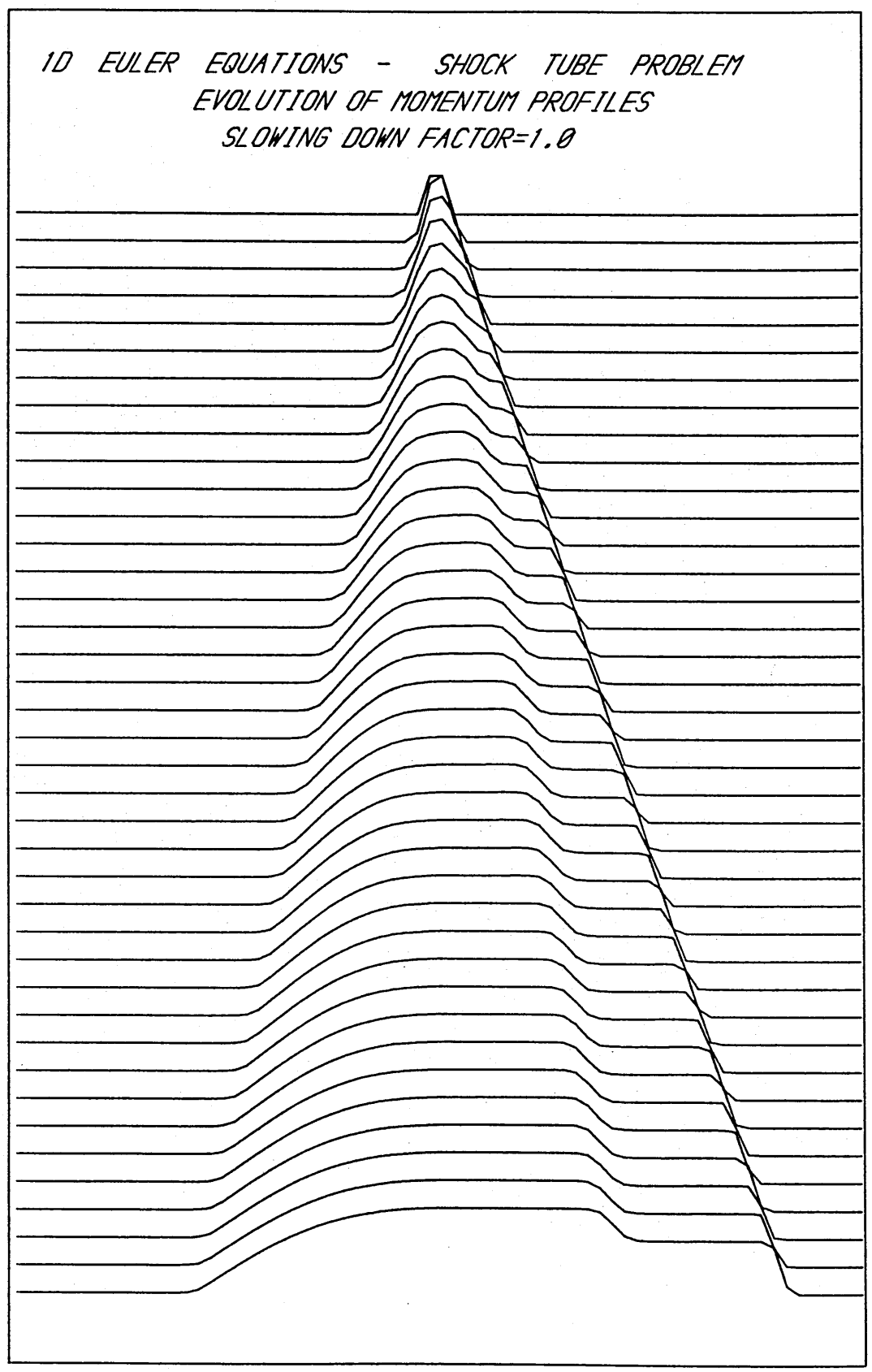

Figure (III.2) - 1D Euler equations with various constant slowing down coefficients (a).

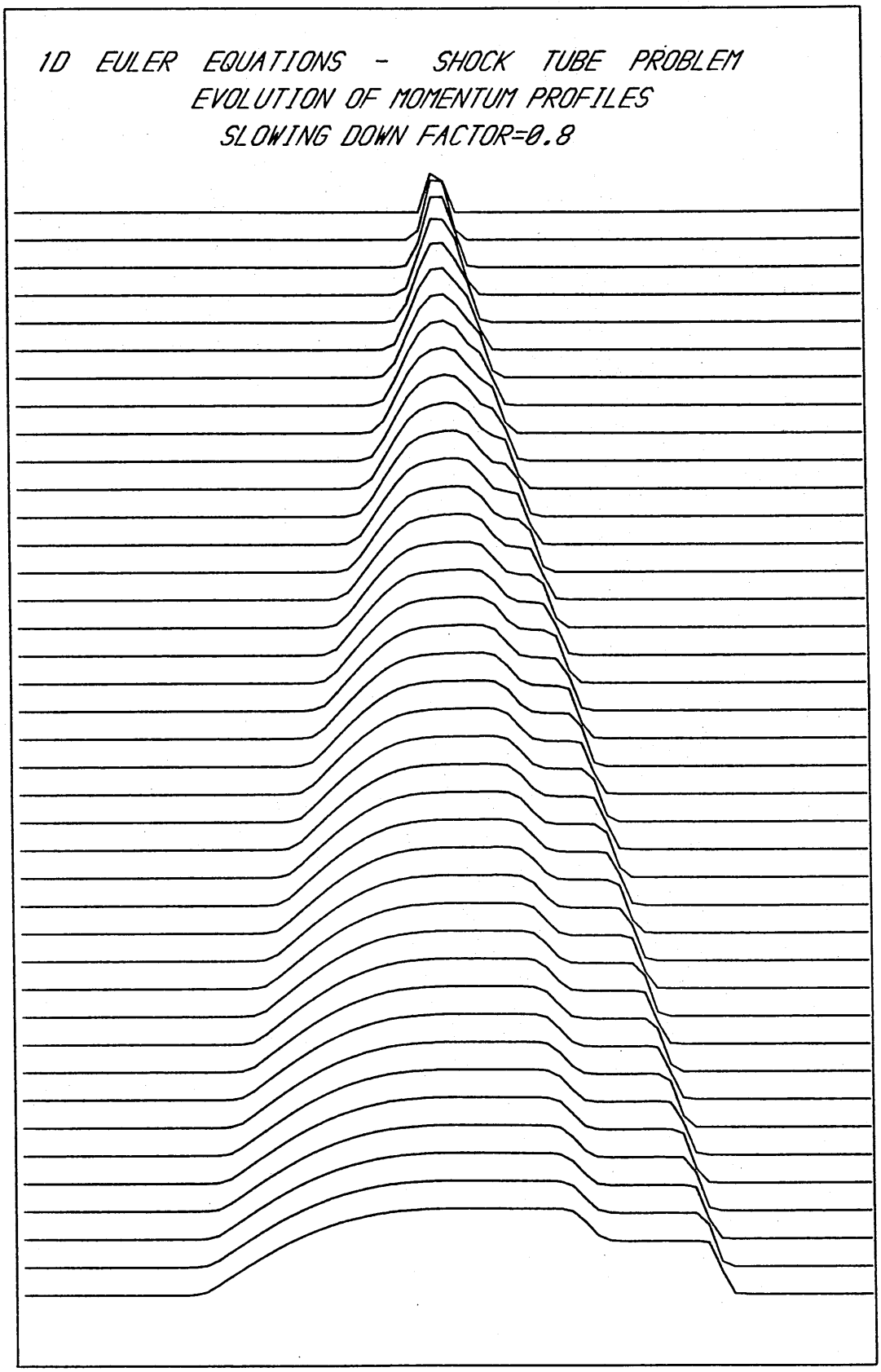

Figure (III.2) - 1D Euler equations with various constant slowing down coefficients (b).

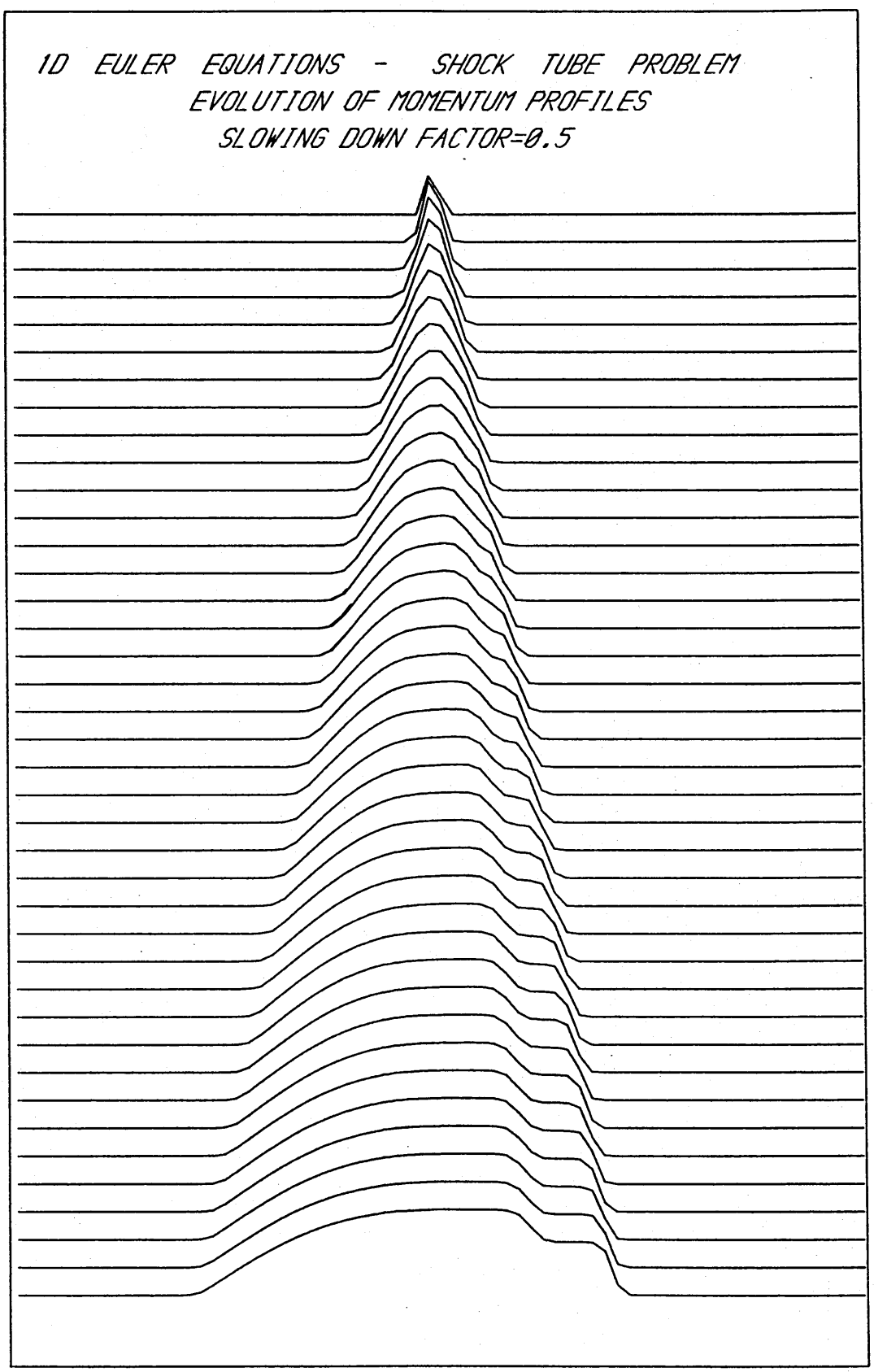

Figure (III.2) - 1D Euler equations with various constant slowing down coefficients (c).

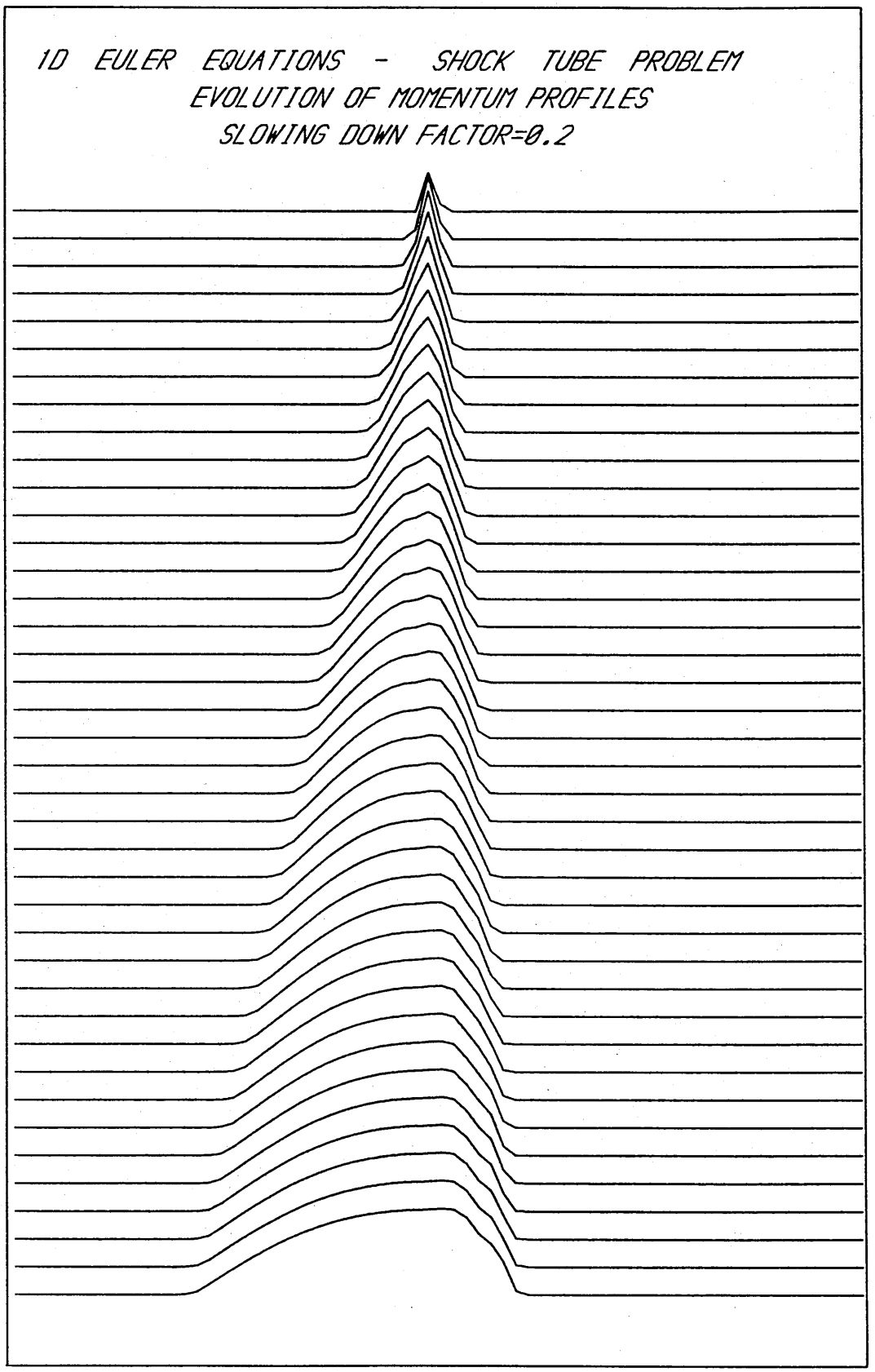

Figure (III.2) - 1D Euler equations with various constant slowing down coefficients (d).

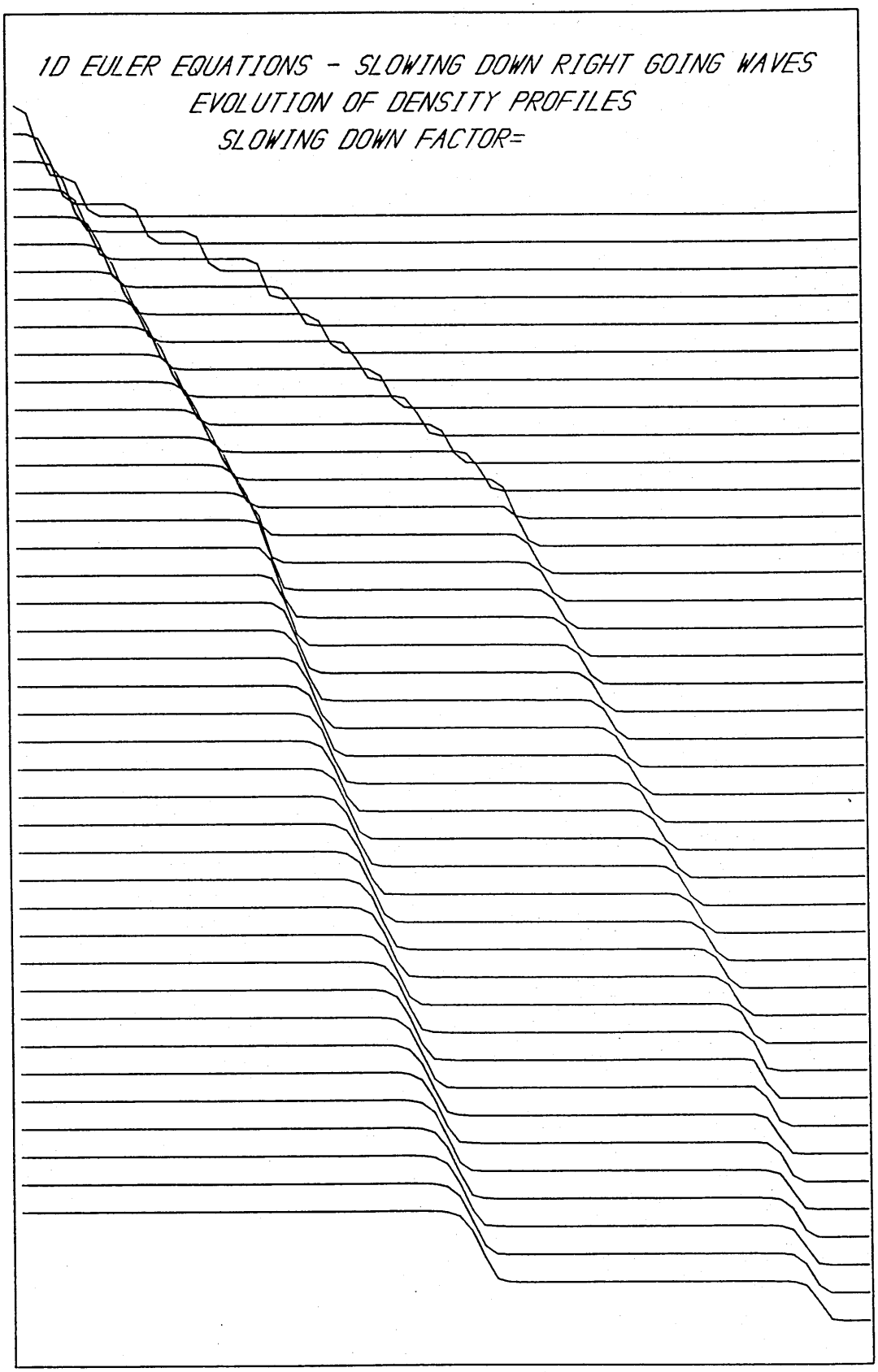

Figure (III.3) - 1D Euler equations - (a) Piecewise constant slowing down coefficients.

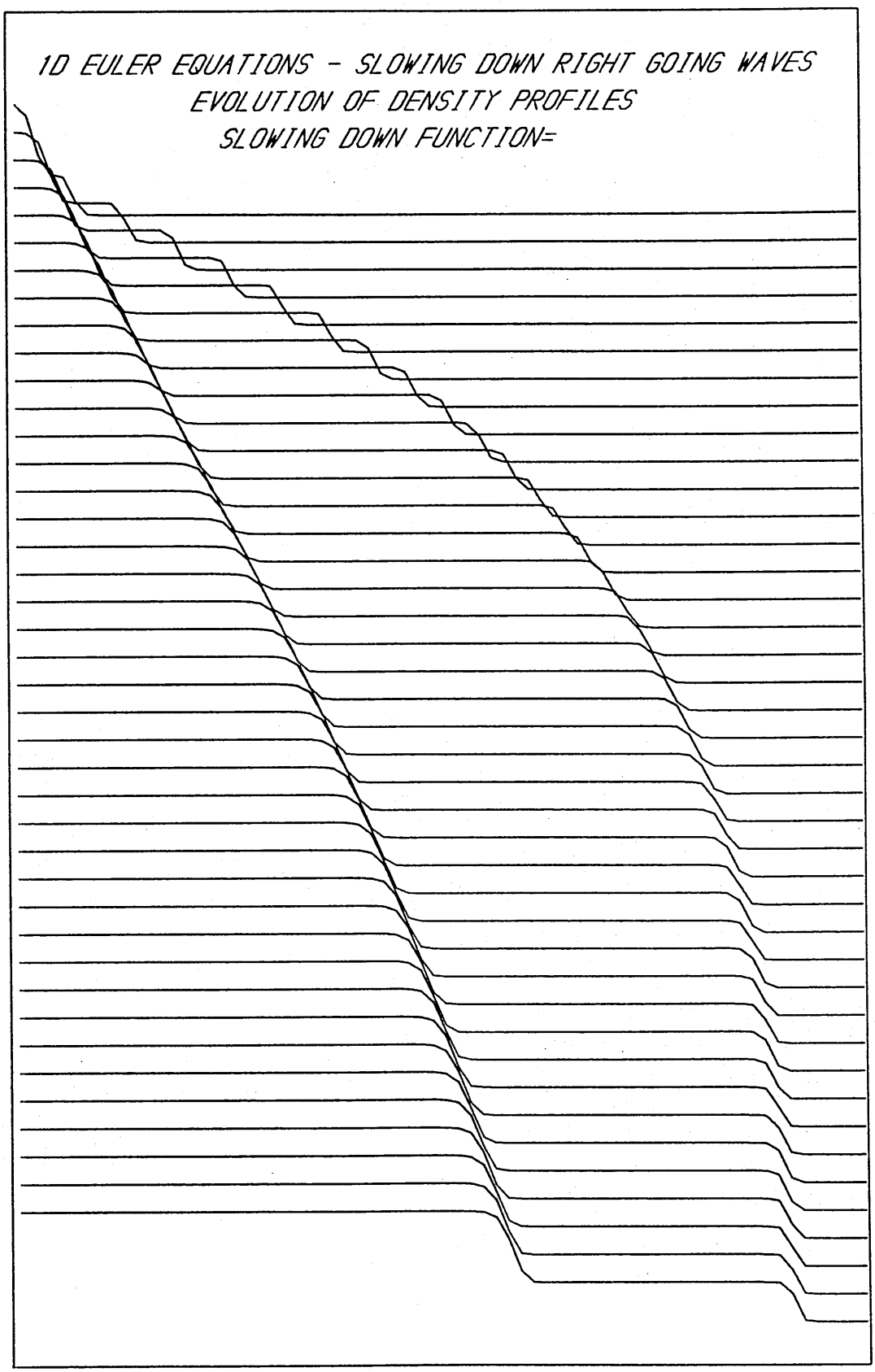

Figure (III.3) - 1D Euler equations - (b) Smoothly varying slowing down coefficients.

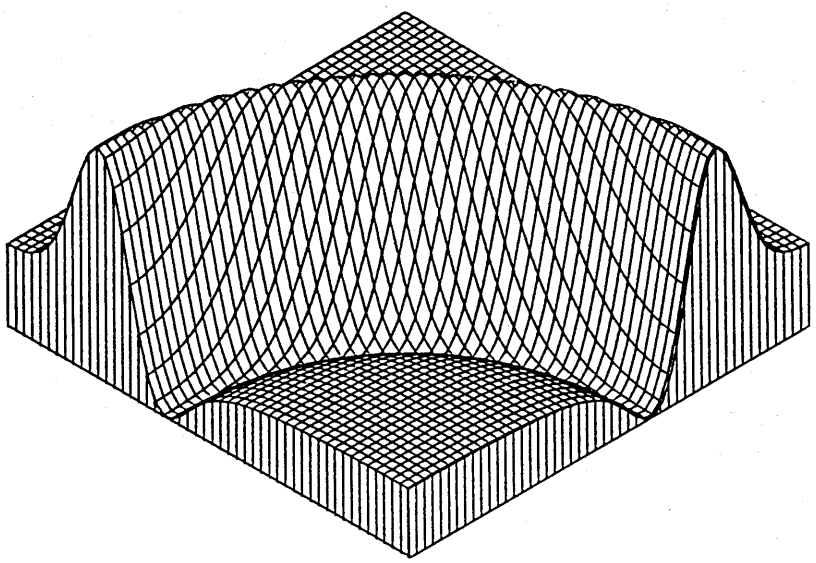

(a) Exact Solution - Projection

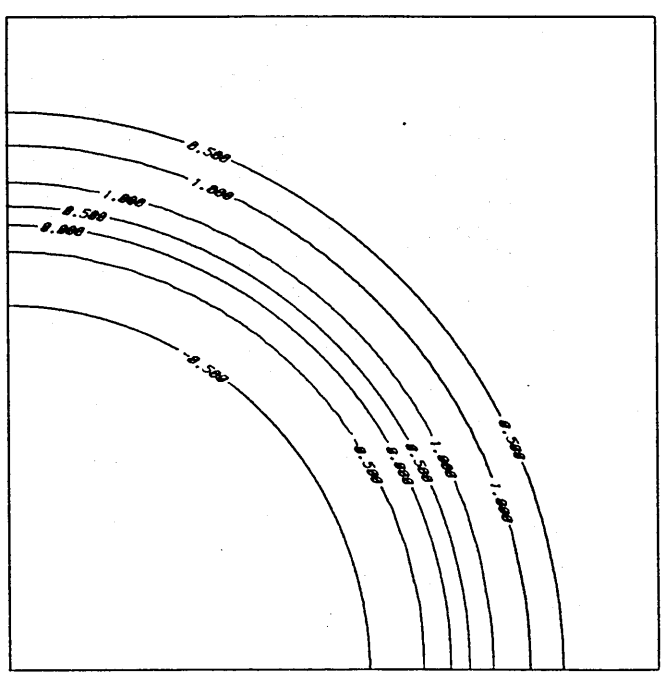

(b) Exact Solution - Contours

Figure (III.4) - 2D linearised Euler equations - Exact solution for initial data (3.8.5).

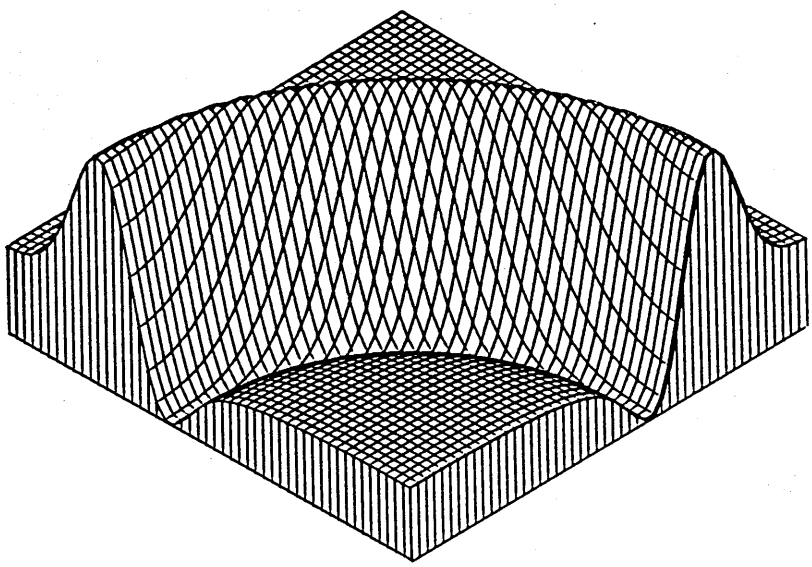

(a) Outgoing Speed = 1.0

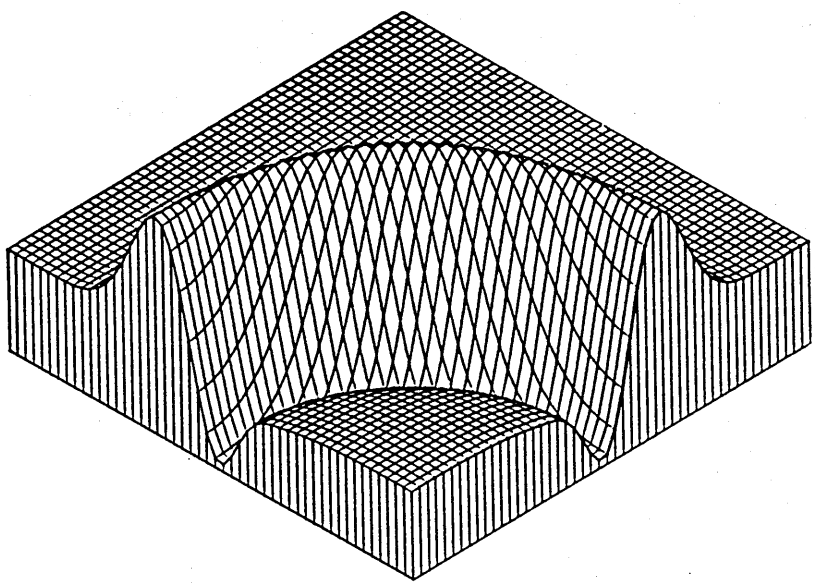

(b) Outgoing Speed = 0.8

Figure (III.5) - 2D linearised Euler equations - Numerical solution for initial data (3.8.5).

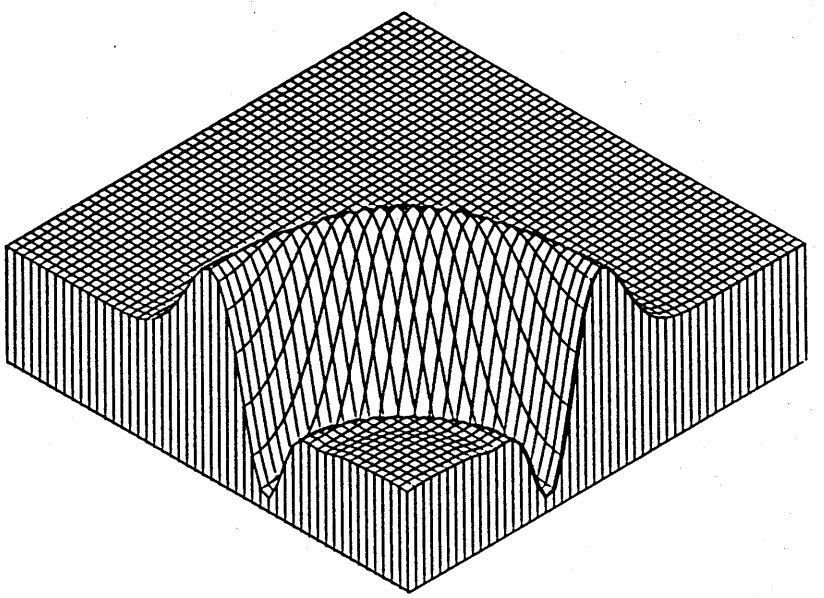

(c) Outgoing Speed = 0.6

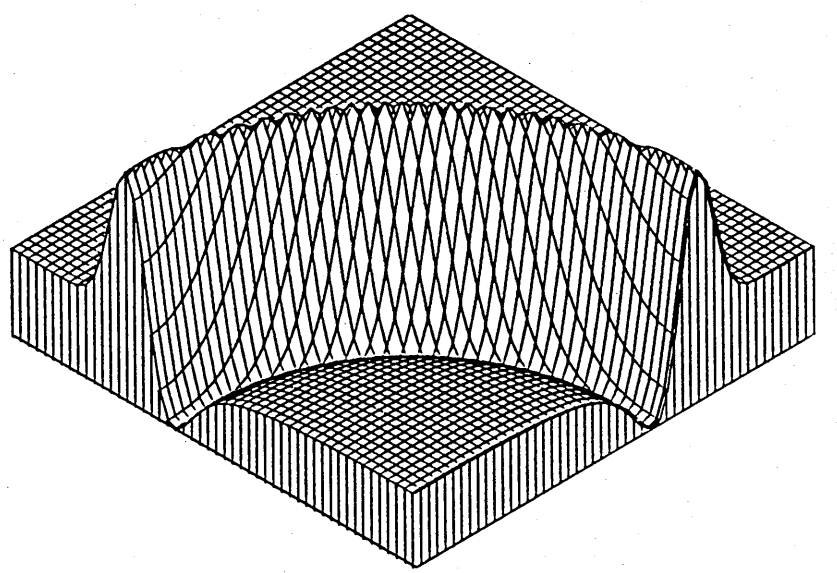

(d) Outgoing Speed = 1 - r

Figure (III.5) - 2D linearised Euler equations - Numerical solution for initial data (3.8.5).

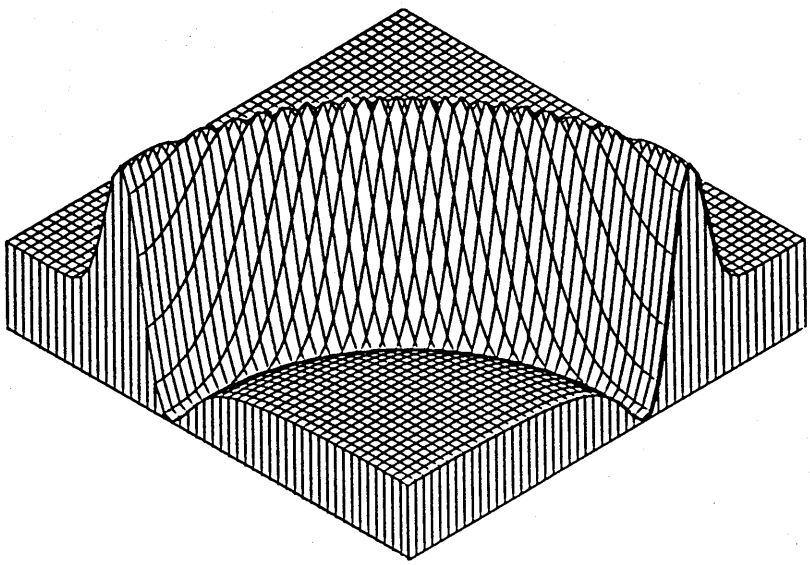

(a) Outgoing Speed = 1 - r
System No I

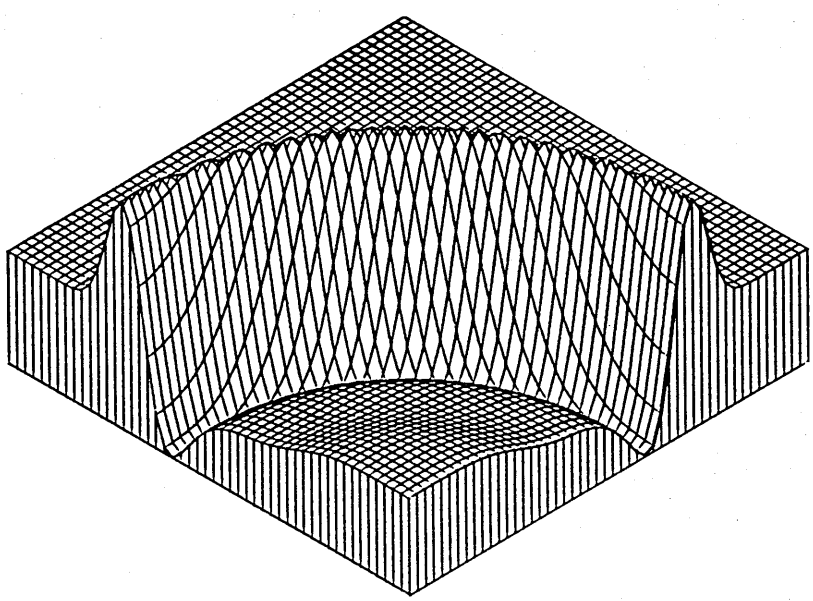

(b) Outgoing Speed = 1 - r
System No II

Figure (III.6) - 2D linearised Euler equations - Numerical solution for initial data (3.8.5).

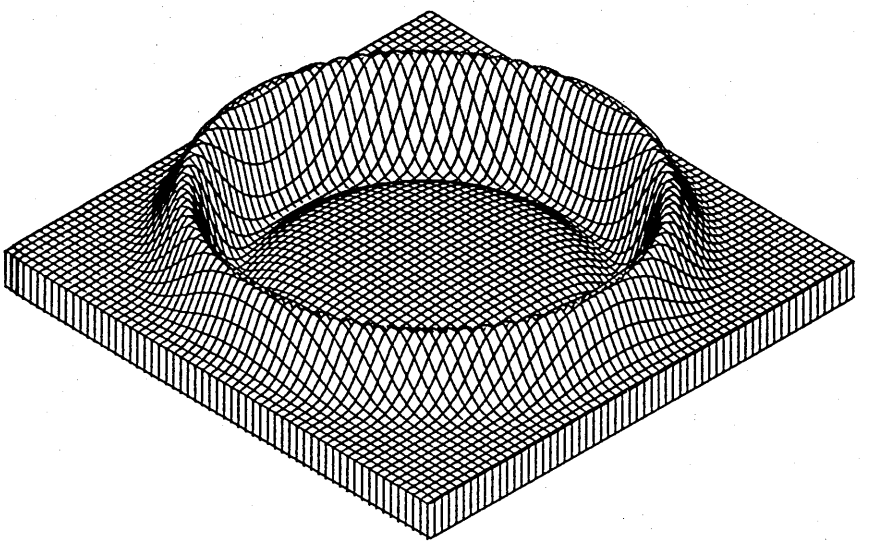

(a) Exact Solution - Projection

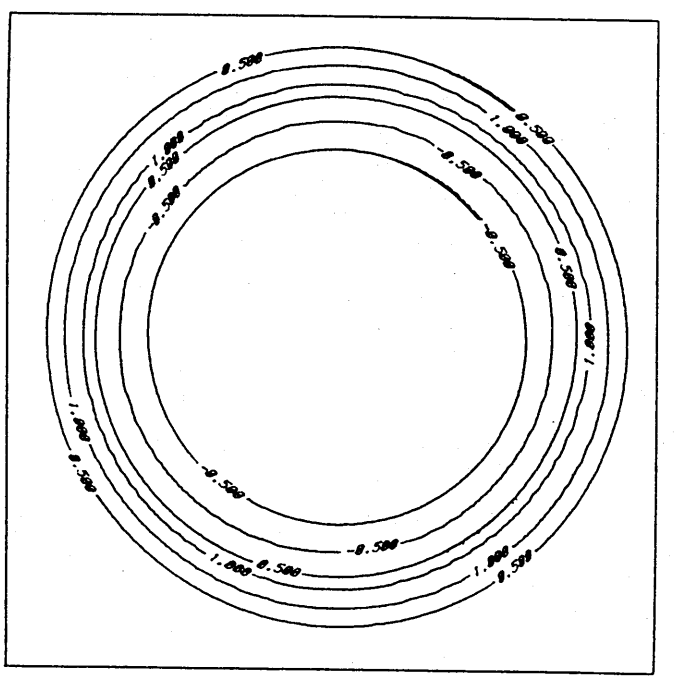

(b) Exact Solution - Contours

Figure (III.7) - 2D linearised Euler equations - Exact solution for initial data (3.8.7).

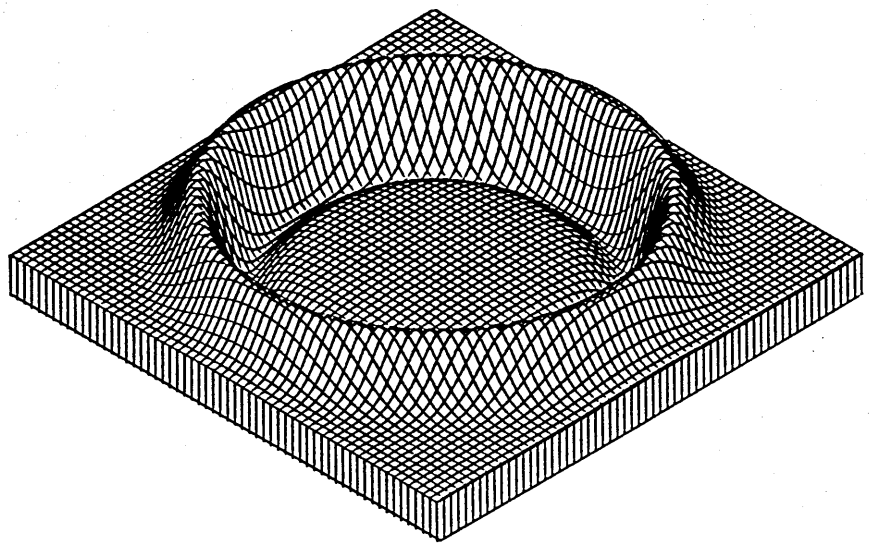

(a) Outgoing Speed = 1.0

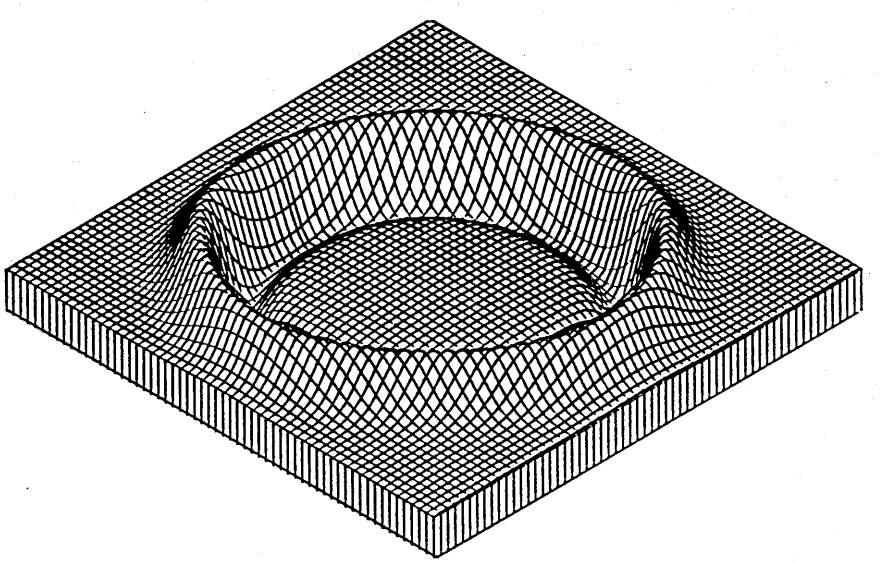

(b) Outgoing Speed = 0.8

Figure (III.8) - 2D linearised Euler equations - Numerical solution for initial data (3.8.7).

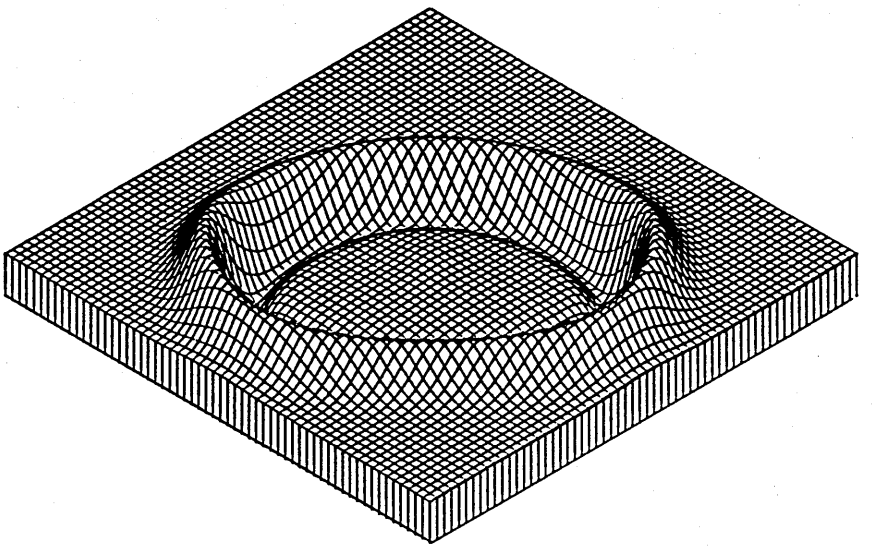

(c) Outgoing Speed = 0.6

Figure (III.8) - 2D linearised Euler equations - Numerical solution for initial data (3.8.7).

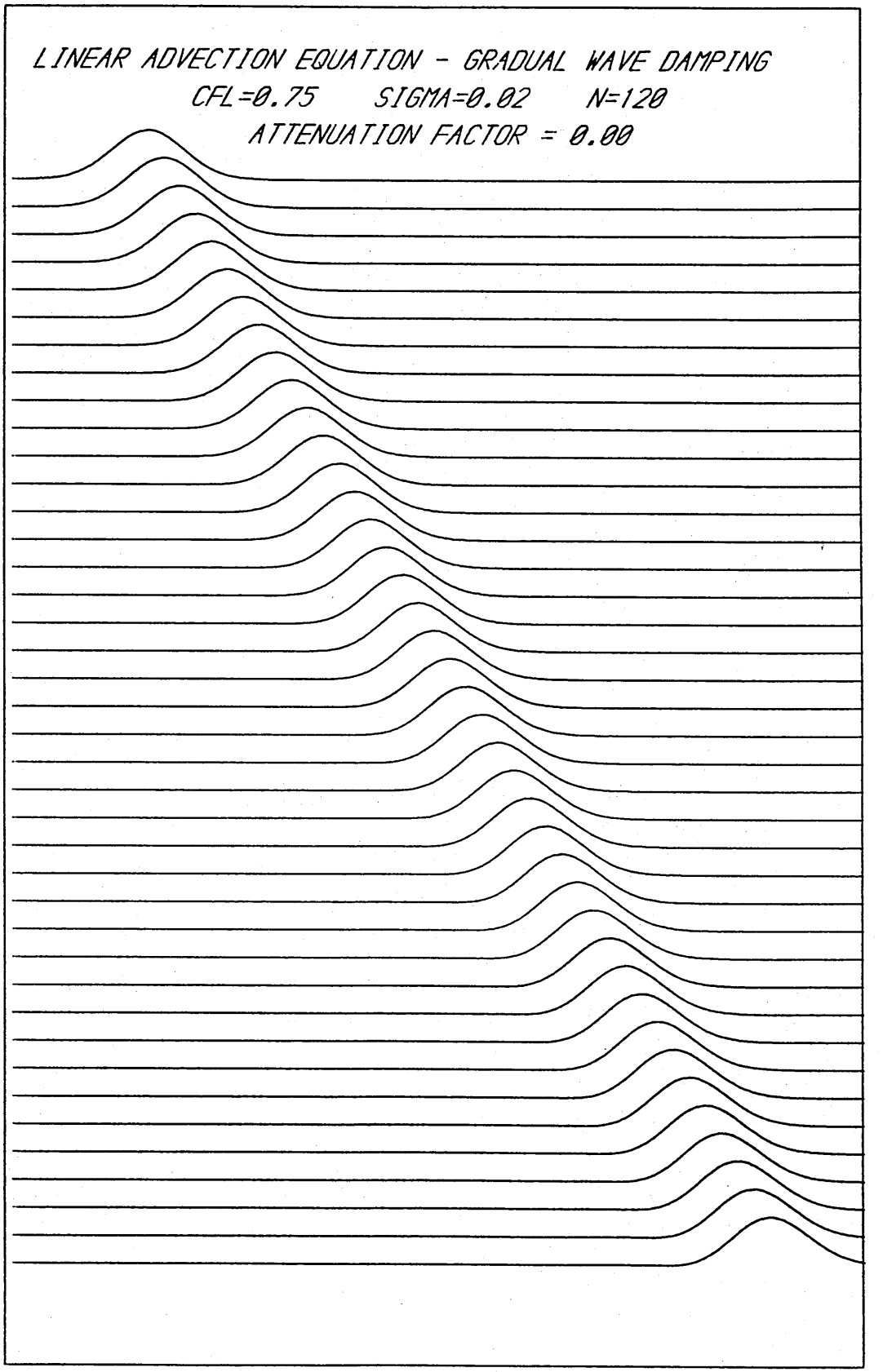

Figure (IV.1) - Linear advection equation - gradually attenuated solution (a).

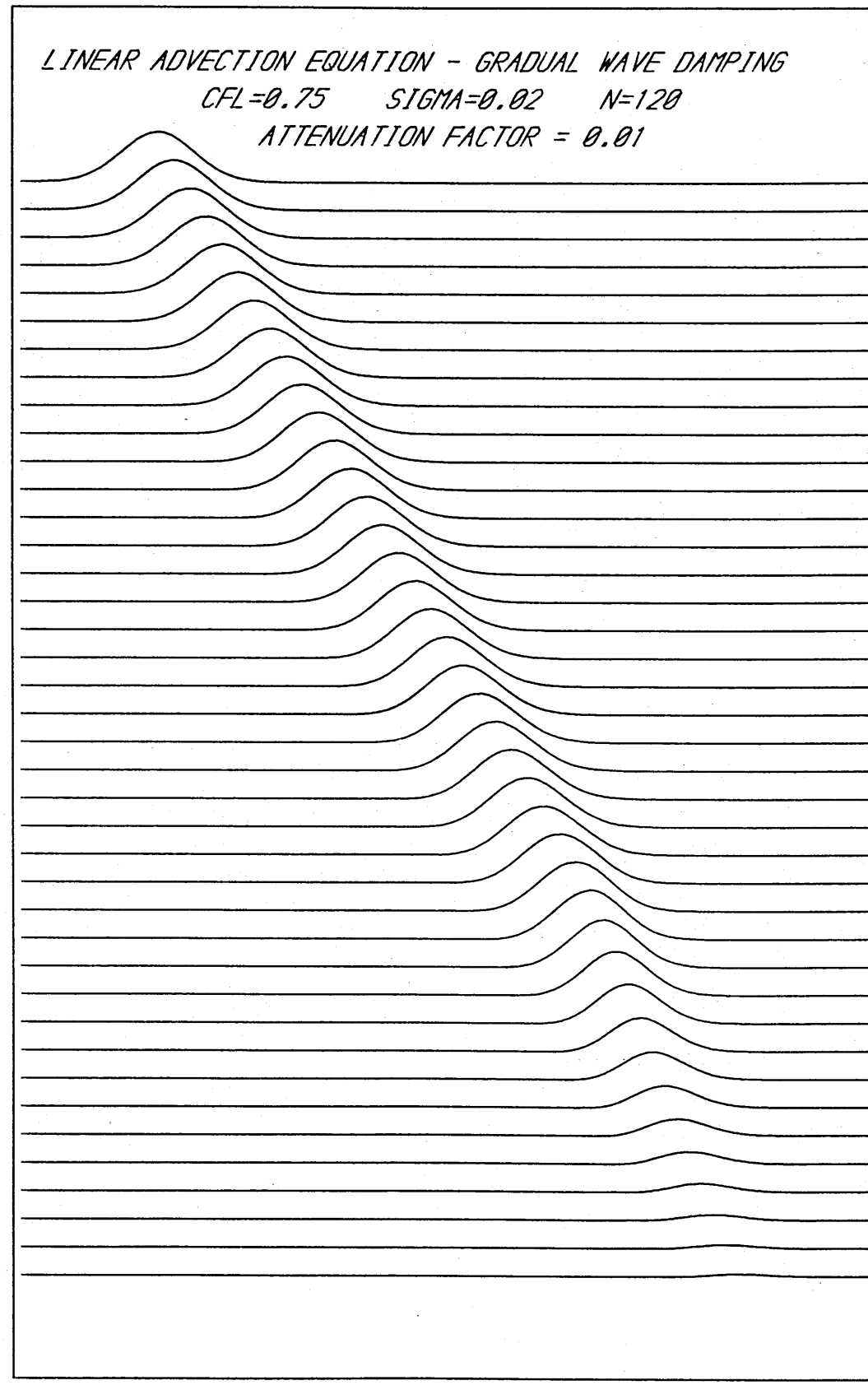

Figure (IV.1) - Linear advection equation - Gradually attenuated solution (b).

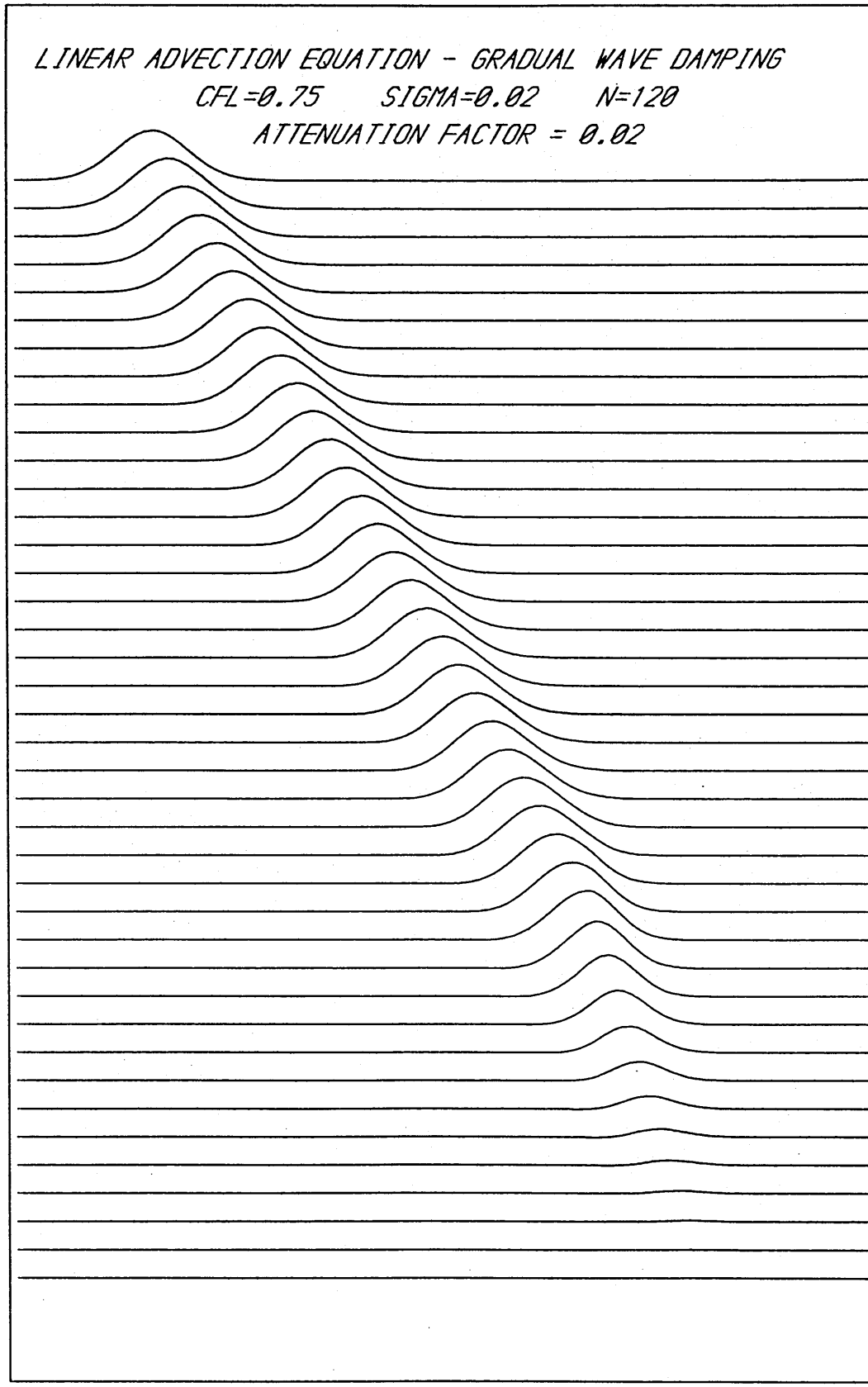

Figure (IV.1) - Linear advection equation - Gradually attenuated solution (c).

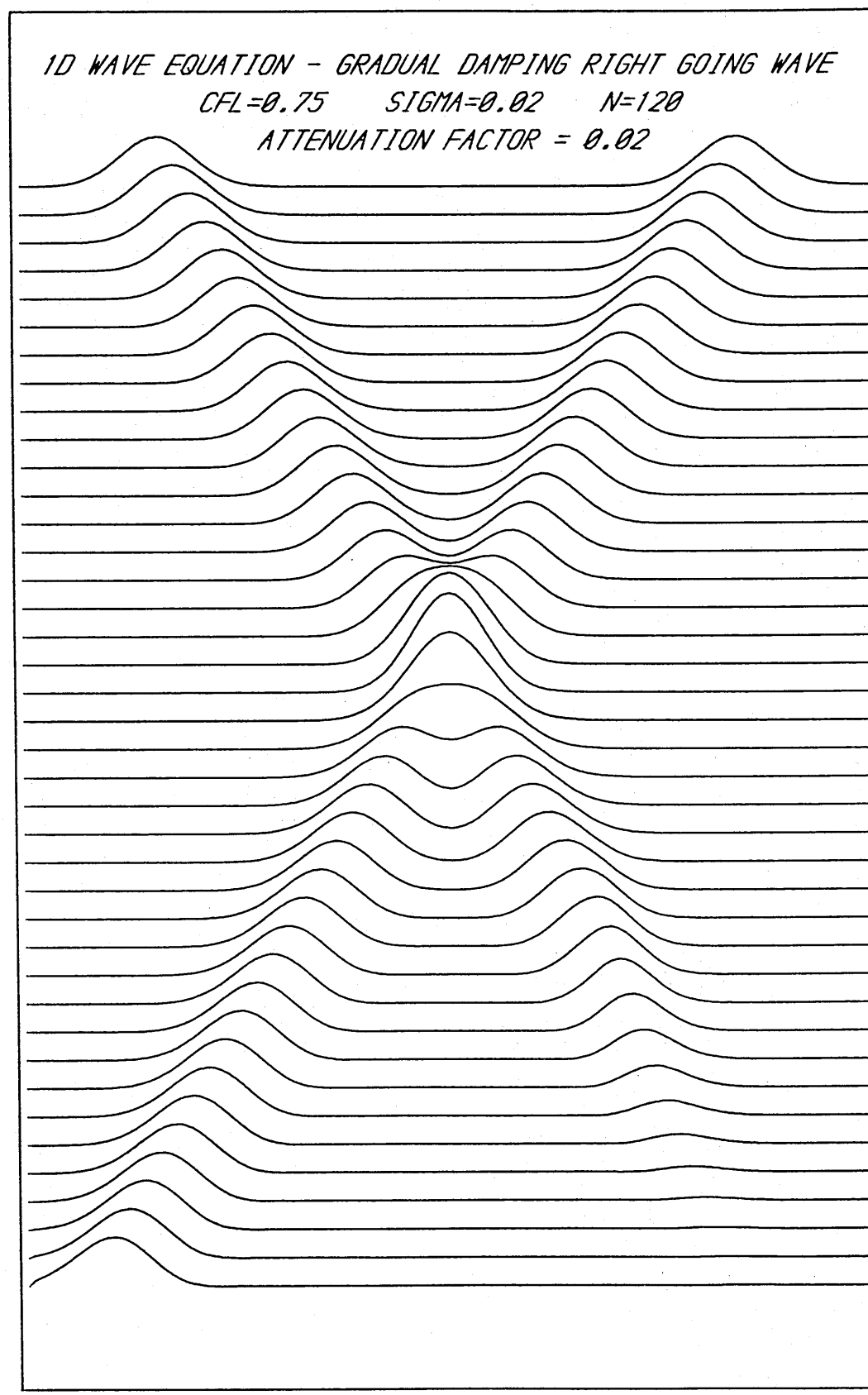
1D WAVE EQUATION - GRADUAL DAMPING RIGHT GOING WAVE
CFL=0.75 SIGMA=0.02 N=120
ATTENUATION FACTOR = 0.02

Figure (IV.2)

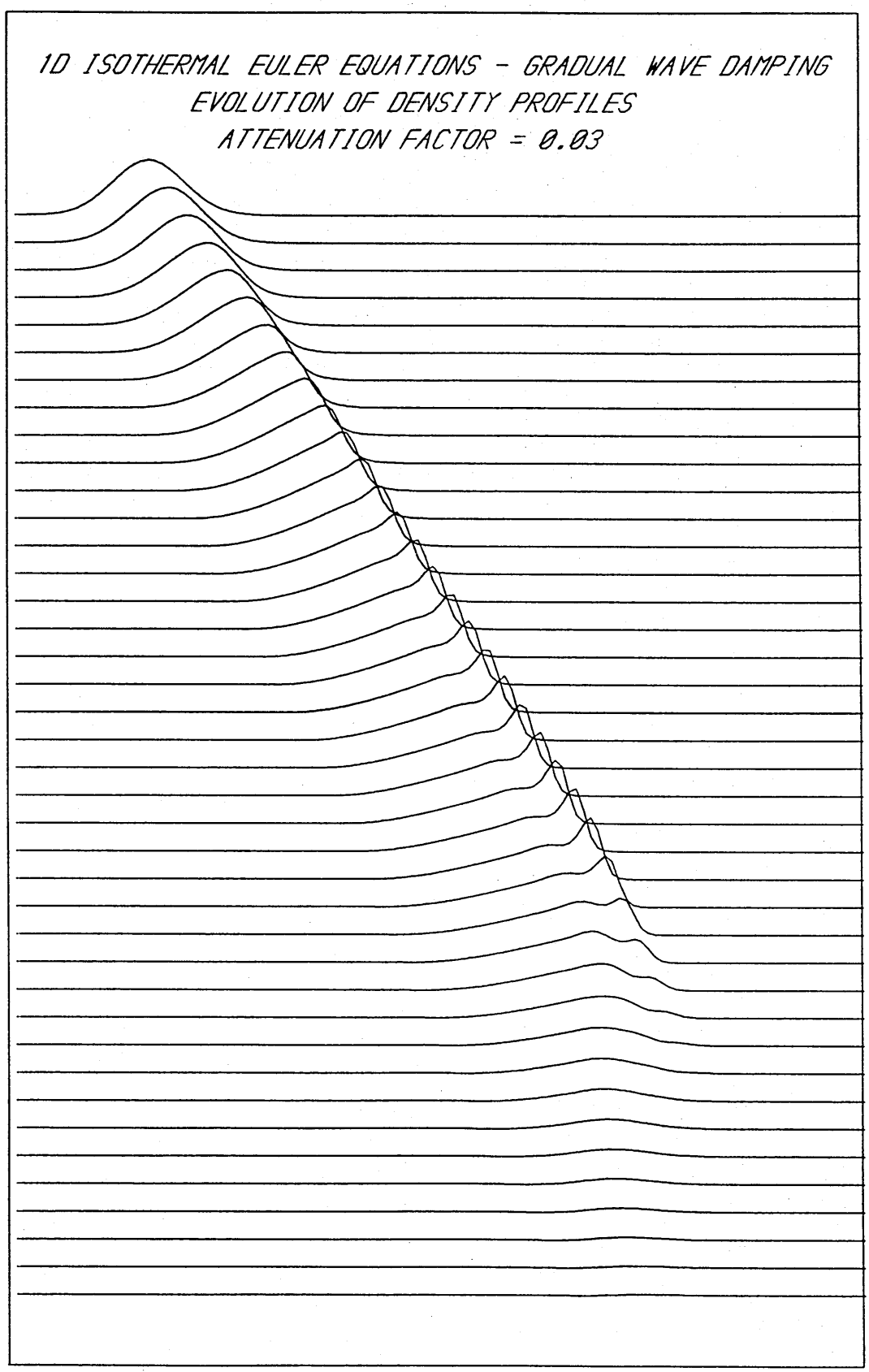

Figure (IV.3) - (a) Gradual attenuation of a outgoing compression wave.

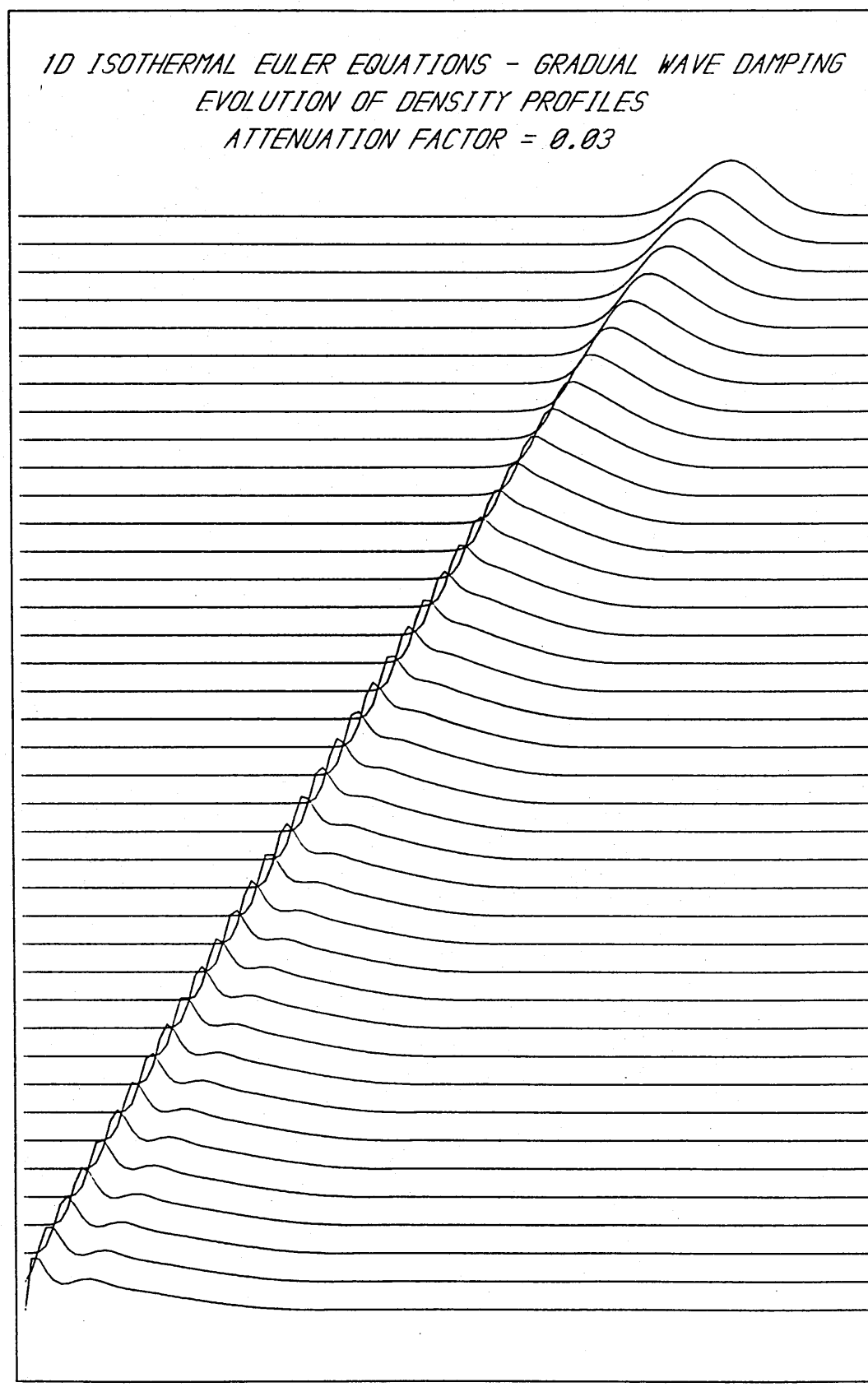

Figure (IV.3) - (b) Incoming compression wave unaffected.

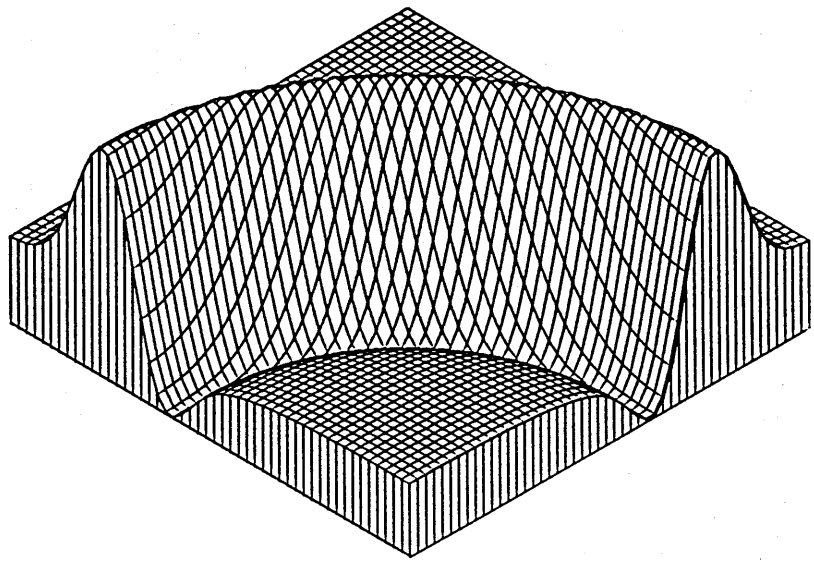

(a) Outgoing Speed = 1.0
Outging Damping Coefficient = 0.00

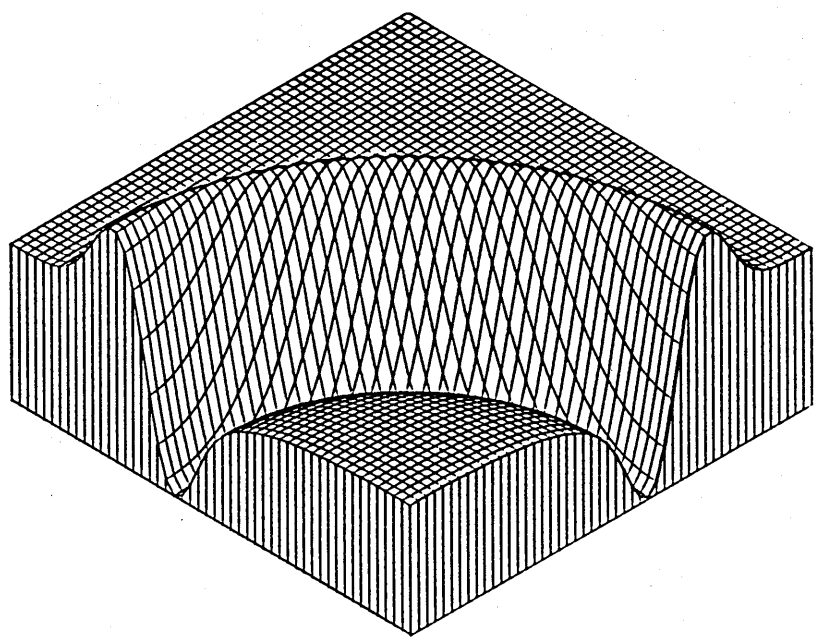

(b) Outgoing Speed = 1.0
Outgoing Damping Coefficient = 0.01

Figure (IV.4) - 2D linearised Euler equations - Gradual attenuation of an outgoing pressure wave.

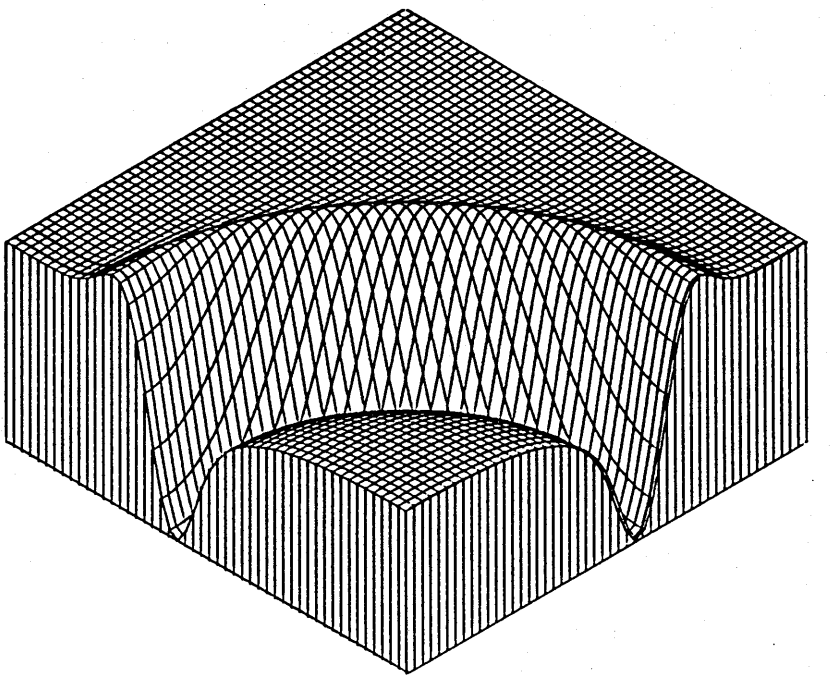

(c) Outgoing Speed = 1.0
Outging Damping Coefficient = 0.02

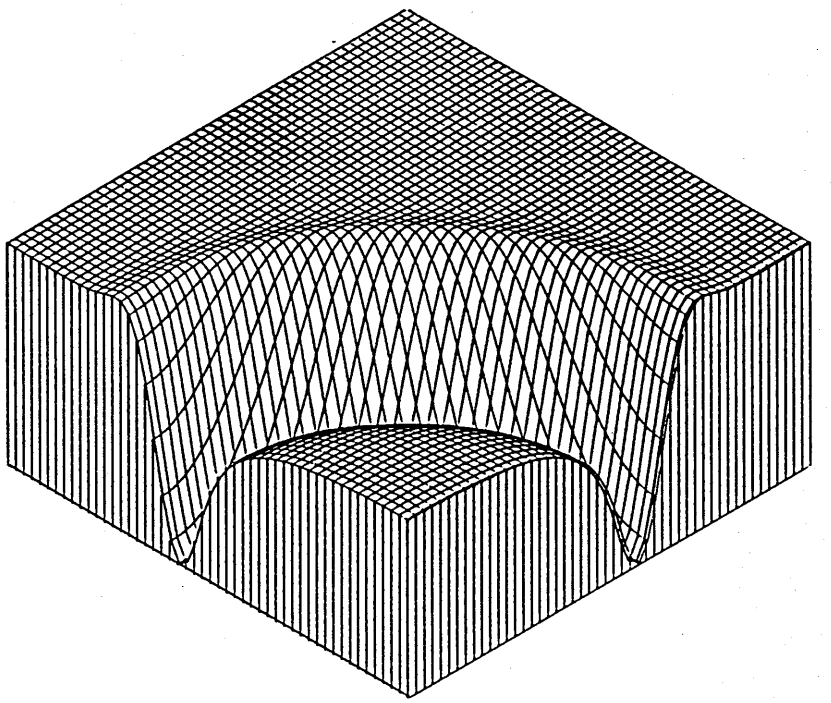

(d) Outgoing Speed = 1.0
Outgoing Damping Coefficient = 0.03

Figure (IV.4) - 2D linearised Euler equations - Gradual attenuation of an outgoing pressure wave.

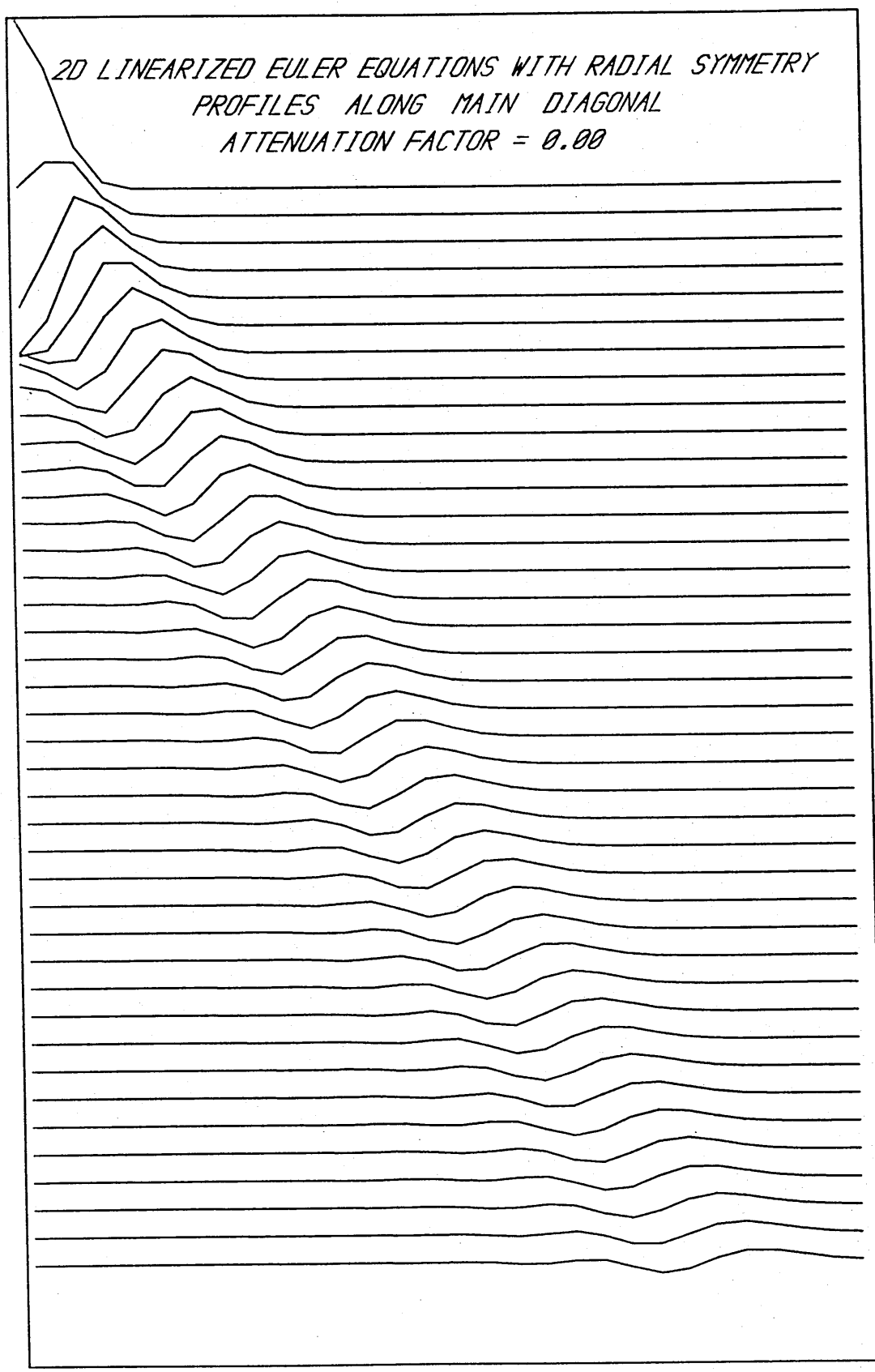

Figure (IV.5) - 2D linearised Euler equations with gradual attenuation - Profiles along main diagonal (a).

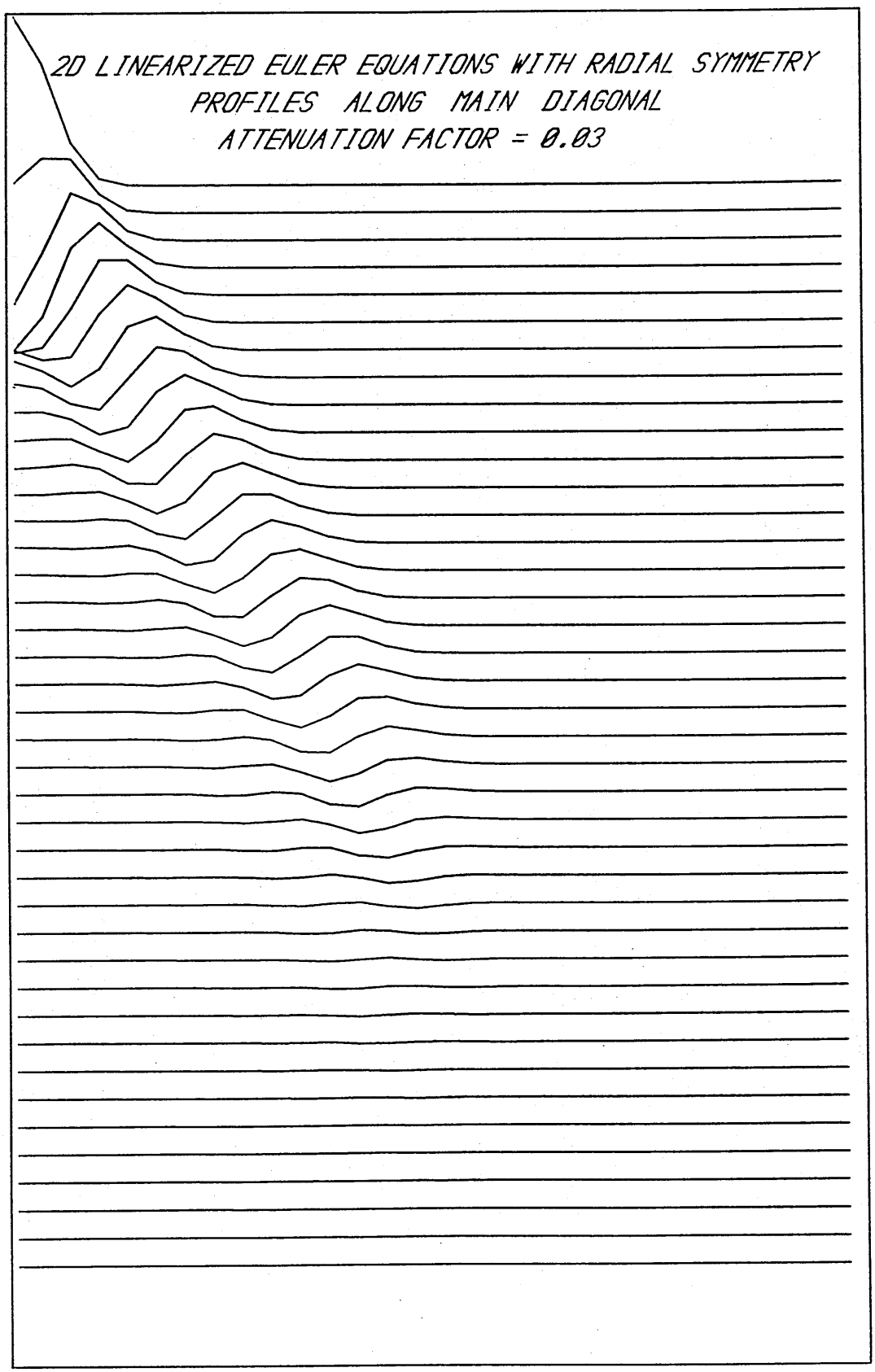

Figure (IV.5) - 2D linearised Euler equation with gradual attenuation - Profiles along main diagonal (b).

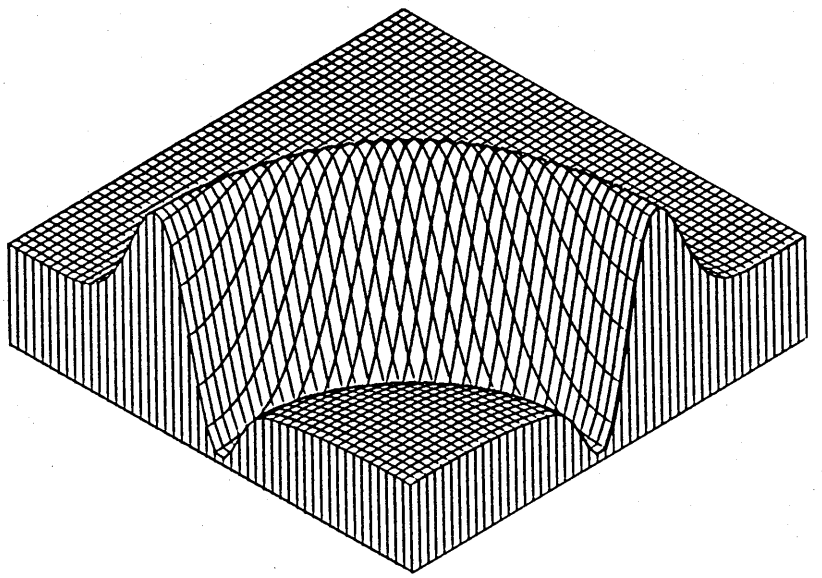

(a) Outgoing Speed = 0.8
Outging Damping Coefficient = 0.00

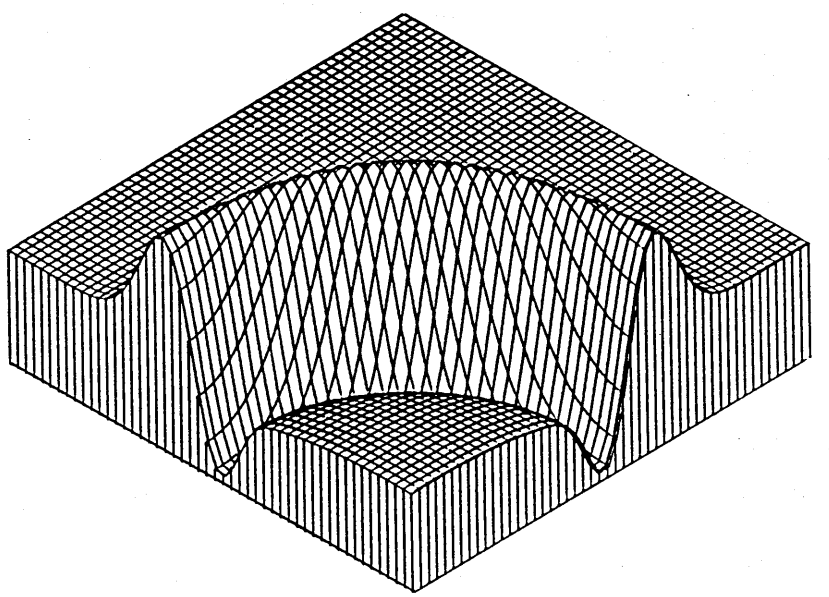

(b) Outgoing Speed = 0.8
Outgoing Damping Coefficient = 0.01

Figure (IV.6) - 2D linearised Euler equations - Numerical solution for initial data (3.8.5).

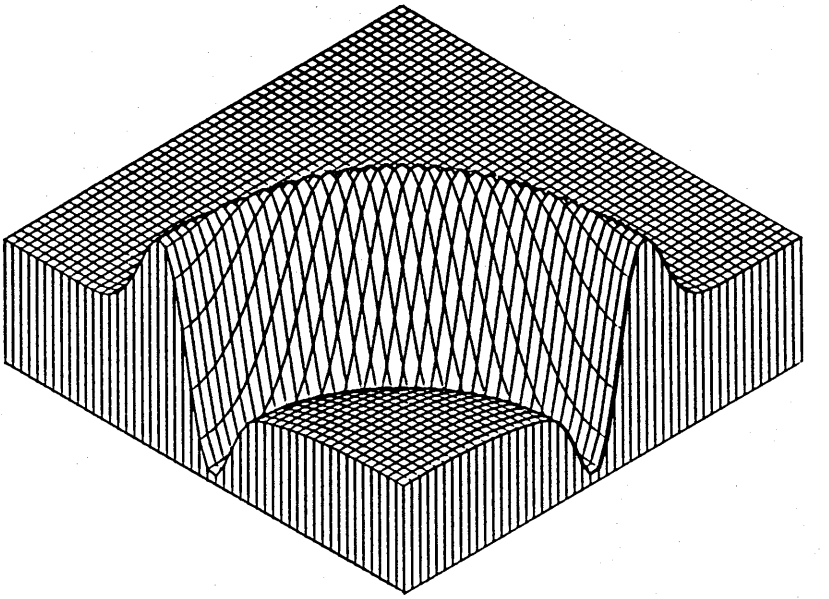

(c) Outgoing Speed = 0.8
Outging Damping Coefficient = 0.02

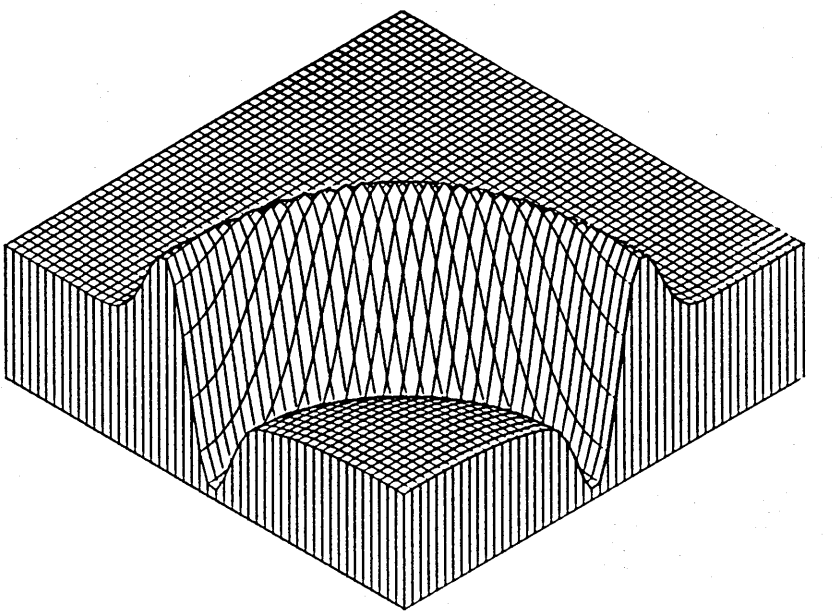

(d) Outgoing Speed = 0.8
Outgoing Damping Coefficient = 0.03

Figure (IV.6) - 2D linearised Euler equations - Numerical solution for initial data (3.8.5).

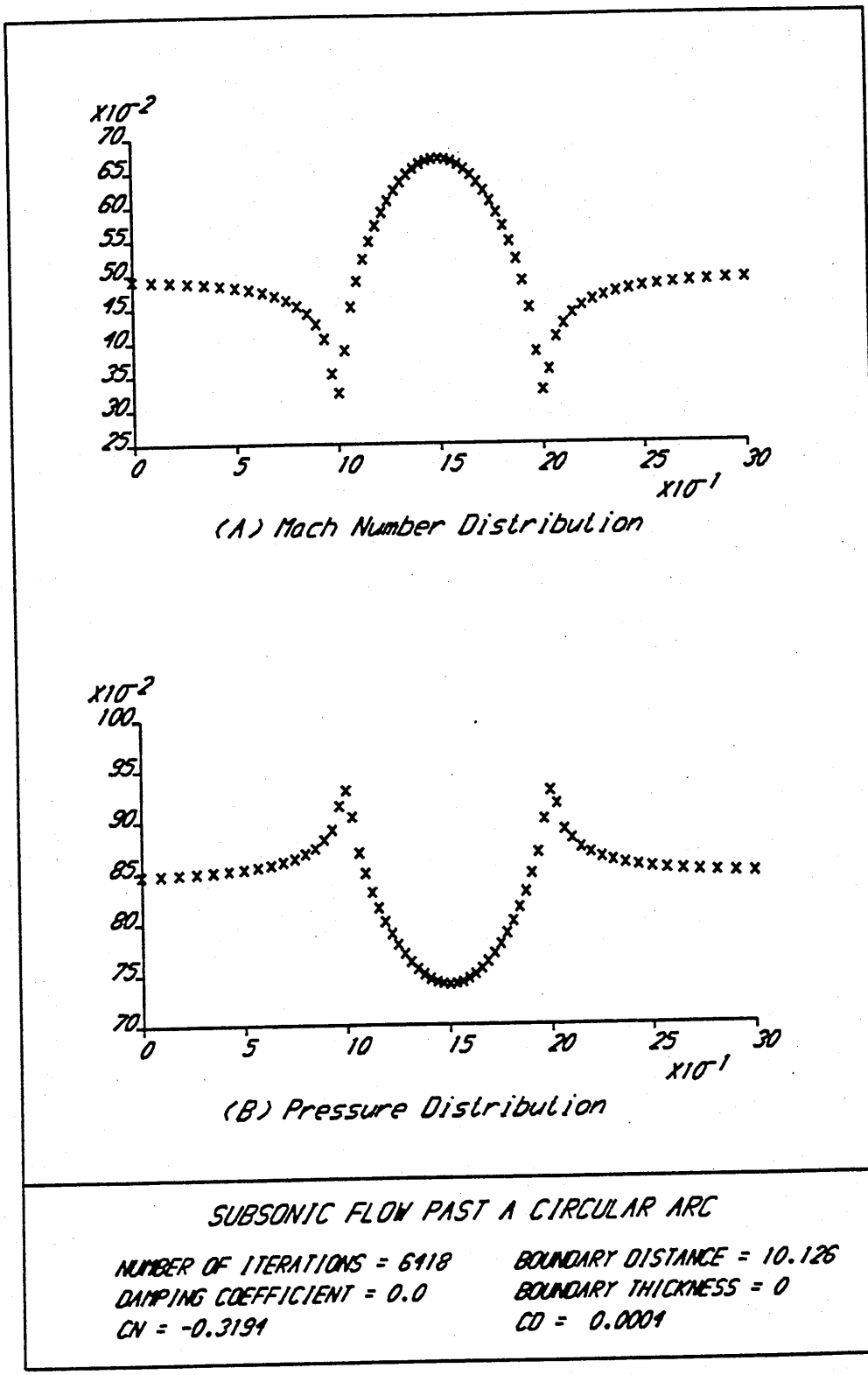
X10-2
70
65
60
55
50
45
40
35
30
25
0
5
10
15
20
25
30
X10-1
(A) Mach Number Distribution
X10-2
100
95
90
85
80
75
70
0
5
10
15
20
25
30
X10-1
(B) Pressure Distribution
SUBSONIC FLOW PAST A CIRCULAR ARC
NUMBER OF ITERATIONS = 6418
DAMPING COEFFICIENT = 0.0
CN = -0.3191
BOUNDARY DISTANCE = 10.126
BOUNDARY THICKNESS = 0
CD = 0.0004

Figure (IV.7)

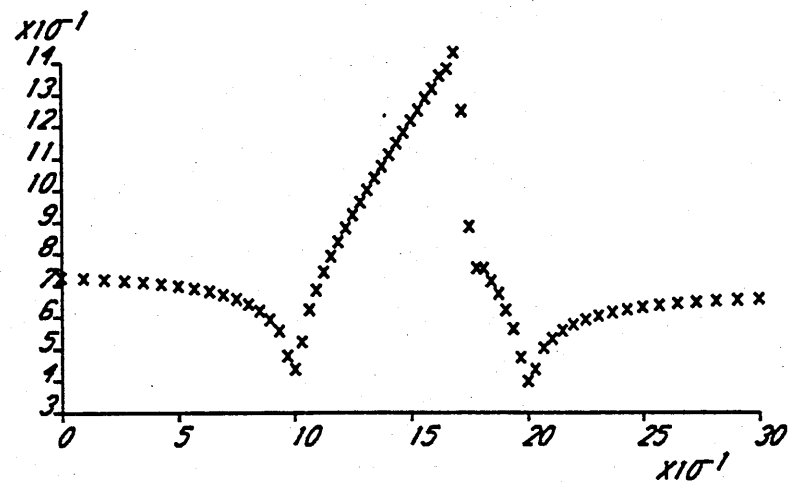

(A) Mach Number Distribution

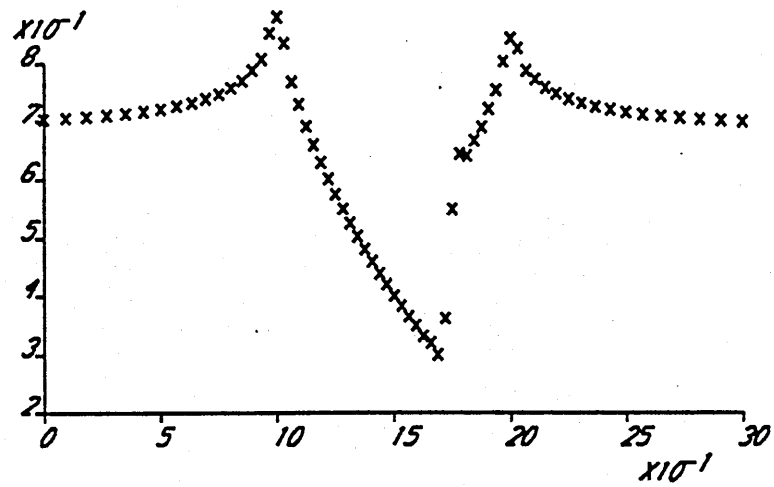

(B) Pressure Distribution

TRANSONIC FLOW PAST A CIRCULAR ARC

NUMBER OF ITERATIONS = 5528	BOUNDARY DISTANCE = 10.126
DAMPING COEFFICIENT = 0.0	BOUNDARY THICKNESS = 0
CN = -0.1628	CD = 0.0118

Figure (IV.8)